

1 **Progress in understanding of Indian Ocean circulation, variability, air-sea exchange and impacts on**  
2 **biogeochemistry**

3 Helen E. Phillips<sup>1,2</sup>, Amit Tandon<sup>3</sup>, Ryo Furue<sup>4</sup>, Raleigh Hood<sup>5</sup>, Caroline C. Ummenhofer<sup>6,7</sup>, Jessica A. Benthuisen<sup>8</sup>,  
4 Viviane Menezes<sup>6</sup>, Shijian Hu<sup>9</sup>, Ben Webber<sup>10</sup>, Alejandra Sanchez-Franks<sup>11</sup>, Deepak Cherian<sup>12</sup>, Emily Shroyer<sup>13</sup>, Ming  
5 Feng<sup>14,15</sup>, Hemantha Wijesekera<sup>16</sup>, Abhisek Chatterjee<sup>17</sup>, Lisan Yu<sup>6</sup>, Juliet Hermes<sup>18</sup>, Raghu Murtugudde<sup>19</sup>, Tomoki  
6 Tozuka<sup>20,4</sup>, Danielle Su<sup>21</sup>, Arvind Singh<sup>22</sup>, Luca Centurioni<sup>23</sup>, Satya Prakash<sup>17</sup>, Jerry Wiggert<sup>24</sup>

- 7  
8 <sup>1</sup>Institute for Marine and Antarctic Studies, University of Tasmania, Hobart, 7005, Australia  
9 <sup>2</sup>Australian Antarctic Program Partnership, [Institute for Marine and Antarctic Studies](#), University of Tasmania, Hobart,  
10 7005, Australia  
11 <sup>3</sup>Department of Mechanical Engineering, College of Engineering, University of Massachusetts Dartmouth, 02747, USA  
12 <sup>4</sup>APL/JAMSTEC, Yokohama, Japan  
13 <sup>5</sup>University of Maryland Center for Environmental Science, Horn Point Laboratory, Cambridge, 21613, USA  
14 <sup>6</sup>Department of Physical Oceanography, Woods Hole Oceanographic Institution, Woods Hole, 02543, USA  
15 <sup>7</sup>ARC Centre of Excellence for Climate Extremes, University of New South Wales, Sydney, Australia  
16 <sup>8</sup>Australian Institute of Marine Science, Indian Ocean Marine Research Centre, Crawley, Australia  
17 <sup>9</sup>Institute of Oceanology, Chinese Academy of Sciences, Qingdao, China  
18 <sup>10</sup>School of Environmental Sciences, University of East Anglia, Norwich, NR4 7TJ, UK  
19 <sup>11</sup>National Oceanography Centre, Southampton, UK  
20 <sup>12</sup>National Center for Atmospheric Research, Boulder, USA  
21 <sup>13</sup>College of Earth, Ocean and Atmospheric Sciences, Oregon State University, Corvallis, 97331, USA  
22 <sup>14</sup>CSIRO Oceans and Atmosphere, Indian Ocean Marine Research Centre, Crawley, Australia  
23 <sup>15</sup>Centre for Southern Hemisphere Oceans Research, Hobart, Australia  
24 <sup>16</sup>U.S. Naval Research Laboratory, [Stennis Space Center, MS, 39529](#), USA  
25 <sup>17</sup>Indian National Centre for Ocean Information Services, Ministry of Earth Sciences, Hyderabad, India  
26 <sup>18</sup>South African Environmental Observation Network, Cape Town, South Africa  
27 <sup>19</sup>Department of Atmospheric and Oceanic Science, University of Maryland, College Park, 20742, USA  
28 <sup>20</sup>Department of Earth and Planetary Science, Graduate School of Science, The University of Tokyo, Tokyo, Japan  
29 <sup>21</sup>Sorbonne Universités, UPMC Université Paris 06, CNRS, UMR 7159 LOCEAN-IPSL, Paris, France  
30 <sup>22</sup>Physical Research Laboratory, Ahmedabad, India  
31 <sup>23</sup>Scripps Institution of Oceanography, University of California San Diego, La Jolla, 92093, USA  
32 <sup>24</sup>University of Southern Mississippi, Hattiesburg, 399406, USA

**Style Definition:** Bullets: Outline numbered + Level: 1 +  
Numbering Style: 1, 2, 3, ... + Start at: 1 + Alignment: Left +  
Aligned at: 0 cm + Tab after: 1.27 cm + Indent at: 1.27 cm

**Deleted:** Wijesekera<sup>16</sup>

**Deleted:** Washington, 20032

35  
36  
37  
38  
39  
40  
41  
42  
43  
44  
45  
46  
47  
48  
49  
50  
51  
52  
53  
54  
55  
56  
57  
58  
59  
60  
61  
62  
63  
64

*Correspondence to:* Helen E. [Phillips \(h.e.phillips@utas.edu.au\)](mailto:h.e.phillips@utas.edu.au)

*Dedicated to Dr Satya Prakash (1979-2021). This manuscript was written during the COVID-19 pandemic while many juggled family and health issues under lockdown. Satya, our co-author and friend, passed away on 22nd July 2021. Satya was the coordinator of the International Indian Ocean Expedition (IIOE-2) at the Indian National Centre for Ocean Information Services (INCOIS). He played an integral part in Indian Ocean research. He is remembered for his enthusiasm, commitment and smile. His passing is a massive loss to the Indian Ocean community, but there will be much that will still be carried on in his memory thanks to his hard work and passion.*

**Abstract.** Over the past decade, our understanding of the Indian Ocean has advanced through concerted efforts toward measuring the ocean circulation and air-sea exchanges, detecting changes in water masses, and linking physical processes to ecologically important variables. New circulation pathways and mechanisms have been discovered, which control atmospheric and oceanic mean state and variability. This review brings together new understanding of the ocean-atmosphere system in the Indian Ocean since the last comprehensive review, describing the Indian Ocean circulation patterns, air-sea interactions and climate variability. Coordinated international focus on the Indian Ocean has motivated the application of new technologies to deliver higher-resolution observations and models of Indian Ocean processes. As a result we are discovering the importance of small-scale processes in setting the large-scale gradients and circulation, interactions between physical and biogeochemical processes, interactions between boundary currents and the interior, and between the surface and the deep ocean. A newly discovered regional climate mode in the southeast Indian Ocean, the Ningaloo Niño, has instigated more regional air-sea coupling and marine heatwave research in the global oceans. In the last decade, we have seen rapid warming of the Indian Ocean overlaid with extremes in the form of marine heatwaves. These events have motivated studies that have delivered new insight into the variability in ocean heat content and exchanges in the Indian Ocean, and have highlighted the critical role of the Indian Ocean as a clearing house for anthropogenic heat. This synthesis paper reviews the advances in these areas in the last decade.

**Contents**

**1. Introduction**

**2 Large-scale setting**

**3 Air-sea interactions**

**3.1 Seasonal cycle and the monsoons**

Deleted: Phillips (h.e.phillips@utas.edu.au)

Deleted: ¶



67	<a href="#"><u>3.2 Intraseasonal air-sea interaction</u></a>
68	<a href="#"><u>3.2.1 Madden-Julian Oscillation - MJO</u></a>
69	<a href="#"><u>3.2.2 Monsoon Intraseasonal Oscillation - MISO</u></a>
70	<a href="#"><u>3.2.3 Intraseasonal drivers of heavy rainfall</u></a>
71	<a href="#"><u>3.3 Ocean internal variability impacts on air-sea interaction</u></a>
72	<a href="#"><u>4 Upper Ocean Circulation and Biogeochemical Variability</u></a>
73	<a href="#"><u>4.1 Overview</u></a>
74	<a href="#"><u>4.2 Southern Indian Ocean</u></a>
75	<a href="#"><u>4.2.1 South Equatorial Current</u></a>
76	<a href="#"><u>4.2.2 Western Boundary</u></a>
77	<a href="#"><u>4.2.3 Interior flows</u></a>
78	<a href="#"><u>4.2.4 Eastern Boundary</u></a>
79	<a href="#"><u>4.2.5 Biogeochemical Variability</u></a>
80	<a href="#"><u>4.3 Equatorial regime</u></a>
81	<a href="#"><u>4.3.1 Wyrtki Jets</u></a>
82	<a href="#"><u>4.3.2 5-30 Day Ocean Waves and Instabilities</u></a>
83	<a href="#"><u>4.3.3 Equatorial Upwelling and Downwelling</u></a>
84	<a href="#"><u>4.3.4 Equatorial Undercurrents</u></a>
85	<a href="#"><u>4.3.5 Cross-Equatorial Circulation</u></a>
86	<a href="#"><u>4.3.6 Biogeochemical Variability</u></a>
87	<a href="#"><u>4.4 Northern Indian Ocean</u></a>
88	<a href="#"><u>4.4.1 Bay of Bengal</u></a>
89	<a href="#"><u>4.4.1.1 Southwest/Northeast Monsoon Currents</u></a>
90	<a href="#"><u>4.4.1.2 East Indian Coastal Currents (EICC)</u></a>
91	<a href="#"><u>4.4.1.3 Undercurrents</u></a>
92	<a href="#"><u>4.4.1.4 Sri Lanka Dome</u></a>
93	<a href="#"><u>4.4.2 Arabian Sea</u></a>
94	<a href="#"><u>4.4.2.1 Somali current System</u></a>
95	<a href="#"><u>4.4.2.2 West India Coastal Current (WICC)</u></a>
96	<a href="#"><u>4.4.3 Biogeochemical Variability</u></a>
97	<a href="#"><u>5 Inter-ocean exchange</u></a>
98	<a href="#"><u>5.1 Indonesian Throughflow</u></a>
99	<a href="#"><u>5.1.1 General features</u></a>
100	<a href="#"><u>5.1.2 Variability, dynamics and influence</u></a>
101	<a href="#"><u>5.2 Agulhas Leakage</u></a>
102	<a href="#"><u>5.2.1 General features</u></a>
103	<a href="#"><u>5.2.2 Variability, dynamics and influence on climate</u></a>
104	<a href="#"><u>5.3 Supergyre connection to the South Pacific</u></a>
105	<a href="#"><u>5.4 Roles of salinity in inter-ocean exchange</u></a>

106	<a href="#"><u>6 Modes of Interannual Climate Variability in the Indian Ocean</u></a>
107	<a href="#"><u>6.1 ENSO teleconnection and the Indian Ocean Basin mode</u></a>
108	<a href="#"><u>6.2 The Indian Ocean Dipole</u></a>
109	<a href="#"><u>6.3 The subtropical Indian Ocean Dipole</u></a>
110	<a href="#"><u>6.4 Ningaloo Niño and marine heatwaves in the Indian Ocean</u></a>
111	<a href="#"><u>6.5 Monsoon variability and links to the Indian Ocean</u></a>
112	<a href="#"><u>7. Multiscale upper ocean processes in the Bay of Bengal</u></a>
113	<a href="#"><u>7.1 The Bay's Forcing and Upper Ocean Structure</u></a>
114	<a href="#"><u>7.2 Lateral Processes</u></a>
115	<a href="#"><u>7.2.1 Stirring from the Margins</u></a>
116	<a href="#"><u>7.2.2 Inter-basin exchange</u></a>
117	<a href="#"><u>7.2.2.1 Andaman Sea Exchange</u></a>
118	<a href="#"><u>7.2.2.2 Arabian Sea Exchange</u></a>
119	<a href="#"><u>7.2.3 Equatorial Connections</u></a>
120	<a href="#"><u>7.3 Vertical Mixing</u></a>
121	<a href="#"><u>7.4 Where vertical and lateral processes meet: The Role of Submesoscale</u></a>
122	<a href="#"><u>7.5 Putting the Pieces Together</u></a>
123	<a href="#"><u>7.5.1 Coupled ocean-atmosphere phenomena</u></a>
124	<a href="#"><u>7.5.2 Implications for biogeochemistry in the Bay</u></a>
125	<a href="#"><u>8. Summary and open questions</u></a>
126	<a href="#"><u>Code Availability</u></a>
127	<a href="#"><u>Data Availability</u></a>
128	<a href="#"><u>Author Contributions</u></a>
129	<a href="#"><u>Competing interests</u></a>
130	<a href="#"><u>Acknowledgements</u></a>
131	<a href="#"><u>References</u></a>
132	
133	

134 **1. Introduction**

135 The physical processes taking place in the Indian Ocean and overlying atmosphere underpin the variability evident in  
136 monsoons, extreme events, marine biogeochemical cycles, ecosystems, and ultimately human experience. The Indian  
137 Ocean rim countries, accounting for one third of the Earth's human population, depend on this ocean for food and  
138 resources, and are dramatically impacted by its variability (Hermes et al., 2019). Increasing our understanding of

139 interactions between geologic, oceanic and atmospheric processes that control the complex physical dynamics of the  
140 Indian Ocean region is a priority for many national, bilateral, and international programmes including the Indian Ocean  
141 Observing System (IndOOS; Beal et al., 2020), the Climate and Ocean: Variability, Predictability and Change  
142 (CLIVAR)/Intergovernmental Oceanographic Commission (IOC) - Indian Ocean Region Panel  
143 ([https://www.clivar.org/sites/default/files/documents/indian/135\\_IOP5.pdf](https://www.clivar.org/sites/default/files/documents/indian/135_IOP5.pdf)), and the second International Indian Ocean  
144 Expedition (IIOE-2), to name a few. While initiated through IIOE-2, this review draws on the collective results of all of  
145 the programmes and individual efforts. We focus, in particular, on questions about the Indian Ocean circulation, climate  
146 variability and change such as: 1) how have the atmospheric and oceanic circulation of the Indian Ocean changed in the  
147 past and how will they change in the future; 2) how do these changes relate to geography and connectivity with the Pacific,  
148 Atlantic and Southern oceans; and 3) what impact does the circulation, variability, and change have on biological  
149 productivity and fisheries.

150 Recent focus on the Indian Ocean has motivated new international efforts in field campaigns and modelling studies, and  
151 leveraged advances in global observations that contribute to the Indian Ocean Observing System (IndOOS; Beal et al.,  
152 2020). The Argo profiling float array (Roemmich et al., 2012) reached full coverage in the Indian Ocean in 2006, the  
153 RAMA moored buoy array (McPhaden et al., 2009) has now delivered multi-year time series of tropical oceanic and  
154 atmospheric variability, with some sites dating back to 2000. Satellite systems continue to provide observations vital to  
155 interpreting spatial and temporal variability in the in situ observations, and new technology is now enabling high resolution  
156 observations of boundary current variability and small scale processes. Thus, since the reviews of Schott and McCreary  
157 (2001) and Schott et al. (2009), the spatial coverage of observations and length of time series have increased substantially  
158 such that the signals of many previously unresolved processes are now able to be observed.

160 These new higher-resolution observations and companion improvements in model simulations have highlighted the  
161 importance of small scale processes in setting the large-scale gradients and circulation, interactions between physical and  
162 biogeochemical processes, interactions between boundary currents and the interior, and between the surface and the deep  
163 ocean. Overlaid on these interior Indian Ocean processes, ocean warming due to increasing greenhouse gas concentrations  
164 has been shown to be pervasive and relentless (Wijffels et al., 2016), and extending to abyssal depths (Johnson et al.,  
165 2008a; Desbruyères et al., 2017).

167 The Indian Ocean plays a key role in the global climate system, enabling upwelling of the lower cell of the meridional  
168 overturning circulation from abyssal to upper-deep and intermediate waters through diffusive mixing (Schmitz, 1995;  
169 Lumpkin and Speer, 2007; McDonagh et al., 2008; Talley, 2013; Hernandez-Guerra and Talley, 2016) and exporting the  
170 largest poleward heat flux of all Southern Hemisphere basins (Roxby et al., 2014). In recent decades, the upper 700 m of  
171 the entire Indian Ocean has warmed rapidly (Desbruyères et al., 2017). In the southern Indian Ocean, the warming was

Deleted: topography

173 directly linked primarily to heat advection from a strengthened ITF and, secondly, to a decrease in mean air-sea flux  
174 cooling (Li et al., 2017b; Zhang et al., 2018a). This coupling between the ocean and atmosphere in the Indian and Pacific  
175 Oceans shifted the balance of global warming, accelerating ocean warming and causing a hiatus in the warming of Earth's  
176 surface atmosphere (Section 6). Marine heatwaves have emerged as an increasing threat to marine ecosystems as ocean  
177 temperatures warm (e.g. Oliver et al., 2018). Increasingly vulnerable populations need more reliable monsoon predictions,  
178 a task complicated by variability across timescales from intraseasonal to interannual, decadal and beyond in a tightly  
179 coupled ocean-atmosphere system (Hazra et al., 2017).

180  
181 The starting point for this synthesis report are the reviews by Schott and McCreary (2001) and Schott et al. (2009),  
182 describing the circulation patterns, air-sea interactions and climate variability on timescales from intraseasonal to  
183 interannual, and relatively large spatial scales. We begin with a description of the large scale setting that has been well  
184 established since Schott et al. (2009) (Section 2). We then consider the structure and propagation of variability in air-sea  
185 interactions at seasonal and intra-seasonal scales, including the contribution of the mesoscale and the ocean's role in air-sea  
186 sea interaction (Section 3). Section 4 discusses new advances in understanding of the upper ocean circulation, organised  
187 by region (southern basin, equatorial and northern basin). This section includes an update of the near-surface circulation  
188 maps of Talley et al. (2011), including recent work on boundary currents around Australia and Madagascar, and a  
189 discussion of the biogeochemical variability observed in each region. The interocean connections with the Pacific, Atlantic  
190 and Southern Oceans are discussed in Section 5. Section 6 describes the variability of the Indian Ocean circulation with  
191 the recent advances in understanding the warming across the basin, climate modes such as the Indian Ocean Dipole,  
192 connection with the El Niño-Southern Oscillation (ENSO), and Indian ocean marine heatwaves. Section 7 focuses on  
193 multiscale processes in the Bay of Bengal as an "ocean laboratory", since there have been multiple international programs  
194 in this Bay in the last decade. Recent advances from the large scales (>100 km) down to sub-mesoscales (100 m to 10 km)  
195 and further down to mixing scales (mm) are discussed. We then link back from mixing to large scales via salinity budgets  
196 and coupled phenomena such as the Madden-Julian Oscillation (MJO) to understand the complexity of these processes  
197 across multiple scales. We end with a short summary and open questions that will need to be addressed over the next  
198 decade.

## 199 **2 Large-scale setting**

200 The oceanic and atmospheric circulation of the Indian Ocean are unlike those in the Pacific and Atlantic oceans, largely  
201 due to geography. The Asian landmass limits the northern extent of the Indian Ocean to around 25°N so that there is no  
202 high-latitude cooling of the ocean, and consequently no dense water formation such as that seen in the North Atlantic and,  
203 to some extent, the North Pacific. The intense seasonal variation in temperature over Asia drives the seasonal monsoons:  
204 the southwest monsoon in boreal summer, and northeast monsoon in boreal winter. The timing of the onset of the monsoon,

205 and associated wet and dry periods in the Indian Ocean rim countries, varies considerably depending on a range of large-  
206 scale climate modes and smaller-scale coupled ocean-atmosphere interactions. The seasonally-reversing winds drive  
207 seasonally-reversing ocean currents in the northern Indian Ocean (Section 4.4), e.g. the southwest/northeast monsoon  
208 current and the Somali Current. Equatorial currents in the Indian Ocean, eastward near the surface above westward  
209 undercurrents (Section 4.3), provide rapid connection between the western and eastern basin and are also subject to  
210 monsoon dynamics.

211 In the southern Indian Ocean (Section 4.2), the connection of the Indian and Pacific Oceans through the Indonesian Seas  
212 also contributes to the unique circulation patterns. The very warm and fresh ITF water is funneled into the tropical southern  
213 Indian Ocean and carried westward by the South Equatorial Current. The warm, fresh waters are much lighter than those  
214 further south, creating a north-south density (pressure) gradient that drives near-surface broad, eastward geostrophic  
215 currents between 16°S and 32°S and between Madagascar and Australia (Niiler et al., 2003). This pressure gradient also  
216 generates the Leeuwin Current, a unique poleward-flowing eastern boundary current (Godfrey and Ridgway, 1985) that is  
217 a downwelling region but is also, counter-intuitively, highly productive (Waite et al., 2007). These two features are not  
218 found in the southeastern Atlantic and Pacific oceans. There, the eastern basin currents are characterised by a clear  
219 subtropical gyre circulation with weak, equatorward flow and upwelling against the coast.

220 The tropical Indian Ocean (Section 4.3) is home to the largest fraction of sea surface temperature (SST) warmer than 28°C  
221 (the tropical warm pool), and is therefore a key region for deep atmospheric convection: the upward part of the Walker  
222 Circulation that drives cloud formation and precipitation over the tropical Indo-Pacific. Variation in SST is the primary  
223 driver of variation in exchanges between the ocean and atmosphere and is thus a key focus in this paper. Sea surface  
224 salinity effects on ocean-atmosphere exchanges have become better understood and are discussed throughout and in  
225 particular in Section 7.

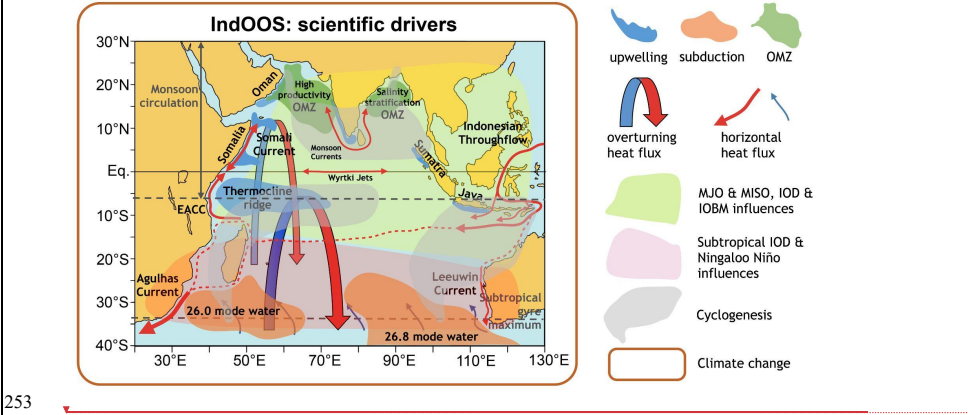
226 The tropical Indian Ocean sea surface temperature (SST) has warmed faster over the period since 1950, than either the  
227 tropical Pacific or Atlantic (Han et al., 2014, Fox-Kemper et al., 2021), with implications for primary productivity (Roxy  
228 et al., 2014, 2016). The Indian Ocean accounts for 50-70% of the total ocean heat uptake in the global upper (700 m) ocean  
229 over the last decade, associated with anthropogenic warming (Lee et al., 2015). The deeper ocean (700-2000 m) is  
230 warming across the globe with a robust signature of anthropogenic warming evident even in the short Argo record since  
231 2005 (Wijffels et al. 2016, Rathore et al. 2020). Warming in the abyss is detectable and widespread, communicated from  
232 the surface of the ocean along pathways from Antarctic Bottom Water formation regions (Purkey and Johnson, 2012).  
233 Considerable variability in the Indian Ocean climate system exists on the backdrop of this strong, long-term warming  
234 trend.

**Deleted:** ~2010

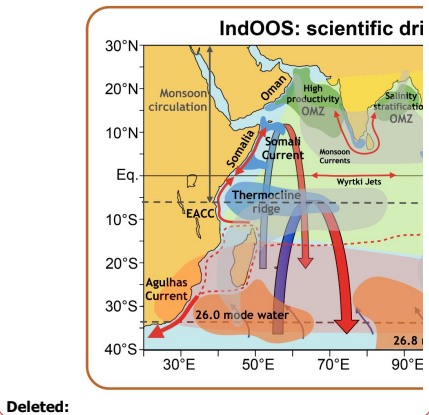
**Deleted:** 2014). Most of this warming (1.2°C over 1901–2012) has occurred in the western Indian Ocean, which has been the largest contributor to the overall global SST trend.

239 An extensive debate erupted in recent years about whether there was hiatus or a reduced rate of global warming  
240 (Lewandowsky et al. 2018). However, persistent cold anomalies in the eastern Pacific have been argued to have enhanced  
241 oceanic heat uptake, and the strengthened trade winds are consistent with this argument (Kosaka and Xie 2013, England  
242 et al. 2014). It has further been argued that the excess heat taken up by the tropical Pacific has been pumped into the Indian  
243 Ocean via the Indonesian throughflow (Lee et al. 2015). The tropical Indian Ocean is likely affected by the Southern  
244 Ocean trends at a rapid timescale of the order of a decade (Yang et al. 2020), and the Indian Ocean warming may accelerate  
245 the Atlantic meridional overturning circulation (Hu et al. 2019) and the Pacific response to anthropogenic forcing (Zhang  
246 et al. 2019). Based on these oceanic tunnels and atmospheric bridges into and out of the Indian Ocean, one could  
247 hypothesise that the Indian Ocean may be acting as the clearinghouse for oceanic warming under anthropogenic forcing.

248 Variability in the oceanic and atmospheric circulation of the Indian Ocean is the result of complex interactions that are  
249 both internal and external to the Indian Ocean. The recent review of the IndOOS plan (Beal et al., 2019, 2020) summarises  
250 the major scientific drivers, of which we still have limited understanding (Fig. 1). The over-arching signal is anthropogenic  
251 climate change, causing a background trend of ocean warming and increasing acidity due to uptake of heat and carbon  
252 dioxide and affecting the nature of large and small scale variability mechanisms.



254 **Figure 1: Schematic view of key phenomena in the Indian Ocean (from Beal et al. 2019). The main scientific drivers**  
255 **of the Indian Ocean Observing System, including the Oxygen Minimum Zones (OMZs), upwelling and subduction**  
256 **zones, major heat flux components, the tropical modes of the Madden-Julian Oscillation (MJO), the Monsoon**



Deleted:

258 **Intra-Seasonal Oscillation (MISO), the Indian Ocean Dipole (IOD) and Indian Ocean Basin Mode (IOBM), the**  
259 **subtropical modes of Ningaloo Niño and subtropical IOD, cyclogenesis, and climate change.**

260 A net poleward flow of heat out of the Indian Ocean is accomplished by a combination of the horizontal circulation along  
261 the boundaries, coupled with the Indian Ocean's part of the global meridional overturning circulation (MOC) and shallow  
262 overturning cells. The ITF delivers heat from the Pacific into the Indian Ocean. The Agulhas Current moves heat rapidly  
263 southward at surface and intermediate depths (Bryden and Beal, 2001), with 30% of Indian Ocean heat export thought to  
264 be carried across 32°S by this gyre circulation (Talley, 2008). The shallow Leeuwin Current makes a smaller direct  
265 contribution to the poleward flow of heat (Smith et al., 1991; Feng et al., 2003; Furue et al., 2017) but generates a rich  
266 field of mesoscale eddies that carry heat and momentum into the Indian Ocean interior, contributing to heat export across  
267 32°S (Domingues et al. 2006, Feng et al., 2007; Dilmahamod et al. 2018).

268 In the upper ocean, the shallow overturning consists of the cross-equatorial cell (Miyama et al. 2003; Schott et al. 2004)  
269 and the subtropical cell (Schott et al. 2004). The ascending branches of these cells connect to different upwelling zones in  
270 the southern and northern Indian Ocean and, therefore, play an important role in regulating the climatological mean,  
271 seasonal, and interannual heat balance in the tropical Indian Ocean (Lee 2004; Lee and McPhaden 2008). At intermediate  
272 depths (500-2000 m), mode waters of varying density enter the Indian Ocean from the Southern Ocean. Along their  
273 northward path they mix with lighter waters above, progressively upwelling to the sea surface in a range of locations north  
274 of 10°S to then return south in a widespread southward Ekman transport of near-surface waters (Schott et al., 2009). The  
275 lower part of the mode water layer mixes with denser waters below and joins the southward flowing deep waters (2000-  
276 4000 m). This southward flow also has a contribution from transformed abyssal waters: Antarctic Bottom Water moves  
277 northward at abyssal depths, mixing with lighter waters above, progressively upwelling along its path from the Southern  
278 Ocean to the Indian Ocean to return southward at shallower depths (Talley, 2013). Cross-equatorial flow is accomplished  
279 both at abyssal levels and via the East Africa Coastal Current, seasonally reversing Somali Current (Schott et al., 2009)  
280 and southward Ekman transport (Schott and McCreary, 2001).

281 The remaining elements of Fig. 1 refer to oxygen minimum zones (OMZ) in the Arabian Sea and Bay of Bengal and the  
282 range of mechanisms that drive strong variations in sea surface temperature leading to shifts in atmospheric convection  
283 and precipitation with major effects on rim countries. These mechanisms include: Madden-Julian oscillation (MJO) and  
284 Monsoon Intraseasonal Oscillation (MISO), Indian Ocean Dipole (IOD), Indian Ocean Basin Mode, Subtropical IOD, and  
285 Ningaloo Niño which are discussed further in Section 6. Cyclogenesis is not discussed in this synthesis. For discussion of  
286 OMZ, the reader is referred to the review papers of McCreary et al. (2013) and Rixen et al. (2020).

287 Extreme precipitation in the Bay of Bengal and evaporation in the Red Sea and Arabian Sea lead to strong variability in  
288 ocean salinity that in turn impacts ocean circulation and air-sea interaction. The surface salinity gradient in the northern

Indian Ocean decreases from the Arabian Sea in the west to the Bay of Bengal in the east. Strong evaporation over the Arabian Sea results in highly saline surface waters (Antonov et al., 2010; Chatterjee et al., 2012), while surface waters in the Bay of Bengal are comparatively fresh and highly stratified as a result of monsoon precipitation and outflow from river systems such as the Ganges-Brahmaputra (Shetye et al., 1996; Vinayachandran et al., 2002). The surface forcing is balanced by the seasonally reversing monsoon currents to maintain the climatological distribution of salinity.

### 3 Air-sea interactions

The tropical Indian Ocean is highly variable across multiple scales, all of which involve atmosphere-ocean interaction: from the locally intense heat and moisture fluxes that drives tropical cyclones to large-scale convection in the ascending branch of the Hadley circulation, and basin scale ocean heat transport carried by overturning cells that contribute to decadal variability and trends. At intermediate time scales, the intraseasonal oscillations involve strong air-sea coupling (e.g., Demott et al., 2015). The Indian Ocean Dipole (IOD) is an example of an inherently coupled mode of variability (Saji et al., 1999, Webster et al. 1999, Murtugudde et al. 2000). The monsoonal rainfall around the Indian Ocean is largely fuelled by warm SSTs and strong sea-to-air moisture fluxes. These phenomena emphasise the need to understand the mechanisms of air-sea interaction within the Indian Ocean, with a particular focus on how these processes can be better represented in models to aid predictions of variability in the Earth system.

#### 3.1 Seasonal cycle and the monsoons

In the open ocean south of 10°S, the wind pattern throughout the year is southeasterly trade winds across the tropics and subtropics and westerlies south of 35°S (Fig. 2). The evaporative cooling of the ocean surface by the trade winds leads to high salinity throughout the subtropics. The curl of the wind stress drives year-round Ekman pumping (downwelling) south of around 15°S (Fig. 2). Downwelling of these denser, high salinity surface waters supplies the downward limb of the shallow Subtropical Cell, STC and Cross-Equatorial Cell, CEC (Schott et al. 2002; Miyama et al. 2003; Schott et al., 2004; Lee 2004; Schott et al., 2009). The subsurface path of the shallow overturning is not well known, and the return to the surface is in any of a number of upwelling zones including the Seychelles-Chagos Thermocline Ridge for the STC and along Somalia, Oman and the west coast of India for the CEC. North of around 10°S, the winds over the Indian Ocean are characterised by seasonal reversals due to the monsoons (Fig. 2), which in turn cause most of the near-surface currents in these regions to seasonally reverse (Schott et al., 2009; Shankar et al., 2002, Section 4.4).



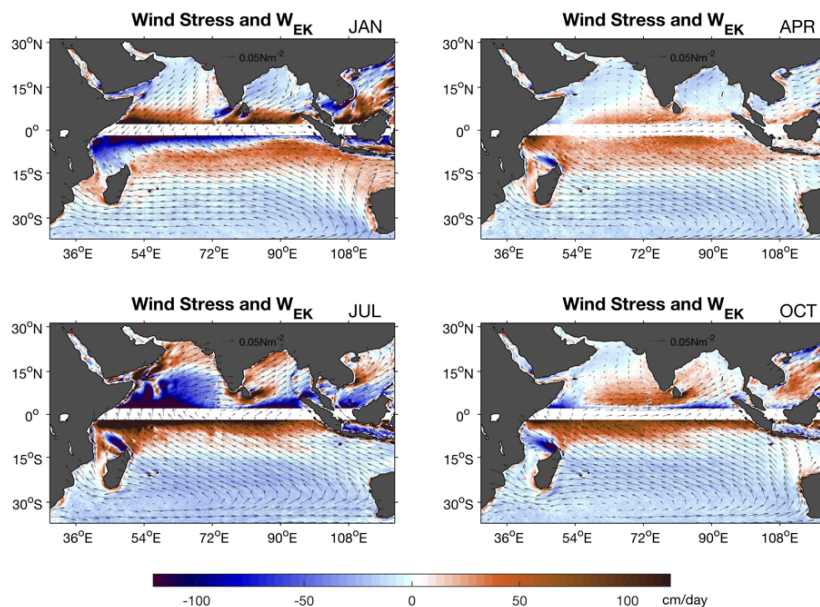
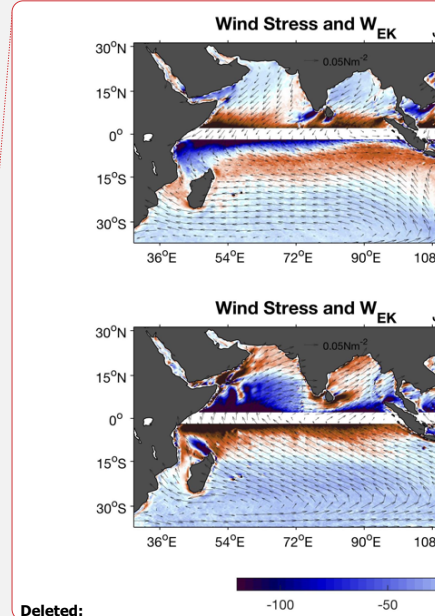


**Figure 2: Climatology (2001–2018) of monsoon wind stress (vectors) and Ekman pumping rate (colour shaded) with positive values denoting Ekman suction (upwelling) and negative values Ekman pumping (downwelling) for (a) January - NE monsoon, (b) April, (c) July - SW monsoon, and (d) October. The climatology was constructed by the Objectively Analyzed air-sea Flux High-Resolution (OAFlux-HR) analysis (adapted from Yu 2019).**

A strong positive correlation between seasonal net heat fluxes into the ocean and SST variability (Fig. 3) suggests that the seasonal cycle of SST is largely due to the seasonal cycle of winds and cloud cover (Yu et al., 2007). One prominent exception is the Seychelles-Chagos thermocline ridge (located between 5°S and 10°S and east of 50°E), where upwelling and horizontal advection exhibit substantial seasonal variations that in turn contribute to the seasonal cycle of SST (Hermes and Reason, 2008; Foltz et al., 2010). On the equator and to the north, seasonally reversing winds drive complex patterns of upwelling and downwelling that lead to complex SST variability.



Deleted:

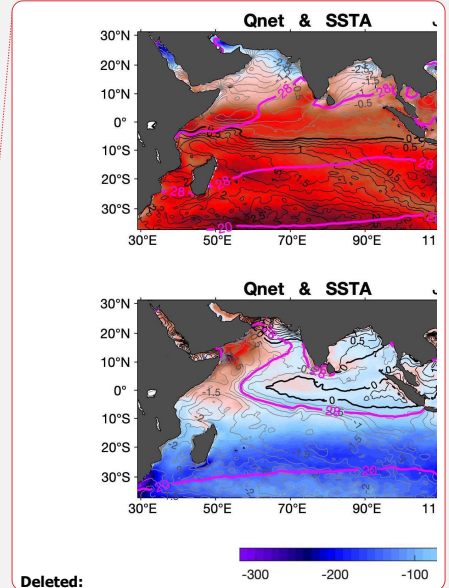
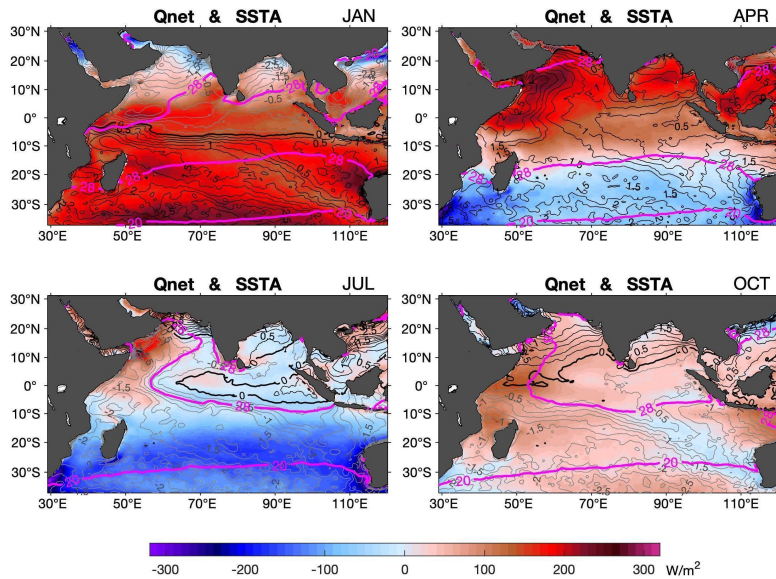
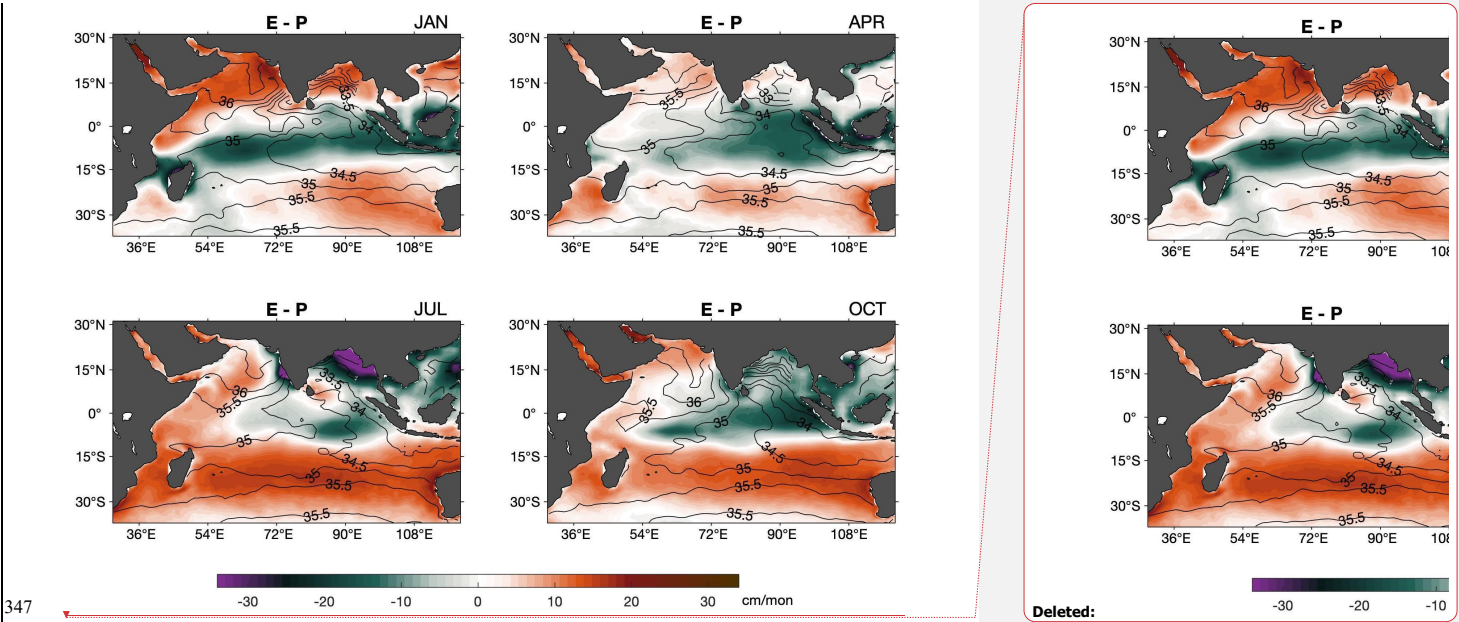


**Figure 3: Climatology (2001–2018) of ocean-surface net heat input (colour shaded; positive values denote ocean heat gain and negative values ocean heat loss), SST anomaly (black contours) and 20°C, 28°C SST contours (pink) for (a) January - NE monsoon, (b) April, (c) July - SW monsoon, and (d) October (adapted from Yu 2019). Net heat flux is the sum of solar radiation, longwave radiation, and turbulent latent and sensible heat fluxes. The turbulent heat flux climatology was constructed by the OAFux-HR analysis and surface radiation climatology by the NASA CERES EBAF (Kato et al., 2013).**

In the Bay of Bengal and Arabian Sea, surface heat fluxes dominate the seasonal cycle of SST, with the exception of the upwelling zone along the western boundary of the Arabian Sea (Chowdary et al., 2015; Yu et al., 2007). However, salinity effects and subsurface processes (barrier layers, vertical entrainment, variations in the depth of penetration of solar radiation and zonal advection also influence SST variability (Thangaprakash et al., 2016). Rainfall variability driven by the monsoons creates near-surface salinity variability, most notably in the Bay of Bengal where there is a pronounced annual cycle of sea surface salinity (SSS; Fig. 4, Akhil et al., 2014). Freshwater input at the northern end of the Bay forms a shallow mixed layer stratified by low salinity and is advected southwards along the east coast of India, where it is eventually eroded by vertical mixing (Akhil et al., 2014). The variability in freshwater input contributes to the seasonal

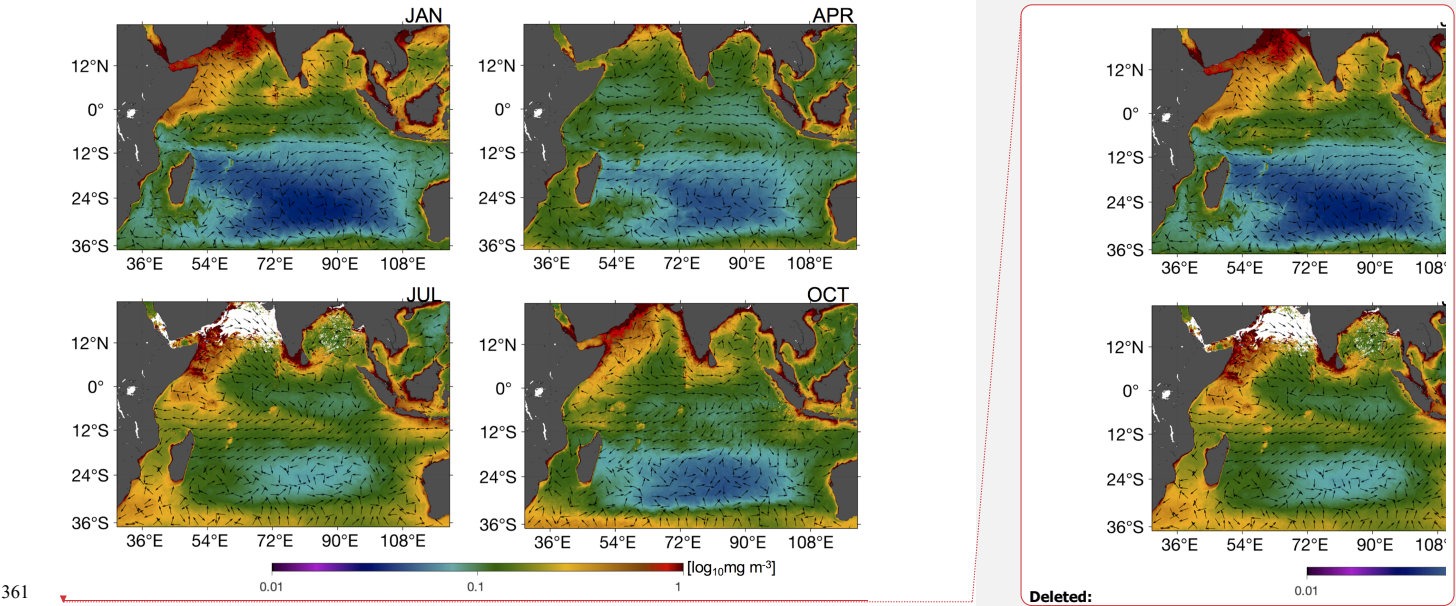
344 cycle of barrier layer thickness in the Bay of Bengal (Howden and Murtugudde, 2001; Thadathil et al., 2007), which in  
 345 turn modulates how strongly SST responds to surface forcing (Li et al., 2017). The seasonally reversing currents that  
 346 connect the salty Arabian Sea and fresh Bay of Bengal also strongly influence sea surface salinity patterns (Section 4.1.3).



348 **Figure 4: Climatology (2001–2018) of evaporation minus precipitation (colour shaded; positive values denote**  
 349 **freshwater leaving the ocean and negative values addition of fresh water to the ocean) and sea surface salinity**  
 350 **(black contours) for (a) January - NE monsoon, (b) April, (c) July - SW monsoon, and (d) October (adapted from**  
 351 **Yu 2019).**

352 The seasonal cycles in the atmosphere and ocean circulation strongly influence the biological productivity of the near-  
 353 surface Indian Ocean (Wiggert et al. 2006). Fig. 5 shows the seasonal cycle of satellite chlorophyll *a* and surface currents.  
 354 The dramatically low productivity in the subtropics, where wind stress curl drives large-scale downwelling (Fig. 2), and  
 355 highly productive coastal boundaries where wind-driven upwelling occurs, highlights the impact of the circulation and  
 356 atmosphere-ocean interaction on biological productivity. In turn, the chlorophyll *a* distribution has important implications  
 357 for air-sea interaction, since higher concentrations of phytoplankton lead to increased absorption of solar radiation (e.g.,

359 Morel and Antoine, 1994; Murtugudde et al. 2002; Giddings et al. 2021). Organisation of chlorophyll *a* at intraseasonal  
360 timescales has also been reported (Section 3.2.1).



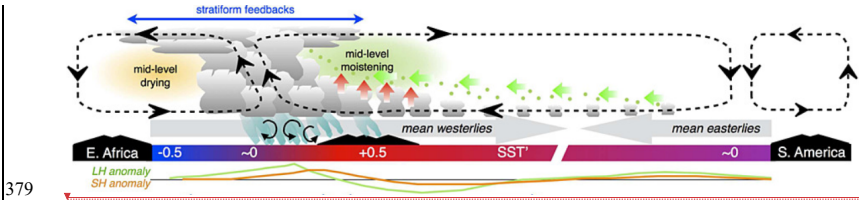
362 **Figure 5: Climatology (2002-2018) of chlorophyll-a concentrations (colormap) and current velocities (arrows) for**  
363 **(a) January (b) April (c) July (d) October. Chlorophyll a climatology was obtained from the MODIS-Aqua product**  
364 **and current velocities were obtained from the third-degree Ocean Surface Current Analysis Real-time (OSCAR)**  
365 **product.**

### 366 3.2 Intraseasonal air-sea interaction

#### 367 3.2.1 Madden-Julian Oscillation - MJO

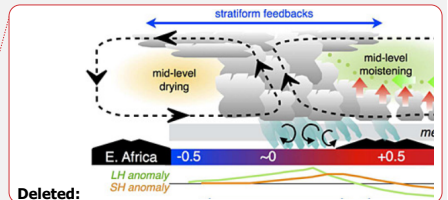
368 The Madden-Julian Oscillation (MJO; Madden and Julian, 1972, 1971) is the dominant mode of variability in the Indian  
369 Ocean at subseasonal time scales. The MJO (Fig. 6) is characterised by eastward-propagating features of enhanced and  
370 reduced convection over distances of more than 10,000 km and with a periodicity of around 30–60 days (Zhang, 2005).

372 The MJO propagates slowly ( $\sim 5 \text{ m s}^{-1}$ ) through the portion of the Indian and Pacific Oceans where the sea surface is  
 373 warm, constantly interacting with the underlying ocean and influencing many weather and climate systems. Within the  
 374 large-scale envelopes of enhanced convection, smaller-scale clusters of clouds propagate westward, and can produce local  
 375 extremes in rainfall. Air-sea interaction is believed to sustain, and perhaps amplify, the patterns of enhanced and reduced  
 376 convection as the MJO propagates eastward (Demott et al., 2015). Indo-Pacific warming trends are warping the life cycle  
 377 of the MJO, which is spending less time over the Indian Ocean, more time over the Pacific and altering mean rainfall  
 378 trends in parts of the globe (Roxy et al, 2019).



380 **Figure 6: Schematic depiction of Indian and Pacific Ocean feedbacks to the MJO when convection (gray cloud**  
 381 **elements) is maximized in the eastern Indian Ocean. Rainfall (aquamarine), circulation anomalies (black dashed**  
 382 **cells), convective downdrafts (black rotor arrows), mean winds (faint gray arrows), and moistening by convective**  
 383 **detrainment (small green dots) and horizontal and vertical advection (thick green and red arrows, respectively) are**  
 384 **overlaid. Net moistening (drying) is shaded green (orange). Positive (red) and negative (blue) SST anomalies for a**  
 385 **strong event are shaded, while latent (sensible) heat flux anomalies are shown with green (orange) curves. Central**  
 386 **and East Pacific spatial scale is compressed relative to the Warm Pool. Adapted from DeMott et al. (2015).**

387 The MJO-related pattern of winds results in anomalous westerly (easterly) winds to the west (east) of the region of  
 388 convergence, convection and enhanced rainfall (Fig. 6). These winds generate Kelvin and Rossby waves along the Equator.  
 389 The Kelvin waves generated by the MJO have been hypothesised (Kessler et al, 1995; McPhaden 1999; Bergman et al.  
 390 2001) to trigger ENSO events in the Pacific. In the Indian Ocean, there is a distinctive sequence of basin-scale ocean waves  
 391 generated by the MJO. Eastward-propagating equatorial ocean Kelvin waves strike the coast of Sumatra, where they  
 392 generate coastally-trapped Kelvin waves that propagate northward and southward away from the generation site. Kelvin  
 393 waves also propagate into the Indonesian seas where they affect the ITF (Pujiana and McPhaden, 2020). Westward-  
 394 propagating equatorial ocean Rossby waves are also formed, either due to direct intraseasonal wind forcing or through  
 395 reflection of Kelvin waves at the eastern boundary (Oliver and Thompson, 2010; Webber et al., 2010; Nagura and  
 396 McPhaden, 2012; Pujiana and McPhaden, 2020). These waves influence local upwelling and currents; they have been  
 397 linked to variability in coastal currents around the Bay of Bengal (Vialard et al., 2009), to enhancement of the spring  
 398 Wyrtki jets in the eastern equatorial Indian Ocean (Prerna et al., 2019), to changes in subsurface equatorial currents in the





central Indian Ocean (Iskandar and McPhaden, 2011) and to changes in upwelling and chlorophyll a concentration in the off-equatorial central Indian Ocean (Webber et al., 2014). Such waves also propagate energy downwards into the deep ocean (e.g., Pujiana and McPhaden, 2020), contributing to deep ocean variability at multiple time scales (e.g., Matthews et al., 2007). Downwelling Rossby waves in the western Indian Ocean create positive SST anomalies through a combination of reduced entrainment of cooler water from below and zonal advection (Rydbeck et al., 2017; Webber et al., 2012b). These waves therefore act as a triggering mechanism for new MJO events (Rydbeck and Jensen, 2017; Webber et al., 2010, 2012b, 2012a), and may also play a role in amplifying existing MJO events.

MJO-related winds also lead to variability in mixing within and at the bottom of the mixed layer. Westerly wind bursts generate zonal currents that create strong vertical current shear (Moum et al., 2014). These currents and the associated mixing persist after the passage of the atmospheric disturbance. Cooler waters from below the surface are mixed with surface waters, leading to a reduction in available ocean heat content for the next MJO event and thus reducing its potential amplitude (Moum et al., 2016). By examining the causes of SST variability in two separate MJO events, McPhaden and Foltz (2013) showed that the presence or absence of barrier layers may play a crucial role in determining how strongly mixing and vertical entrainment influence SST. They also found that zonal advection plays a relatively stronger role when a barrier layer is present. Chi et al. (2014) confirmed the importance of barrier layers in influencing the turbulent heat flux, but found that thin barrier layers can be eroded by strong current shear that occurs during active phases of the MJO. Wind mixing and surface heat and freshwater fluxes both contribute in roughly equal proportions to intraseasonal variability in mixed layer depth (Keerthi et al., 2016).

Various studies have investigated the relative importance of surface heat fluxes and subsurface ocean processes for the evolution of SST at intraseasonal time scales. The Seychelles-Chagos Thermocline Ridge (SCTR), is a region of high intraseasonal SST variability (Saji et al. 2006, Hermes and Reason, 2008). Several observational studies have concluded that the SST variability here is predominantly generated by variability in surface heat fluxes (Jayakumar et al., 2011; Vialard et al., 2008), while Drushka et al. (2012) suggest this finding applies across most of the tropical Indian Ocean. Such studies, however, typically exhibit large uncertainty in the subsurface ocean terms. The shallow thermocline and strong high frequency winds in the SCTR region enhance near-inertial waves and lead to strong mixing at the base of the mixed layer as well as in the thermocline (e.g. Cuypers et al. 2013; Sabu et al. 2021). Modelling studies have shown that ocean dynamics play an important role in generating SST variability (Halkides et al., 2015; Han et al., 2007). For example, Fig. 7 from the study of Halkides et al. (2015) shows the relative contribution of modelled ocean dynamical processes and thermodynamical processes (i.e., surface heat fluxes) in forcing intraseasonal SST variability. Fig. 7a shows that ocean dynamical processes (green shading), including horizontal and vertical advection, are the dominant source of intraseasonal SST variability on the equator and in upwelling regions off Indonesia, Sri Lanka and along the western boundary. The ocean dynamical processes are in turn dominated by horizontal advection along the equator and tropical coastlines (Fig. 7b, pink shading), and vertical advection (blue shading) in the off-equatorial ocean interior.

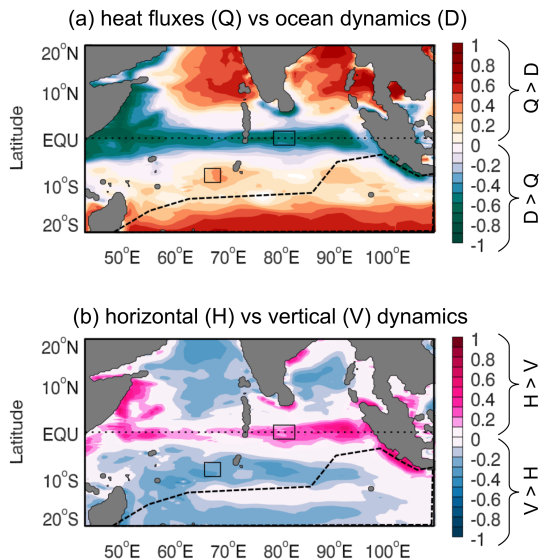
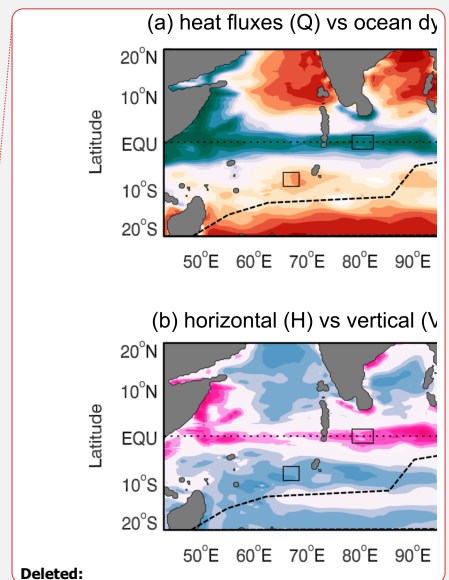


**Figure 7: Modelled balance of processes driving intraseasonal SST variability. (a) Relative role of heat fluxes (Q) and ocean dynamics (D) in driving SST variability, with red (green) colours implying Q (D) dominates forcing, (b) Relative role of horizontal (H) and vertical (V) processes in the dynamical forcing, with pink (blue) colours implying that H (V) processes dominate. All fields are derived from the ECCO-JPL ocean state estimate. The dotted line marks the Equator, dashed line in the southern hemisphere outlines a region in which the model does not fully resolve the ocean heat budget, and the boxes on the Equator and at 10°S mark regions for further analysis not described here. Modified from Halkides et al. (2015).**

Organisation of chlorophyll a at intraseasonal timescales has also been reported, with model studies indicating potential biophysical feedbacks due to the variability of penetrative radiation into the water column (Waliser et al. 2005, Jin et al. 2013a; Giddings et al., 2021). In the Bay of Bengal, the proportion of incoming solar radiation absorbed within the mixed layer varies between 60% and 97% due to a combination of variability in chlorophyll a concentration and mixed layer depth (Lotlikar et al., 2016) and an increase in chlorophyll of 0.3 mg/m<sup>3</sup> can lead to SST increase of up to 0.35°C on intraseasonal time scales (Giddings et al., 2021). Representing the seasonal cycle of chlorophyll a concentration in the Arabian Sea in a coupled model led to substantial changes in the simulated SST and monsoon rainfall over India (Turner

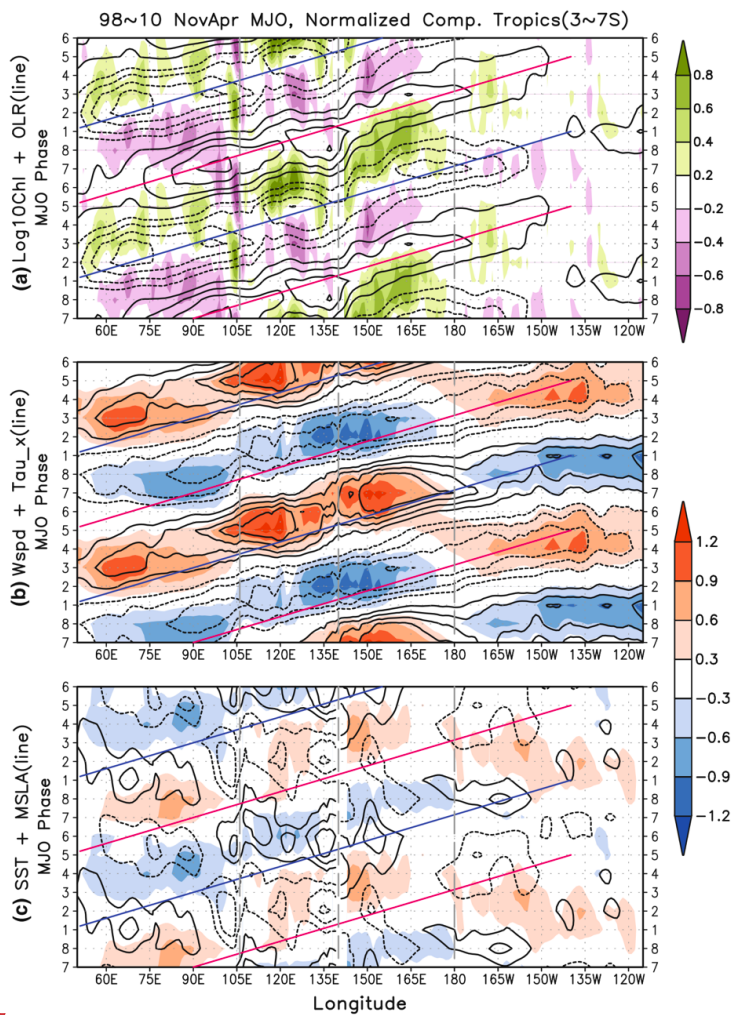


449 et al., 2012), suggesting that incorporating this process into coupled models may be important to improve simulation of  
450 monsoon rainfall and circulation around the Indian Ocean.

451 Figure 8 illustrates propagation of surface patterns in an MJO composite constructed by Jin et al. (2013a). In each panel  
452 the peak in outgoing longwave radiation (OLR, a proxy for convection) is indicated by a red diagonal line. The MJO  
453 generates substantial surface heat flux anomalies that create a pattern of surface heat fluxes and SST anomalies such that  
454 warm (cool) SSTs lead enhanced (reduced) convection by a quarter of a phase (e.g., Shinoda et al., 1998). The MJO also  
455 leads to low-frequency rectifications in the mean state of physical and ecosystem responses (Fig. 8, Waliser et al. 2003,  
456 Jin et al., 2013a,b).

**Deleted:** ), in particular semi-annual variability can rectify into mean flows along the equator (Nagura and McPhaden, 2014





459

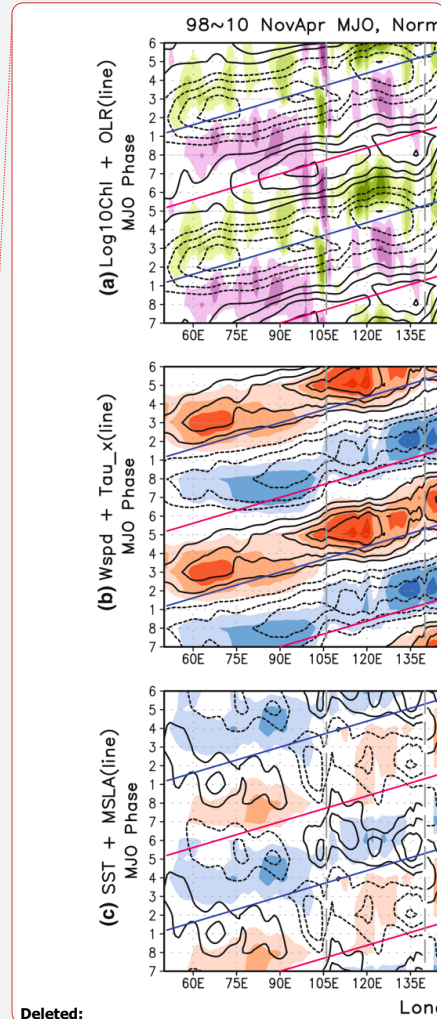


**Figure 8: MJO composite evolution for the Boreal winter (Nov-Apr) averaged over latitudes 3°–7°S for the period of November 1st, 1997 to October 31st, 2010, of a) Log<sub>10</sub>Chl from SeaWIFS satellite observations (shaded) and satellite-derived outgoing longwave radiation (contour), b) wind speed (shaded) and zonal wind stress (contour), both from the cross-calibrated multi-platform (CCMP) dataset, and c) NOAA-OI satellite SST anomalies (shaded) and AVISO mean sea level anomaly (contour). All contour intervals match shading levels in (c), and solid (dash) line indicates positive (negative) values. All variables are normalised, and the same MJO composite is repeated for two cycles for convenience. There are between 127-227 events in the composite for each MJO phase. Red diagonal lines indicate peak signals of positive OLR, and blue lines indicate negative OLR peak, so these are guides for the MJO propagation. The relative location of each propagation line in all panels is the same. Left and center gray vertical dashed line indicates the western and eastern boundary of the Maritime Continent, and the right gray line is on the Dateline where chlorophyll a propagation stops. From Jin et al. (2013a).**

### 3.2.2 Monsoon Intraseasonal Oscillation - MISO

While the MJO dominates intraseasonal variability during October to April, during May to September (boreal summer, southwest monsoon), the Monsoon Intraseasonal Oscillation (MISO; Goswami, 2012; Suhas et al., 2013) dominates. [The dominant timescale for MISOs is 30-60 days but MISOs can also occur on 10-20 day time scales \(Goswami et al, 2016\) and there are studies that have identified a 3-7 day time scale for MISOs \(e.g. Roman-Stork et al, 2020\).](#) MISOs can be seen as low pressure systems laden with moisture which deliver rain from atmospheric instabilities (Fig. 9). The MISO is also known as the Boreal Summer Intraseasonal Oscillation (BSISO; Lau and Waliser, 2012; Lee et al., 2013). The MISO oscillations are dynamically linked to the equatorial MJO (e.g., Sperber and Annamalai, 2008), but exhibit northeastward and northwestward propagating features, with the main centre of action being the Bay of Bengal. These northward-propagating bands of enhanced and reduced rainfall exhibit a similar relationship with SST to the MJO: warm SST leading increased rainfall (cool SST leading reduced rainfall) that then determine the wet/dry (or active/break) cycles of the South Asian monsoon (Vecchi and Harrison, 2002; Roxy et al., 2013; Suhas et al., 2013; Zhang et al., 2018). These SST anomalies are primarily forced by variations in surface heat fluxes in the Bay of Bengal (Girishkumar et al., 2017; Vialard et al., 2012), while variations in wind-induced mixing, Ekman pumping and entrainment drive SST variability in the Arabian Sea (Duncan and Han, 2012; Vialard et al., 2012).

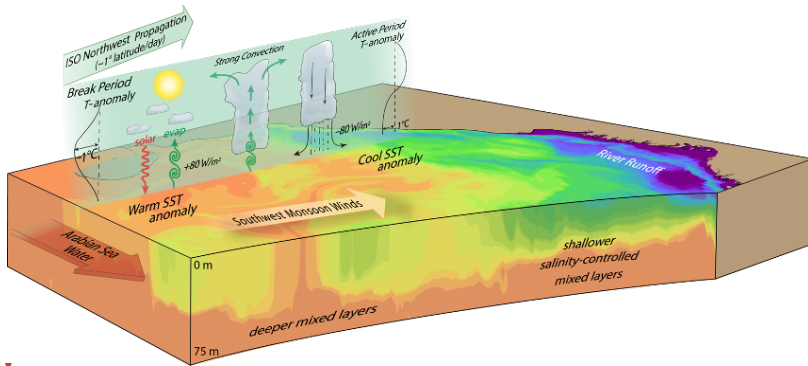
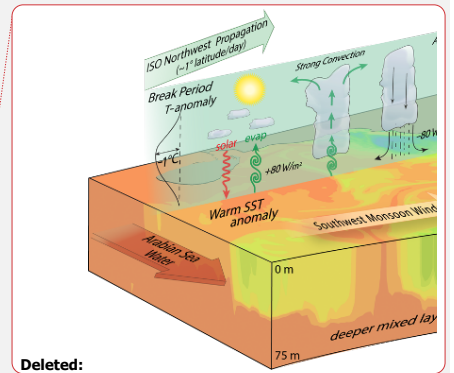


**Figure 9: A schematic of the Monsoon Intraseasonal Oscillation (MISO) in the Bay of Bengal, showing the coupled ocean-atmosphere 30–60 day mode northwestward propagation and associated processes in the atmosphere and the ocean. (From Mahadevan et al., 2016a).**

Simulations of the MISO are still generally poor in state-of-the-art coupled models (e.g., Goswami et al., 2013; Jayakumar et al., 2017; Sabeerali et al., 2013; Sharmila et al., 2013) and re-analysis products (e.g. Sanchez-Franks et al., 2018). Evidence exists from observations of low-level convergence and OLR, as well as from forced atmospheric and coupled ocean-atmosphere model experiments, that both MJOs and MISOs are phenomena that require coupling between the ocean and atmosphere to exist. This is even though the scales of SST anomalies tend to be an order of magnitude smaller than the scales of the propagating atmospheric systems (Waliser et al., 1999; Zhou and Murtugudde, 2009). Including air-sea coupling in simulations of the MISO has been identified as key to improving simulation of this oscillation in some models (e.g., Jayakumar et al., 2017; Li et al., 2018; Roxy et al., 2013; Sharmila et al., 2013), and has been shown to improve aspects of simulation in others (e.g., Bellon et al., 2008; Peatman and Klingaman, 2018).

While new theories continue to be proposed for MJOs (e.g., Wang et al., 2016), MISOs have not received similar attention likely due to their more local nature compared to the global impacts of MJOs (e.g. their impact on ENSO). The mechanism that causes the northward propagation of the MISO is still a topic of research. The most recent theory for MISOs proposed by Zhou et al. (2017a, b) invokes an explicit coupling between the ocean and the atmosphere in a so-called Central Indian Ocean mode. Zonal winds at intraseasonal timescales over the Indian Ocean are argued to be coupled to SSTs to produce a barotropic instability in the meridional gradient of the zonal winds. The horizontal atmospheric eddy fluxes generated by the barotropic instability are invoked to explain the northward propagation and the advection of momentum and moisture as a coupled phenomenon. Key questions remain about the oceanic and air-sea interaction processes that



Deleted:

509 reorganise the SSTs in the Central Indian Ocean mode as well as the respective roles of the vertical and horizontal shears  
510 in driving northward propagation of MISOs.

511 Observations and models indicate that MISOs may be slowing down because of the warming in the Indian Ocean  
512 (Sabeerali et al., 2013), which needs to be understood better for providing reliable monsoon predictions and projections in  
513 this climate vulnerable region. This is underscored by the observational evidence that climate variability and change are  
514 increasing the frequency of dry spells and the intensity of wet spells in the Indian summer monsoon, which are directly  
515 related to MISO (Singh et al., 2014).

516 **3.2.3 Intraseasonal drivers of heavy rainfall**

517 As the MJO season begins to wind down in April, northward propagating MISOs begin to become dominant in the northern  
518 Indian Ocean, north of around 5°N. While the southwesterlies produce some of the strongest coastal upwelling off Somalia  
519 and cool the Arabian Sea, the Bay of Bengal remains warm and largely above the convective threshold (28°C) owing to  
520 the freshwater input from rainfall as well as rivers discharging into the Bay (Roxy and Tanimoto, 2007). The freshwater  
521 input creates a shallow density stratification (barrier layer) within the temperature mixed layer and thereby weakens the  
522 upwelling of cold water from the thermocline. MISOs deliver rain from atmospheric instabilities, but what controls the  
523 rainfall at intraseasonal timescales during the summer can be expected to be region specific with moisture supply  
524 determining the rainfall variability over land (Pathak et al., 2017).

525 Over the ocean, the largely evaporative Arabian Sea is relatively cool but the southwesterlies begin to slow down as they  
526 approach the Western Ghats mountain range on the west coast of India, leading to maximum rainfall there during the  
527 boreal summer monsoon season (Xi et al., 2015). Rather counterintuitively, the warm SST in the Bay of Bengal remains  
528 above the convective threshold (Gadgil et al., 1984; Roxy, 2013) and yet, the ocean is not in direct control of the  
529 intraseasonal rainfall events. Once the SSTs are warm enough to support atmospheric convection, it is baroclinic  
530 instabilities, and not static instabilities induced by warm SSTs, that drive the majority of rainfall over the Bay of Bengal  
531 (Xi et al., 2015).

532 **3.3 Ocean internal variability impacts on air-sea interaction**

533 Mesoscale eddies are ubiquitous in the ocean. In the tropical Indian Ocean, however, linear dynamics dominate and the  
534 impacts of eddies are (or seem) small. While the Indian Ocean has the largest SST variability occurring at seasonal  
535 timescales, strong mesoscale variability is also observed along the Somali coast where the western boundary current  
536 crosses the Equator. The slope of the East African coastline and the equatorial crossing of the low-latitude jet produce  
537 multiple eddies (Nof and Olson, 1993), which are shown to generate strong air-sea coupling at mesoscales (Schott and  
538 McCreary, 2001; Schott et al., 2009; Vecchi et al., 2004; Seo et al., 2008). Some intraseasonal oscillations in the ocean

**Deleted:** These findings should provide a proper paradigm for understanding the role of SST in monsoon and MISO in terms of the ocean dynamics and air-sea interaction processes that matter most.

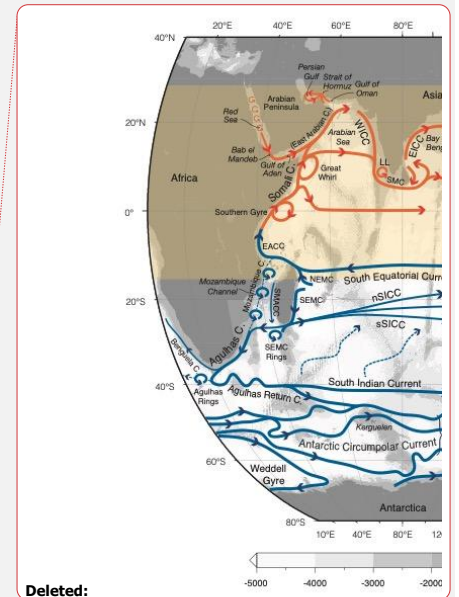
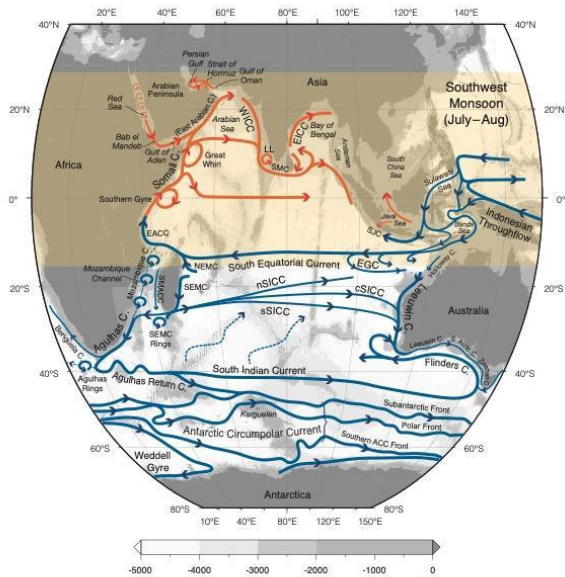
were reported in the southwestern tropical Indian Ocean (Kindle and Thompson, 1989) but generally, the impact of ocean internal variability on SSTs in the tropical Indian Ocean has not been widely studied. At the eastern boundary of the subtropical Indian Ocean, instability of the poleward Leeuwin Current generates a rich field of mesoscale eddies that carry heat into the Indian Ocean interior, contributing to air-sea exchange of heat and the oceanic interior poleward heat transport (Domingues et al. 2006, Feng et al., 2007; Dilmahamod et al. 2018). In the subtropical southeast Indian Ocean, mesoscale eddies, and possibly annual and semiannual Rossby waves propagating from the eastern boundary, were found to influence the seasonal variation of the surface layer heat balance through horizontal advection (Cyriac et al. 2019).

Low-frequency internal variability is also possible. Jochum and Murtugudde (2004) performed forced ocean model experiments with climatological forcing alone to demonstrate that significant low-frequency variability at interannual timescales is generated in the Indian Ocean by mesoscale eddies and other types of nonlinearity. The role of internal variability in regional coupled climate variability as well as ecosystem and biogeochemistry remain interesting problems for this already warm ocean, in which even small SST anomalies can be important for generating large-scale ocean atmosphere interactions (Palmer and Mansfield, 1994).

## **4 Upper Ocean Circulation and Biogeochemical Variability**

### **4.1 Overview**

The near surface circulation in the Indian Ocean consists of the monsoon-dominated, seasonally reversing currents north of around 10°S, and the steady currents to the south, as illustrated in Fig. 10a for the southwest monsoon (July-August) and Fig. 10b for the northeast monsoon (January-February). This figure has been updated from Talley et al. (2011) to recognise recent advances in understanding of circulation patterns. In the northern Indian Ocean, additions are a revision of the Red Sea circulation (Menezes et al., 2019). In the southern Indian Ocean, moving in an anti-clockwise direction from the Maritime Continent, additions are: 1) seasonally reversing flows in the Java Sea; 2) the Holloway Current along Australia's Northwest Shelf (Holloway and Nye, 1985; Holloway, 1995; Brahmanpour et al., 2016); 3) revised position of the salinity-driven Eastern Gyral Current that flows eastward from around 90°E along approximately 15°S, recirculating Indonesian Throughflow Water from the South Equatorial Current and supplying the poleward-flowing Leeuwin Current (Meyers et al., 1995; Domingues et al., 2007; Menezes et al., 2013, 2014); 4) the near-surface South Indian Countercurrent with 3 distinct branches, northern, central and southern, flowing from the southern tip of Madagascar to Australia where they merge with the poleward-flowing Leeuwin Current (Menezes et al., 2014 and references therein); and 5) the splitting of the Flinders Current near 110°E, with one branch recirculating back toward Australia, and the other a westward continuation of the Flinders Current, previously not shown (Duran et al., 2020).



Deleted:

**Figure 10a: Schematic near-surface circulation during the Southwest Monsoon (July–August).** Blue: year-round mean flows with no seasonal reversals. Orange: monsoonally reversing circulation (after Schott & McCreary, 2001). The ACC fronts are taken directly from Orsi, Whitworth, and Nowlin (1995). Acronyms: EACC, East African Coastal Current; NEMC, Northeast Madagascar Current; SEMC, Southeast Madagascar Current; SMACC, Southwest Madagascar Coastal Current; WICC, West Indian Coastal Current; EICC, East Indian Coastal Current; LH and LL, Lakshwadeep high and low; SJC, South Java Current; EGC, Eastern Gyrar Current; SICC, South Indian Countercurrent (south, central and southern branches); NEC, Northeast Monsoon Current. Updated from Talley et al. (2011), originally based on Schott and McCreary (2001). The light gray shading shows seafloor bathymetry.



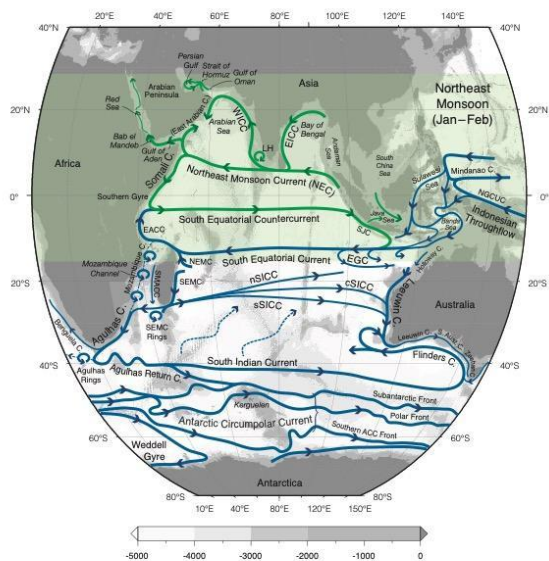


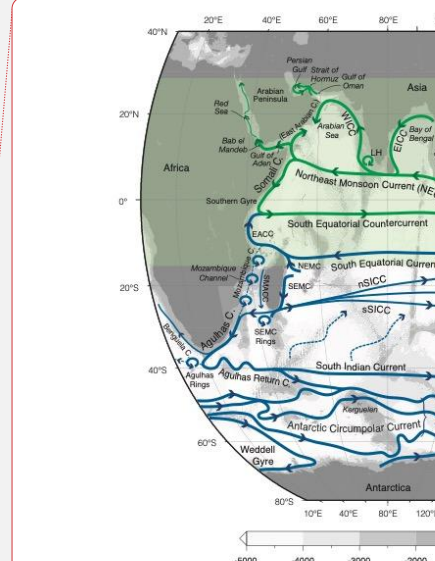
**Figure 10b: Schematic near-surface circulation during the Northeast Monsoon (January-February). Details as for Fig. 10a.**

The intermediate and deep circulation and overturning cells will not be examined in this synthesis. The reader is referred to Talley et al. (2011) and references therein, and in addition, Nagura and McPhaden (2018) who used Argo and CTD data to map out the circulation and water masses in density classes associated with the shallow overturning circulation, with emphasis on the southern hemisphere. There has been some progress on understanding circulation at intermediate and deeper depths in the equatorial band, which is summarised in Huang et al (2018).

## 4.2 Southern Indian Ocean

### 4.2.1 South Equatorial Current

The South Equatorial Current (SEC), the northern limb of the southern Indian Ocean subtropical gyre, carries Indonesian Throughflow (ITF) waters into the interior Indian Ocean, flowing westward between 10–20°S (Fig. 10a and 10b). Upon



Deleted:

597 reaching the northern tip of eastern Madagascar, it bifurcates and supplies the Northeast Madagascar Current (NEMC;  
 598 Schott and McCreary, 2001; Song et al., 2004; Valsala and Ikeda, 2007) and the Southeast Madagascar Current (SEMC)  
 599 and contributes to the development of Mozambique Channel eddies. The mean flow through the Mozambique Channel is  
 600 weak (Song et al., 2004), although there is an indication from ocean model results that the eddy-dominated flow contributes  
 601 on the order of 20 Sv southward (Durgadoo et al., 2013). The Mozambique Channel eddies, eddies from the SEMC and  
 602 recirculation combine to feed into the Agulhas Current (Schott and McCreary, 2001).  
 603  
 604 Between 50 and 80°E the SEC is coincident with the southern half of the Seychelles-Chagos Thermocline Ridge (SCTR,  
 605 Vialard et al., 2009). The SCTR is characterized by a relatively shallow thermocline and thin mixed layer (~30m) across  
 606 the southern tropical Indian Ocean in the latitude band 5-15°S. Between 50 and 80°E the SCTR/SEC is a region of  
 607 significant upwelling (Hermes and Reason, 2008; Vialard et al., 2009; Resplandy et al., 2009; Dilmahamod, 2014), which  
 608 affects biogeochemistry, and even fisheries (Resplandy et al., 2009; Robinson et al., 2010; Dilmahamod, 2014).  
 609  
 610 In the eastern IO, the intraseasonal variation of the SEC is mostly attributed to the baroclinic instability of the mean current  
 611 (Feng and Wijffels, 2002), which is important for the meridional heat transport in the region and contributes to the demise  
 612 of Indian Ocean Dipole events (Ogata and Masumoto, 2011; Yang et al. 2015). Barotropic instability of the SEC has also  
 613 been proposed to be a key mechanism for generating intraseasonal variability (Yu and Potemra, 2006). These intraseasonal  
 614 signals propagate westward as Rossby Waves, influencing the SEC variability in the western Indian Ocean (Zhou and  
 615 Murtugudde, 2008).  
 616  
 617 Interannual variability in the ITF due to ENSO, IOD and other influences is communicated into the interior Indian Ocean  
 618 along the SEC and via Kelvin and Rossby waves (Godfrey, 1989, 1996; Meyers et al., 1995; Meyers, 1996; Wijffels and  
 619 Meyers, 2004). Pressure anomalies associated with ENSO and IOD are communicated through the Indonesian seas as  
 620 Kelvin and Rossby waves. These anomalies propagate westward into the Indian Ocean as Rossby waves. At the same time  
 621 the pressure anomalies drive variations in ITF and SEC transport and induce temperature/salinity variability via advection.  
 622 Geostrophic transport variability in the long-time repeat XBT line IX1 shows that the SEC is stronger during La Niña and  
 623 positive Indian Ocean Dipole events (Meyers, 1996; Liu et al., 2015). Similarly, the Pacific Decadal Oscillation alters the  
 624 SEC and ITF transports and associated water properties (Section 6.1). During the climate change hiatus period of 2000-  
 625 2011, the enhanced heat transport of the SEC/ITF was a key mechanism for the fast warming trend in the southern  
 626 subtropical Indian Ocean (Section 6.1).  
 627



#### 4.2.2 Western Boundary

The Agulhas Current (Fig. 10) has long been known as one of the strongest western boundary currents in the global oceans, with an average transport of 75 Sverdrups and current speeds in excess of  $2 \text{ m s}^{-1}$  (Beal et al., 2015; Beal et al., 2011). The Agulhas Current plays a vital role in the global thermohaline circulation, advecting warm, salty, subtropical water southwards, following the continental shelf of South Africa and meandering less than 150 km offshore (Gründlingh, 1983; Lutjeharms 2006). The strength and warmth of the Agulhas Current influences atmospheric storm tracks and storm development. The large moisture source of the warm Agulhas Current region contributes significantly to the frequency and strength of African precipitation, which significantly impacts rain-fed subsistence farming (Hermes et al. 2019 and references therein).

South of the tip of Africa, the Agulhas Current retroflects eastwards into the South Indian Ocean (Fig. 10). This retroflection area is highly variable, occluding rings that propagate into the South Atlantic Ocean. The Agulhas variability is linked upstream to modes of variability including ENSO (Elipot and Beal, 2018, Trott et al., 2021) and downstream with the Atlantic meridional overturning circulation, providing an essential link between the Pacific, Indian and Atlantic Oceans (Beal et al., 2011). Estimates of the rate of mass and heat exchange carried by Agulhas leakage south of Africa (and the number of rings shed per year) vary and are difficult to verify reliably (Weijer et al., 2014). Daher et al (2020) recently used a combination of drifters and Argo floats to derive an estimate of Agulhas leakage of 20 Sv. van Sebille et al. (2011) and le Bars et al. (2014) suggested upstream variability of the Agulhas Current has an effect on inter-ocean exchange between the South Indian and South Atlantic oceans, primarily by influencing the frequency of ring shedding at the Agulhas retroflection. However, a few recent papers suggest instead that its variability is driven by the Southern Hemisphere Westerlies (Durgadoo et al, 2013; Loveday et al., 2014; Elipot and Beal, 2015).

The Agulhas Current has a seasonal cycle and is strongest in summer (Krug and Tournadre, 2012; Beal and Elipot, 2016) and tied to a baroclinic adjustment of near-field winds (Hutchinson et al, 2018). Seasonal changes in the Agulhas retroflection region (Lutjeharms and van Ballegooyen, 1988; Quartly and Srokosz, 1993) and in the southwest Indian Ocean (Ffield et al., 1997) have been suggested from hydrographic and satellite data (Krug et al., 2012), but with weak statistical significance due to a lack of sufficiently long time series.

Although long term observations in this region are limited there are numerous recent studies that have further elucidated our understanding of the Agulhas Current. Beal and Elipot (2016) used 3 years of in situ data to show that, contrary to expectations, the Agulhas Current has not intensified since the early 1990s. Instead, it has broadened as a result of more eddy activity, driven by intensifying winds. Variability in the path and strength of the Agulhas Current has mostly been attributed to solitary Agulhas meanders within the Current system (also known as Natal pulses) which drive upwelling

and cross-shelf transports, affecting marine productivity, fisheries and recruitment over the Agulhas Bank (Beal and Bryden, 1999; Roberts et al., 2010, Elipot and Beal, 2015). Recent work has highlighted the importance of submesoscale eddies in the Agulhas Current frontal region driving an inshore edge flow reversal which can have important consequences on fisheries (Krug et al., 2017).

The advance in models has also helped improve our understanding of the Agulhas Current, which is generally not well represented in global ocean models. Hutchinson et al. (2018) used idealized models to expose a link between the seasonality of the Agulhas Current and propagation of first baroclinic mode Rossby waves communicating the wind stress signal across the western portion of the Southern Indian Ocean, with the signal from winds further east having little effect.

#### 4.2.3 Interior flows

In the central-eastern South Indian Ocean between 20°S and 30°S, the surface geostrophic flow is generally eastward, opposite to the prediction of both the Ekman and Sverdrup theories (Sharma 1976; Sharma et al., 1978; Godfrey and Ridgway, 1985; Schott et al., 2009). This flow is driven by the large-scale, poleward drop in the dynamic height (steric height) near the sea surface (Godfrey and Ridgway, 1985; Schott et al., 2009) related to the meridional transition from the very fresh and warm SEC waters to the increasingly cooler, saltier and denser waters to the south. The flow generally extends from the sea surface to ~200–300 m (Domingues et al., 2007; Palastanga et al., 2007; Divakaran and Brassington, 2011; Menezes et al., 2014). The mechanisms that determine the vertical extent of the interior eastward flow remains unclear, although this depth coincides with the depth of the shelf break at the eastern boundary and the bottom of the Leeuwin Current along that boundary. This correspondence may be achieved by the westward propagation of baroclinic Rossby waves (Weaver and Middleton, 1989; Furue et al., 2013). Below the near-surface eastward flows, the flow is weakly westward (Domingues et al., 2007; Schott et al., 2009; Furue et al., 2017).

Embedded in this general eastward flow are narrower eastward jets (Maximenko et al., 2009; Divakaran and Brassington, 2011; Menezes et al., 2014), collectively known as the South Indian (Ocean) Countercurrent (SICC; Palastanga et al. 2007; Siedler et al. 2006; Menezes et al., 2014). They start out as a single jet emanating from the southern tip of Madagascar around 25°S, possibly fed by a partial retroflexion of the SEMC (Palastanga et al., 2007; Siedler et al., 2006, 2009) and divide into separate jets around the Central Indian Ridge (65°E–68°E) (Menezes et al., 2014). Eastward flows exist in similar latitude bands in the North and South Pacific and North and South Atlantic (Yoshida and Kidokoro, 1967; Merle et al., 1969; Takeuchi, 1984; Kubokawa, 1999; Qiu and Chen, 2004; Kobashi and Kubokawa, 2012). However, the jets in these basins are weaker and shallower than the SICC and do not extend all the way to the eastern boundary (Menezes, 2015).

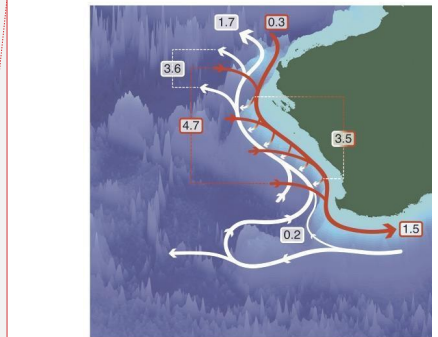
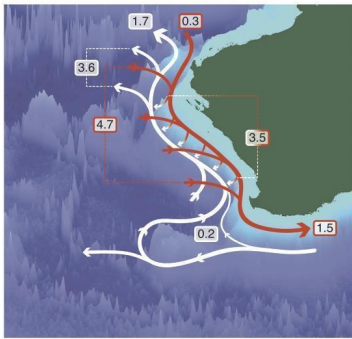
Three main jets (Fig. 10a) are evident in geostrophic velocity calculated from both altimetric sea surface height and hydrography and are captured in OGCMs (Maximenko et al., 2009; Divakaran and Brassington, 2011; Menezes et al., 2014). The stronger southern jet (3–4 Sv) crosses the basin around 26°S and has an associated thermal front at depths around 100–200 m (Sharma 1976; Siedler et al., 2006; Menezes et al., 2014; Palastanga et al., 2007). This front suggests that the southern SICC has physics similar to the Subtropical Countercurrents (STCCs) of the Pacific Ocean (Kubokawa, 1999; Kobashi and Kubokawa, 2012; Menezes et al., 2014). The location and strength of the SICC vary between studies, from well-defined jets (Siedler et al. 2006, Palastanga et al. 2007, Divakaran and Brassington 2011, Menezes et al. 2014) to a mean velocity structure (Jia et al., 2011a), or even absence of the SICC (Srokosz et al. 2015). Depending on the region and time in which its characteristics were determined, the SICC varies from a weak mean current of 2–3 cm/s (Jia et al., 2011a) to a strong jet of 50 cm/s eastward flow (Siedler et al., 2006).

The eastward flowing Eastern Gyral Current (EGC) is part of an anticyclonic recirculation centred at the Indonesian-Australian basin (5°S–20°S and 100°E–125°E) (Domingues et al., 2007; Menezes et al., 2013, and references therein). Part of the northern SICC merges with the EGC around 15°S, 100°E (Fig. 10a). The EGC supplies ITF-origin water to the Leeuwin Current (LC) and is an essential component of the LC dynamics (Domingues et al., 2007; Benthuyssen et al., 2014; Lambert et al., 2016; Furue et al., 2013, 2017; Yit Sen Bull and van Sebille, 2016). The geostrophic flow of the EGC is controlled by the meridional salinity gradient, making its dynamics distinct from the temperature dominated SICC (Menezes et al., 2013). This salinity front is formed by the encounter of the fresh Indonesian Throughflow Water carried westward by the SEC and the salty subtropical underwater formed at the Southern Indian Ocean subtropical salinity maximum. The seasonal cycles of the EGC and the SICC are also distinct: the EGC is stronger in austral winter (3–5 Sv) and weaker (<0.5 Sv) in summer with the cycle in phase with the Leeuwin Current (Feng et al., 2003; Menezes et al., 2013; Furue et al., 2017). The SICC is overall stronger in spring-summer and weaker in winter (Palastanga et al., 2007; Jia et al., 2011a; Menezes et al., 2014) and experiences strong interannual variability, which peaks at biennial timescales and is decadal modulated (Menezes et al., 2016).

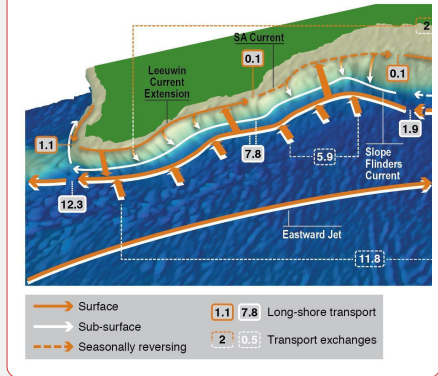
The multiple jets of the SICC are embedded in a zone of high eddy kinetic energy, with eddies generated by instabilities of the Leeuwin Current and of the SICC itself (Palastanga et al., 2007; Divakaran and Brassington, 2011; Huhn et al., 2012; Jia et al., 2011a, 2011b; Menezes et al., 2014, 2016; Siedler et al., 2006). By co-locating Argo floats and satellite data, Dilmahamod et al. (2018) described the passage of surface and subsurface South Indian Ocean eddies (SIDDIES). These westward-propagating, long-lived features (>3 months) originate in areas of high evaporation in the eastern Indian Ocean and prevail over a preferential latitude band, forming a permanent structure linking the eastern to the western Indian Ocean (the “SIDDIES Corridor”). This corridor of eddy passage allows the advection of water masses and biogeochemical properties across the basin (Dilmahamod et al., 2018).

4.2.4 Eastern Boundary

Unlike any other eastern boundary current, the Leeuwin Current (LC; Figs. 10 and 11a) flows poleward, along the shelf break of the west coast of Australia (Smith et al., 1991). Figure 11a presents the long-term average volume transport of the LC System from an observational climatology with similar structure found in a 1/10° ocean general circulation model (Furue et al., 2017). The primary source waters for the LC are the interior eastward flows (Section 4.2.3) that turn southeastward as they approach the coast and merge with the LC (Fig. 11a; Domingues et al., 2007; D'Adamo et al., 2009; Menezes et al., 2013, 2014; Furue et al., 2017, 2019). On average, the LC carries 0.3 Sv southward at 22°S, gains 4.7 Sv from the Indian Ocean interior, loses 3.5 Sv through downwelling to the layer beneath, and carries 1.5 Sv at its southern limit. The LC is approximately 200–300 m deep, extends from 22°S (North West Cape) to 34°S (Cape Leeuwin) and exists throughout the year despite significant seasonality (Feng et al., 2003; Ridgway and Godfrey, 2015; Furue et al., 2017). The Holloway Current, which flows southwestward on the North West Shelf (D'Adamo et al., 2009; Bahmanpour et al., 2016), is another weaker source to the LC from the north. Inshore of the LC, there exist seasonal equatorward flows that recirculate waters of distinct watermass properties influenced by air-sea interaction over the continental shelf (Woo et al., 2006).



Deleted:



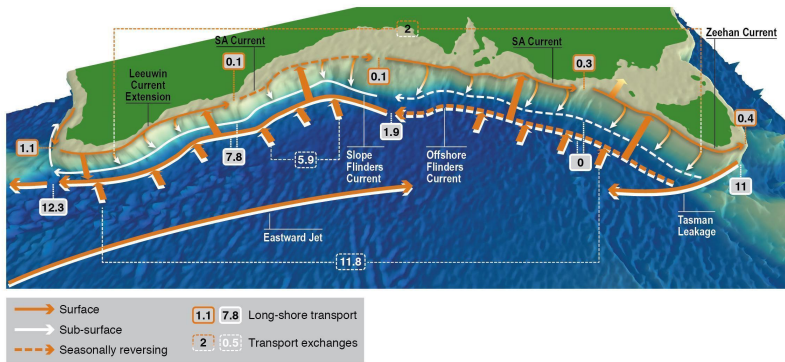


**Figure 11: a) Schematic summary of Australia's Leeuwin Current System three-dimensional transports (Sv). The red arrows and red-outline numbers represent the upper-layer (0–200 m) meridional transport of the poleward Leeuwin Current and meridionally-integrated zonal transport of the shallow eastward flows. The white arrows represent the lower-layer (200–900 m) flows of the Leeuwin Undercurrent. Taken from Furue et al. (2017). © American Meteorological Society. Used with permission. b) Schematic summary of the Southern Australia Current System three-dimensional transports (Sv). Long-shore transport for the Shelf Break Currents and Flinders Current in grey box with orange and white outlines, respectively. Integrated vertical and onshore flow transport in dashed outline box. Reprinted from Duran et al. (2020), with permission from Elsevier, *Progress in Oceanography*. Both schematics are based on a geostrophic calculation in the CARS 1/4-degree climatology.**

The mean state of the LC is driven by the meridional pressure gradient in the upper ocean (e.g., Godfrey and Ridgway, 1985; Godfrey and Weaver, 1989, 1991), evident as a large poleward decrease in SSH balanced by an eastward surface geostrophic current (Section 4.2.3.1). The eastward flow approaches the eastern boundary, inducing downwelling and a surface poleward current (Fig. 11; Godfrey and Ridgway, 1985; McCreary et al., 1986; Thompson, 1987; Weaver and Middleton, 1989, 1990; Furue et al., 2013; Benthuyssen et al., 2014), in opposition to the prevailing southerly winds. As a poleward boundary current, the LC waters are relatively fresh and warm from tropical origins (Rochford, 1969; Andrews, 1977; Legeckis and Cresswell 1981; Domingues et al., 2007; Woo and Pattiaratchi, 2008). Saltier Indian Central Water, the surface water of the Subtropical South Indian Ocean, joins the LC as it flows poleward (Section 4.2.3) increasing the mean density of the LC. Surface cooling along the poleward path also contributes to the increase in density (Woo and Pattiaratchi, 2008; Furue, 2019).

The LC flows around the southwestern corner of Australia and continues to flow eastward along the shelf break of the south coast of Australia to reach the southern tip of Tasmania near 42°S, 140°E (Fig. 11b, Oliver et al., 2016; Oke et al., 2018; Duran et al., 2020). This 5500-km long boundary current was first documented as a continuous flow by Ridgway and Condie (2004). When the longshore current is weak, however, it tends to be somewhat fragmentary (Oke et al., 2018; Duran et al., 2020) and sometimes even reverses in places (Duran et al., 2020). For this reason, and additionally because of the scarcity of observational sampling, the current is not traditionally regarded as a single current. Along southern Australia, the boundary currents can be described following Ridgway and Condie's (2004) naming convention. The current's western sector is called the Leeuwin Current Extension, the central part, to the south of the Great Australian Bight, is called the South Australian Current, and the easternmost part along Tasmania is called the Zeehan Current. They are collectively known as the Shelf-Break Currents (SBCs) of the Southern Australia Current System (Duran et al., 2020). It is not clear whether the SBCs along the south coast of Australia are, dynamically, an extension of the LC. The SBCs are at least consistent with the local northward Ekman drift (Ridgway and Condie, 2004; Duran et al., 2020) and hence would exist without the LC.

On seasonal timescales, the LC transport generally tends to be strongest in austral autumn and weakest in austral summer (McCreary et al., 1986; Smith et al., 1991; Feng et al., 2003; Furue et al., 2017). There are two theories to explain this seasonality. In one, the local winds, which generally induce an offshore Ekman drift and therefore tend to weaken the LC, reach their annual maximum or minimum when the LC transport reaches its minimum or maximum, respectively (McCreary et al., 1986; Furue et al., 2013). In the other, a seasonal pressure anomaly originates in the Gulf of Carpentaria and propagates counterclockwise along the shelf break, driving the seasonality of the LC and of the SBCs to the south of Australia (Ridgway and Godfrey, 2015). Like the LC, the SBCs tend to be strongest in austral autumn and weakest in austral summer (Ridgway and Condie, 2004; Oke et al., 2018; Duran et al., 2020). In particular, the eastern part of the South Australian Current is seen to reverse in summer (Duran et al., 2020). This variability is consistent with the counterclockwise propagation of pressure anomaly shown by Ridgway and Godfrey (2015) and also with the seasonality of the wind stress along the south coast of Australia, with onshore (offshore) Ekman drift tending to drive eastward (westward) shelf-break flow (Duran et al. 2020).

On interannual time scales, the LC is modulated by the El Niño Southern Oscillation owing to the steric height anomalies in the western equatorial Pacific Ocean propagating through the Indonesian Seas and along Western Australia (Feng et al., 2003). During El Niño and La Niña periods, the LC transport weakens and strengthens, respectively, and is correlated with Fremantle sea level (Feng et al., 2003). During the strong 2010–2011 La Niña event, the LC reached record strength speeds (Feng et al., 2013) and the consequences of the unprecedented marine heat wave that resulted are described in Section 6.4. On multidecadal timescales, the major boundary currents around Australia, including the LC, are reported to have strengthened during 1979–2014 in an eddy-resolving OGCM, consistent also with observations (Feng et al., 2016; see

799 Section 6.1 for associated changes). At intraseasonal timescales, winds or heat anomalies on the North West Shelf region  
800 due to MJO events lead to intraseasonal variability of the Holloway Current on the North West Shelf and then of the LC  
801 (Marshall and Hendon, 2014; Marin and Feng, 2019).

802  
803 The LC is accompanied by mesoscale eddies that cause the LC to meander energetically (Pearce and Griffiths, 1991; Feng  
804 et al., 2005; Waite et al., 2007; Meulenens et al., 2008). Those eddies are, at least partially, generated by barotropic,  
805 baroclinic, or mixed instability of the LC itself (Pearce and Griffiths, 1991; Feng et al., 2005; Meulenens et al., 2008). The  
806 eddy kinetic energy is greatest when the LC transport is strongest, in May–June (Fang and Morrow, 2003; Feng et al.,  
807 2005). Some of these eddies cause a large meander of the LC: a large anti-cyclonic eddy often forms at 28°–29°S and at  
808 31°–32°S (Feng et al., 2003; Feng et al., 2007) steering the LC offshore to return to the continental shelf further south.  
809 This state typically starts during May–June and ends in July–August (Feng et al., 2007). Similarly, it is suggested that the  
810 eastern part of the SBCs becomes unstable in boreal autumn and winter, generating eddies, which subsequently propagate  
811 westward south of Australia (Oke et al., 2018). Turbulent mixing has been found to be enhanced in anticyclonic eddies  
812 near the surface, and in cyclonic eddies at deeper levels (500–1000 m) due to the interaction of the eddies and near-inertial  
813 waves, which has implications for watermass modifications and the meridional overturning circulation (Cyriac et al. 2021).

814  
815 Just below the Leeuwin Current is the equatorward Leeuwin Undercurrent (LUC; Thompson, 1984; Church et al., 1989;  
816 Smith et al., 1991; Fig. 11a). The LUC hugs the continental slope and extends from 200 m to 900 m (Furue et al., 2017).  
817 The LUC begins at Cape Leeuwin (34°S, 114°E) and is fed by a northward bend of a small fraction of the Flinders Current  
818 (FC; Fig. 10, 11; Furue et al., 2017). The remaining part of the FC continues westward but another small fraction of it  
819 appears to retroflect eastward and join and augment the LUC (Duran, 2015; Furue et al., 2017). Near 22°S, most of the  
820 LUC volume leaves the continental slope and flows offshore (Duran, 2015), apparently following the southern flank of  
821 the Exmouth Plateau although its bottom at 900 m is much shallower than the topographic feature (Fig. 11a).

822  
823 To the south of Australia, an undercurrent has been recently identified below the Zeehan Current in a numerical simulation  
824 (Oke et al., 2018) and in a geostrophic calculation based on a gridded T–S climatology (Duran et al., 2020). Traditionally  
825 this flow was identified as a branch of the FC (Cirano and Middleton, 2004; Rosell-Fieschi et al., 2013; Feng et al., 2016)  
826 because the former flows in the same direction as the latter, but the FC as the northern boundary current of the subtropical  
827 gyre cannot exist on an eastern boundary (Anderson and Gill, 1975; Philander and Yoon, 1982; McCreary et al., 1992)  
828 and it lacks the vertical structure of an undercurrent (Duran et al., 2020). This northwestward- or westward-flowing  
829 undercurrent appears to exist all the way from the west coast of Tasmania to Cape Leeuwin (the southwestern tip of  
830 Australia) but its separation from the FC is less clear to the south of the Great Australian Bight and further west, where  
831 the FC accelerates and tends to overwhelm the undercurrent (Duran et al., 2020). Below, we call this current “slope FC”  
832 following Duran et al. (2020).

The mechanisms responsible for the LUC and undercurrent off southern Australia remain an open question, although models have been developed to investigate potential processes. The linear, continuously stratified models of McCreary et al. (1986) and Kundu and McCreary (1986) produce a surface poleward and a subsurface equatorward current, resembling the LC and LUC, along the eastern boundary. This class of model, however, requires large vertical diffusivity to produce a realistic LC and LUC (McCreary, 2013, personal communication). Along a continental slope, alongshore and cross-shelf buoyancy advection cause a shelf break front, forming a surface intensified poleward current, like the LC, and an equatorward undercurrent by thermal wind shear (Benthuisen et al., 2014). Analytical shelf models have been extended to include cross-shelf buoyancy gradients to derive a poleward undercurrent like the LUC (Schloesser, 2014). These process-based analytical theories have not been tested in an eddy-resolving model.

The LUC and the slope FC are connected to the LC and the SBCs, respectively, by downwelling (Fig. 11; Furue et al., 2017; Duran et al., 2020), suggesting a common, but as yet unexplained, dynamics. Note, however, that for the LC–LUC pair, the mean downwelling appears to occur along isopycnal surfaces, and hence the LC water mass is not found in the LUC (Furue, 2019). For the SBCs and the slope FC, the nature of the downwelling is not known. The seasonality of these undercurrents are not well known. No systematic seasonal variability of the LUC was evident in a hydrographic climatology and ocean general circulation model (Furue et al., 2017).

#### 4.2.5 Biogeochemical Variability

The ITF impacts both ocean currents and basin-scale biogeochemistry (Talley and Sprintall, 2005; George et al., 2013; van Sebille et al., 2014). Talley and Sprintall (2005) mapped silicate on the 31.96 potential density surface, revealing a striking silicate maximum associated with the SEC that extends westward to at least 60°E, highlighting the broad reach of ITF nutrient influence into the Indian Ocean. Ayers et al. (2014) estimated the depth- and time-resolved nitrate, phosphate, and silicate fluxes at the three main exit passages of the ITF that feed into the SEC: Lombok Strait, Ombai Strait, and Timor Passage. They found that the nutrient flux is significant relative to basin wide new production, and that the majority of ITF nutrient supply to the Indian Ocean via the SEC is to thermocline waters, where it is likely to support primary production and significantly impact biogeochemical cycling.

Satellite chlorophyll and primary production estimates suggest that values in the SEC are considerably higher than those found in the southern hemisphere subtropical gyre to the south, with Chla from ~0.10 to 1.0 mg/m<sup>3</sup> and primary production from ~400 to 1000 mgC m<sup>-2</sup> d<sup>-1</sup> (Fig. 5; Figs. 5 and 6 in Hood et al., 2017). The highest concentrations and rates in the SEC are observed in the Eastern Indian Ocean in July and August during austral winter, associated with the ITF nutrient sources and upwelling off Java. The lowest chlorophyll concentrations and rates are observed in January (austral summer).



Model results and satellite observations show that the SEC/SCTR region exhibits an annual cycle in surface chl<sub>a</sub> concentration and primary production, with the highest values in austral winter (June-August;  $> 0.20 \text{ mg/m}^3$  and  $> 600 \text{ mgC m}^{-2} \text{ d}^{-1}$ , respectively) due to the strong southeasterly winds that increase wind stirring and induce upwelling (Resplandy et al., 2009; Dilmahamod, 2014; Fig. 5; Figs. 5 and 6 in Hood et al., 2017). Vertical sections of the SEC/SCTR region also reveal a deep chl<sub>a</sub> maximum (George et al., 2013). Along  $65^\circ\text{E}$  this maximum shoals from  $> 100 \text{ m}$  at  $16^\circ\text{S}$  to  $\sim 50 \text{ m}$  at  $10^\circ\text{S}$  due to upwelling. The increases in surface Chl-*a* concentrations in austral winter are associated with decreases in the subsurface chl<sub>a</sub> maximum (Resplandy et al., 2009; Dilmahamod, 2014). Surface freshening associated with the core of the SEC also influences the chl<sub>a</sub> distribution in the SCTR region by modulating the static stability and mixed layer depth (George et al. (2013).

The SEC provides relatively oligotrophic (low nutrient, low chlorophyll and low primary production) tropical source waters that feed into the EACC, NEMC, SEMC and the Mozambique channel. Chlorophyll *a* concentrations and production rates in Mozambique Channel surface waters are generally low ( $< 0.4 \text{ mg/m}^3$  and  $< 700 \text{ gC m}^{-2} \text{ d}^{-1}$ , Fig. 5), and not significantly different in cyclonic and anticyclonic eddies (Lamont et al., 2014; Barlow et al., 2014; Figs. 5, 6 and 20 in Hood et al., 2017). Deep chlorophyll maxima are observed between 25 and 125 m depth depending on the proximity to the shelf and the influence of mesoscale eddies (Barlow et al., 2014; Lamont et al., 2014). Eddies in the Mozambique Channel also have a strong influence on the lateral transport of nutrients and chlorophyll from the coasts of Madagascar and Africa. Indeed, enhanced phytoplankton production within both cyclonic and anticyclonic eddies in the Mozambique Channel often occurs in response to lateral nutrient inputs into the euphotic zone by horizontal advection from the coasts of Madagascar and Africa rather than through eddy induced upwelling and downwelling (José et al., 2014; Lamont et al., 2014; Roberts et al., 2014). In contrast, in the Southeast Madagascar Current, topographically-induced coastal upwelling brings cold, nutrient-rich water up to the surface, which supports high rates of primary production (Lutjeharms and Machu, 2000; Ho et al., 2004; Quartly and Srokosz, 2004). This upwelling and its impacts are observed in both the austral summer and winter (Ho et al., 2004).

The Agulhas Current itself is warm and oligotrophic with sources derived from low nutrient and low chlorophyll surface waters from the Mozambique Channel, Southeast Madagascar Current and the southwestern tropical Indian Ocean (Fig. 5; Lutjeharms, 2006). Chlorophyll *a* concentrations and production rates in Agulhas Current surface waters are particularly low during austral summer ( $< 0.2 \text{ mg/m}^3$  and  $< 500 \text{ mgC m}^{-2} \text{ d}^{-1}$ ) with higher concentrations and rates in the austral winter (Machu and Garcon, 2001; Figs. 5, 6 and 20 in Hood et al., 2017). The Agulhas Current can drive upwelling and elevate primary production in the coastal zone through meandering and topographic interactions, but it can also dramatically suppress primary production when it impinges onto the shelf (Schumann et al., 2005).

900 In general, chlorophyll concentrations and primary production are elevated in the coastal zone of southeast Africa along  
901 the inshore side of the Agulhas Current (Fig. 5; Machu and Garcon, 2001; Goschen et al., 2012; Figs. 5, 6 and 20 in Hood  
902 et al., 2017). This enhancement is most pronounced in austral summer and further southward downstream, and it is  
903 associated with upwelling-favourable (easterly) winds and the aforementioned topographically-induced upwelling.

904 The near-surface eastward flows are generally associated with very low (oligotrophic) nutrient and chlorophyll-*a* (Chl-*a*)  
905 concentrations ( $< 0.1 \text{ mg/m}^3$ ) and also very low primary production ( $< 500 \text{ mgC m}^{-2} \text{ d}^{-1}$ ; Fig. 5 Figs. 5 and 6 in Hood et  
906 al., 2017). A well-defined deep Chl-*a* maximum is observed between 50 and 150 m during the austral fall along 55°E  
907 between 20 and 30°S (Coles et al., unpublished data). An exception to this, however, is the South-East Madagascar bloom  
908 (SMB). The SMB occurs in near-surface waters off the southeastern coast of Madagascar in the late austral summer/fall  
909 (Jan-April). It was first described as a dendroid bloom by Longhurst (2001), owing to its branching shape that projects  
910 eastward (Fig. 12). The bloom can extend over a 2,500 km<sup>2</sup> area with Chl-*a* concentrations reaching 2-3 mg/m<sup>3</sup> (Longhurst,  
911 2001), making it a 'hot spot' for primary production in an otherwise oligotrophic region. Fig. 12 illustrates the bloom's  
912 large spatial variability, with high Chl-*a* filaments apparently co-occurring and being transported with mesoscale and  
913 submesoscale eddies and jets.

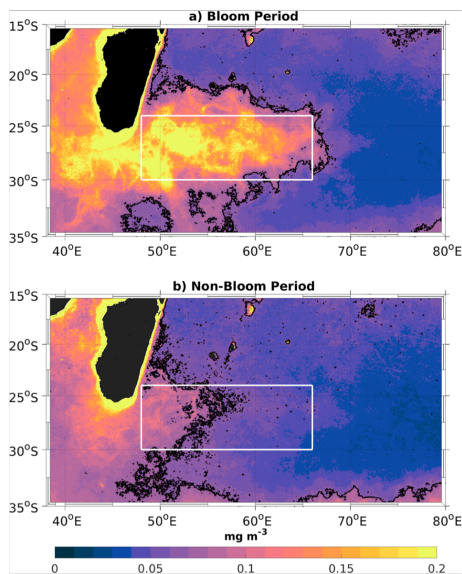
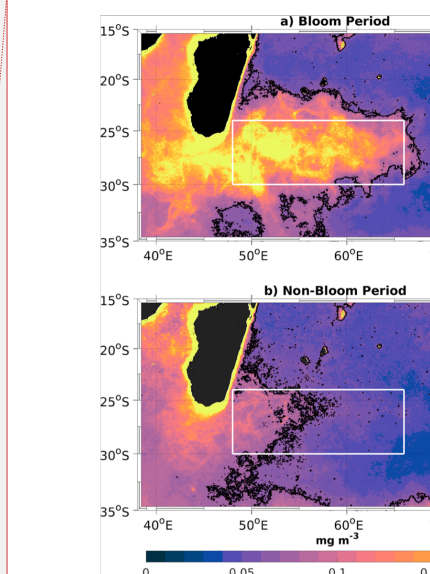


**Figure 12: (a) Spatial maps of mean Chl-*a* concentration (mg/m<sup>3</sup>) during months of maximum austral summer bloom. (b) Same as (a) but during January of minimum Chl-*a* concentration in austral summer. The black contour denotes the 0.07 mg/m<sup>3</sup> threshold used to distinguish between bloom and non-bloom years. From Dilmahamod et al. (2019).**

Why the SMB flourishes in late austral summer is unclear. Longhurst (2001) attributed SMB development to mixed layer deepening and entrainment of nutrients by the vigorous mesoscale eddy field. These nutrients could stimulate phytoplankton growth in the photic zone, with the eddies shaping the eastward propagation of the enhanced surface Chl-*a* concentrations. However, Uz (2007), Srokosz and Quartly (2013), and Dilmahamod et al. (2019) subsequently showed that the bloom occurs within a warm (> 26.5°C), shallow mixed layer (~30 m) overlying a strong pycnocline. Furthermore, they suggested that diazotrophs known to inhabit the region (Poulton et al., 2009) might introduce new nitrogen (N) from N<sub>2</sub> fixation that could support the enhanced Chl-*a* concentration as observed elsewhere (Mulholland et al., 2014; Hood et al. 2004; Coles et al., 2004). Subsequent studies also highlight the role of mesoscale eddies (Fig. 12), that could advect,



Deleted:

929 disperse and co-mingle nutrients and/or phytoplankton biomass (Dilmahamod et al. 2019; Huhn et al., 2012; Raj et al.,  
930 2010; Srokosz and Quartly, 2013; Srokosz et al., 2004, 2015; Uz, 2007).

931 A different explanation of the SMB and its eastward projection was proposed by Srokosz et al. (2004). In their proposed  
932 mechanism, the bloom initiates off Madagascar due to coastal processes that bring limiting nutrients to the photic zone  
933 and phytoplankton are transported horizontally by mesoscale eddies, resulting in an eastward propagation of the bloom.  
934 Dilmahamod et al. (2020) extend this further using a model to suggest that, from a nutrient flux analysis, horizontal  
935 advection of low-salinity nutrient-rich Madagascan coastal waters can indeed trigger a phytoplankton bloom.  
936 Alternatively, the apparent eastward propagation of the SMB has recently been attributed to advection by the SICC (Fig.  
937 10; Dilmahamod et al., 2019; Huhn et al., 2012; Wilson and Qiu, 2008). Indeed, Huhn et al. (2012) further suggested that  
938 the bloom is shaped by a meridional barrier of jet-like Lagrangian coherent structures associated with the SICC.

939 At the eastern boundary, the tropical source waters and downwelling tendency of the Leeuwin Current combine to create  
940 a warm, oligotrophic current with low productivity. Chl-*a* concentrations are usually < 30 mgChl  $\text{m}^{-2}$  and rates of primary  
941 production rates generally do not exceed 500 mgC  $\text{m}^{-2} \text{d}^{-1}$  (Koslow et al., 2008; Lourey et al., 2006; Lourey et al., 2013).  
942 Productivity in the Leeuwin Current is lowest during austral summer, when the water column is stratified. During summer,  
943 subsurface chlorophyll maxima are found between 50 and 120 m depth (Hanson et al., 2007) as observed in open ocean  
944 subtropical oligotrophic waters (e.g., Venrick, 1991). However, rates of primary production in near shore upwelling  
945 regions (e.g., off of the North West Cape during summer) can sometimes attain very high levels (3000–8000 mgC  $\text{m}^{-2}$   
946  $\text{day}^{-1}$ ) as observed in other eastern boundary upwelling zones (Furnas, 2007).

947 In all seasons, meanders in the Leeuwin Current give rise to warm core, anticyclonic eddies that carry moderately high  
948 chlorophyll coastal water offshore. The elevated chlorophyll concentrations in these eddies is due to the presence of  
949 coastal diatom communities. These diatoms are transported offshore into cooler oligotrophic waters that are dominated  
950 by much smaller open ocean phytoplankton species (Waite et al., 2007a; Paterson et al., 2008; Waite et al., 2016). These  
951 eddies, which can extend to more than 2000 m depth, are unusual because they are downwelling (anticyclonic) circulations  
952 that should inhibit the input of new nutrients from depth. Nonetheless, these eddies, and the elevated chlorophyll  
953 concentrations that are associated with them, persist for months (Feng et al., 2007; Moore et al., 2007; du Fois et al., 2014).  
954 It has been hypothesized that the diatom communities in these eddies are supported by internal nutrient recycling and/or  
955 lateral supply (Waite et al., 2007a; Paterson et al., 2013; Thompson et al., 2007, 2011).

956 Generation of these warm (and cold) core eddies by the Leeuwin Current is prolific between 20° and 35° S (Gaube et al.,  
957 2013). Most of these eddies move directly westward and some may be very long-lived (Feng et al., 2005; Feng et al.,  
958 2007; Moore et al., 2007; Gaube et al., 2013; du Fois et al., 2014). The persistence and potential biogeochemical/ecological  
959 impacts of these eddies in the open ocean have not been investigated fully.

960

## 961 **4.3 Equatorial regime**

### 962 **4.3.1 Wyrтки Jets**

963 Owing to the seasonally reversing monsoon winds, the equatorial Indian Ocean (EIO) exhibits unique characteristics and  
964 is in contrast with the equatorial Atlantic and Pacific Oceans. Unlike the other basins, the annual winds along the EIO are  
965 very weak and mostly meridionally oriented except during the two intermonsoon seasons between boreal winter (April-  
966 May) and summer (Oct-Nov) when strong westerly wind bursts prevail along the EIO (see Schott and McCreary, 2001  
967 and references therein). The semi-annual cycle in the zonal wind is well known observationally and was shown to be due  
968 to the meridional advection of easterly momentum by the cross-equatorial monsoon winds (Ogata and Xie, 2011). The  
969 westerly winds force strong eastward jets in the top 100 m along the equator that are known as spring and fall Wyrтки Jets,  
970 respectively (Wyrтки, 1973). These surface jets are usually confined within the top 100 m of the water column (Han et al.,  
971 1999; Iskander et al., 2011) and deepen (shoal) the thermocline and elevate (lower) the sea level in the east (west) (Rao et  
972 al., 1989; Schott and McCreary, 2001; Nagura and McPhaden, 2010a). These jets play a major role in zonal redistribution  
973 of mass, heat, salt and other water properties at the Equator and in off-equatorial basins (Reppin et al., 1999; Murtugudde  
974 and Busalacchi, 1999; Han et al., 1999; McPhaden et al., 2015; Chatterjee et al., 2017). Long term ADCP observations  
975 from the RAMA equatorial mooring suggest that the fall jet in the central EIO is usually stronger with a maximum transport  
976 of  $\sim 19.7$  Sv compared to the spring jet which shows maximum transport of  $\sim 14.9$  Sv with comparable standard deviations  
977 (McPhaden et al., 2015).

978 These eastward surface zonal currents tend to propagate westward during spring and eastward during fall (Nagura and  
979 McPhaden, 2016). The westward phase propagation speed during spring is estimated to be on average between 0.7-1.5 m  
980  $s^{-1}$  (Qiu et al., 2009; Nagura and McPhaden, 2010a) and driven primarily by the westward propagating surface zonal winds  
981 associated with atmospheric deep convection that moves from the Maritime Continent to the northern Bay of Bengal  
982 during spring (Nagura and McPhaden, 2010b; Nagura and McPhaden, 2016). Equatorial Rossby waves may also contribute  
983 to this westward propagation (Nagura and McPhaden, 2010a). In contrast, during fall, as the deep convection moves  
984 southeastward, the surface equatorial zonal winds, and thus surface currents, propagate eastward.

985 The spring and fall Wyrтки Jets also show considerable intraseasonal and interannual variability. While the intraseasonal  
986 variability of the Wyrтки Jets has been shown to be influenced by their own instability (Sengupta et al., 2001, 2007; Han  
987 et al., 2004) and local winds (Masumoto et al., 2005; Sengupta et al., 2007; Iskander et al., 2009; Prerna et al., 2019), the  
988 interannual variability of the Wyrтки Jets is mainly caused by the anomalous wind forcing along the EIO associated with  
989 ENSO (Murtugudde et al., 2000; Gnanaseelan et al., 2012; Joseph et al., 2012) and IOD (Nagura and McPhaden, 2010b;  
990 Nyadjro and McPhaden (2014); Prerna et al., 2019): IOD weakens (strengthens) the equatorial zonal winds during its

991 positive (negative) phase. While IOD modulates the zonal winds along the entire equator, the influence of ENSO is  
992 primarily limited to the eastern part of the EIO (Gnanaseelan et al., 2012). Moreover, it has been shown that these climate  
993 modes affect the boreal fall jet more significantly than the boreal spring jet. Recent modelling studies suggest that MJO  
994 convection can lead to a stronger spring Wyrki jet particularly in the eastern EIO. The interannual variability of MJO can,  
995 therefore, contribute to the observed interannual variability of this equatorial jet as well (Deshpande et al., 2017; Prerna et  
996 al., 2019).

#### 997 4.3.2 5-30 Day Ocean Waves and Instabilities

998 Meridional velocity along the equator shows prominent high frequency variability at all depths, in the periodic band of  
999 10-20 days with a peak at ~15 days (referred to as biweekly variability) and in the 20-30 days band with a peak at ~25  
1000 days (Masumoto et al., 2005; David et al., 2011; Chatterjee et al., 2013; Smyth et al., 2014). This variability is attributed  
1001 to Yanai waves, first discovered in the atmosphere (also referred to as mixed Rossby-Gravity waves; Yanai and Maruyama  
1002 1966; Arzeno et al., 2020; Pujiana and McPhaden, 2021). Unlike Kelvin and Rossby waves, Yanai wave phases can  
1003 propagate westward or eastward depending upon their frequency, but their group velocity is always eastward (Miyama et  
1004 al., 2006). These waves lead to convergent meridional heat flux into the equatorial regime (Shinoda, 2009; Smyth et al.,  
1005 2014). While these waves were first observed in the ocean in the late 1990s, the establishment of the equatorial RAMA  
1006 moorings (McPhaden et al., 2009) over the last two decades has provided more insight into these processes. Bi-weekly  
1007 (10-20 day) is shown to be forced by the direct meridional wind stress (Sengupta et al., 2004) and to some extent by the  
1008 meridional gradient of the zonal wind stress (Miyama et al., 2006). The 20–30-day band can be excited by off-equatorial  
1009 barotropic/baroclinic instabilities in addition to direct wind forcing. A detailed review of the biweekly variability is  
1010 provided in Schott et al. (2009) and hence, we focus on the 20-30 day variability in this review.

1011 While the 20-30-day oscillation in meridional velocity is reported near the surface in the central EIO (David et al., 2011),  
1012 in the eastern EIO these variabilities are seen only in subsurface layers (100-200 m depth) of the water column (Masumoto  
1013 et al., 2005). This indicates a possible downward energy propagation of a vertical beam that carries energy to deeper  
1014 depths. In the central EIO, these 20-30-day Yanai waves are excited by horizontal shear between the westward-flowing  
1015 South Equatorial Current and the eastward-flowing Southwest Monsoon Current during IOD events (Fig. 10a; David et  
1016 al., 2011). In the western EIO, these waves are primarily driven by cross equatorial meridional winds (Chatterjee et al.,  
1017 2013). During early boreal summer (June/July), when the Somali current begins to cross the Equator along the western  
1018 boundary of the basin, it bends offshore to conserve potential vorticity (Schott and McCreary, 2001) and forms a gyral  
1019 circulation known as the Southern Gyre (Fig. 10a). Subsequently, these swift currents turn barotropically unstable and  
1020 generate eddy flow that is advected southward to the Equator near the western boundary i.e. at ~50-55°E. They generate  
1021 a westward propagating cross-equatorial flow with a wavelength set by the eddy field which is similar to the wavelength  
1022 of 20-30 day Yanai waves and thus excite these frequencies efficiently (Chatterjee et al., 2013).

Deleted: 2010

1024 The ocean response to convectively coupled Kelvin waves (CCKW) in the atmosphere was investigated using ocean glider  
1025 measurements from the CINDY/DYNAMO field experiment (Webber et al., 2014; Matthews et al., 2014). CCKW are  
1026 atmospheric weather systems that propagate eastward along the Equator and are an important constituent of the MJO  
1027 convection (Baronowski et al., 2016). CCKW enhance surface wind speed and latent heat flux during their passage  
1028 suppressing the diurnal cycle of SST and leading to sustained decrease in bulk SST of around 0.1°C, one third of the SST  
1029 anomaly due to a single, average MJO event, suggesting the oceanographic impact could have a strong feedback on the  
1030 MJO cycle (Baronowski et al., 2016). Using RAMA moored measurements of upper ocean and surface atmosphere  
1031 variability, Pujiana and McPhaden (2018) demonstrated that CCKW force oceanic Kelvin waves, affect surface heat fluxes  
1032 and generate upper ocean turbulence.

### 1033 4.3.3 Equatorial Upwelling and Downwelling

1034 In the Pacific and Atlantic Oceans, permanent easterlies drive permanent equatorial upwelling due to Ekman  
1035 divergence, but in the Indian Ocean where the mean winds are weak and westerly, permanent upwelling does not  
1036 exist (Schott and McCreary, 2001). Mean westerly winds along the Equator are downwelling favorable, driving  
1037 surface convergence and thermocline divergence, which has been observed and described with Argo and RAMA data  
1038 (Wang and McPhaden, 2017). Instead of upwelling along the equator, coastal upwelling along the coasts of Sumatra  
1039 and Java is prominent. During June-October, south-easterly trade winds blow close to the Equator and drive the  
1040 offshore Ekman transport away from the Sumatra-Java coast (Quadfasel and Cresswell, 1992; Sprintall et al., 1999;  
1041 Susanto et al., 2001). The associated wind-driven upwelling intensifies as the monsoon progresses, reaching its peak  
1042 by August and finally weakening by October as the monsoon winds wane. Recent studies suggest that when the  
1043 easterly winds prevail during summer, upwelling favourable Kelvin waves also contribute to intensifying the  
1044 equatorial upwelling (Iskander et al., 2009; Chen et al., 2016). During boreal winter-early spring (December-March),  
1045 an intermittent/weaker subsurface thermocline shoaling is evident (Chen et al., 2016). Subsequently, the prevalence  
1046 of westerly winds, which drive downwelling Kelvin waves, depress the thermocline in the east (Susanto et al., 2001;  
1047 Prerna et al., 2019). Apart from this seasonal cycle, interannual climatic variability associated with ENSO and IOD  
1048 events (Saji et al., 1999; Vinayachandran et al., 1999; Nyadjiro and McPhaden, 2014) also influences the upwelling  
1049 intensity in this region (Section 6.2).

1050

### 1051 4.3.4 Equatorial Undercurrents

1052 In the Pacific and Atlantic, easterly winds produce an eastward mean undercurrent in the thermocline but in the  
1053 Indian Ocean westerly winds do not produce a mean westward undercurrent. The reason is that nonlinear momentum  
1054 advection drives mean eastward currents in the thermocline that flow up the zonal pressure gradient (Nagura and  
1055 McPhaden, 2014). The Indian Ocean Equatorial Undercurrent (EUC) is, therefore, a much weaker and seasonally

Formatted: Indent: Hanging: 0 cm

varying transient feature driven by seasonally reversing monsoon winds (Reppin et al., 1999; Schott and McCreary, 2001). The equatorial RAMA moorings have recorded an eastward EUC with a core within the thermocline during boreal winter and spring (Chen et al., 2015, 2019) and occasionally in summer and fall at a depth of 90-170 m (Iskandar and McPhaden, 2011). During winter, the eastward EUC is forced by the upwelling Kelvin and Rossby waves that are in turn forced by easterly winds along the equator in that season. During summer, the westward EUC is primarily forced by the eastward pressure gradient generated by the downwelling reflected Rossby waves off the eastern boundary of the basin. On intraseasonal timescales of 30-70-days, the EUC variability is dominated by that of Kelvin and Rossby waves of lower order baroclinic modes (Iskander and McPhaden, 2011). The undercurrents also undergo significant interannual variations related to the IOD. These variations are important in the mass and heat balance on IOD time scales, with significant impacts on upwelling and SST (Zhang et al., 2014; Nyadjro and McPhaden, 2014)

#### 4.3.5 Cross-Equatorial Circulation

The cross-equatorial circulation in the upper ocean is achieved by the Cross-Equatorial Cell (CEC), driven by southern hemisphere southeasterly winds and the seasonally-reversing monsoon winds in the northern hemisphere (Miyama et al. 2003; Schott et al. 2002, 2004, 2009). Thermocline waters subducted in the subtropical southeast Indian Ocean move equatorward and enter the northern hemisphere via the western boundary to upwell off Somalia and Oman. The return across the Equator, the surface branch of the CEC, is via the near-surface meridional flow in the interior Indian Ocean that is southward in the mean at nearly all longitudes (Miyama et al., 2003; Lee, 2004). This cell is unique to the Indian Ocean and is consistent with Sverdrup dynamics, being driven by the predominantly negative wind stress curl (Godfrey et al., 2001; Miyama et al., 2003; Wang and McPhaden, 2017). It carries most of the cross-equatorial transport of mass and heat (Schott and McCreary, 2001) and helps to moderate the seasonal climate of the region. The seasonal cross-equatorial mass flux is oppositely directed along the western boundary and in the interior (Beal et al., 2013). Flow in the interior is directed from the summer to the winter hemisphere (Horii et al., 2013; Wang and McPhaden, 2017) consistent with monsoon wind forced Ekman and Sverdrup dynamics as proposed in the model study of Miyama et al. (2003).

In OGCMs, the southward flow of the CEC was found to occur just below the surface, beneath a northward surface current (Wacogne and Pacanowski, 1996; Miyama et al. 2003). This “equatorial roll”, also unique to the Indian Ocean, is only of order 100 m depth and so has little impact on the cross-equatorial heat transport of the CEC. Horii et al. (2013) and Wang and McPhaden (2017) presented the first observational evidence for the equatorial roll.

The spatial structure and time evolution of the cross-equatorial circulation is difficult to depict due to its dependence



1089 on the fluctuating monsoon winds. Consequently, the flow patterns obtained from an Eulerian average as in Fig. 10  
1090 cannot capture the monsoon-dependent streamlines that a flow will follow at a given moment. Lagrangian methods  
1091 based on ocean drifter velocities (Laurindo et al. 2017) and real and simulated surface drifter trajectories identify  
1092 pathlines that connect the monsoonal Indian Ocean, revealing three cross-equatorial gyre pathways that connect the  
1093 Somali Current with the interior flow north and south of the Equator (Fig. 7 in l'Hegaret et al., 2018).

#### 1094 4.3.6 Biogeochemical Variability

1095 Much of the current understanding of biogeochemical variability in the equatorial zone of the Indian Ocean is based on  
1096 satellite ocean color observations and models, augmented by some additional, relatively sparse, in situ measurements.  
1097 Seasonal climatologies of near-surface chlorophyll concentrations and primary production show a significant seasonality  
1098 in equatorial waters that is clearly associated with monsoon forcing (Fig. 5, Wiggert et al., 2006; Strutton et al., 2015;  
1099 Figs. 5 and 6 in Hood et al., 2017). In general, Chl-*a* concentrations and primary production increase northward from the  
1100 equator with the lowest concentrations ( $< 0.1 \text{ mg m}^{-3}$ ) and rates ( $< 800 \text{ mg C m}^{-2} \text{ d}^{-1}$ ) occurring during the boreal spring  
1101 intermonsoon period. During the southwest monsoon, Chl-*a* concentrations and rates of primary production increase in  
1102 western equatorial waters in response to monsoon-forced mixing and upwelling. However, concentrations and rates in the  
1103 central and eastern equatorial waters stay relatively low ( $< 0.5 \text{ mg m}^{-3}$ ,  $< 800 \text{ mgC m}^{-2} \text{ d}^{-1}$ , respectively). Island wake  
1104 effects can be seen advecting high chlorophyll water ( $> 0.5 \text{ mg m}^{-3}$ ) along the equator from the Chagos-Laccadive ridge  
1105 at  $73^\circ\text{E}$  eastward during the autumn intermonsoon period and westward during spring (see Fig. 1 in Strutton et al., 2015).

1106 Well-developed deep Chl-*a* maxima have been observed in the equatorial Indian Ocean along  $65^\circ\text{E}$  centered at about 50  
1107 m depth in November-December (George et al., 2013) and along  $80^\circ\text{E}$  centered at about 75 m in August-September  
1108 (Sorokin et al., 1985). It is unknown whether or not this subsurface Chl-*a* maximum exists along the equator throughout  
1109 the year, but it is probably present whenever the water column is stratified. Models predict the presence of a subsurface  
1110 (60 m) Chl-*a* maximum in eastern Indian Ocean equatorial waters along  $87^\circ\text{E}$  (Wiggert et al., 2006) that is present  
1111 throughout the year except during the southwest monsoon when high chlorophyll surface water is advected into the region.

1112 Physical processes at time scales from intraseasonal to interannual (i.e., Wyrki Jets, MJO and IOD) have been shown to  
1113 influence biogeochemistry. For example, IOD events can significantly increase chlorophyll concentrations and primary  
1114 production in eastern Indian Ocean equatorial waters (Wiggert *et al.*, 2009). In addition, relaxation of an IOD can deplete  
1115 upper ocean nutrients, decreasing biological productivity (Kumar *et al.*, 2012). Biogeochemical responses to the IOD also  
1116 have significant higher trophic level impacts (Marsac and Le Blanc, 1999).

1117 Satellite observations and biophysical model simulations show how chlorophyll concentrations and primary production  
1118 near the Seychelles-Chagos thermocline ridge, can be increased by MJO-induced wind mixing and nutrient entrainment  
1119 (Resplandy et al., 2009). They also concluded that IOD-driven interannual variability of thermocline depth influences the

1120 biogeochemical response to MJO: the deepened nutricline following IOD events inhibits nutrient input into the mixed  
1121 layer and thus decreases the biogeochemical response to MJO.

1122 In model simulations, Wyrтки jets depress the thermocline and nitracline along the equator on the eastern side of the basin  
1123 and, as a result, lower equatorial primary production when they arrive in the spring and autumn (Wiggert et al. 2006). This  
1124 pattern was observed in a 25 day time series study on the equator at 80.5°E in late 2006 that showed a deepening of the  
1125 surface layer, nutracline and subsurface Chl-*a* maximum during the autumn Wyrтки jet period (Kumar et al., 2012).

1126 Finally, Strutton et al. (2015) examined time-series measurements of near-surface chlorophyll concentration from a  
1127 mooring deployed in 2010 at 80.5 E in the equatorial Indian Ocean. These data revealed at least six spikes in chlorophyll  
1128 from October through December, separated by approximately 2-week intervals and coinciding with the development of  
1129 the fall Wyrтки jets. The chlorophyll pulses were associated with increases in eastward surface winds and eastward currents  
1130 in the mixed layer and inconsistent with upwelling dynamics because eastward winds that cause intensification of the  
1131 Wyrтки jet should drive downwelling. Strutton et al. (2015) concluded that the chlorophyll spikes could be explained by  
1132 two alternative mechanisms: (1) turbulent entrainment of nutrients and/or chlorophyll from across the base of the mixed  
1133 layer by wind stirring or Wyrтки jet-induced shear instability or (2) enhanced southward advection of high chlorophyll  
1134 concentrations into the equatorial zone associated with wind-forced biweekly Yanai waves.

#### 1135 **4.4 Northern Indian Ocean**

1136 The two main basins of the northern Indian Ocean, the Bay of Bengal (BoB) and the Arabian Sea (AS), are characterized  
1137 at the surface by remarkably contrasting sea surface salinity with differences of the order of 3 psu (e.g. Chatterjee et al.  
1138 2012, Gordon et al. 2016, Hormann et al. 2019) decreasing from west to east (Fig. 4). The fresh surface layer of the BoB  
1139 is maintained by large freshwater input deriving from direct rainfall over the ocean and river runoff, especially during the  
1140 South Asian monsoon. The salt balance of the BoB is maintained by the subsurface supply of salt water via the Southwest  
1141 Monsoon Current (Fig. 10, Vinayachandran et al., 2013). The saltier SSS of the AS is the consequence of an evaporative  
1142 regime (e.g., Rao & Sivakumar, 2003; Sengupta et al., 2006). A reversing monsoonal near-surface circulation (Fig. 10 a,b)  
1143 plays a central role in the exchanges of freshwater and heat between the BoB and the AS (McCreary et al. 1993, Hormann  
1144 et al. 2019).

1145 Recent multi-year deployments of satellite tracked surface drifters drogued at 15 m depth (Wijesekera et. al, 2016,  
1146 Centurioni et al. 2018) have helped to better constrain the amplitude and structure of the circulation and the exchange  
1147 processes between the two basins, and to refine the findings reported by other authors (e.g. Schott and McCreary, 2001).  
1148 Additionally, implementation of a moored buoy network along the slope and shelf of the Indian coast has helped

1149 significantly in enhancing our understanding of the east India Coastal Current (EICC) and west India Coastal Current  
1150 (WICC) (Fig. 10, Mukherjee et al., 2014; Amol et al., 2014; Mukhopadhyay et al., 2020; [Chaudhuri et al. 2020](#)).

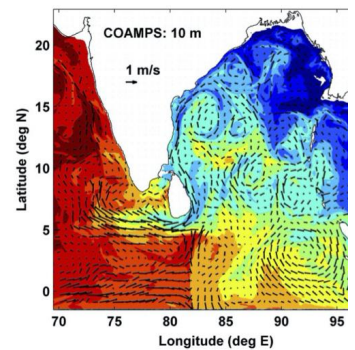
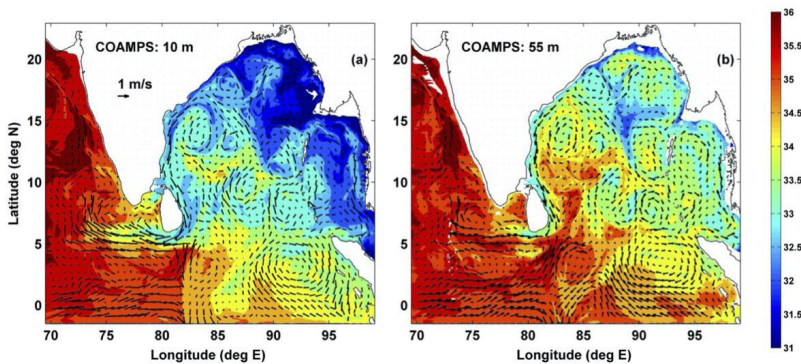
Deleted: Anya

1151 **4.4.1 Bay of Bengal**

1152 In a climatological sense, the main features of the near-surface circulation of the western BoB (Figs. 10a and 10b) are the  
1153 reversing EICC, the Southwest/Northeast Monsoon Current (SMC/NMC) and the seasonally variable Sri Lanka Dome.  
1154 The eastern side of the BoB, extending into the Andaman Sea, is characterised by a sluggish circulation.

1155 **4.4.1.1 Southwest/Northeast Monsoon Currents**

1156 During the boreal summer SW monsoon, the Southwest Monsoon Current (SMC, Fig. 10a) flows eastward around the  
1157 Indian subcontinent supplying salty water from the Arabian Sea to the fresher Bay of Bengal (e.g., Jensen, 2001; Jensen  
1158 et al., 2016; Vinayachandran et al., 2013; Wijesekera et al., 2015, 2016). During the winter monsoon, the Northeast  
1159 Monsoon Current (NMC, Fig. 10b) reverses the flow carrying fresher water into the Arabian Sea. Figure 13 provides a  
1160 snapshot from an operational forecast system, the Coupled Ocean-Atmosphere Mesoscale Prediction System (COAMPS),  
1161 of the NMC flow and route for freshwater to enter the Arabian Sea (Wijesekera et al., 2015).



Deleted:

1162 **Figure 13: COAMPS velocity vectors (arrows) and salinity (psu, color shading) at (a) 10 m and (b) 55 m on 18**  
1163 **December 2013. Modified from Wijesekera et al. (2015).**

1165 A more recent study has found that the origins of the Arabian Sea high salinity water are specifically from the western  
1166 Arabian Sea and western Equatorial Indian Ocean, and they reach the Bay of Bengal via a combination of the Indian Ocean

1169 EUC and the SMC (Sanchez-Franks et al., 2019; Section 8.2). Changes in the supply of salty water to the Bay of Bengal  
1170 varies interannually due to the strength in the equatorial currents, forced by the local wind field and ENSO (Sanchez-  
1171 Franks et al., 2019), and is expected to influence the salinity budget of the Bay of Bengal (Vinayachandran et al., 2013)  
1172 and thus modulate SST variability (Fig. 10a, Jensen, 2001; Jensen et al., 2016; Li et al., 2017; Vinayachandran et al., 2013,  
1173 2018; Webber et al., 2018).

#### 1174 4.4.1.2 East Indian Coastal Currents (EICC)

1175 The EICC forms the western boundary current of the Bay of Bengal and plays an important role in the basin-scale heat  
1176 and salt budget of the Indian Ocean, and hence in determining the local climate (Shenoi et al, 2002), biological processes  
1177 (Madhupratap et al, 2003; Vinayachandran et al, 2005; Naqvi et al, 2006; Dileepkumar, 2006; McCreary et al, 2009) and  
1178 marine fisheries (Vivekananda and Krishnakumar, 2010) of this region. It reverses its direction seasonally north of 10°N  
1179 in response to a combination of local alongshore winds, remote alongshore winds in the eastern BoB, remote forcing from  
1180 the equatorial Indian Ocean and the interior Ekman pumping of the basin (Shankar et al., 1996; McCreary et al., 1996;  
1181 Vinayachandran et al., 1996; Mukherjee et al., 2018). The EICC is generally equatorward south of 10°N throughout the  
1182 year. While local winds dominate the EICC forcing during summer and winter, remote forcing dominates during the inter-  
1183 monsoon periods (Shankar et al., 1996; McCreary et al., 1996; Suresh et al., 2013).

1184 Climatological ship-drift and hydrographic data suggest the EICC flows poleward during February-September (Shetye et  
1185 al., 1993) and turns equatorward during November-January (Shetye et al., 1996; Fig. 10). While the annual cycle is driven  
1186 by local alongshore winds and interior Ekman pumping, the semiannual cycle is the result of asymmetry in the monsoon  
1187 and equatorial forcing (Mukherjee et al., 2018). During boreal spring (March-May), the EICC is strongest with a magnitude  
1188 exceeding 1m/s with unidirectional currents to about 150 m, forming the western boundary current of a cyclonic basin-  
1189 wide gyre of the BoB. The local alongshore winds are weakest and the stronger EICC is primarily forced by the interior  
1190 anticyclonic Ekman pumping over the basin (McCreary et al., 1996; Shankar et al., 1996; Vinayachandran et al., 1996;  
1191 Mukherjee et al., 2018). During boreal summer, the EICC is weaker and is restricted to within the top 70 m of the water  
1192 column. The poleward flow is generally limited to the central part of the coast between 10-18°N and often switches to  
1193 short pulses of poleward currents along the coast (Mukherjee et al., 2018; Francis et al., 2020). The poleward flow is  
1194 driven by local winds, but the response of the interior cyclonic Ekman pumping and equatorial winds driving an opposite  
1195 flow along the coast causes a weaker poleward EICC in summer than in spring (McCreary et al., 1996; Vinayachandran  
1196 et al., 1996; Shankar et al., 2002). The basin-scale gyre also disappears in summer and the EICC then consists of several  
1197 eddies along the coast. The EICC turns equatorward during November-January (Shetye et al., 1996).

1198 Near-surface alongshore currents also display significant 120 day and intraseasonal variability. The magnitude of the 120  
1199 day variability is generally weaker than the semiannual period, particularly in the southern part of the coast. As for the

Deleted: 2017

Deleted: 2017

1202 annual period, upward phase propagation along the coast is also evident for the semiannual and 120 day period, except at  
1203 Cuddalore where downward phase propagation is common during summer and winter months (Mukherjee et al., 2014;  
1204 Mukhopadhyay et al., 2020). Further, unlike annual and semiannual periods, the 120 day and intraseasonal variability  
1205 decorrelate along the coast indicating that these high frequencies are dominated by local responses rather than remote  
1206 forcing (Mukherjee et al., 2018; Mukhopadhyay et al., 2020).

1207 **4.4.1.3 Undercurrents**

1208 ADCP observations suggest that during summer and winter, when the near-surface current is shallow, the EICC often  
1209 exhibits undercurrents along the continental slope. As the EICC is deeper in the north, the undercurrent is observed at a  
1210 depth of 100-150 m and can extend up to 700 m. However, in the south undercurrents are seen at relatively shallow depths  
1211 of about 70-75 m (Francis et al., 2020). While these undercurrents are observed throughout the coast, they are much more  
1212 prominent and more frequent at Cuddalore, the southernmost station of the coast (Fig. 14, Mukherjee et al., 2014;  
1213 Mukhopadhyay et al., 2020).

Deleted: 2020a

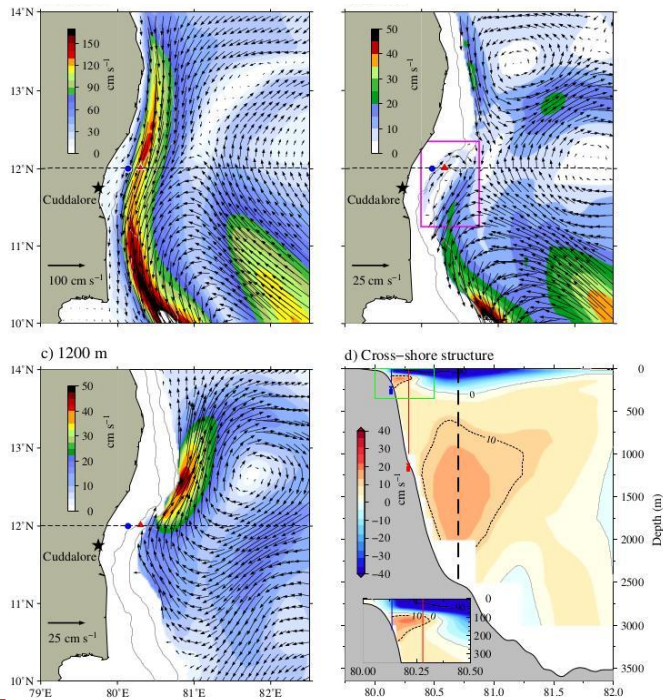
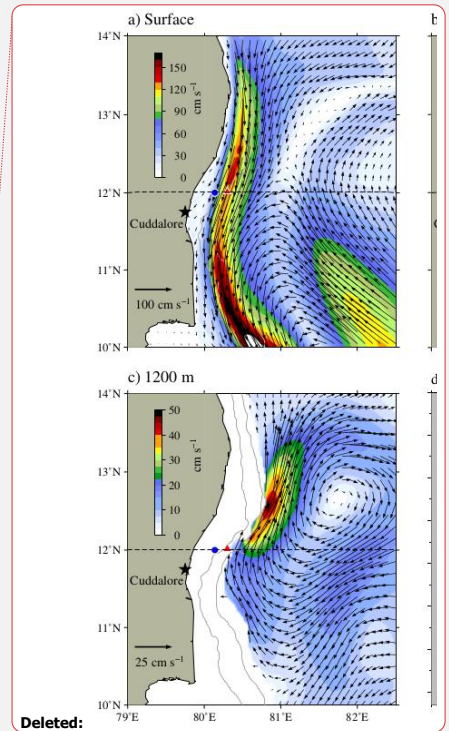


**Figure 14:** Circulation pattern in the southwestern Bay of Bengal at (a) surface (b) 200 m and (c) 1200 m on 15 November 2014. Vectors show the current direction, and overlaid is the current magnitude ( $\text{cm s}^{-1}$ ). Note that the scales of current vectors and color bars are different at each subplot. Blue circle (red triangle) represents the location of ADCP deployed on the shelf (slope) off Cuddalore. Dashed black line represents the  $12^\circ\text{N}$  latitude. Continuous gray lines represent the 100 m and 1000 m bathymetric contours. Rectangular box (magenta) indicates the subsurface eddy near the shelf break. (d) Cross-shore structure of alongshore currents across  $12^\circ\text{N}$ . Dashed black vertical line shows the core of the undercurrent, and red (blue) vertical lines show the location of ADCP mooring on the slope (shelf). Inset plot is the zoomed view of shelf break region indicated by green box (Reproduced from Francis et al., 2020).

The prominent upward phase propagation of the annual signal in the subsurface layers, particularly in the southern stations, suggests downward propagation of energy and is thereby attributed as one of the main causes of the undercurrents



1228 (Mukherjee et al., 2014). A recent modelling study suggests that the wintertime undercurrent off Cuddalore consists of  
1229 two separate subsurface anticyclonic eddy circulations: a shallow small scale circulation at a depth range of 100-200 m  
1230 and a broader and deep flow below 500 m depth off the continental slope (Francis et al., 2020). The shallow subsurface  
1231 anticyclonic eddy was found to spin off from the zonal shear of the mean near-surface EICC along the shelf break (Fig.  
1232 14). These eddies exhibit high frequency fluctuations and have 20-30 km length scales. Since the zonal share of the EICC  
1233 is primarily linked to the strength of the EICC itself, the variability and strength of this undercurrent is also linked with  
1234 the EICC.

#### 1235 **4.4.1.4 Sri Lanka Dome**

1236 The Sri Lanka Dome (Vinayachandran et al. 1999; Schott and McCreary, 2001; Wijesekera et. al, 2016, Cullen and  
1237 Shroyer, 2019) is mainly visible as a closed anticyclonic (clockwise) eddy in the near-surface geostrophic current velocity  
1238 field starting in May and lasting through October (Fig. 15c). It is a recurring upwelling dome that forms east of Sri Lanka  
1239 between 5-10°N, 83-87°E. The SLD is embedded within the Southwest Monsoon Current (SMC) system (Gadgil, 2003)  
1240 and enhances the SMC exchange from the Arabian Sea to the Bay of Bengal (Anutaliya et al., 2017). Upwelling associated  
1241 with the SLD influences the vertical exchange of water properties, enhances biological productivity, and cools sea surface  
1242 temperature (SST) which affects local atmospheric convection (Vinayachandran et al., 2004; de Vos et al., 2014).

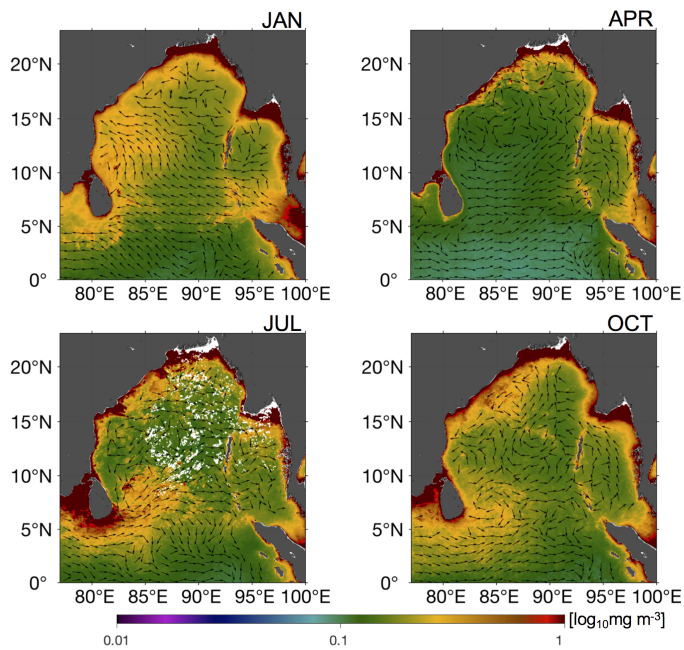
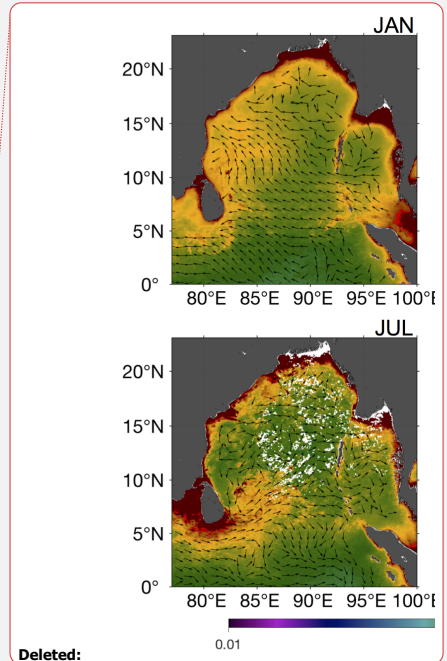


**Figure 15: Climatology (2002-2018) of chlorophyll-a concentrations (colormap) and current velocities (arrows) in the Bay of Bengal for (a) January (b) April (c) July (d) October. Chlorophyll climatology was obtained from the MODIS-Aqua product and current velocities were obtained from the third-degree Ocean Surface Current Analysis Real-time (OSCAR) product.**

#### 4.4.2 Arabian Sea

Like the Bay of Bengal (BoB), the Arabian Sea (AS) near surface circulation is also driven primarily by the seasonally reversing monsoon winds. The AS is connected to the BoB through the passage between the southern tip of India and the equatorial wave guide, and to the southern hemisphere by the cross equatorial flow via the Somali current system. The Somali current (Fig. 10) forms one of the western boundary currents of the AS. Another major boundary current system



Deleted:



is along the west coast of India, the WICC (Fig. 10), which transports heat and salt from the northern Arabian Sea to the BoB, and vice-versa. Recent observations (Chatterjee et al., 2012) and modelling studies (Shankar et al., 2016; Vijith et al., 2016) indicate that the northern extent of the WICC reaches up to 20°N during the winter monsoon, carrying fresher BoB water to the northern latitudes and modulating the wintertime convection there. In the last couple of decades, the strengthening of WICC and NMC has decreased the SSS in the eastern Arabian Sea (Varna et al., 2021).

#### 4.4.2.1 Somali current System

The Somali Current is a seasonally reversing western boundary current and is often composed of discontinuous non-linear eddy driven flows. During summer it flows poleward and the upwelling here is nearly as large as for the eastern boundary upwelling regimes of the Pacific and Atlantic Oceans (See Schott and McCreary, 2001 for a detailed review). Unfortunately, owing to piracy, direct in-situ observations are very rare in this region and mostly date back to the early 1960s and 1970s. Hence, the scientific community has mostly relied on numerical model simulations to enhance understanding of this region over the last few decades.

Recent modelling studies suggest that during the summer monsoon, unlike other western boundary currents, the Somali Current system can be divided into three dynamically distinctive regions (Wang et al., 2018; Chatterjee et al., 2019): northern (north of 8°N), central (3-8°N) and the southern (south of 3°N) part. The northern and southern parts are driven by the large anticyclonic gyres called the Great Whirl (GW) and the southern Gyre (SG), respectively (Fig. 10a). Local southwesterly alongshore winds known as the Findlater Jet (Findlater, 1969) drives Ekman transport all along the Somali coast (Schott and McCreary, 2001) with varied magnitude which is strongest in the southern part, and significantly weakens northward (Chatterjee et al., 2019). The wind stress forcing leads to Ekman Pumping in the central Arabian Sea, setting up a bowl-shaped mixed layer and warming at the 100 m level. Ekman downwelling velocities are strongest in the northern part and likely contribute to the formation of the Great Whirl front which upwells cold subsurface water in this part of the coast. The central part, in contrast, is mainly driven by the local winds and remotely forced Rossby waves. In fact, the annual Rossby waves radiated out of the southwestern coast of Sri Lanka seem to play a major role in the reversal of currents to poleward flow in the northern part of the Somali coast as early as mid April. This reversal likely initiates the generation of the Great Whirl (Beal and Donohue, 2013; Vic et al., 2014), a month before the strong northeastward Findlater Jet commences along the Somali coast. As the monsoon progresses, these downwelling favourable Rossby waves oppose the coastal Ekman upwelling and thereby start to weaken the upwelling all along the coast. Moreover, as the alongshore winds peak, this favours enhanced mixing at the bottom of the mixed layer, which deepens the thermocline further. This process is more conspicuous in the central part of the coast, where the depth of the 22°C isotherm deepens by about 30-40 m from June to August (Chatterjee et al., 2019). By this time, the upwelling becomes limited to the northern part of the coast along the Great Whirl front of the Somali region.

Deleted: 2015

1288 Climatological characteristics of the Somali Undercurrent (SUC) have been revealed by a new multi-decadal time series  
1289 of temperature, salinity and geostrophic velocity constructed from repeat XBT transects and Argo observations (Zang et  
1290 al. 2021). They find that the SUC flows southeastward during the monsoon transition periods in boreal spring (April-June)  
1291 and fall (September-November), against the northeastward flow of the Somali Current. The depth of the SUC core is  
1292 shallower during the spring transition (~500 dbar in April) and has a maximum depth of ~1200 dbar in September. Core  
1293 speeds are 2.5–4 cm s<sup>-1</sup> in spring; in fall the core speed strengthens from 0.2 to 10.6 cm s<sup>-1</sup> from September to November  
1294 and then disappears in December. Volume transport of the Somali Current and SUC (0–2000 dbar) has a maximum of 29.6  
1295 Sv northeastward in the summer monsoon and minimum of 13 Sv southwestward during the fall transition when the SUC  
1296 is strong.

#### 1297 4.4.2.2 West India Coastal Current (WICC)

1298 The WICC reverses its direction annually: flowing equatorward (upwelling favourable) during the summer monsoon (May  
1299 to September; Fig. 10a) and poleward (downwelling favourable) during the winter monsoon (November to February; Fig.  
1300 10b). The equatorward flow during the summer characterises the WICC as a classical eastern boundary current (Shetye  
1301 and Shenoi, 1988). Interestingly, as the monthly mean alongshore winds off the west coast of India are always equatorward  
1302 throughout the year, the surface currents flow against the winds during the winter, driven by coastally-trapped Kelvin  
1303 waves forced remotely in the BoB and along the east coast of India (McCreary et al., 1993; Shankar and Shetye, 1997;  
1304 Shankar et al., 2002; Suresh et al., 2016). Recent observations based on satellite data and alongshore ADCP moorings  
1305 reveal strong interannual variability of this seasonal cycle. Vialard et al. (2009b), based on a short ADCP record during  
1306 2006–2008, reported an absence of seasonal cycle off Goa and they attributed this absence to the radiation of Rossby waves  
1307 south of the critical latitude. As the longer record of ADCP data became available, a clear seasonal cycle in the WICC  
1308 became evident with weaker amplitudes in the south, stronger poleward (Amol et al., 2014).

1309 The WICC also shows significant intraseasonal variability at times, particularly during boreal winter, exhibiting much  
1310 stronger energy in the intraseasonal band than in the seasonal band (Vialard et al., 2009b; Amol et al., 2014). Unlike the  
1311 seasonal cycle, intraseasonal variability is stronger in the south and weakens poleward. Vialard et al. (2009b) attributed  
1312 this intraseasonal variability to the atmospheric MJO forcing. Recently, a modelling study suggested that interception of  
1313 the intraseasonal equatorial Rossby waves by the southern tip of India and Sri Lanka excites coastal Kelvin waves which  
1314 contribute significantly (~60–70%) to the intraseasonal variability along the west coast (Suresh et al., 2013). A satellite  
1315 sea level study by Dhage and Sturb (2016) confirmed the model-based findings of Suresh et al. (2013) and revealed that  
1316 large-scale winds from the south of India and Sri Lanka also contribute to the coastal signals along the west coast of India.

1317 Another striking feature observed in these ADCP data is the clear signature of upward phase propagation in all timescales  
1318 during both monsoon seasons. This upward phase propagation is more conspicuous for the seasonal period than for the

Formatted: Normal, Space Before: 0 pt, Don't keep lines together

Deleted: 2009

Deleted: 2009

Deleted: 2009

intraseasonal. As a result, the phase of the surface currents often tends to be opposite that in the subsurface layers (Amol et al., 2014). Moreover, it is found that the strength of this undercurrent intensifies northward along the west coast with strongest undercurrent off Mumbai and the weakest off Kanyakumari (southernmost point of Indian mainland), indicating a possible downward propagation of energy along the ray path as suggested earlier by Nethery and Shankar (2007). Since the ray angle ( $\theta$ ) depends on the frequency ( $\sigma$ ) and stratification ( $N_b$ ) according to  $\theta = \sigma / N_b$  (McCreary, 1984; Nethery and Shankar, 2007) the angle the beam makes from the horizontal is deeper for the intraseasonal band than for the seasonal. As a result, intraseasonal beams propagate energy deeper into the water column. Therefore, while the WICC shows some coherence along the coast in the seasonal time scale, it completely decorrelates horizontally for the intraseasonal period.

1330

#### 1331 4.4.3 Biogeochemical Variability

In the Bay of Bengal, the large freshwater input gives rise to enhanced stratification that inhibits upwelling and wind-mixing and therefore nutrient supply to surface waters (Kumar et al., 2002; Vinayachandran et al., 2002; Madhupratap et al., 2003; Vinayachandran, 2009). Nonetheless, increased productivity is observed along the coast primarily in association with riverine nutrient inputs (Vinayachandran, 2009). These nutrients stimulate diatom blooms (Sasamal et al., 2005) leading to significant increases in Chl-*a* concentration ( $\sim 30\text{--}100 \text{ mgChl a m}^{-2}$ ) and production ( $\sim 0.55\text{--}1 \text{ gC m}^{-2} \text{ d}^{-1}$ ) near the coast (Gomes et al., 2000; Fig. 15). This high Chl-*a* river water flows either along the coast or offshore, up to several hundred kilometers, depending on the coastal current pattern (Vinayachandran, 2009). Along the Indian coast, the flow of Chl-*a*-rich water is determined by the EICC, which flows northward during the spring intermonsoon period and Southwest Monsoon and southward during the autumn intermonsoon and Northeast Monsoon (Fig. 15). When the EICC meanders seaward from the Indian coast, it leads to offshore increases in high chlorophyll water. During the spring intermonsoon and Southwest Monsoon the northward-flowing EICC is upwelling favorable, which may contribute to increases in Chl-*a* concentration and primary production along the coast (Hood et al., 2017)

1344

Elevated productivity is observed further offshore in the southwestern Bay of Bengal during the Northeast Monsoon (Vinayachandran and Mathew, 2003; Vinayachandran, 2009). Modeling studies suggest that this is caused by wind-driven entrainment, not only of subsurface nutrients, but also of phytoplankton from the subsurface chl maximum that is present during the autumn intermonsoon period (Vinayachandran et al., 2005). In contrast, productivity near the coast is suppressed during the Northeast Monsoon when the EICC flows southward (Fig. 14). Presumably, this is due to a combination of the downwelling-favorable currents and winds. However, primary production over the shelf in the northern part of the Bay increases during the Northeast Monsoon (Gomes et al., 2000; Fig. 15), possibly due to river nutrient inputs (Vinayachandran, 2009) and / or wind-stress and buoyancy-driven nutrient entrainment as is observed in the northern Arabian Sea during the Northeast Monsoon (Wiggert et al., 2000; 2005; Hood et al., 2017).

1354  
1355 Subsurface Chl-*a* maxima are observed in the Bay of Bengal during all seasons whenever and wherever wind forcing  
1356 and/or currents are insufficiently strong to upwell or entrain them into the surface layer (Sarma and Aswanikumar, 1991;  
1357 Murty et al., 2000; Sarjini and Sarma, 2001; Kumar et al., 2007). During the intermonsoon periods the Bay of Bengal  
1358 transitions to more oligotrophic conditions with relatively low surface chlorophyll concentrations ( $< 0.6 \text{ mg/m}^3$ ; Fig. 15)  
1359 and production rates ( $< 700 \text{ mgC m}^{-2} \text{ d}^{-1}$ ; see Fig. 6 in Hood et al., 2017). *Trichodesmium erythraeum* blooms have been  
1360 observed during the intermonsoon periods along with high abundances of *Synechococcus* and heterotrophic dinoflagellates  
1361 (Sarjini and Sarma, 2001; Jyothibabu et al., 2008). In offshore waters subsurface chlorophyll maxima are generally located  
1362 between 40 and 70m in autumn and 60 and 90m in spring (Kumar et al., 2007). These deep Chl-*a* maxima tend to shoal  
1363 near the coast (Sarma and Aswanikumar, 1991; Murty et al., 2000) and their depth and chlorophyll concentrations are  
1364 strongly influenced by eddies (Kumar et al., 2007).  
1365  
1366 Strong upwelling also occurs along the southern coast of Sri Lanka during the Southwest Monsoon (Vinayachandran,  
1367 2004; 2009; de Vos et al., 2014). Satellite SST and chlorophyll images reveal dramatic eastward advection of cool ( $< 28^\circ$   
1368 C) chlorophyll rich upwelled water by the SMC (Vinayachandran, 2004; 2009; de Vos et al., 2014). Chlorophyll-rich  
1369 waters from the southwestern coast of India are also advected by the SMC towards Sri Lanka during the Southwest  
1370 Monsoon (Vinayachandran, 2004; 2009; Strutton et al., 2015). Surface chlorophyll concentrations and rates of primary  
1371 production along the southern coast of Sri Lanka during the Southwest Monsoon can exceed  $10 \text{ mgChla m}^{-3}$  (de Vos et  
1372 al., 2014) and  $1000 \text{ mgC m}^{-2} \text{ d}^{-1}$  (Fig. 6 in Hood et al., 2017), respectively, compared to much lower concentrations and  
1373 rates during the Northeast Monsoon when the NMC flows westward (de Vos et al., 2014; Hood et al., 2017).  
1374 Vinayachandran (2004; 2009) attribute the productivity response during the Southwest Monsoon to nutrient enrichment  
1375 from coastal upwelling driven by monsoon winds. Presumably, these high chlorophyll concentrations and production rates  
1376 are associated with diatom blooms. This elevated productivity extends to the east of Sri Lanka during the peak of the  
1377 Southwest Monsoon (Vinayachandran et al., 1999; Vinayachandran, 2004; 2009). This eastward extension into the  
1378 southern Bay of Bengal occurs along the path of the SMC (Vinayachandran et al., 1999) and is associated with upward  
1379 Ekman pumping east of Sri Lanka. This Ekman pumping also leads to the formation of the aforementioned Sri Lanka  
1380 Dome (Vinayachandran and Yamagata, 1998).  
1381  
1382 The western side of the northern Indian Ocean transitions during the southwest monsoon to a eutrophic coastal upwelling  
1383 system in response to the upwelling favorable winds and currents (Wiggert et al., 2005; Hood et al., 2017 and references  
1384 cited therein; Fig. 5 ; Figs. 5 and 6 in Hood et al., 2017; [Lakshmi et al., 2020](#)). These changes can be seen in ocean color  
1385 data as substantial increases in chl $a$  concentrations along the coasts of Somalia, Yemen and Oman (e.g., Brock and  
1386 McClain, 1992; Banse and English, 2000; Kumar et al., 2000; Lierheimer and Banse, 2002; Wiggert et al., 2005; George  
1387 et al., 2013; Hood et al., 2017). Chlorophyll-*a* concentrations in the western Arabian Sea can exceed  $40 \text{ mgChla m}^{-2}$  during

Deleted: ).

1389 the southwest monsoon with production rates  $> 2.5 \text{ gC m}^{-2}\text{d}^{-1}$  (Marra et al. 1998; Fig. 6 in Hood et al., 2017). However,  
1390 the environmental conditions vary significantly between the eutrophic coastal zones to the west and the oligotrophic open  
1391 ocean waters offshore that are influenced by wind-curl induced downwelling to the southwest of the Findlater Jet (Lee et  
1392 al., 2000; [Lakshmi et al., 2020](#)). The surface nitrate and Chl-*a* concentrations decline dramatically from  $> 10$  to  $< 0.02$   
1393  $\mu\text{M}$  and from  $> 1.0$  to  $< 0.2 \text{ mgChla m}^{-3}$ , respectively, from the west coast to open ocean in the Arabian Sea (Brown et al.,  
1394 1999; Wiggert et al., 2005; Hood et al., 2017). In general, the phytoplankton community structure transitions to larger  
1395 cells (diatoms) during the southwest monsoon in the western Arabian Sea (Brown et al., 1999; Tarran et al., 1999;  
1396 Shalapyonok et al., 2001; [Lakshmi et al., 2020](#)). However, small primary producers remain important, even in areas  
1397 strongly influenced by coastal upwelling (Brown et al., 1999; [Lakshmi et al., 2020](#)). In contrast, during the oligotrophic  
1398 spring and fall intermonsoon periods, surface waters in the western Arabian Sea are dominated by picoplankton (Garrison  
1399 et al., 2000). Subsurface Chl-*a* maxima are observed between 40 and 140 meters in the central southeastern Arabian Sea  
1400 during all seasons (Gundersen et al., 1998; Goericke et al., 2000; Ravichandran et al., 2012), at times occurring in layers  
1401 below the oxyclines of the oxygen minimum zone (Goericke et al., 2000). These features are strongly influenced by  
1402 mesoscale features (Gundersen et al., 1998).

1403  
1404 During the southwest monsoon off Oman and Somalia, the presence of the topographically-locked eddies generate strong  
1405 offshore flows that advect high nutrient, high Chl-*a* concentrations and coastal phytoplankton communities hundreds of  
1406 kilometers offshore (Keen et al., 1997; Latasa and Bidigare, 1998; Manghnani et al., 1998; Gundersen et al., 1998;  
1407 Hitchcock et al., 2000; Lee et al., 2000; Kim et al., 2001). These advective effects can be seen, for example, in association  
1408 with the Great Whirl off the coast of northern Somalia (Hitchcock et al., 2000) and in the filaments that develop off the  
1409 Arabian Peninsula during the southwest monsoon (Wiggert et al. 2005; Hood et al., 2017). In contrast, during the northeast  
1410 monsoon, the circulation and winds transition to downwelling favourable. During the northeast monsoon, cold dry  
1411 northeasterly winds from southern China and the Tibetan Plateau flow across the northern Arabian Sea. The sheer from  
1412 these winds, combined with surface cooling and buoyancy-driven convection, drive mixing and entrainment of nutrients  
1413 that, in turn, promote modest increases in chlorophyll and primary production over the northern Arabian Sea (Wiggert et  
1414 al., 2000; Wiggert et al., 2005; Fig. 5; Figs. 5 and 6 in Hood et al., 2017). These increases in Chl-*a* have been associated  
1415 with increased diatom abundance (Banse and McClain, 1986; Sawant and Madhupratap, 1996). In the last decade,  
1416 however, there appears to have been a shift in the composition of winter phytoplankton blooms in the northern and central  
1417 Arabian Sea from diatom dominance to blooms of a large, green mixotrophic dinoflagellate, *Noctiluca scintillans* (Gomes  
1418 et al., 2014; Goes et al., 2020).

1419  
1420 During the southwest monsoon, the upwelling-favorable WICC induces upwelling along the west coast of India, which  
1421 increases Chl-*a* concentrations by more than 70% compared to the central Arabian Sea (Kumar et al., 2000; Naqvi et al.,  
1422 2000; Luis and Kawamura, 2004; Hood et al., 2017). The increased Chl-*a* concentrations near the coast are associated

Deleted: ).

Deleted: ).

with increases in diatom abundance (Sawant and Madhupratap, 1996). However, these increases in Chl-*a* and their offshore extent are modest compared to the western Arabian Sea (Fig. 5; Fig. 5 in Hood et al., 2017). In contrast, during the northeast monsoon the WICC is downwelling-favorable and tends to suppress primary production off the southwestern coast of India. The depletion of nutrients in this region during the northeast monsoon coincides with blooms of *Trichodesmium* and dinoflagellate species (Parab et al., 2006; Matondkar et al., 2007) resulting in the extremely high rates of nitrogen fixation (Gandhi et al., 2011, Kumar et al., 2017). However, as discussed above, further north and offshore, nutrient entrainment enhances phytoplankton biomass and primary production during the northeast monsoon (Wiggert et al., 2000; McCreary et al., 2001; Luis and Kawamura, 2004; Gomes et al., 2014; Goes et al., 2020; Fig. 5). Near-surface Chl-*a* and primary production off the west coast of India (estimated from satellite ocean color measurements) increases from ~9 to 24 mgChl *a* m<sup>-2</sup> and from ~1 to 2.25 g C m<sup>-2</sup> d<sup>-1</sup>, respectively, from winter to the summer monsoon (Luis and Kawamura, 2004; Fig. 5; Figs. 5 and 6 in Hood et al., 2017). The elevated productivity during the southwest monsoon is modulated by the coastal Kelvin waves that originate from the Bay of Bengal and propagate along the West Indian Shelf, modifying circulation patterns and upwelling (Luis and Kawamura, 2004).

## 5 Inter-ocean exchange

### 5.1 Indonesian Throughflow

#### 5.1.1 General features

The Indonesian Throughflow (ITF) transfers low-salinity tropical waters from the Pacific to the Indian Ocean via the Indonesian seas (Fig. 10). The ITF is the only tropical oceanic pathway that links ocean basins and plays an important role in the global ocean circulation and climate system (Sprintall et al., 2014; 2019). The simultaneous measurements in the exit channels of the ITF from the International Nusantara Stratification and Transport (INSTANT) program during 2004-2006 (Gordon et al., 2008; Sprintall et al., 2009) suggested that the ITF has a mean transport of 15 Sv into the Indian Ocean. The ITF pathway is composed of many narrow channels within the Indonesian seas, among which about 80% of the total ITF is through the Makassar Strait (Fig. 10, Gordon et al., 2008, 2010). The remaining passages include the Maluku Sea, Lifamatola Passage, Karimata Strait and Sibutu Passage (Fang et al., 2010; Gordon et al., 2012; Susanto et al., 2013).

#### 5.1.2 Variability, dynamics and influence

The interannual variability of the ITF is mainly dictated by the ENSO-related wind forcing through the Pacific waveguide with stronger transport during La Niña years (Meyers, 1996; England and Huang, 2005; Hu and Sprintall, 2016), but the IOD occasionally offsets the Pacific ENSO influences through the Indian Ocean wind variability and Indian Ocean

1454 waveguide (Sprintall and Révelard, 2014; Liu et al. 2015; Feng et al., 2018). For the strong negative IOD event in 2016,  
1455 the Indian Ocean influence overwhelmed that of the Pacific leading to record low ITF volume transports because of the  
1456 reduction in the interbasin pressure gradient (Pujiana et al., 2019). Strong wind forcing over the equatorial Indian Ocean  
1457 triggers equatorial Kelvin waves and influences the ITF variability on intraseasonal, semi-annual and interannual time  
1458 scales (Drushka et al., 2010; Pujiana et al., 2013; Shinoda et al., 2012). Kelvin waves through the Indian Ocean waveguide  
1459 are suggested to influence the interannual variability in the tropical Pacific Ocean (Yuan et al., 2013; Pujiana and  
1460 McPhaden, 2020).

1461 The ENSO cycle also influences the outflowing ITF transport through the salinity effect in the downstream buoyant pool,  
1462 contributing about 36% of the total ITF interannual transport variation (Hu and Sprintall, 2016; Section 6.1). Fresh  
1463 anomalies in the buoyant pool during La Nina years can be as large as 0.2 in practical salinity averaged over the upper 180  
1464 m of the water column (Phillips et al. 2005). Such salinity anomalies can strengthen the volume transport of the LC through  
1465 an increase in the zonal density gradient driving stronger southward flow (Feng et al., 2015a). The Inter-decadal Pacific  
1466 Oscillation/Pacific Decadal Oscillation (IPO/PDO), through modulations of decadal wind stress in the tropical Pacific, has  
1467 also directly influenced the strength of the ITF (Feng et al., 2011; Hu et al., 2015; Mayer et al., 2018). This has, in turn  
1468 influenced heat and freshwater transports, causing upper ocean heat content to increase in the southern Indian Ocean (Feng  
1469 et al., 2010; Schwarzkopf and Böning, 2011; Nidheesh et al., 2013; Sprintall, 2014; Lee et al., 2015; Nieves et al., 2015;  
1470 Du et al., 2015; Ummenhofer et al., 2017) and produced interhemispheric contrasts in sea surface temperature (Dong and  
1471 McPhaden, 2016). During the negative IPO phase, such as during the hiatus in warming of the globally averaged surface  
1472 atmosphere (1998-2012), enhanced trade winds in the Pacific strengthened the ITF volume and heat transport into the  
1473 Indian Ocean, driving a rapid warming trend in the Southern Indian Ocean (England et al., 2014; Nieves et al., 2015; Lee  
1474 et al., 2015; Liu et al., 2015, Zhang et al., 2018). Contributions from air-sea exchanges (Jin et al. 2018a,b) have also been  
1475 suggested to be important, as has a reduction in the oceanic heat exported from the Indian Ocean at its southern boundary  
1476 (Lisa Beal, personal communication).

1477 Using a combination of theory, ocean reanalyses, OGCM simulations, and coupled climate model simulations, Jin et al.  
1478 (2018a,b) found eastern and western Indian Ocean heat content to be affected by remote Pacific forcing through two  
1479 distinct mechanisms: oceanic influences transmitted through the ITF and the atmospheric bridge. The intensified  
1480 freshwater input within the Maritime Continent during the past decade was found to strengthen the ITF and its heat and  
1481 freshwater transports into the Indian Ocean, causing significant warming and freshening trends and accelerated sea-level  
1482 rise in the eastern Indian Ocean (Hu and Sprintall, 2017a, 2017b; Zhang et al., 2018; Jyoti et al., 2019). The decadal  
1483 enhancement of the ITF transport has increased upper ocean heat content anomalies in the southeast Indian Ocean and  
1484 increased the likelihood of marine heatwaves off the west coast of Australia (Feng et al., 2015b; Section 6.4).

## 1485    **5.2 Agulhas Leakage**

### 1486    **5.2.1 General features**

1487    At the tip of Africa, the southward-flowing Agulhas Current retroflects with most of the flow heading eastwards along the  
1488    northern edge of the ACC, recirculating back into the Indian Ocean (Fig. 10, Section 4.2.2). Around 20-30% of the  
1489    Agulhas Current enters the Atlantic Ocean as Agulhas leakage in the form of Agulhas rings and cyclones (van Seville,  
1490    2010a). Agulhas leakage estimates are sensitive to the definition used to calculate the leakage, ranging roughly between  
1491    10 and 20 Sv (van Seville et al., 2010b; Beron-Vera et al., 2013; Cheng et al., 2016; Holton et al., 2017). Bars et al. (2014)  
1492    proposed an algorithm to measure Agulhas leakage anomalies using absolute dynamic topography data from satellites.

1493    The division of flow between Agulhas Leakage and Agulhas retroflexion can be influenced by the upstream Agulhas  
1494    Current. In a Lagrangian particle tracking experiment, van Seville et al. (2009) found that a weaker Agulhas Current,  
1495    detaching farther downstream and generating anti-cyclonic vorticity, potentially leads to more Agulhas leakage and larger  
1496    Indian-Atlantic inter-ocean exchange. However, eddy-resolving model results suggest that as model resolution increases,  
1497    the sensitivity of the leakage to Agulhas Current transport anomalies is reduced (Loveday et al., 2014). In addition, the  
1498    ITF potentially influences the Agulhas leakage (Le Bars et al., 2013) as model outputs suggest that the Indian Ocean  
1499    contributes 12.6 Sv to the Agulhas leakage, half of which is from the ITF (Durgadoo et al., 2017).

### 1500    **5.2.2 Variability, dynamics and influence on climate**

1501    The magnitude of the Agulhas leakage is controlled by wind forcing including the trade winds and the Southern  
1502    Hemisphere Westerlies (e.g., Durgadoo et al., 2013). The poleward shift in the Southern Hemisphere westerlies associated  
1503    with anthropogenic forcing induced a clear increase in the Agulhas leakage during 1995-2004 as shown in numerical  
1504    simulations (Biaostoch et al., 2009; Biaostoch and Böning, 2013). Increased wind stress curl in the South Indian Ocean  
1505    associated with the southward shift of westerlies led to significant warming in the Agulhas Current system since the 1980's  
1506    (Rouault et al., 2009); however further work showed that this is due to an increase in eddies leading to a broadening of the  
1507    current as opposed to intensification (Beal and Elipot, 2016). Given the non-linear nature of Agulhas leakage, the difficulty  
1508    of observing it and ocean model biases in the region, quantifying Agulhas leakage is very challenging (Holton et al., 2017).  
1509    At seasonal time scales, the Agulhas leakage variability is controlled by eddies, however recent studies have shown that  
1510    eddies might not contribute as significantly to leakage as was thought and the non-eddy leakage transport is likely to be  
1511    constrained by large-scale forcing at longer time scales (e.g., Cheng et al., 2018). A recent study shows that the subsurface  
1512    signal from the ENSO cycle influences the Agulhas leakage through Rossby waves with a time lag of 2 years (Paris et al.,  
1513    2018).



1514 The Agulhas leakage carries warm and saline water from the Indo-Pacific Ocean into the Atlantic Ocean. The Agulhas  
1515 leakage has been suggested to influence the Atlantic Meridional Overturning Circulation strength (AMOC; Beal et al.  
1516 2011; Weijer and van Sebille, 2014; Biastoch et al. 2015) and modify the AMOC convective stability (e.g., Haarsma et  
1517 al., 2011; Caley et al., 2012; Castellanos et al., 2017). It is suggested that the increases in the Agulhas leakage due to  
1518 anthropogenic warming during the past decades would act to strengthen the Atlantic overturning circulation (e.g., Beal et  
1519 al., 2011).

1520 The Agulhas leakage is an important source of decadal variability in the AMOC through Rossby waves (Biastoch et al.,  
1521 2008; 2015). Source waters from the Agulhas Current take more than four years and mostly one to four decades to arrive  
1522 in the North Atlantic Ocean (van Sebille et al., 2011; Rühls et al., 2013). The increased Agulhas leakage during 1995-2004  
1523 has contributed to the salinification of the South Atlantic thermocline waters (Biastoch et al., 2009). Hindcast experiments  
1524 suggest that the Agulhas leakage increased by about 45% during the 1960s-2000s, leading to the observed warming trend  
1525 in the upper tropical Atlantic Ocean (Lübbecke et al., 2015).

### 1526 **5.3 Supergyre connection to the South Pacific**

1527 The extreme strong westerly wind stress in the Southern Hemisphere gives rise to a wide and energetic subtropical  
1528 supergyre (Figure 16), the Southern Hemisphere supergyre, that connects three ocean basins (e.g., Ridgway and Dunn,  
1529 2007; Speich et al., 2007; Lambert et al., 2016; Maes et al., 2018; Cessi, 2019). Although the near-surface circulation is  
1530 eastward across the southern Indian Ocean, there are subsurface westward flows beneath (Section 4.2.3; Schott and  
1531 McCreary 2001; Domingues et al. 2007; Furue et al. 2017), and the depth-integrated circulation reveals the westward  
1532 return flow of the equatorward side of the Indian Ocean's anti-clockwise subtropical gyre. In Figure 16, the southern side  
1533 of the Indian Ocean subtropical gyre extends eastward south of Australia to connect with the western Pacific subtropical  
1534 gyre. The return flow is accomplished via a pathway that includes the East Australian Current, the South Pacific's western  
1535 boundary flow; the Tasman Leakage, a westward flow south of Tasmania that carries Pacific Ocean water back to the  
1536 Indian Ocean (distinct from the Flinders Current that hugs the continental slope, Duran et al 2020; Section 4.2.4); and  
1537 northwestward flow in the eastern Indian Ocean to close the circulation. The ITF and Leeuwin Current are also part of the  
1538 supergyre, connecting the Indian and Pacific Oceans through the Indonesian seas (e.g. Ridgway and Dunn, 2007).

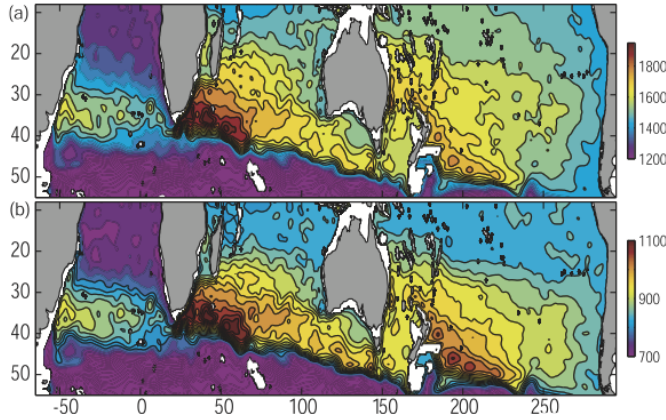
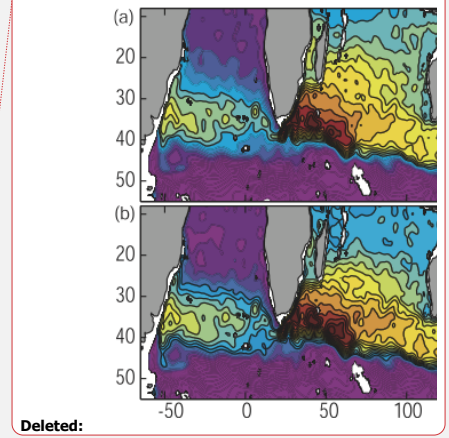


**Figure 16: The interbasin supergyre system for the Pacific and Indian Oceans as shown by the depth-integrated steric height (a)  $P_0/2000$ , and (b)  $P_{400}/2000$ , derived from the CARS climatological temperature and salinity fields. The contour interval in (a) is  $50 \text{ m}^2$  and in (b) is  $25 \text{ m}^2$ . Taken from Ridgway and Dunn 2007.**

The supergyre is the subtropical gyre of the southern hemisphere. As such, its flow is primarily determined by the westward integration of wind stress curl from the eastern boundaries as determined by Sverdrup dynamics. The latitudinal position of the Subtropical Front at the southern edge of the supergyre is found to be controlled by strong bottom pressure torque due to the interaction between the ACC and the ocean floor topography (De Boer et al., 2013). According to one analysis in SODA (Simple Ocean Data Reanalysis), the water masses in the supergyre became cooler and fresher and shifted southward by about  $2.5^\circ$  due to changes in the basin-scale wind forcing during 1958–2007 (Duan et al., 2013). A recent study using altimeter observations shows a clear strengthening of the Southern Hemisphere supergyre in all three oceans since 1993 as indicated in the large trends of sea surface height and their contrast. Argo observations and ECCO assimilations suggest that the strengthening extends to deeper than 2000 m (Qu et al., 2019). The spin-up of the Southern Hemisphere supergyre is attributed to the poleward shift and strengthening of westerly winds that are linked to an increasingly positive southern annular mode (Qu et al., 2019).

#### 5.4 Roles of salinity in inter-ocean exchange

Ocean salinity is one of the basic variables that determines the oceanic stratification, sea level change and climate change (e.g., Llovel and Lee, 2015; Kido and Tozuka, 2017; Sprintall et al., 2019). However, the role of salinity in ocean circulation has been largely underestimated until the recent decade when *in situ* observations of subsurface and surface



Deleted:

1559 salinity from Argo and satellite salinity missions became available. These new observations have revolutionized our  
1560 understanding of the influence of salinity on ocean circulation and dynamics (Vinogradova et al. 2019, and references  
1561 therein).

1562

1563 Four major processes control the salinity in the Indian Ocean: net air-sea fluxes (evaporation minus precipitation),  
1564 freshwater inflow from large rivers in the Bay of Bengal, inflow of relatively fresh waters from the Pacific Ocean via the  
1565 Indonesian Throughflow, and inflow of saltier waters from the Red Sea and the Persian and Arabian Gulfs. These different  
1566 drivers combine to give the Indian Ocean salinity its unique flavour: a strong east-west gradient in the North Indian Ocean  
1567 (salty in the Arabian Sea and fresh in the Bay of Bengal) and strong north-south gradients in the South Indian Ocean (fresh  
1568 in the tropics, and salty in the subtropics) (Fig. 4).

1569

1570 Salinity is a crucial variable to understand Indian Ocean dynamics. For instance, salinity has strong ties with the Indian  
1571 Ocean Dipole (e.g., Du and Zhang, 2015; Durand et al., 2013; Grunseich et al., 2011; Kido and Tozuka, 2017; Nyadjro  
1572 and Subrahmanyam, 2014; Zhang et al. 2016; Section 6.2), the EGC (Menezes et al., 2013; Section 4.2.3), LC transport,  
1573 Ningaloo Niño and marine heatwaves off western Australia (e.g., Feng et al., 2015a), and the El Niño/La Niña climate  
1574 mode (e.g., Hu and Sprintall, 2016; Zhang et al., 2016). Salinity plays an essential role in the dynamics of the seasonal  
1575 Wyrtki Jets in the equatorial zone (e.g., Masson et al., 2003), extra-equatorial Rossby waves (Heffner et al., 2008; Menezes  
1576 et al., 2014b; Vargas-Hernandez et al., 2015; Banks et al., 2016), Madden-Julian and Intraseasonal Oscillations (e.g.,  
1577 Grunseinch et al., 2013; Guan et al., 2014; Subrahmanyam et al., 2018), barrier-layer dynamics (e.g., Drushka et al., 2014;  
1578 Felton et al., 2014), and the North Indian Ocean (e.g., D’Addezio et al., 2015, Fournier et al., 2017; Mahadevan et al.,  
1579 2016; Nyadjro et al., 2011, 2012, 2013; Wilson and Riser, 2016; Spiro Jaeger and Mahadevan, 2018).

1580

1581 Salinity variability within the Indonesian Seas has been shown to control the transport of the ITF. Andersson and  
1582 Stigebrandt (2005) proposed that a downstream buoyancy pool in the outflowing ITF region acts to regulate the ITF  
1583 transport. Gordon et al. (2003, 2012) pointed out that low salinity surface water from the South China Sea is drawn into  
1584 the Java Sea. Combined with the monsoonal precipitation over the Maritime Continent and seasonal monsoon winds, this  
1585 freshwater plug contributes to the seasonal fluctuation of the Makassar Strait Throughflow transport and inhibits the inflow  
1586 of tropical Pacific surface water from the Mindanao Current (e.g., Gordon et al., 2012; Lee et al., 2019). Recently, Hu and  
1587 Sprintall (2016) found that about 36% of the interannual ITF transport is attributable to the salinity effect associated  
1588 with freshwater input anomalies due to the ENSO cycle. Jyoti et al. (2019) further examined this salinity effect and found  
1589 that the unprecedented sea-level rise in the southern Indian Ocean since the beginning of the 21st Century is attributed to  
1590 the accelerated heat and freshwater intrusion by the ITF. A significant strengthening of the ITF transport in the 2000s has  
1591 given rise to a subsequent warming and freshening of the eastern Indian Ocean (e.g., Hu and Sprintall, 2017a, 2017b,

1592 Section 6.1). The southeast Indian Ocean is one of the few places in the global ocean where the halosteric component of  
1593 sea level rise is as large as the thermosteric component (Llovel and Lee, 2015).  
1594

1595 **6 Modes of Interannual Climate Variability in the Indian Ocean**

1596 **6.1 ENSO teleconnection and the Indian Ocean Basin mode**

1597 ENSO influences the Indian Ocean circulation through the Pacific-to-Indian Ocean oceanic waveguide and atmospheric  
1598 teleconnections. Through the atmospheric bridge, El Niño conditions in the Pacific induce an anticyclonic wind anomaly  
1599 pattern in the southeast Indian Ocean (Xie et al., 2002), whereas La Niña induces a cyclonic wind anomaly pattern (Feng  
1600 et al., 2013). The ENSO teleconnection also drives SST variability over the western Indian Ocean during ENSO  
1601 development. The tropical Indian Ocean experiences prolonged warming (cooling) that peaks in the following boreal  
1602 spring and persists into boreal summer, after the decay of El Niño (La Niña) events, the so-called Indian Ocean Basin  
1603 (IOB) mode (Yang et al., 2007). The westward propagating Rossby waves induced by ENSO may also help sustain the  
1604 warming (cooling) of the tropical Indian Ocean (Xie et al., 2002), fueled by regional air-sea coupling (Du et al., 2009).  
1605 The IOB warming has a capacitor effect for El Niño to influence boreal summer climate, such as for the Indian monsoon  
1606 (Zhou et al., 2019), and remote impacts in the northwest Pacific (Xie et al., 2009, 2016), including China and Japan (Hu  
1607 et al., 2019). Details of the Indo-Western North Pacific capacitor effect are summarized in Xie et al. (2016) and Kosaka et  
1608 al. (2021). The relationship between ENSO and IOB varies on decadal time scales (e.g., Xie et al., 2010; Chowdary et al.,  
1609 2012 and under global warming scenarios. The IOB warming tends to persist longer after El Niño events according to  
1610 CMIP5 model simulations (Zheng et al., 2013).

1611 The ITF variability lags ENSO by 8-9-months, found in ocean model results (England and Huang, 2005) and derived from  
1612 the geostrophic transport across an Australia-Indonesia XBT section (Liu et al., 2015). The variability of the ITF transport  
1613 drives sea level and upper ocean heat content anomalies in the southeast Indian Ocean. Through the waveguide, ENSO  
1614 has a direct influence on the strength of the Leeuwin Current (Section 4.2.4), with a stronger poleward volume and heat  
1615 transport during a La Niña event (Feng et al., 2008). A stronger Leeuwin Current during La Niña events leads to greater  
1616 baroclinic instability of the current and enhanced generation of eddies that leads to interannual variability of the eddy  
1617 kinetic energy in the southeast Indian Ocean (Feng et al., 2005; Zheng et al., 2018). The increase of the ITF transport and  
1618 enhancement of rainfall in the Indonesian Seas during strong La Niña events can drive up to 0.2-0.3 psu freshening  
1619 anomalies in the upper southeast Indian Ocean (Phillips et al., 2005; Feng et al., 2015a; Hu and Sprintall, 2017a; Section  
1620 5.1.2), which may have a compound effect in accelerating the Leeuwin Current (Feng et al., 2015a). Both ENSO and the

- Deleted:** evolves
- Deleted:** a
- Deleted:** scale, and the persistent IOB warming after El Niño has been evident since the 1970s (
- Deleted:** ). Based on the CMIP5 multi-model experiments, the
- Deleted:** the
- Deleted:** under global warming scenarios

1628 IOD (see Section 6.2) influence the ITF and thus the exchange of heat from the Pacific into the Indian Ocean, but in  
1629 concurrent IOD and ENSO events it appears that the influence from the IOD dominates (Sprintall and Revelard, 2014).

1630 Due to the opposing effects of the winds and dissipation, ENSO induced sea level and upper ocean heat content anomalies  
1631 in the southeast Indian Ocean do not propagate far into the western Indian Ocean; instead, wind anomalies generate sea  
1632 level and heat content anomalies of opposite signs in the western Indian Ocean through Rossby wave propagations  
1633 (Masumoto and Meyers, 1998; Xie et al., 2002; Zhuang et al., 2013; Ma et al., 2019; Volkov et al., 2020; Nagura and  
1634 McPhaden, 2021). Thus, the joint forcing of the oceanic waveguide and atmospheric teleconnection results in variations  
1635 of meridional overturning circulation and heat transport in the Indian Ocean on a multi-year time scale, in phase with the  
1636 ITF variability (Ma et al., 2019).

## 1637 **6.2 The Indian Ocean Dipole**

1638 There is increasing evidence that positive IOD events are more frequent and intense during the 20th century (e.g., Abram  
1639 et al., 2008; Cai et al., 2013; Abram et al., 2020a,b; and references therein). A rare occurrence of three consecutive positive  
1640 IOD events took place in 2006–2008 (Cai et al., 2009b). The skewness towards more positive and fewer negative IOD  
1641 events (Cai et al., 2009a) is due potentially to an anthropogenically-driven shoaling thermocline in the eastern Indian  
1642 Ocean (Cai et al., 2008). The three consecutive positive IOD events rarely occurred in Coupled Model Intercomparison  
1643 phase 5 (CMIP5) models and the more recent frequent occurrence was consistent with regional Indo-Pacific Walker  
1644 circulation trends (Cai et al., 2009c,d). An anthropogenic contribution was proposed since positive IOD events became  
1645 more frequent over the period 1950–1999 in the CMIP5 models. Projected mean-state changes in the Indian Ocean with  
1646 stronger easterly winds and a shoaling thermocline in the southeast Indian Ocean during austral spring favour positive  
1647 IOD development, with a reduction in skewness between positive and negative IOD events likely (Cai et al., 2013; Figure  
1648 17), and a three-fold increase in frequency of extreme positive IOD events by 2100 compared to the previous century (Cai  
1649 et al., 2014a). However, model biases in Indian Ocean mean-state and IOD variability challenge these projected changes:  
1650 models with excessive IOD amplitude bias tend to project a strong IOD-like warming pattern and increase in extreme  
1651 pIOD occurrences, consistent with an enhanced Bjerknes feedback, and hence the projected IOD changes could represent  
1652 spurious artefacts of model biases (Li et al., 2016). Yet, paleoclimate evidence supports trends observed in recent decades:  
1653 based on a millennial IOD reconstruction from corals, extreme positive IOD events, as were observed in 1997 and 2019,  
1654 were historically rare (Abram et al., 2020b). In the reconstruction, only ten extreme positive IOD events occurred and yet  
1655 four events occurred in the last 60 years (Abram et al., 2020b). The increase in event frequency and intensity highlights  
1656 the need to improve preparedness in regions affected by IOD events to minimize future climate risks posed by them.

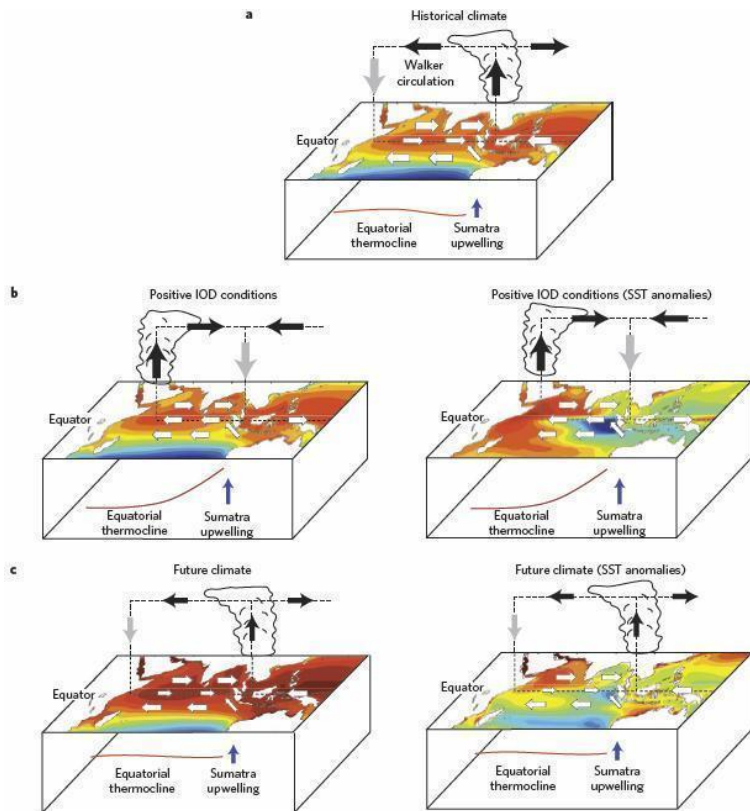
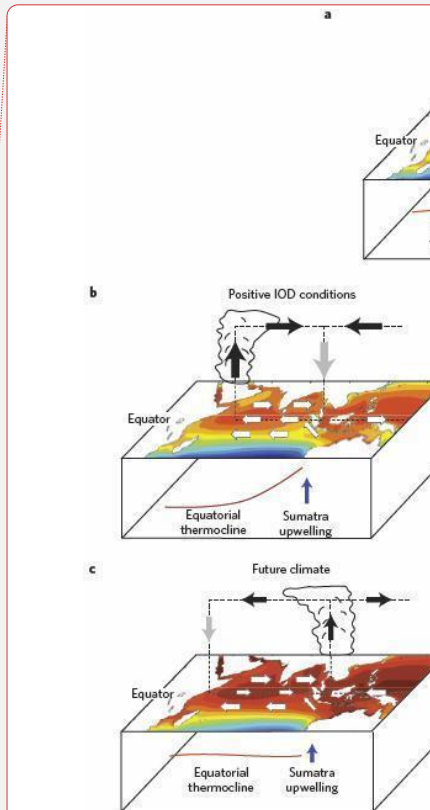


Figure 17: Historical austral spring mean climate and positive IOD conditions for the twentieth century, and future austral spring mean climate. a, Historical mean climate, indicating SSTs, surface winds, the associated atmospheric Walker circulation, the mean position of convection and the thermocline. In the western Indian Ocean, the descending branch is broad and not well-defined, as indicated by a grey arrow. b, Typical conditions during a positive IOD event. c, Projected future mean climate based on a CMIP5 multi-model ensemble average. Diagrams with total SST fields are shown on the left; diagrams with SST anomalies referenced to the 1961–1999 mean for b,



1665 and referenced to the basin mean for c, are shown on the right. Reprinted from Cai et al. (2013) with permission  
1666 from Springer Nature.

1667 While model simulations and paleo proxy records suggest changes in the frequency and magnitude of IOD events in a  
1668 warming climate, there is less observational evidence from other sources. Given the short observational record in the  
1669 Indian Ocean, the role of decadal to multi-decadal variability across the broader Indo-Pacific region has recently emerged  
1670 as a compounding factor: the number and frequency of IOD events have been observed to vary on decadal timescales.  
1671 Decadal variations in SST featuring an IOD-like out-of-phase pattern between the western and eastern tropical Indian  
1672 Ocean have been linked to the PDO (Krishnamurthy and Krishnamurthy, 2016) or IPO (Dong et al., 2016). A combination  
1673 of processes transmits the signal from the Pacific to the Indian Ocean through both the atmospheric and oceanic bridges,  
1674 leading to variations in the subsurface temperature structure in the Indian Ocean (Zhou et al., 2017; Jin et al., 2018a).  
1675 Decadal modulations of the background state of the eastern Indian Ocean thermocline depth can thus pre-condition the  
1676 Indian Ocean to more or less IOD events (Annamalai et al., 2005). Consequently, positive IOD events were unusually  
1677 common in the 1960s and 1990s with a relatively shallow eastern Indian Ocean thermocline, while the deeper thermocline  
1678 in the 1970s and 1980s was associated with frequent negative IOD and rare positive IOD events (Ummenhofer et al.,  
1679 2017). The Indian Ocean stands out as a region with high skill in decadal predictions (Guemas et al., 2013) and improved  
1680 understanding of decadal modulation of IOD events can aid in decadal prediction efforts for the Indian Ocean region.

1681 The relationship between ENSO and the IOD has been subject to ongoing debate. Recent research has shown that around  
1682 two-thirds of IOD variability arises as a remote response to ENSO (Stuecker et al., 2017; Yang et al., 2015), with the  
1683 remaining variability being independent of ENSO. Stuecker et al. (2017) argue that the ENSO-driven IOD can be seen as  
1684 a combination of remotely driven wind and heat flux anomalies modulated by seasonally-varying Bjerknes feedback in  
1685 the Indian Ocean. Further, they suggest that the ENSO-independent IOD events arise out of white noise atmospheric  
1686 forcing coupled to these feedbacks (Stuecker et al., 2017). Variability internal to the Indian Ocean basin and unrelated to  
1687 ENSO, arising from ocean-atmosphere feedback processes, does however modulate the evolution of IOD events and can  
1688 lead to early termination of IOD events; as a result, including internal variability improves the predictability of the IOD  
1689 (Yang et al., 2015). IOD variability internal to the Indian Ocean resembles recharge oscillator dynamics for ENSO, but  
1690 equatorial heat content is less effective as a precursor for the IOD than for ENSO because of the strong impact of remote  
1691 forcing from the Pacific on the IOD. Internal Indian Ocean dynamics however may contribute to the biennial nature of  
1692 the IOD through the cycling of Kelvin/Rossby wave energy across the basin (McPhaden and Nagura, 2014). The  
1693 relationship between ENSO and the IOD is not only one-way: IOD events have also been shown to influence the  
1694 development of ENSO in the following year (Izumo et al., 2010; Wang et al., 2019; Cai et al., 2019; and references therein).

1695 Different types of IOD events have been described, each with distinct evolution and regional impacts (Du et al., 2013;  
1696 Endo and Tozuka, 2016). Du et al. (2013) distinguished three types of IOD events according to the timing of their peak

1697 amplitude and overall duration: ‘unseasonable’ events that develop and mature mostly within June-August (JJA), ‘normal’  
1698 events that develop and mature mostly within September-November (SON), and ‘prolonged’ events that develop in JJA  
1699 and mature in SON, with the latter two described as the canonical IOD events (Du et al., 2013). The unseasonable IOD  
1700 events have only been observed since the mid-1970s and have been suggested to be a response to the rapidly warming  
1701 Indian Ocean SST and a weakened Walker circulation during austral winter (Du et al., 2013). The seasonal evolution and  
1702 type of ENSO also seems to play a role in determining the IOD evolution and type, with atmospheric influences transmitted  
1703 through variations in the Walker Circulation and oceanic ones through anomalous oceanic Rossby waves affecting timing  
1704 and evolution of IOD events, especially during their developing phase (Guo et al., 2015; Zhang et al. 2015; Fan et al.,  
1705 2017). However, Sun et al. (2015) suggested more IOD events independent of ENSO since the 1980s, along with higher  
1706 correlations between the IOD and Indian summer monsoon activity, likely due to mean-state change in the tropical Indian  
1707 Ocean due to weaker equatorial westerlies. The relationship between ENSO and the IOD has weakened in recent decades,  
1708 linked to changes in the ENSO-induced rainfall anomalies over the Maritime Continent (Han et al., 2017).

1709 Recent advances in understanding variability and change in IOD characteristics have implications for the relationships  
1710 between SST and regional rainfall patterns in Indian Ocean rim countries. For example, different types of IOD events  
1711 exhibit distinct regional impacts, with only the canonical events associated with enhanced rainfall over East Africa due to  
1712 the low-level moisture convergence over the region (Endo and Tozuka, 2016). The effect of Indian Ocean SST on East  
1713 African rainfall is most pronounced during the short rains (September-November), though Williams and Funk (2011)  
1714 argued that warming Indian Ocean SST in recent decades was also associated with reduced long rains for the March-June  
1715 season in Ethiopia and Kenya. Changes in the tropical atmospheric circulation across the Indo-Pacific on multi-decadal  
1716 timescales (Vecchi and Soden, 2007; L’Heureux et al., 2013) have further implications for the relationship between Indian  
1717 Ocean SST and regional rainfall: When the Pacific Walker cell weakened and the Indian Ocean one strengthened post-  
1718 1961, the East African short rains became more variable and wetter (Nicholson, 2015). Similarly, Manatsa and Behera  
1719 (2013) described an epochal strengthening in the relationship between the IOD and East African rainfall post-1961, with  
1720 73% of short rain variability in East Africa explained by the IOD, up from 50% in previous decades. After 1997, this  
1721 increased further to 82%, explaining spatially coherent events across the region and frequent rainfall extremes (Manatsa  
1722 and Behera, 2013). Recent observed and projected changes in frequency and intensity of IOD events highlight the  
1723 increasing need for preparedness in vulnerable regions affected by these events. One such event is the recent 2019 positive  
1724 IOD, the largest IOD on record since the 1960s (Du et al. 2020), which was linked to unusual hydroclimate around the  
1725 Indian Ocean rim and further afield. It was linked to extreme rainfall and floods in East Africa (e.g., Wainwright et al.,  
1726 2021), anomalously wet Indian monsoon season (Ratna et al., 2021), abnormally warm conditions in many parts of East  
1727 Asia (Doi et al., 2020), unusually wet subsequent summer monsoon season in Japan and China due to downwelling Rossby  
1728 waves that had affected Western Pacific SST (Takaya et al. 2020; Zhou et al., 2021), and was seen as a contributing factor  
1729 to the severe bushfire season experienced in Australia in 2019/2020 (e.g., Wang and Cai, 2020). The 2019 IOD was unique

Deleted: Indian Ocean Dipole

Deleted: caused

Deleted: over

Deleted: 2021).



1734 in that it developed independently from any El Nino events and resulted from westward propagating Rossby waves in the  
1735 southwest tropical Indian Ocean (Du et al., [2020](#)) and/or an interhemispheric pressure gradient over the Maritime continent  
1736 ([Lu and Ren, 2020](#)).

#### 1737 **6.2.1 Biogeochemical Variability**

1738 IOD events are associated with distinct changes in primary productivity, as measured by chlorophyll. During positive IOD  
1739 events, increased chlorophyll indicative of phytoplankton blooms is apparent in the normally oligotrophic eastern Indian  
1740 Ocean in fall (Wiggert et al., 2009; Currie et al., 2013). Positive chlorophyll anomalies occur in the southeastern Bay of  
1741 Bengal in boreal winter, while negative anomalies are observed over much of the Arabian Sea and southern tip of India.  
1742 In a case study of the 2006 positive IOD event, Iskandar et al. (2010) using an eddy-resolving biophysical model found  
1743 the offshore chlorophyll signal in the southeastern Indian Ocean to be associated with regions of high eddy kinetic energy  
1744 implying that cyclonic eddies injected nutrient-rich water into the upper layer enabling the bloom. Currie et al. (2013)  
1745 emphasize the importance of assessing the relative contributions of IOD events and remote impacts from ENSO on primary  
1746 productivity in the Indian Ocean through their respective influence on upper-ocean properties for improved understanding  
1747 and ultimately predictions of productivity, ecosystems, and fisheries within the basin. Little attention has been paid so far  
1748 to resultant effects of these blooms on biogeochemical cycling (Wiggert et al., 2009).

#### 1749 **6.3 The subtropical Indian Ocean Dipole**

1750 The subtropical Indian Ocean Dipole (SIOD) is a climate mode in the southern Indian Ocean, which tends to arise and  
1751 peak in the austral summer (Behera and Yamagata, 2001). During the SIOD's positive phase, the climate mode has positive  
1752 SST anomalies in the southwestern Indian Ocean and negative SST anomalies in the northeastern region (Behera and  
1753 Yamagata, 2001; Suzuki et al., 2004; Hermes and Reason, 2005). During the positive phase, enhanced precipitation occurs  
1754 over southern Africa (Behera and Yamagata 2001; Reason 2001, 2002). Recent studies have shown that the SIOD affects  
1755 the Indian summer monsoon rainfall (Terry et al., 2003), rainfall over southwestern Australia (England et al., 2006) and  
1756 tropical cyclone trajectories in the southern Indian Ocean (Ash and Matyas, 2012).

1757 Initially, SST anomalies associated with the SIOD were considered to be generated directly by latent heat flux anomalies  
1758 (Behera and Yamagata, 2001). However, recent studies (Morioka et al. 2010, 2012) based on a mixed layer heat budget  
1759 analysis revealed the importance of mixed layer depth anomalies generated by latent heat flux anomalies. Wind anomalies  
1760 associated with the anomalous Mascarene High suppress latent heat loss and shoal the mixed layer in the southwestern  
1761 part, while latent heat release is enhanced and the mixed layer deepens anomalously in the northeastern part (Morioka et  
1762 al. 2010, 2012). With these changes in the upper ocean heat capacity, warming of the surface mixed layer by the

1763 climatological shortwave radiation is enhanced in the southwestern part and becomes less effective in the northeastern  
1764 part. As a result, the dipole SST anomalies appear in the southern Indian Ocean.

1765 Because the above mechanism operates more effectively as the thickness of the mixed layer becomes thinner, the return  
1766 period of the SIOD is becoming shorter associated with the shoaling trend of the mixed layer (Yamagami and Tozuka,  
1767 2015). Whether this mechanism is associated with decadal-to-interdecadal variations and/or global warming awaits further  
1768 study. Many coupled models are relatively successful in simulating the SIOD with some biases in the location and structure  
1769 of the SST anomaly (Kataoka et al., 2012). However, no study has examined if the SIOD is modulated by climate modes  
1770 of variability with decadal-to-interdecadal timescales or changes with global ocean warming.

#### 1771 **6.4 Ningaloo Niño and marine heatwaves in the Indian Ocean**

1772 The Ningaloo Niño (Niña) phenomenon is an interannual climate mode associated with anomalously warm (cold) water  
1773 in the eastern Indian Ocean (Feng et al., 2013; see Figure 18). This mode is seasonally phase-locked, with a peak during  
1774 austral summer (Kataoka et al., 2014). The mode exerts significant impacts on rainfall over Australia (Kataoka et al., 2014)  
1775 and affects marine ecosystems and fisheries (e.g. Pearce et al. 2011). The phenomenon can alter biological productivity,  
1776 with negative chlorophyll anomalies during Ningaloo Niño (Narayanasetti et al., 2016). Ningaloo Niños can develop in  
1777 response to remote ENSO forcing from the western Pacific transmitted as a coastally trapped wave (Kataoka et al., 2014).  
1778 During the La Niña events, high sea level anomalies propagate poleward along the west coast of Australia, intensifying  
1779 the Leeuwin Current and causing poleward advection of heat and anomalously warm waters (e.g. Benthuisen et al., 2014;  
1780 Section 4.2.4). Poleward transport of tropical, low salinity waters can further enhance the total geostrophic transport of  
1781 the Leeuwin Current (Feng et al., 2015a).

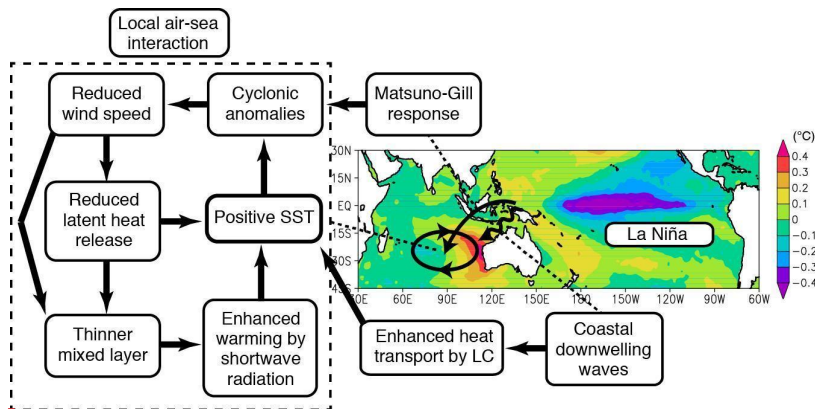
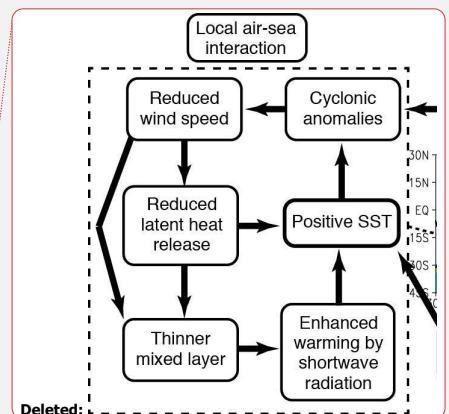


**Figure 18: Schematic diagram illustrating generation mechanisms (i.e. local air-sea interaction, atmospheric teleconnection, and oceanic wave propagation) of the Ningaloo Niño. SST anomalies are regressed against the Ningaloo Niño Index to illustrate typical SST anomalies associated with the phenomenon.**

Atmospheric teleconnection can further enhance the development of Ningaloo Niño. A reduction in southerly winds over the shelf, which would strengthen the Leeuwin Current, can arise through a Gill-type response with low sea level pressure anomalies in the southeast Indian Ocean owing to the Niño3.4 SST anomalies (Feng et al., 2013; Tozuka et al., 2014). Ningaloo Niños can arise from local air-sea interactions off western Australia, through the wind-evaporation-SST feedback during its initial stage (Marshall et al., 2015) and coastal SST-wind-Leeuwin Current (Bjerknes) feedback (Kataoka et al. 2014). In the coastal feedback mechanism, positive SST anomalies lead to northerly alongshore wind anomalies and coastal downwelling anomalies, causing enhancement of the positive SST anomalies (Kataoka et al., 2014). During the Ningaloo Niño's development phase, estimates of air-sea heat flux contributions have been found to be dependent on products and their resolution and bulk flux algorithms (Feng and Shinoda, 2019). Since the late 1990s, Ningaloo Niño events have occurred more frequently (Feng et al., 2015b). This decadal increase is corroborated by coral proxy records of Leeuwin Current strength, with the most extreme SST anomalies associated with Ningaloo Niños occurring since 1980 (Zinke et al., 2014).

More generally, marine heatwaves refer to prolonged, extremely warm water events. Over the past decade, most studies on marine heatwaves in the Indian Ocean have focused on the eastern sector of the Indian Ocean. Major events in the Indian Ocean have been associated with phases of ENSO. Along the west coast of Australia, marine heatwaves have occurred predominantly at subtropical reefs during La Niña events due to increased heat transport (Zhang et al., 2017).



1803 The term “marine heatwave” was first coined owing to a +5°C warm water event in 2011 off Western Australia during a  
1804 strong La Niña (Pearce et al., 2011). The 2011 event was associated with the strongest recorded Leeuwin Current transport  
1805 anomaly, bringing warm tropical waters south, and was partly due to air-sea heat fluxes (Feng et al., 2013; Benthuisen et  
1806 al., 2014).

1807 Across Australia’s northwestern shelf, marine heatwaves have been found to occur at tropical coral reefs from El Niño  
1808 due to solar radiation and a weakened monsoon (Zhang et al., 2017). During the strong El Niño of 2015-2016, the southeast  
1809 tropical Indian Ocean experienced the warmest and longest marine heatwave on record, with weakened monsoon activity  
1810 and anomalously high air-sea heat flux into the ocean (Benthuisen et al., 2018). The anomalously warm water conditions  
1811 persisted into winter, during one of the strongest negative IOD events (Benthuisen et al., 2018). The 2016 marine heatwave  
1812 was associated with coral bleaching spanning Australia’s inshore Kimberley region to remote coral reef atolls (Gilmour et  
1813 al., 2019). More broadly across the Indian Ocean during 2016, marine heatwaves have been studied in terms of their  
1814 ecological impacts, such as coral bleaching in the western Indian Ocean (e.g. Gudka et al., 2018), the Maldives (e.g.  
1815 Ibrahim et al., 2017) and consequences for fishes in the Chagos Archipelago (Taylor et al., 2019).

1816 Trends in marine heatwave metrics indicate widespread regions across the Indian Ocean where events have increased in  
1817 frequency, based on SST from 1982-2016, especially in the central and southwestern sectors (Oliver et al., 2018). Over  
1818 the same time period, the duration and intensity of marine heatwaves have increased in the Indian Ocean and globally  
1819 (Oliver et al. 2018, Marin et al. 2021). Primary climate modes of variability correlated with an increased occurrence of  
1820 marine heatwaves include the following: (1) the positive phase of the Dipole Mode Index for the northwestern sector, the  
1821 tropical sector, and south to the Seychelles Islands, (2) the positive phase of the Niño3.4 index for the south-central sector,  
1822 and (3) the negative phase of the El Niño Modoki index, which measures the strength of the Central Pacific ENSO, for the  
1823 eastern Indian Ocean (Holbrook et al., 2019). While the marine heatwaves in the eastern Indian Ocean have been well  
1824 documented, there have been fewer studies into the physical mechanisms causing marine heatwaves across the basin and  
1825 other regions and less confidence, for example in the Bay of Bengal, in the local processes causing reported events on a  
1826 range of time scales (Holbrook et al. 2019). There are indications that increased extremes in El Niño (Cai et al., 2014b)  
1827 and La Niña events (Cai et al., 2015) due to mean ocean warming trends increase the likelihood of marine heatwave  
1828 occurrence in the southeast Indian Ocean (Zhang et al., 2017).

## 1829 **6.5 Monsoon variability and links to the Indian Ocean**

1830 Several monsoon systems surround the Indian Ocean, notably the South Asian monsoon, the East Asian monsoon and  
1831 the Australian monsoon. These monsoon systems are remotely influenced by global coupled modes of variability such as  
1832 ENSO, which is often associated with dry conditions in the South Asian monsoon (e.g., Rasmusson and Carpenter,  
1833 1983; Ropelewski and Halpert, 1987) and Australian monsoon (e.g., Risbey et al., 2009; Jourdain et al., 2013), although

the relationship with the Indian monsoon has recently weakened (e.g., Kumar et al., 1999). In the Indian Ocean, the IOD has a strong influence on the Asian monsoon systems, but is weak during the Australian monsoon period. The IOD tends to oppose the ENSO teleconnection to the South Asian monsoon by enhancing monsoon rainfall (e.g., Ashok et al., 2004; Chowdary et al., 2015; Krishnaswamy et al., 2015; Pokhrel et al., 2012). However, the exact combination of SST patterns between the Indian Ocean and the Pacific is crucial for determining the rainfall response in the Asian monsoons (e.g., Lau and Wu, 2001; Ratna et al., 2020; Yuan and Yang, 2012), and the relative strengths of the teleconnections have varied over time (Krishnaswamy et al., 2015). Furthermore, there is evidence that the Indian Ocean forcing of the South Asian monsoon may be primarily driven by ENSO, with pure IOD events only weakly influencing monsoon rainfall (Cretat et al., 2017).

The monsoon systems around the Indian Ocean tend to vary in phase and are also linked to the western North Pacific Monsoon (e.g., Gu et al., 2010). There is a biennial oscillation in the strength of the monsoon systems, with a strong Asian monsoon preceding a negative IOD and coinciding with cold eastern Pacific SSTs, followed by a strong Australian monsoon and subsequently by a reversal in the SST patterns (Loschnigg et al., 2003; Meehl & Arblaster, 2011). Thus, each monsoon system interacts with the ocean dynamics and thermodynamics and with the other monsoon systems through a complex set of teleconnections.

At a regional scale, upwelling in the Arabian Sea reduces rainfall along the western Ghats of India during the monsoon due to a reduction in evaporation and water vapour transport (Izumo et al., 2008). Moisture fluxes across the Arabian Sea are crucial to accurate simulation of the Indian Monsoon, yet many models fail to accurately capture these (Levine and Turner, 2012). In the Bay of Bengal, the shallow surface mixed layer, supported by the vertical salinity gradient, leads to rapid variations in SST (e.g., Sengupta and Ravichandran, 2001; Vecchi and Harrison, 2002) that interact with intraseasonal oscillations (Gao et al., 2019) in the atmosphere and thus with the active/break cycles on the monsoon (e.g., Lucas et al., 2014). This strong and rapid variability in upper ocean conditions in the Bay of Bengal, and the potential feedbacks on the monsoon, motivated multiple observational research programmes with field campaigns in the Bay of Bengal, as discussed in the next section.

## 7. Multiscale upper ocean processes in the Bay of Bengal

Reflective of its name, the Bay of Bengal is in many ways analogous to a large-scale estuary with seasonally reversing winds and boundary currents that facilitate the transport, stirring, and mixing of water masses. To the north, the Ganga-Brahmaputra-Meghna watershed delivers on average 1300 km<sup>3</sup> in annual runoff of freshwater with a seasonal peak in discharge from July to September (Sengupta et al., 2006). During the southwest monsoon (boreal summer), the Summer Monsoon Current (Fig. 10) flows eastward advecting high salinity waters from the Arabian Sea into the southern Bay of

1866 Bengal, balancing the Bay's net outflow of freshwater. Instabilities and eddies result in mesoscale stirring of these different  
1867 water types and create a strongly filamented and complex near-surface thermohaline structure. Lateral and vertical  
1868 gradients in stratification are further modified by submesoscale processes, instabilities, and mixing. The resultant shallow  
1869 stratification allows for rapid coupling with the atmosphere. Collectively, these conditions present a natural laboratory to  
1870 study multi-scale mixing processes and their link to air-sea interaction. This section discusses new understanding of  
1871 physical processes in the Bay from the large-scale to sub-mesoscale and finally at the smallest mixing scales.

1872 Recent focus on the Bay of Bengal's upper ocean structure has been prompted by the need to understand atmosphere and  
1873 ocean coupling with the aim of ultimately informing monsoon forecasting efforts at the intraseasonal timescale and shorter.  
1874 Several bi-lateral international collaborations (Lucas et al., 2014; Wijesekera et al., 2016; Mahadevan et al., 2016;  
1875 Vinaychandran et al., 2018; Gordon et al., 2019, 2020) have collectively supported multiple field campaigns, beginning  
1876 in 2013 and concluding in 2019, using a combination of shipboard, moored, and autonomous platforms. These atmospheric  
1877 and oceanic measurements have provided new insights into the BoB's structure and the processes that regulate that  
1878 structure, particularly at fine lateral scales (<5 km).

1879 Results from these combined efforts span from large-scales, e.g., the quantification of coastal transport along the Sri  
1880 Lankan coast (Lee et al., 2016) and the mesoscale stirring of freshwater (Sree Lekha et al., 2018), to intermediate scales,  
1881 e.g., high-resolution (order 100 m) frontal surveys that hint at the roles of submesoscale (Ramachandran et al., 2018) and  
1882 non-hydrostatic processes in setting stratification (Sarkar et al., 2016), to small-scales with direct measurements of  
1883 microstructure yielding new insights into the BoB's mixing regimes (Jinadasa et al., 2016; Thakur et al., 2019; Cherian et  
1884 al. 2020).

## 1885 **7.1 The Bay's Forcing and Upper Ocean Structure**

1886 At the largest scales, the Bay is forced by air-sea fluxes of buoyancy and momentum, which are strongly modulated by  
1887 the monsoon and vice versa. Precipitation and multiple river systems, including the Ganga-Brahmaputra-Meghna system,  
1888 contribute to freshwater input that creates a barrier layer in the surface Bay of Bengal, which is strongest in the northern  
1889 Bay weakening toward the south. The Bay's stratification, in particular its barrier layer, is unique in how it impacts the  
1890 evolution of seasonal SST, in turn setting the lower boundary condition for the development of the monsoon (Li et al.,  
1891 2017). For this reason, recent emphasis has been placed on understanding processes that determine the Bay's upper ocean  
1892 salinity and temperature structure.

1893 The monsoon cycle of surface forcing plays a first-order role in controlling the Bay's upper ocean temperature structure.  
1894 Direct flux measurements are a critical component in our ability to accurately capture/represent and predict the magnitude  
1895 and variability of monsoon air-sea coupling. Recent studies have shown that of the air-sea heat flux terms, shortwave

radiation and latent heat flux are the largest drivers of variability to the total heat tendency. These variables are also those which reanalysis products struggle most to accurately represent, showing biases up to 75 W/m<sup>2</sup> (Sanchez-Franks et al., 2018). High-quality air-sea surface flux measurements over the BoB historically have been limited to the few sites maintained by the RAMA array (McPhaden et al., 2009). However, regional measurement efforts have expanded and baseline surface measurements are now collected and sustained through India's National Institute of Ocean Technology's met-ocean buoy program (Venkatesan et al., 2018), as well as the recent transition of an 18°N air-sea flux buoy from Woods Hole Oceanographic Institution to Indian National Centre for Ocean Information Services (Weller et al., 2016).

Precipitation and riverine discharge along the Bay's margins respectively contribute roughly 60% and 40% of the 0.14 Sv net freshwater delivered to the Bay (Sengupta et al. 2006; Wilson and Riser, 2016). Precipitation peaks in early summer (June) with a value near 0.4 m month<sup>-1</sup>, while discharge peaks slightly later in summer (August) with a value near 0.3 m month<sup>-1</sup>. Evaporative loss (included in the net 0.14 Sv) is relatively steady throughout the year at 0.1 m month<sup>-1</sup> (Wilson and Riser, 2016). Estimates of river discharge from gauged sources are known to have uncertainties (underestimates) related to unmonitored tributaries and streams. For large deltas, altimeter-based elevations offer a means of extrapolating gauge data over space and time. Papa et al. (2010, 2012) applied such an approach to the Ganga-Brahmaputra River system for the period 1998-2011. This time series allows for assessment of interannual variability over time ranges not spanned by gauged efforts. Papa et al. (2012) note a 12,500 m<sup>3</sup>/s standard deviation in interannual variability in the Ganga-Brahmaputra discharge. Importantly, such data sets are also easily accessible by the general public, facilitating progress and understanding by the scientific community.

The Bay's upper ocean temperature and salinity structure is an integrated representation of the above summarized sources/sinks of heat and freshwater, combined with the physical processes that redistribute these quantities. The thermohaline structure of the Bay is remarkable in several regards—for shallow mixed layer depths (< 5 m, Sengupta and Ravichandran, 1998), for inversions of temperature (Shroyer et al., 2016, 2019; Thadathil et al. 2016), for large-scale coherent layering that spans 100 kms (Shroyer et al., 2019), an active mesoscale field and the strong influence of river discharge over the interior basin. The Bay's salinity stratification is a critical, if not dominant, contributor to the upper ocean density stratification. It supports the formation of barrier layers that are frequently observed to be warmer than the mixed layer thereby providing a substantial subsurface heat reservoir with the potential to modify air-sea interaction (Girishkumar et al., 2011; Shroyer et al., 2016). For example, in conditions supportive of formation of a diurnal warm layer (low winds, strong insolation), subsurface turbulent fluxes can act to modulate the diurnal SST cycle by transporting (typically) warm barrier layer waters into the mixed layer at night while still cooling the base of the diurnal warm layer (DWL) during the day (Shroyer et al., 2016). A similar phenomenon, albeit on a much different scale, results with passage of cyclones, which often show a salty wake even in the absence of a cool wake which is common for cyclones elsewhere (for e.g. Chaudhuri et al. 2019, Qiu et al. 2019). Below, we review recent progress on understanding of processes that determine the Bay's upper ocean thermohaline structure.

1929     **7.2 Lateral Processes**

1930     **7.2.1 Stirring from the Margins**

1931     The Bay of Bengal has an active mesoscale eddy field that stirs diverse source waters into the interior of the Bay of Bengal.  
1932     The origins of these source waters are the Arabian Sea waters to the west, the Ganga-Brahmaputra-Meghna at the northern  
1933     tip, Andaman Sea waters to the east, and Equatorial waters to the south. This stirring effectively contributes to a quasi-  
1934     stationary balance of the fresher waters from the north and the high salinity waters from the west and south over time.  
1935     Lateral advection is a fundamental contributor to the formation of the barrier layer (George et al., 2019) and the freshwater  
1936     budget of the Bay (e.g. Sree Lekha et al., 2018). In the northern Bay, the dispersal of water from the periphery into the  
1937     interior depends critically on mesoscale stirring and the time varying Ekman transport, as indicated from mooring (Sree  
1938     Lekha et al., 2018) and ship-based surveys (Shroyer et al., 2019), and constrained by modelling results (Sree Lekha et al.,  
1939     2018). Here, the advection of freshwater by the mesoscale stirring also plays an important role in determining SST over  
1940     the northern BoB (Buckley et al. 2020), as these waters are typically associated with relatively shallow mixed layers. In  
1941     the southern Bay, measurements have suggested the competing influences of mixing and advection of salty Arabian Sea  
1942     water in the erosion and reformation of the barrier layer during the southwest monsoon (George et al., 2019;  
1943     Vinayachandran et al., 2018). In particular, George et al. (2019) show that maintenance of the barrier layer and the  
1944     associated maximum depth of mixing was critically dependent on horizontal advection through its impact on stratification.  
1945     Surface freshwater input also has an impact on barrier layer evolution; several freshening events were captured at various  
1946     stages of their seasonal evolution in the southern Bay of Bengal in recent observations (Vinayachandran et al., 2018).  
1947     These events play a significant role in the formation of a thick barrier layer, showing that during the southwest monsoon  
1948     the shoaling of the mixed layer in the southern BoB has a similar magnitude and behaviour to that in the northern BoB  
1949     (Vinaychandran et al., 2018).

1950     **7.2.2 Inter-basin exchange**

1951     Inter-basin exchange is critical to the Bay's salinity budget; since the Bay receives net freshwater input, this freshwater  
1952     must be balanced by salty water imported from either the Arabian Sea or the western equatorial Indian Ocean (Jensen et  
1953     al., 2001; Sanchez-Franks et al., 2019), and turbulent transport of salt into the fresh water layer is necessary to maintain  
1954     the BoB's long-term salinity balance. Observations show that intrusion of high salinity water from the Arabian Sea enters  
1955     the BoB between 80°-90°E during the southwest monsoon, (e.g. Murty et al, 1992; Vinayachandran et al., 2013) and has  
1956     been found in several models (e.g. Vinayachandran et al., 1999; Han and McCreary, 2001 and Jensen, 2001). More recent  
1957     observational and modeling studies show that both lateral and vertical transfer of heat and salt occur at multiple space-  
1958     time scales. Seasonal currents play an important role in transporting heat and salt in and out of the BoB, but the role of  
1959     mesoscale eddies on lateral transports is not well known.



Using unique year-long mixing measurements detailed in Section 7.3, Cherian et al. (2020) tentatively estimated a turbulent salt flux of  $1.5\text{e-}6 \text{ psu ms}^{-1}$  out of Arabian Sea water averaged between  $85^{\circ}\text{E}$  and  $88.5^{\circ}\text{E}$  at  $8^{\circ}\text{N}$  through the  $34.75 \text{ psu}$  isohaline between August and January. Over those 6 months, this flux would increase the salinity of a  $75\text{m}$  layer of water by  $0.3 \text{ psu}$ , though much of this would be cancelled out by surface fluxes. The magnitude and timing of this salt flux roughly match that necessary to restore the Bay's near-surface salinity after the large freshwater input in August as estimated by a few modelling studies (Akhil et al., 2014; Benshila et al., 2014; Wilson and Riser, 2016). This is the first direct measurement of turbulence that supports the hypothesis of intrusion of high salinity water from the Arabian Sea during the southwest monsoon (Vinayachandran et al., 2013).

#### 7.2.2.1 Andaman Sea Exchange

The Irrawady river drains into the Andaman Sea, a marginal sea at the eastern edge of the Bay. Export from the Andaman is then another source of freshwater for the Bay, particularly at intermediate densities ( $22\text{-}25 \text{ kg m}^{-3}$ ). A striking example of the interaction between strong surface forcing and an anticyclonic eddy can be found in the fortuitous crossing of an intrathermocline eddy (ITE) in 2013 as reported by Gordon *et al.* (2017). The water mass characteristics clearly identify ITE waters from the Andaman Sea; and, analysis of ancillary Argo data suggest a similar water type often penetrates westward into the Bay extending from the three passages connecting the two basins. While at the time of transit the observed ITE had a very weak surface expression, a week prior to encountering the ITE a clear sea surface high ( $>10 \text{ cm}$ ) is evident in AVISO SSHA. Tropical cyclone Lehar passed near the location of this sea surface high in the interim, and the working conjecture is that the winds associated with Lehar were sufficient to modify a typical mode-1 anticyclone into the observed ITE.

#### 7.2.2.2 Arabian Sea Exchange

Near-surface exchange from the Arabian Sea into the Bay of Bengal is influenced by the Sri Lanka Dome (SLD), an upwelling thermal dome that recurs seasonally within the SMC in the wind shadow of Sri Lanka (Vinayachandran and Yamagata 1998, de Vos et al. 2014, Burns et al. 2017). The SLD has long been recognized as a prominent circulation feature in the southwestern bay during the summer monsoon; and it has been noted as a region of enhanced productivity (Vinayachandran et al., 2004, de Vos et al. 2014), cool SST (Burns et al. 2017), and consequently depressed convection (Figure 15). The SLD displays pronounced interannual variability (Cullen and Shroyer 2019). In some years the SLD has a strong surface manifestation (amplitude of the low  $\sim 30 \text{ cm}$ ) that persists well beyond the southwest monsoon; in other years the SLD has a weak expression that is intermittent and short-lived ( $\sim 1\text{-}2$  months). The SLD is not fixed in location despite its strong association with the wind stress curl. Its position varies from year-to-year as well as over the course of one season. Variations in its location and strength may influence the properties of waters entrained and upwelled within the SLD.

At intermediate depths ( $< \sim 200$  m), the signature of the neighboring Arabian Sea is notable across much of the basin (Gordon et al., 2016). During summer, Arabian Sea High Salinity Water (ASHSW; density near  $22\text{--}24 \text{ kg m}^{-3}$ ) is carried/advectioned into the Bay of Bengal as a ‘high salinity core’ via the Southwest Monsoon Current (SMC, Webber et al., 2018; Sanchez-Franks et al., 2019) and then spread north along the bay’s central spine (Hormann et al., 2019). During this journey, salt is mixed upward into the near-surface fresh layer (Cherian et al 2020; Section 7.3). A nearly two-year long moored current record in the southern BoB captured seasonally varying large eddies generated by the SMC and Northeast Monsoon Current. These eddies included a cyclonic eddy, the SLD, and an anticyclonic eddy south of the SLD (Wijesekera et al. 2016c). These observations revealed that the average transport over a nearly two year period into the BoB was about  $2 \text{ Sv}$  ( $1 \text{ Sv} = 10^6 \text{ m}^3 \text{ s}^{-1}$ ) but likely exceeded  $15 \text{ Sv}$  during summer of 2014, which is consistent with the transport associated with the SMC (e.g., Schott et al. 2009; Webber et al. 2018). The observations further indicate that the water exchange away from coastal boundaries, in the interior of the BoB, may be largely influenced by the location and strength of the two eddies that modify the path of the SMC. The strength and location of the SMC itself is dependent on a combination of local and remote forcing (Webber et al., 2018).

As discussed above several hypotheses have been suggested for cyclonic eddy (SLD) and anticyclonic eddy formation in the southern BoB. It has been suggested that the cyclonic wind stress-curl over southwestern BoB generates the SLD (McCreary et al., 1996; Vinayachandran and Yamagata 1998; Schott et al., 2001; Cullen and Shroyer 2019). Based on numerical simulations, de Vos et al., (2014) argued that the separation of SMC from the (southern) boundary of Sri Lanka may lead to SLD, where a cyclonic vorticity is generated by lateral frictional effects. A mechanism for the anticyclonic eddy formation has been proposed by Vinayachandran and Yamagata (1998), where the interaction of the SMC with Rossby waves arriving from the eastern boundary leads to the anticyclonic eddy. Pirro et al (2020a) proposed a new hypothesis wherein the anticyclonic eddy is generated by a topographically trapped Rossby wave response of the SMC to perturbations by the Sri Lankan coast. They reported that observations of the size, location and origins of the SLD were broadly consistent with their hypothesis, based on a laboratory experiment designed to mimic natural flow in the BoB by creating an eastward jet (SMC) on a simulated  $\beta$  plane.

High-resolution sampling of the interior BoB has provided a more detailed look at the lateral extent of typical ‘patches’ of Arabian Sea water, which tend to remain well-defined over scales of  $10\text{--}50 \text{ km}$ , suggesting the importance of eddy activity in exchange (Shroyer et al., 2019). While many studies have traced origins of ASHSW from the eastern Arabian Sea, entering the Bay of Bengal directly via the southwest monsoon current (e.g., Jensen et al, 2016); a recent study suggests an equatorial pathway may also be relevant (Sanchez-Franks et al., 2019; Section 7.2.3). Highly salty and highly oxygenated waters from the Persian Gulf and the Red Sea have also been noted in the southern regions of the Bay of Bengal (Jain et al., 2017). These waters are injected into the Bay of Bengal via current systems (equatorial and the southwest monsoon current) with important repercussions for the oxygen concentrations of the Bay of Bengal oxygen minimum zone (Sheehan et al., 2020).

Velocity and hydrographic profiles from a shipboard survey in December 2013 combined with drifter observations, satellite altimetry, global ocean nowcast/forecast products, and coupled model simulations were used to examine the circulation in the southern Bay of Bengal during the Northeast monsoon (Wijesekera et al. 2015). The observations captured the southward flowing East India Coastal Current (EICC, e.g., Shetye et al. 1994) off southeast India and east of Sri Lanka. The EICC was approximately 100 km wide, with speeds exceeding  $1 \text{ m s}^{-1}$  in the upper 75 m. East of the EICC, a subsurface-intensified 300-km-wide, northward current was observed, with maximum speeds as high as  $1 \text{ m s}^{-1}$  between 50 m and 75 m. The EICC transported low-salinity water out of the bay and the subsurface northward flow carried high-salinity water into the bay during typical northeast monsoon conditions (Wijesekera et al. 2015; Jensen et al. 2016).

### 7.2.3 Equatorial Connections

The Equatorial undercurrent (EUC) in the Indian ocean is seasonally variable. The summer–fall EUC tends to occur in the western basin in most years but exhibits evident interannual variability in the eastern basin (Chen et al. 2015), with different processes dominating its generation in the western and eastern basins. In the eastern basin reflected Rossby waves from the eastern boundary play a crucial role in the EUC, whereas directly forced Kelvin and Rossby waves control the EUC in the western basin.

Equatorial Kelvin waves, commonly interpreted as Wyrtki (1973) jets, propagate eastward along the equator during April/May and September/October. Upon reflection from the IO eastern boundaries, energy of Wyrtki jets is reflected back in part as long Rossby waves that disperse slowly during the following two months and reach the central-eastern BoB during July–August (Han et al., 1999, 2001; Han, 2005; Nagura and McPhaden, 2010a). The remaining energy is partitioned into two coastally-trapped Kelvin waves traveling poleward (Moore, 1968), which excite long Rossby waves propagating westward. Therefore it is suggested that planetary waves driven by remote forcing from the interior IO contribute significantly to the formation, strength and intensity of the BoB circulation (Vinayachandran et al. 1998; Nagura and McPhaden, 2010b; Chen, 2015). A subset of these planetary waves are the mainstay of intraseasonal oscillations (ISOs), a sub-seasonal phenomenon of period less than 120 days. The genesis of oceanic ISOs has been attributed to multiple mechanisms: external forcing (e.g., atmospheric ISOs and Ekman pumping, e.g. Duncan and Han 2012) and internal processes (upper ocean processes and instabilities e.g. Zhang et al. 2018).

Observations in the IO have captured a range of variabilities in the 30 – 120 days frequency band (e.g., Girishkumar et al., 2013), and past research has identified roughly three distinct ISO bands in the context of the thermocline: 30–60 days, 60–90 days, and 120 days (Han et al., 2001; Girishkumar et al., 2013). Pirro et al. (2020b) discussed interaction between 30–60 day ISOs and the SMC in the southern BoB using long-term moored observations. They estimated that the background mean flow acceleration resulting from the meridional divergence of wave momentum flux in the thermocline was about  $10^{-8} \text{ m s}^{-2}$ . As a result, within a wave period, ISOs can enhance the eastward flow in the thermocline by about 25%. The

negative shear production computed for the same period is consistent with this finding suggesting that the mean flow gained kinetic energy at the expense of the ISO band. The meridional heat-flux divergence was  $-10^{-7} \text{ }^{\circ}\text{C s}^{-1}$  and has a tendency for cooling the thermocline by about  $0.5^{\circ}\text{C}$  when ISOs are active (Pirro et al., 2020b). Observations have also captured energetic and consequential 5-20 day convectively coupled Kelvin waves in the atmosphere (Baranowski et al, 2016) that generate oceanic Kelvin waves, affect surface heat fluxes and generate upper ocean turbulence (Pujiana and McPhaden, 2018).

High salinity waters from the western Arabian Sea and the western Equatorial Indian Ocean can route to the Bay of Bengal via the Somali Current and the Indian Ocean EUC (Sanchez-Franks et al., 2019). Changes in strength of the Bay of Bengal high salinity core are linked to the convergence of the East Africa Coastal Current and the wintertime southward-flowing Somali Current, with anomalously strong equatorial Undercurrent (Fig. 19). Because of the seasonal reversal of currents, two junctions form naturally, one in the western equatorial Indian Ocean (Somali Current) and another south of India (monsoon currents), which effectively act as ‘railroad switches’ rerouting water masses to different basins in the Indian Ocean depending on the season (Fig. 19, Sanchez-Franks et al., 2019).

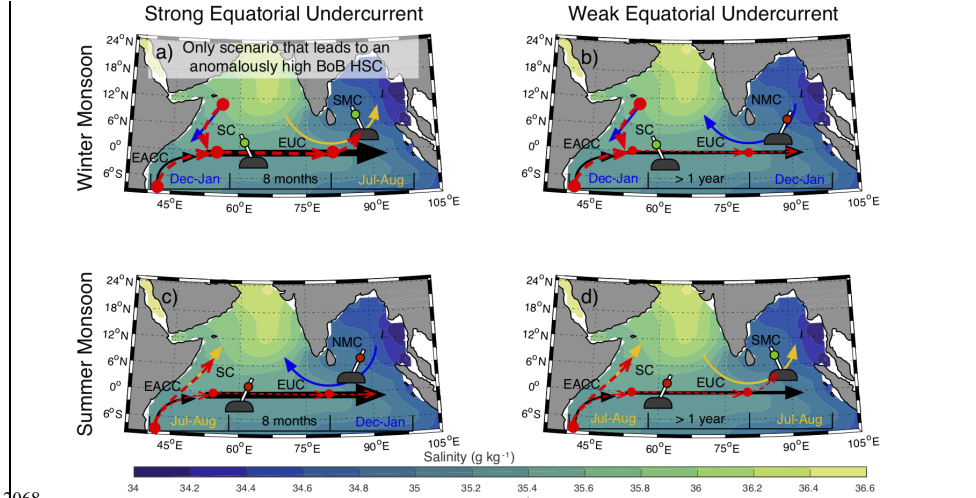
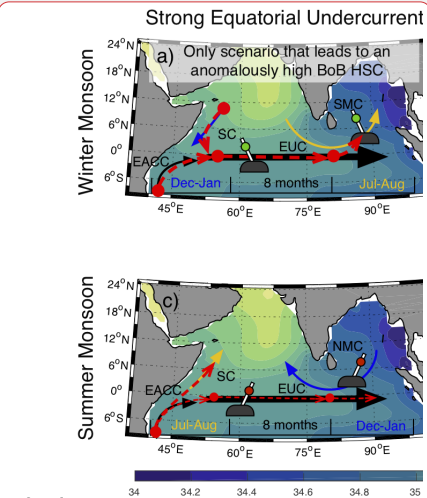


**Figure 19: Seasonal circulation pathways in the northern Indian Ocean, or Railroad Switch schematic, on subsurface (90 m) salinity climatology (psu; shaded) from the Argo optimally interpolated product for the four Equatorial Undercurrent scenarios: (a, b) winter monsoon and strong (weak) Equatorial Undercurrent and (c, d)**



2073 **summer monsoon and strong (weak) Equatorial Undercurrent. Red dashed arrows indicate high-salinity advection.**  
2074 **BoB = Bay of Bengal; HSC = high-salinity core; SMC = Southwest Monsoon Current; SC = Somali Current; EUC**  
2075 **= Equatorial Undercurrent; EACC = East African Coastal Current. From Sanchez-Franks et al. (2019).**

### 2076 **7.3 Vertical Mixing**

2077 Strong stratification in the Bay of Bengal plays a critical role in setting the upper ocean turbulence, notably leading to  
2078 relatively weak mixing compared to other regions (e.g. Gregg et al., 2006). However, large-scale inferences suggest that  
2079 mixing must play a key role in at least two regards. First, the net surface flux during the southwest monsoon on average is  
2080 warming but yet the SST cools (Shenoi et al, 2002). Second, the large-scale salt balance must be closed through upward  
2081 mixing of high-salinity water carried into the Bay via the Summer Monsoon Current (Vinayachandran et al., 2013).

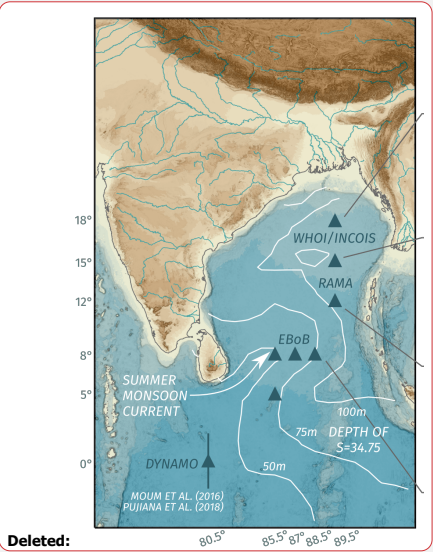
2082 Recent year-long direct measurements of mixing in the Bay have helped link the seasonal cycle in mixing to the seasonal  
2083 cycle of winds, currents and freshwater. These year-long measurements were recorded by mixing meters called  $\chi$ pods.  
2084  $\chi$ pods consist of two temperature microstructure sensors and a suite of ancillary sensors necessary to infer the rate of  
2085 dissipation of temperature variance at 1Hz frequency for up to a year (Moum & Nash, 2009).  $\chi$ pods have been deployed  
2086 on moorings in three different regions of the Bay (Figure 20): the air-sea buoy at 18°N, top 65m (Thakur et al., 2019),  
2087 RAMA moorings along 90°E (mixing measurements at 15m, 30m and 45m; Warner et al. 2016), and the EBoB array in  
2088 the south-central Bay (mixing measurements spanning between 30m and 100m at sites in the region 85°E-88°E, 5°N-8°N,  
2089 Cherian et al., 2020). Across the basin, turbulence within and near the base of the mixed layer shows strong seasonality  
2090 that parallels the monsoon cycle in winds (Thakur et al., 2019, Warner et al., 2016). In the thermocline of the south-central  
2091 Bay (EBoB array), mixing is correlated with packets of downward propagating near-inertial waves implicating wind  
2092 forcing. As depicted in Figure 20, both near-surface and thermocline mixing are relatively high during the NE and SW  
2093 monsoons (Dec-Feb, May-Sep) and relatively low during the transition (Mar, Apr). Cyclones during the post-monsoon  
2094 months of October and November can drive a hundredfold increase in near-surface mixing both locally and throughout  
2095 the Bay (Warner et al. 2016). Turbulence profiles collected by a fast thermistor on a CTD rosette during a basin-wide  
2096 survey before and after the passage of cyclone Madi (6-12 Dec, 2013) show a basin-wide increase in diffusivity linked to  
2097 near-inertial waves forced by the cyclone (Wijesekera et al., 2016b).

2098 Indirect estimates of turbulent diffusivity and turbulent heat fluxes at the base of the mixed layer can be found as the  
2099 residual of a mixed layer heat budget whose terms are estimated using a combination of mooring and satellite  
2100 measurements. Girishkumar et al. (2020) use this approach to indirectly estimate seasonal median turbulent diffusivities  
2101 using decade-long RAMA mooring records at 90°E. They find a robust seasonal cycle of mixing at 8°N, 12°N, and 15°N;  
2102 and strong latitudinal variability in turbulence, with larger diffusivities inferred at 8°N relative to 12°N and 15°N in all

seasons. When comparisons are possible, the indirect estimates compare well against the more direct but time-limited estimates of Warner et al (2016) at 90°E, 12°N.

**Figure 20: Annual cycle of daily averaged temperature diffusivities derived from xpod measurements. The data are from two different years, 2014 and 2015, depending on location. Note the similar wind-forced seasonal cycle at 12°N, 15m and 15°N, 15m and the dramatically different seasonal cycle at 8°N, 105m (reflecting near-inertial wave activity) and at 18°N, 65m reflecting freshwater influence.**

The influence of freshwater is a critical caveat to the above generalizations: the arrival in August of the Ganga-Brahmaputra-Meghna freshwater plume at 18°N has been observed to suppress turbulence (diffusivity  $K_T < 10^{-5} \text{ m}^2 \text{ s}^{-1}$ ) for multiple months (Aug-Nov) at depths of approximately 50-65 m (Figure 20). This buoyant lens limited the vertical extent of the influence of Tropical Cyclone Komen as compared to a previous (weaker) storm (Chaudhuri et al 2019, Thakur et al 2019). Similar observations of extremely weak turbulence below strong, salinity-stratified surface layers have been reported throughout the Bay using data from a variety of platforms: ship-based microstructure (Jinadasa et al, 2016) profiling floats with a temperature microstructure sensor (Shroyer et al, 2016) and glider-based microstructure measurements (St. Laurent and Merrifield, 2017). Lucas et al (2016) find that near-inertial shear was elevated at the base of the mixed layer but not elevated at the base of the barrier layer — direct evidence that salinity stratification can insulate



2120 deeper depths from the effects of near-surface forcing (downward propagating near-inertial waves in this case). Li et al.  
2121 (2017) use a combination of observations and modelling results to demonstrate that barrier layers in the Bay of Bengal  
2122 influence the amplitude of intraseasonal oscillations in SST and precipitation. However, a recent coarse resolution coupled  
2123 modelling study suggests that freshwater has little influence on SST or rainfall, since the SST tendency caused by a  
2124 reduction in mixing is offset by changes in surface heat fluxes (Krishnamohan et al., 2019)

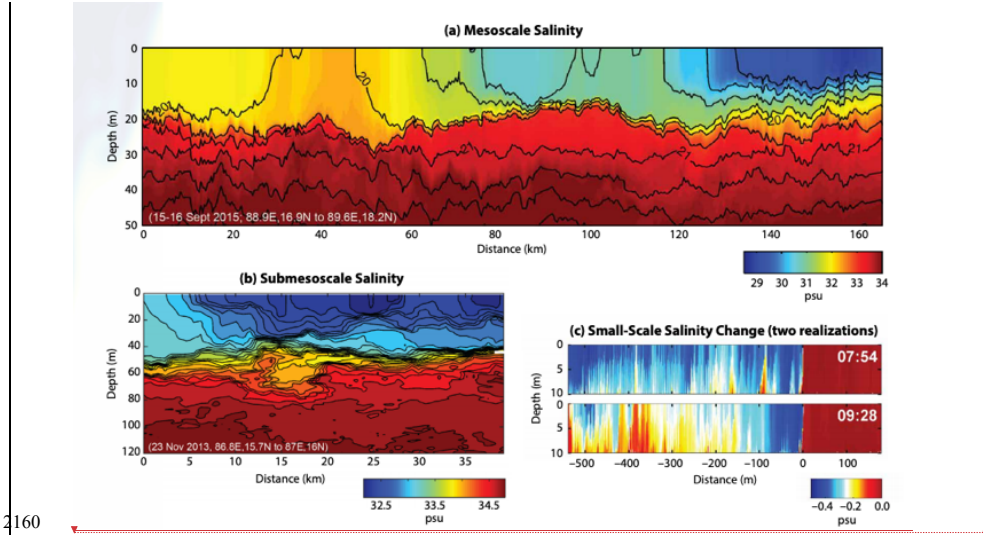
2125 Surface freshwater advection can create subsurface reservoirs of heat and salt that can be accessed when the winds are  
2126 strong enough, such as during cyclones that regularly form in the Bay during October and November. In one dramatic  
2127 example Qiu et al (2019) report up to 5 psu increases in SSS and only a smaller 0.5°C decrease in SST following the  
2128 passage of Cyclone Phailin (2013). In this case, mooring records indicate that mixing was limited to the isothermal layer  
2129 (Chaudhuri et al. 2019). Subsurface warm layers (i.e. temperature inversions stabilized by strong salinity stratification)  
2130 are also observed, representing a reservoir of heat that can be accessed if a storm excites enough turbulence, as appears to  
2131 have happened during the passage of Cyclone Hudhud (Warner et al, 2016). The influence of stratification in limiting the  
2132 extent of vertical mixing and creating subsurface warm layers mean that cyclone-induced cooling is generally either weak  
2133 or negligible in the Bay, unlike in other ocean basins (Sengupta et al, 2008). Subsurface warm layers influence SST on  
2134 longer timescales too: Girishkumar et al (2013) find that the wintertime SST at 8°N, 90°E is quite sensitive to the thickness  
2135 of the barrier layer, and to the presence of temperature inversions (subsurface warm layers) in the barrier layer on  
2136 intraseasonal and interannual timescales.

2137 Long periods of near-molecular diffusivities (weeks to a month) were also inferred at multiple  $\gamma$ pods along 8°N between  
2138 50 m and 100 m during transition months of March and April. Here freshwater insulation does not appear to be the major  
2139 factor. Instead the period of weak turbulence may be linked to low levels of near-inertial energy (a consequence of weak  
2140 wind forcing in March and April) and the absence of strong mean oceanic flows during these transition months (Cherian  
2141 et al 2020). Relatively weak diffusivities are also present in the LADCP fine structure estimate of depth-integrated  
2142 (thermocline to bottom) turbulent kinetic energy dissipation  $\epsilon$  (Kunze et al, 2006) and the Argo fine structure-based 250-  
2143 500 m diffusivity estimates of Whalen et al. (2012). The extended presence of such weak turbulence suggests that the  
2144 Bay's internal wave field is weaker than might be expected from the Garrett-Munk internal wave spectrum at least during  
2145 some months of the year. Another (related) question is the issue of representation of such weak background mixing in  
2146 climate models and whether that matters to known biases in such models.

2147 Published efforts so far have been directed towards understanding the modulation of turbulence by larger-scale variations  
2148 in the wind, currents and freshwater. Questions remain as to the impact of small-scale mixing on the large-scale long-term  
2149 T-S structure in the Bay as well as the influence of subsurface mixing and the ensuing modification of SST on coupled  
2150 ocean-atmosphere phenomena such as the MJO and the MISO (Section 3.2)

2151 **7.4 Where vertical and lateral processes meet: The Role of Submesoscale**

2152 Freshwater inflow from the Ganga-Brahmaputra-Meghna (GBM) and the Irrawady river in the Bay of Bengal is stirred by  
2153 the mesoscale eddies into sharp frontal gradients (in salinity and in density) at  $O(1-10\text{km})$  scales with shallow vertical  
2154 extent. These fronts are acted upon by winds seasonally, setting up complex sub-mesoscale structures with salinity  
2155 differences  $O(1\text{ psu})$  over  $1-10\text{ km}$ , developing bore-like features with  $O(0.5\text{ psu})$  difference over a few meters horizontally  
2156 (Nash et al 2016; Figure 21). Wavenumber spectra of temperature at  $O(1-10\text{km})$  scale show a  $-2$  slope in many regions  
2157 of the Bay (Mackinnon et al 2016), a signature of frontogenesis in the Bay at these scales. The BoB is thus replete with  
2158 fronts which evidently slump at sub-mesoscales due to both symmetric and baroclinic instabilities (Ramachandran et al.  
2159 2018), and show higher stratification near fronts (Sree Lekha 2019).



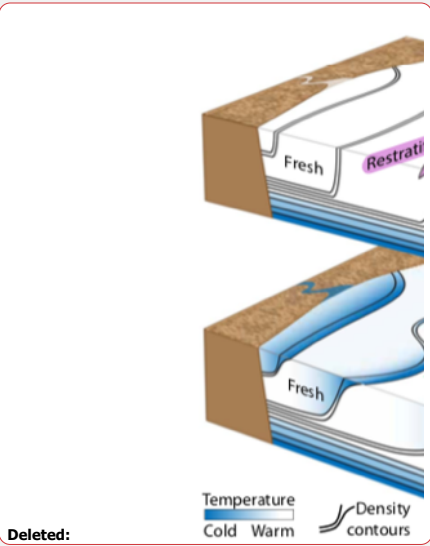
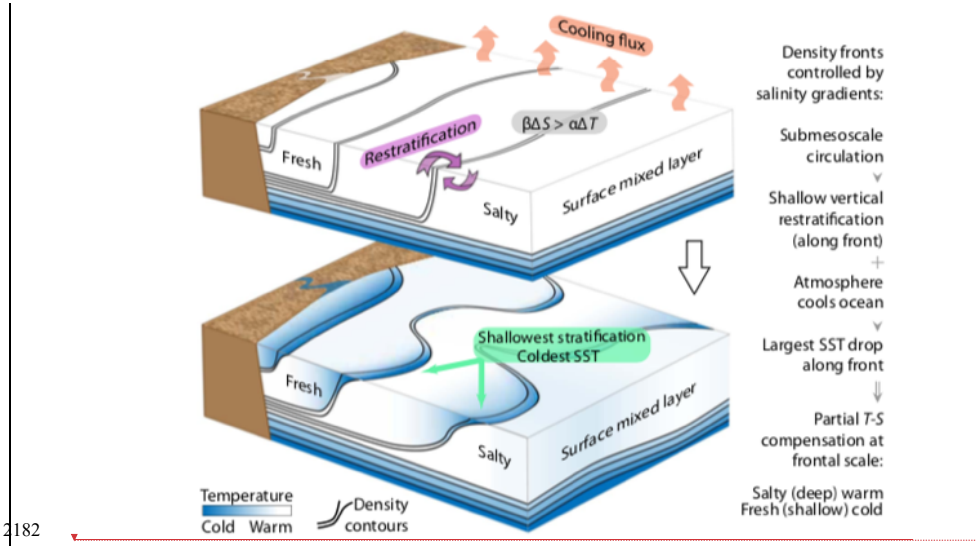
2161 **Figure 21: Observed salinity gradients at mesoscale, sub-mesoscales and small horizontal scales from in the Bay of**  
2162 **Bengal (Nash et al. 2016).**

2163 The fronts and filaments at  $O(1-10\text{km})$ , which are dominated by salinity gradients and weakly compensated, have strong  
2164 implications for setting up the density stratification in the top 50-100m in the BoB (Section 4.4.1). The stratification in  
2165 this depth range often has multi-layered structure with stratification varying at  $O(1-10\text{km})$  scales (Lucas et al 2016),  
2166 showing evidence that the stratification in the Bay cannot be explained simply in terms of vertical processes, and horizontal



submesoscale processes are intimately coupled with the vertical processes at these scales. Ramachandran et al. (2018) show that a mesoscale strained region with strong fronts ( $O(1\text{kg/m}^3 \text{ over } 40\text{km})$ ) and weak down front wind shows multiple dynamical signatures of sub-mesoscale instabilities. Ageostrophic secondary circulations arising near the fronts and the accompanied sheared advection plays an important role in setting the stratification (Pham and Sarkar 2019). Both observations and process modeling show  $O(1\text{-}10\text{km})$  patches of low potential vorticity consisting of subducted warm water patches due to a combination of baroclinic and forced symmetric instabilities, creating barrier layers whose thickness varies laterally at sub-mesoscales (Ramachandran and Tandon, 2020 JGR-in review).

During winter, the temperature gradients in the horizontal compensate for the salinity gradients to reduce the density gradient, and the sub-mesoscale processes in BoB lead to a unique situation. Jaeger & Mahadevan (2018) show that surface cooling fluxes combined with submesoscale instabilities of the haline fronts during wintertime leads to shallower mixed layers on the less saline (cooler) side. Therefore, cold SSTs in wintertime in the Bay mark surface trapped waters (Fig. 22), whereas in other regions of the world ocean, cold filaments mark upwelling of nutrient-rich waters. Further, since the shallow fresher mixed layers lead to larger drops in temperature, this develops the correlation between SST and SSS at  $O(1\text{-}10\text{km})$  scales.



Deleted:

2184 **Figure 22: Interaction of submesoscale salinity gradients with atmospheric cooling leads to shallow cold regions**  
2185 **(From Spiro Jaeger and Mahadevan, Science Advances 2018)**

## 2186 **7.5 Putting the Pieces Together**

### 2187 **7.5.1 Coupled ocean-atmosphere phenomena**

2188 Due to the presence of a barrier layer over much of the Bay of Bengal, entrainment and upwelling of waters from the  
2189 thermocline are inhibited, and the evolution of SST is largely driven by net air-sea heat flux variability (Duncan and Han,  
2190 2009). However, the dependency of SST on surface fluxes is controlled by subsurface processes such as formation of  
2191 barrier layers, entrainment warming and cooling of the mixed layer, penetrative solar radiation and zonal advection  
2192 (Thangaprakash et al., 2016). Advection is important in influencing the SST as lateral variations in the mixed layer depth  
2193 alone can result in variations in air-sea fluxes of roughly  $20 \text{ Wm}^{-2}$  over distances of kilometers (Adams et al., 2019). This  
2194 magnitude is similar to uncertainty in air-sea flux products (Weller et al. 2016) thus implying that variations in sub-  
2195 mesoscales are important for heat balance in the northern BoB. The coupling of the ocean-atmosphere over BoB at large  
2196 scales implicates the air-sea interaction and the mixed layer heat budget in the BoB (Rahaman et al. 2019), although at  
2197 oceanic mesoscale and finer scales in the horizontal and at sub-seasonal timescales this coupling is a topic of active  
2198 research.

### 2199 **7.5.2 Implications for biogeochemistry in the Bay**

2200 Eddies in the central BoB arise not by the baroclinic instability of boundary currents but rather due to planetary wave  
2201 dynamics off the equator that triggers coastal Kelvin waves around the Bay. The Kelvin waves then trigger south-westward  
2202 propagating Rossby waves, which result in large mesoscale structures in the Bay (Cheng et al. 2018). The Andaman and  
2203 Nicobar Islands are also shown to be very important for the generation of these eddies; without these islands the number  
2204 of eddies would have reduced to almost half in the western bay of Bengal (Mukherjee et al., 2019). These eddies provide  
2205 much of the horizontal stretching and stirring of the tracers, including those relevant to the ecosystems

2206 Eddies have tremendous potential to influence ocean biogeochemistry by providing “new” nutrients to the ocean’s  
2207 euphotic layer (Stramma et al., 2013). However, we do not fully understand the spatial distribution of nutrients within the  
2208 eddy surface area – e.g., there is a debate whether nutrients upwell at the core and downwell at the edge of the eddy, or  
2209 vice versa. Further, such discrepancy also continues in the type of eddies – i.e., whether upwelling occurs in cyclonic and  
2210 downwelling occurs in anticyclonic eddies and vice versa (Mahadevan, 2014; Mahadevan et al., 2012; Martin and  
2211 Richards, 2001). But there is a consensus that eddies do impact biogeochemistry (McGillicuddy et al., 2007).

2212 There have been only a handful of studies on the role of eddies in biological productivity in this region (Kumar et al.,  
2213 2007; Singh et al., 2015). Kumar et al. (2007) observed an increase in surface nutrients in the Bay through eddies during  
2214 both fall-2002 and spring-2003 followed by higher biomass. Despite being highly eutrophic, biological activity did not  
2215 increase following cyclonic eddies during the summer-2003 in the northern Bay (Muraleedharan et al., 2007). But primary  
2216 production switched from 'regenerated' to 'new' production during summer-2003. In a  $^{15}\text{N}$  based new production estimate  
2217 to assess the role of cyclonic eddies in enhancing primary production, Singh et al. (2015) carried out measurements of  
2218 primary production at four stations in the Bay of Bengal (around a cyclonic eddy close to  $17.8^\circ\text{N}$ ,  $87.5^\circ\text{E}$ ) during winter  
2219 2007. The measurements sampled one cyclonic eddy during the campaign. The highest surface productivity ( $2.71 \mu\text{M C}$   
2220  $\text{d}^{-1}$ ) and chlorophyll a ( $0.18 \mu\text{g L}^{-1}$ ) were observed within the eddy due to intrusion of nutrients from subsurface waters.  
2221 Given new nitrogen input via vertical mixing, river discharge or aerosol deposition, the additional primary production due  
2222 to this new nutrient input and its contribution to the total production increased from 40% to 70%. Eddies could be a reason  
2223 for the otherwise unexplained high new production rates in the Bay of Bengal (Singh and Ramesh, 2015). Eddies also  
2224 seem to have a potential for transferring a high fraction of fixed carbon to the deep. [A couple of recent studies have](#)  
2225 [highlighted the role of mesoscale eddies in changing the elemental proportions of carbon:nitrogen:phosphorus in the](#)  
2226 [organic and nutrient pools in the euphotic layer of the Bay \(Sahoo et al., 2020, 2021\).](#)

Deleted:  $^{13}\text{C}$  based

## 2228 8. Summary and open questions

2229 This paper summarises a suite of new studies in the Indian Ocean that have been made possible through national, bilateral,  
2230 and international programmes, including the IIOE-2. An increase in high quality observations (both increased spatial  
2231 resolution and the acquisition of longer time series) has led to a substantial increase in our understanding of processes and  
2232 interactions. These in-situ observations, in combination with remote sensing, detailed syntheses and modeling have  
2233 increased our knowledge of the surface circulation and its complex implications for biological production, along with an  
2234 increased understanding of air-sea interaction in the Indian ocean.

2235 There are, however, a number of outstanding questions that require prioritised efforts. Compared to the Atlantic and  
2236 Pacific, where the important boundary currents are now being monitored with a suite of gliders with repeated and sustained  
2237 sections (Todd et al. 2019), the boundary currents and their variability in the Indian Ocean remain poorly constrained.  
2238 Given the anomalous warming of the Indian Ocean, the frequency of heatwaves, and the population supported by the  
2239 Indian Ocean and Monsoons, the air-sea fluxes and the coupled atmosphere-ocean exchange in this ocean remain poorly  
2240 understood at many scales. Understanding of the intermediate, deep and abyssal layer circulation and the vertical  
2241 overturning cells that connect these layers in the Indian Ocean is lacking.

2243 There are still many gaps in current understanding of Indian Ocean biogeochemical cycles, which we have presented here  
2244 in the context of the physical processes that affect them. Although the characterization of the temporal and spatial  
2245 variability in chlorophyll concentration and primary production has greatly improved as a result of recent in situ  
2246 measurements and satellite remote sensing, there are still many areas where there is little or no information about how this  
2247 relates to changes in planktonic food web structure and particulate organic matter export to the deep ocean. Although  
2248 nutrient limitation patterns were not discussed in this review, it should be pointed out that the importance of nitrogen  
2249 verses iron and silica limitation in the Arabian Sea and elsewhere in the Indian Ocean is still a subject of debate - more  
2250 nutrient and trace metal measurements are needed along with nutrient limitation bioassays throughout the Indian Ocean.

2251 The number of nitrogen fixation rate measurements in the Indian Ocean has increased significantly over the last decade,  
2252 but the importance of this process as a source of new nitrogen to the surface ocean has been quantified in only a few  
2253 regions (e.g., off northwest Australia) and its contribution to bloom formation (e.g., the Madagascar Bloom) is still  
2254 uncertain. From a spatial standpoint, the quantification of biogeochemical variability in the northern Indian Ocean  
2255 (Arabian Sea and Bay of Bengal) has benefited, in particular, from numerous shipboard measurements, moorings and  
2256 biogeochemical Argo float deployments in the last decade. Many questions still remain, for example, related to the  
2257 influence of freshwater inputs on biogeochemical cycles in the Bay of Bengal. Remarkably, the biogeochemical and  
2258 ecological impacts of the Indonesian Throughflow have been examined in only a handful of studies. Similarly, there are  
2259 very few studies that focus on the biogeochemical and ecological impacts of the Seychelles-Chagos Thermocline Ridge  
2260 (SCTR). The ITF and the SCTR are unique features of the Indian Ocean, yet the understanding of their biogeochemical  
2261 and ecological impacts is rudimentary at best. Finally, the quantification of biogeochemical variability in the Leeuwin  
2262 and Agulhas Currents and adjacent waters has also benefited from recent measurements, though it is important to point  
2263 out that the biogeochemical impacts of boundary currents in the Indian Ocean are still poorly understood compared to the  
2264 Atlantic and Pacific.

2265 There are still large uncertainties in air-sea fluxes. Even in the regional basin of the Bay of Bengal where there have been  
2266 focused international efforts, the river discharge and rain need to be better represented in models, as do the processes that  
2267 set the shallow salinity stratification. These have important feedbacks on the SST which impacts atmospheric convection  
2268 with a global reach. At longer time scales, the salinity feedbacks to climate at interannual to decadal timescales need to be  
2269 investigated in further detail. The decadal variability of the Indian Ocean Dipole and its link to the Pacific decadal  
2270 variability also needs to be better understood, particularly given events like the record breaking 2019 positive IOD that  
2271 developed independently from ENSO conditions. Marine heatwaves are an increasing threat to marine ecosystems fuelled  
2272 by increasing mean temperatures in the ocean and atmosphere. There are still large gaps in our understanding of the Indian  
2273 Ocean dynamics that lead to these extremes, and consequently in our ability to predict the onset, intensity and frequency  
2274 of extreme weather such as rainfall, flooding and heatwaves, associated with anomalously strong climatic mode events,  
2275 that have major socioeconomic impacts.

Deleted: and

Deleted: ,

2278 Modeling and observational efforts have both pointed to the increased role of air-sea coupling at higher frequencies to  
2279 improve the predictions of sub-seasonal Monsoon forecasts. Observations and models indicate that MISOs may be slowing  
2280 down because of the warming in the Indian Ocean (e.g. Sabeerali et al. 2013), which needs to be understood better for  
2281 providing reliable monsoon predictions and projections in this climate vulnerable region.

2282 On the influence of small-scale mixing, increased measurements of ocean mixing both along the equator and new long-  
2283 term measurements in the Bay of Bengal, have shown intensively enhanced mixing during the passage of eddies and during  
2284 cyclones. However, there are still significant uncertainties in subsurface ocean mixing in setting the large-scale balance in  
2285 the Indian ocean.

2286 It has been proposed that the hiatus in warming of the surface atmosphere may have ceased as the Pacific Ocean enters an  
2287 El Nino like state (Cha et al. 2018). However, the secular trends in the Pacific Ocean trade winds are expected to continue  
2288 to affect the Indo-Pacific Ocean heat content through the Indonesian Throughflow (Maher et al. 2018). The Indian Ocean  
2289 thus remains a critical component of the Earth's global response to the continued anthropogenic forcing and the ocean's  
2290 role as a clearing house for distributing heat to modulate global warming.

2291 **Code Availability**

2292 No original data analyses were undertaken as part of this review paper.

2293 **Data Availability**

2294 No original data analyses were undertaken as part of this review paper. All data presented in this manuscript have been  
2295 previously published and are available from sources identified in the original manuscripts.

2296 **Author Contributions**

2297 HEP and AT designed the review, wrote the introductory and concluding parts and sections in their areas of expertise. HP  
2298 and AT reviewed the contributions of the authors and made editorial adjustments. RH wrote the sections on  
2299 biogeochemical variability in Section 4. All co-authors contributed to the writing of sections relevant to their areas of  
2300 expertise and response to reviewer questions. All authors contributed to refining the manuscript for submission. RF, CU,  
2301 JB, BW, AS-F, JH and RM contributed editorial advice.

2302     **Competing interests**

2303     The authors declare that they have no conflict of interest.

2304     **Acknowledgements**

2305     The authors acknowledge the sustained efforts of researchers and funding agencies in observing and modelling the oceanic  
2306     and atmospheric processes that control climate variability in the Indian Ocean region. These contributions during the  
2307     International Indian Ocean Expeditions (I and II) and in the intervening years through national and international programs,  
2308     such as CLIVAR and GOOS, are fundamental to improving our knowledge of these systems and increasing our skill at  
2309     forecasting variability and extreme events. We thank the IIOE-2 leadership team (<https://iioe-2.incois.gov.in/>) for their  
2310     unwavering efforts to share new discoveries and promote understanding of the importance of the Indian Ocean to the  
2311     climate system and Earth’s inhabitants. We are very grateful to Michael McPhaden, Lisa Beal and an anonymous reviewer  
2312     for their encouraging and constructive comments that have led to a more comprehensive and balanced synthesis of recent  
2313     advances. HEP acknowledges [support from the Earth Systems and Climate Change Hub and Climate Systems Science](#)  
2314     [Hub of](#) the Australian Government’s National Environmental Science Programme and [the ARC Centre of Excellence for](#)  
2315     [Climate Extremes](#). AT acknowledges the US Office of Naval Research.

Deleted: AT

Deleted: , for their support

2316     **References**

2317     Abram, N. J., Gagan, M. K., Cole, J. E., Hantoro, W. S., and Mudelsee, M.: Recent intensification of tropical climate  
2318     variability in the Indian Ocean. *Nature Geoscience*, 1, 849–853, <https://doi.org/10.1038/ngeo357>, 2008.  
2319     Abram, N. J., Hargreaves, J. A., Wright, N. M., Thirumalai, K., Ummenhofer, C. C., and England, M. H.: Palaeoclimate  
2320     perspectives on the Indian Ocean Dipole. *Quat. Sci. Rev.*, 237, 106302,  
2321     <https://doi.org/10.1016/j.quascirev.2020.106302>, 2020a.  
2322     Abram, N. J., Wright, N. M., Ellis, B., Dixon, B. C., Wurtzel, J. B., England, M. H., Ummenhofer, C. C., Philibosian, B.,  
2323     Cahyarini, S. Y., Yu, T.-L., Shen, C.-C., Cheng, H., Edwards, R. L., and Heslop, D.: Coupling of Indo-Pacific climate  
2324     variability over the last millennium, *Nature*, 579, 385–392, <https://doi.org/10.1038/s41586-020-2084-4>, 2020b.  
2325     Akhil, V. P., Durand, F., Lengaigne, M., Vialard, J., Keerthi, M. G., Gopalakrishna, V. V., Deltel, C., Papa, F. and De  
2326     Boyer Montégut, C.: A modeling study of the processes of surface salinity seasonal cycle in the Bay of Bengal, *J.*  
2327     *Geophys. Res. Ocean.*, doi:10.1002/2013JC009632, 2014.  
2328     [Amol, P., Shankar, D., Fernando, V., Mukherjee, A., Aparna, S. G., Fernandes, R., Michael, G. S., Khalap, S. T.,](#)  
2329     [Satelkar, N. P., Agarvadekar, Y., Gaonkar, M. G., Tari, A. P., Kankonkar, A. and Vernekar, S. P.: Observed](#)  
2330     [intraseasonal and seasonal variability of the West India Coastal Current on the continental slope; J. Earth Syst. Sci.](#)  
2331     [123 1045–1074, https://doi.org/10.1007/s12040-014-0449-5, 2014.](#)  
2332     Alory, G., Wijffels, S., and Meyers, G.: Observed temperature trends in the Indian Ocean over 1960–1999 and  
2333     associated mechanisms. *Geophys. Res. Lett.*, 34, L02606, <https://doi.org/10.1029/2006GL028044>, 2007.  
2334     Anderson, D. L. T., and Gill, A. E.: Spin-up of a stratified ocean, with applications to upwelling, *Deep Sea Res.*, 22(9),  
2335     583–596, [https://doi.org/10.1016/0011-7471\(75\)90046-7](https://doi.org/10.1016/0011-7471(75)90046-7), 1975.

2338 Andrews, J.C.: Eddy structure and the West Australian current, *Deep Sea Research*, 24(12), 1133–1148,  
2339 [https://doi.org/10.1016/0146-6291\(77\)90517-3](https://doi.org/10.1016/0146-6291(77)90517-3), 1977.

2340 Annamalai, H., Potemra, J., Murtugudde, R., and McCreary, J. P.: Effect of preconditioning on the extreme climate  
2341 events in the tropical Indian Ocean, *J. Climate*, 18, 3450–3469, <https://doi.org/10.1175/JCLI3494.1>, 2005.

2342 Anutaliya, A., Send, U., Mclean, J., Sprintall, J., Rainville, L., M. Lee, C., Jinadasa, S., Wallcraft, A, J., Metzger, E.:  
2343 An undercurrent off the east coast of Sri Lanka. *Ocean Sci. Discuss.* 13, 1–15, 2017.

2344 Arzeno, I. B., S. N. Giddings, G. Pawlak, and R. Pinkel: Generation of Quasi Biweekly Yanai Waves in the Equatorial  
2345 Indian Ocean. *Geophys Res Lett*, 47, e2020GL088915. <https://doi.org/10.1029/2020GL088915>, 2020.

2346 Ash, K. D., and Matyas, C. J.: The influences of ENSO and the Subtropical Indian Ocean Dipole on tropical cyclone  
2347 trajectories in the South Indian Ocean, *Int. J. Climatol.*, 32, 41–56, <https://doi.org/10.1002/joc.2249>, 2012.

2348 Ayers, J. M., Strutton, P. G., Coles, V. J., Hood, R. R. and Matear, R. J.: Indonesian throughflow nutrient fluxes and  
2349 their potential impact on Indian Ocean productivity, *Geophys. Res. Lett.*, doi:10.1002/2014GL060593, 2014.

2350 Bahmanpour, M. H., Pattiaratchi, C., Wijeratne, E. M. S., Steinberg, C., and D'Adamo, N.: Multi-year observation of  
2351 Holloway Current along the shelf edge of North Western Australia, *J. Coast. Res.*, 517–521,  
2352 <https://doi.org/10.2112/S175-104.1>, 2016.

2353 Banse, K. and English, D. C.: Geographical differences in seasonality of CZCS-derived phytoplankton pigment in the  
2354 Arabian Sea for 1978-1986, *Deep. Res. Part II Top. Stud. Oceanogr.*, doi:10.1016/S0967-0645(99)00157-5, 2000.

2355 Banse, K. and McClain, C.: Winter blooms of phytoplankton in the Arabian Sea as observed by the Coastal Zone Color  
2356 Scanner, *Mar. Ecol. Prog. Ser.*, doi:10.3354/meps034201, 1986.

2357 Baranowski, D. B., M. K. Flatau, P. J. Flatau, and A. J. Matthews (2016), Impact of atmospheric convectively coupled  
2358 equatorial kelvin waves on upper ocean variability, *Journal of Geophysical Research-Atmospheres*, 121(5), 2045–  
2359 2059, doi:10.1002/2015jd024150.

2360 Barlow, R., Lamont, T., Kyewalyanga, M., Sessions, H. and Morris, T.: Phytoplankton production and physiological  
2361 adaptation on the southeastern shelf of the Agulhas ecosystem, *Cont. Shelf Res.*, doi:10.1016/j.csr.2010.05.007, 2010.

2362 Barlow, R., Lamont, T., Morris, T., Sessions, H. and van den Berg, M.: Adaptation of phytoplankton communities to  
2363 mesoscale eddies in the Mozambique Channel, *Deep. Res. Part II Top. Stud. Oceanogr.*,  
2364 doi:10.1016/j.dsr2.2013.10.020, 2014.

2365 Beal, L. M. and Bryden, H. L.: The velocity and vorticity structure of the Agulhas Current at 32°S, *J. Geophys. Res.*  
2366 *Ocean.*, doi:10.1029/1998jc000056, 1999.

2367 Beal, L. M., De Ruijter, W. P. M., Biastoch, A., Zahn, R., Cronin, M., Hermes, J., Lutjeharms, J., Quartly, G., Tozuka,  
2368 T., Baker-Yeboah, S., Bormman, T., Cipollini, P., Dijkstra, H., Hall, I., Park, W., Peeters, F., Penven, P., Ridderinkhof,  
2369 H. and Zinke, J.: On the role of the Agulhas system in ocean circulation and climate, *Nature*, doi:10.1038/nature09983,  
2370 2011.

2371 Beal, L. M. and Donohue, K. A.: The Great Whirl: Observations of its seasonal development and interannual variability,  
2372 *J. Geophys. Res. Ocean.*, doi:10.1029/2012JC008198, 2013.

2373 Beal, L. M., Hormann, V., Lumpkin, R., & Foltz, G. R.: The Response of the Surface Circulation of the Arabian Sea to  
2374 Monsoonal Forcing, *Journal of Physical Oceanography*, 43(9), 2008-2022.  
2375 <https://journals.ametsoc.org/view/journals/phoc/43/9/jpo-d-13-033.1.xml>, 2013.

2376 Beal, L. M., Elipot, S., Houk, A., and Leber, G. M.: Capturing the Transport Variability of a Western Boundary Jet:  
2377 Results from the Agulhas Current Time-Series Experiment (ACT)\*, *Journal of Physical Oceanography*, 45, 1302–  
2378 1324, <https://doi.org/10.1175/jpo-d-14-0119.1>, 2015.

2379 Beal, L. and Elipot, S.: Broadening not strengthening of the Agulhas Current since the early 1990s. *Nature*, 540, 570–  
2380 573, <https://doi.org/10.1038/nature19853>, 2016.

2381 Beal, L. M., Vialard, J., Roxy, M. K. and lead authors: IndOOS-2: A roadmap to sustained observations of the Indian  
2382 Ocean for 2020-2030. CLIVAR-4/2019, GOOS-237, 204 pp. doi: <https://doi.org/10.36071/clivar.rp.4.2019>, 2019.

2383 Beal, L. M., Vialard, J., Roxy, M. K., Li, J., Andres, M., Annamalai, H., Feng, M., Han, W., Hood, R., Lee, T.,  
2384 Lengaigne, M., Lumpkin, R., Masumoto, Y., McPhaden, M. J., Ravichandran, M., Shinoda, T., Sloyan, B. M.,

Deleted: , 2020

Formatted: Font colour: Auto

Formatted: Font colour: Auto

Formatted: Font colour: Auto

Formatted: Font colour: Auto

2386 Strutton, P. G., Subramanian, A. C., Tozuka, T., Ummenhofer, C. C., Unnikrishnan, A. S., Wiggert, J., Yu, L., Cheng,  
 2387 L., Desbruyères, D. G., & Parvathi, V.: A Road Map to IndOOS-2: Better Observations of the Rapidly Warming  
 2388 Indian Ocean, *Bulletin of the American Meteorological Society*, 101(11), E1891-E1913,  
 2389 <https://journals.ametsoc.org/view/journals/bams/101/11/bamsD190209.xml>, 2020.  
 2390 Behera, S.K., and Yamagata, T.: Subtropical SST dipole events in the southern Indian Ocean, *Geophys. Res. Lett.*, 28,  
 2391 327–330, <https://doi.org/2000GL011451>, 2001.  
 2392 Bellon, G., Sobel, A. H., and Vialard, J.: Ocean-atmosphere coupling in the monsoon intraseasonal oscillation: A simple  
 2393 model study, *J. Clim.*, 21(20), 5254–5270, <http://doi.org/10.1175/2008JCLI2305.1>, 2008.  
 2394 Benthuyssen, J., Feng, M., and Zhong, L.: Spatial patterns of warming off Western Australia during the 2011 Ningaloo  
 2395 Niño: quantifying impacts of remote and local forcing, *Continental Shelf Res.*, 91, 232–246,  
 2396 <https://doi.org/10.1016/j.csr.2014.09.014>, 2014a.  
 2397 Benthuyssen, J., Furue, R., McCreary, J. P., Bindoff, N. L., and Phillips, H. E.: Dynamics of the Leeuwin Current: Part 2.  
 2398 Impacts of mixing, friction, and advection on a buoyancy-driven eastern boundary current over a shelf, *Dyn. Atmos.*  
 2399 *Oceans*, 65, 39–63, <https://doi.org/10.1016/j.dynatmoce.2013.10.004>, 2014b.  
 2400 Benthuyssen, J. A., Oliver, E.C.J., Feng, M., and Marshall, A. G.: Extreme marine warming across tropical Australia  
 2401 during austral summer 2015–2016, *J. Geophys. Res.: Oceans*, 123, 1301–1326, <https://doi.org/10.1002/2017JC013326>,  
 2402 2018.  
 2403 Bergman, J. W., Hendon, H. H., and Weickmann, K. M.: Intraseasonal air-sea interactions at the onset of El Nino, *J.*  
 2404 *Climate*, 14, 1702–1719, 2001.  
 2405 Beron-Vera, F. J., Wang, Y., Olascoaga, M. J., Goni, G. J. and Haller, G.: Objective detection of oceanic eddies and the  
 2406 agulhas leakage, *J. Phys. Oceanogr.*, doi:10.1175/JPO-D-12-0171.1, 2013.  
 2407 Biastoch, A., Böning, C. W. and Lutjeharms, J. R. E.: Agulhas leakage dynamics affects decadal variability in Atlantic  
 2408 overturning circulation, *Nature*, doi:10.1038/nature07426, 2008.  
 2409 Biastoch, A., Böning, C. W., Schwarzkopf, F. U. and Lutjeharms, J. R. E.: Increase in Agulhas leakage due to poleward  
 2410 shift of Southern Hemisphere westerlies, *Nature*, doi:10.1038/nature08519, 2009.  
 2411 Biastoch, A. and Böning, C. W.: Anthropogenic impact on Agulhas leakage, *Geophys. Res. Lett.*, doi:10.1002/grl.50243,  
 2412 2013.  
 2413 Biastoch, A., Durgadoo, J. V., Morrison, A. K., Van Sebille, E., Weijer, W. and Griffies, S. M.: Atlantic multi-decadal  
 2414 oscillation covaries with Agulhas leakage, *Nat. Commun.*, doi:10.1038/ncomms10082, 2015.  
 2415 Boyd, A. J. and Shillington, F. A.: Physical forcing and circulation patterns on the Agulhas Bank, *S. Afr. J. Sci.*, 90(3)  
 2416 114–122, 1994.  
 2417 Brock, J. C. and McClain, C. R.: Interannual variability in phytoplankton blooms observed in the northwestern Arabian  
 2418 Sea during the southwest monsoon, *J. Geophys. Res.*, doi:10.1029/91JC02225, 1992.  
 2419 Brown, S. L., Landry, M. R., Barber, R. T., Campbell, L., Garrison, D. L. and Gowing, M. M.: Picophytoplankton  
 2420 dynamics and production in the Arabian Sea during the 1995 Southwest Monsoon, *Deep. Res. Part II Top. Stud.*  
 2421 *Oceanogr.*, doi:10.1016/S0967-0645(99)00042-9, 1999.  
 2422 Bryden, H. and Beal, L.: Role of the Agulhas Current in Indian Ocean circulation and associated heat and freshwater  
 2423 fluxes. *Deep-Sea Research I*, 48(8), 1821–1845, 2001.  
 2424 Burchall, J. : An evaluation of primary productivity studies in the continental shelf region of the Agulhas Current near  
 2425 Durban (1961–1966), Investigational Report, Oceanographic Research Institute, 20: 16 pp, 1968.  
 2426 Cai, W., Sullivan, A., and Cowan, T.: Shoaling of the off-equatorial south Indian Ocean thermocline: Is it driven by  
 2427 anthropogenic forcing? *Geophys. Res. Lett.*, 35, <https://doi.org/10.1029/2008GL034174>, 2008.  
 2428 Cai, W., Cowan, T., and Sullivan, A.: Recent unprecedented skewness towards positive Indian Ocean Dipole  
 2429 occurrences and their impact on Australian rainfall. *Geophys. Res. Lett.*, 36, <https://doi.org/10.1029/2009GL037604>,  
 2430 2009a.

Deleted: . ,



2432 Cai, W., Pan, A., Roemmich, D., Cowan, T., and Guo, X.: Argo profiles a rare occurrence of three consecutive positive  
2433 Indian Ocean Dipole events, 2006–2008, *Geophys. Res. Lett.*, 36, <https://doi.org/10.1029/2008GL037038>, 2009b.

2434 Cai, W., Sullivan, A., and Cowan, T.: Climate change contributes to more frequent consecutive positive Indian Ocean  
2435 Dipole events. *Geophys. Res. Lett.*, 36 (L23704), <https://doi.org/10.1029/2009GL040163>, 2009c.

2436 Cai, W., Sullivan, A., and Cowan, T.: How rare are the 2006–2008 positive Indian Ocean Dipole events? An IPCC AR4  
2437 climate model perspective, *Geophys. Res. Lett.*, 36 (L08702), <https://doi.org/10.1029/2009GL037982>, 2009d.

2438 Cai, W., Zheng, X.-T., Weller, E., Collins, M., Cowan, T., Lengaigne, M., Yu, W., and Yamagata, T.: Projected  
2439 response of the Indian Ocean Dipole to greenhouse warming, *Nat. Geosci.*, 6, 999–1007,  
2440 <https://doi.org/10.1038/ngeo2009>, 2013.

2441 Cai, W., Santoso, A., Wang, G., Weller, E., Wu, L., Ashok, K., Masumoto, Y., and Yamagata, T.: Increased frequency  
2442 of extreme Indian Ocean Dipole events due to greenhouse warming, *Nature*, 510, 254–258,  
2443 <https://doi.org/10.1038/nature13327>, 2014a.

2444 Cai, W., Borlace, S., Lengaigne, M., van Rensch, P., Collins, M., Vecchi, G., Timmermann, A., Santoso, A., McPhaden,  
2445 M. J., Wu, L., and England, M. H.: Increasing frequency of extreme El Niño events due to greenhouse warming, *Nat.*  
2446 *Clim. Change*, 4, 2, 111–116, <https://doi.org/10.1038/nclimate2100>, 2014b.

2447 Cai, W., Wang, G., Santoso, A., McPhaden, M. J., Wu, L., Jin, F. F., Timmermann, A., Collins, M., Vecchi, G.,  
2448 Lengaigne, M., and England, M. H.: Increased frequency of extreme La Niña events under greenhouse warming, *Nat.*  
2449 *Clim. Change*, 5, 2, 132–137, <https://doi.org/10.1038/nclimate2492>, 2015.

2450 Cai, W. et al.: Pantropical climate interactions. *Science*, 363, doi:10.1126/science.aav4236, 2019.

2451 Caley, T., Giraudeau, J., Malaizé, B., Rossignol, L. and Pierre, C.: Agulhas leakage as a key process in the modes of  
2452 Quaternary climate changes, *Proc. Natl. Acad. Sci. U. S. A.*, doi:10.1073/pnas.1115545109, 2012.

2453 Caputi, N., de Lestang, S., Feng, M., and Pearce, A. F.: Seasonal variation in the long-term warming trend in water  
2454 temperature off the Western Australian coast. *Mar. Freshw. Res.*, 60, 129–139, 2009.

2455 Carter, R. A. and Schleyer, M. H.: Plankton distributions in Natal coastal waters., E. H. Schumann (ed.), *Coastal Ocean*  
2456 *Studies off Natal, South Africa* (Springer-Verlag: New York), 2012.

2457 Castellanos, P., Campos, E. J. D., Piera, J., Sato, O. T. and Silva Dias, M. A. F.: Impacts of Agulhas leakage on the  
2458 tropical Atlantic western boundary systems, *J. Clim.*, doi:10.1175/JCLI-D-15-0878.1, 2017.

2459 Cessi, P.: The Global Overturning Circulation, *Annual Review of Marine Science*, 11(1), 249–270,  
2460 <https://doi.org/10.1146/annurev-marine-010318-095241>, 2019.

2461 Cha, S.-C., Moon, J.-H., and Song, Y. T.: A recent shift toward an El Niño-like ocean state in the tropical Pacific and  
2462 the resumption of ocean warming. *Geophysical Research Letters*, 45, 11,885– 11,894.  
2463 <https://doi.org/10.1029/2018GL080651>, 2018.

2464 Chatterjee, A., Shankar, D., Shenoi, S. S. C., Reddy, G. V., Michael, G. S., Ravichandran, M., Gopalkrishna, V. V., Rao,  
2465 E. P. R., Bhaskar, T. V. S. U. and Sanjeevan, V. N.: A new atlas of temperature and salinity for the North Indian  
2466 Ocean, *J. Earth Syst. Sci.*, 121(3), 559–593, doi:10.1007/s12040-012-0191-9, 2012.

2467 Chatterjee, A., Shankar, D., McCreary, J. P. and Vinayachandran, P. N.: Yanai waves in the western equatorial Indian  
2468 Ocean, *J. Geophys. Res. Oceans*, 118, 1556–1570, doi:10.1002/jgrc.20121, 2013.

2469 Chatterjee, A., Shankar, D., McCreary, J. P., Vinayachandran, P. N. and Mukherjee, A.: Dynamics of Andaman Sea  
2470 circulation and its role in connecting the equatorial Indian Ocean to the Bay of Bengal, *J. Geophys. Res. Ocean.*,  
2471 doi:10.1002/2016JC012300, 2017.

2472 Chatterjee, A., Kumar, B. P., Prakash, S., and Singh, P.: Annihilation of the Somali upwelling system during summer  
2473 monsoon, *Scientific reports*, 9(1), 7598. <https://doi.org/10.1038/s41598-019-44099-1>, 2019.

2474 Chaudhuri, D., Sengupta, D., D’Asaro, E., Venkatesan, R. and Ravichandran, M.: Response of the salinity-stratified bay  
2475 of Bengal to Cyclone Phailin, *J. Phys. Oceanogr.*, doi:10.1175/JPO-D-18-0051.1, 2019.

Deleted: <https://doi.org/10.1029/2018GL080651>.

- Chaudhuri, A., Shankar, D., Aparna, S. G., Amol, P., Fernando, V., Kankonkar, A., Micheal, G. S., Satelkar, N. P., Khalap, S. T., tari, A. P., Gaonkar, M. G., Ghatkar, S., Khedekar, R. R.: Observed variability of the West India Coastal Current on the continental slope from 2009–2018, *J. Earth Syst. Sci.*, 129, <https://doi.org/10.1007/s12040-019-1322-3>, 2020.
- Chen, G., Han, W., Li, Y., Wang, D. and McPhaden, M. J.: Seasonal-to-interannual time-scale dynamics of the equatorial undercurrent in the Indian Ocean, *J. Phys. Oceanogr.*, doi:10.1175/JPO-D-14-0225.1, 2015.
- Chen, G., Han, W., Shu, Y., Li, Y., Wang, D. and Xie Q.: The role of Equatorial Undercurrent in sustaining the Eastern Indian Ocean upwelling, *Geophys. Res. Lett.*, 43, 6444–6451, doi:10.1002/2016GL069433, 2016.
- Chen, G., Han, W., Li, Y., Yao, J. and Wang, D.: Intraseasonal Variability of the Equatorial Undercurrent in the Indian Ocean, *Journal of Physical Oceanography*, 49(1), 85–101, 2019.
- Cheng, Y., Putrasahan, D., Beal, L. and Kirtman, B.: Quantifying Agulhas leakage in a high-resolution climate model, *J. Clim.*, doi:10.1175/JCLI-D-15-0568.1, 2016.
- Cheng, Y., Beal, L.M., Kirtman, B.P., and Putrasahan, D.: Interannual Agulhas Leakage Variability and Its Regional Climate Imprints, *J. Climate*, 31(24), 10105–10121, 2018.
- Cheng, X., McCreary, J. P., Qiu, B., Qi, Y., Du, Y. and Chen, X.: Dynamics of Eddy Generation in the Central Bay of Bengal, *J. Geophys. Res. Ocean.*, doi:10.1029/2018JC014100, 2018.
- Chi, N.-H., Lien, R.-C., D'Asaro, E. A., and Ma, B. B.: The surface mixed layer heat budget from mooring observations in the central Indian Ocean during Madden-Julian Oscillation events, *J. Geophys. Res. Ocean.*, 119(7), 4638–4652, <https://doi.org/10.1002/2014JC010192>, 2014.
- Chowdary, J. S., Xie, S., Tokinaga, H., Okumura, Y. M., Kubota, H., Johnson, N., and Zheng, X.: Interdecadal variations in ENSO teleconnection to the Indo–Western Pacific for 1870–2007, *Journal of Climate*, 25(5), 1722–1744, 2012.
- Chowdary, J. S., Bandgar, A. B., Gnanaseelan, C., and Luo, J. J.: Role of tropical Indian Ocean air-sea interactions in modulating Indian summer monsoon in a coupled model, *Atmos. Sci. Lett.*, 16(2), 170–176, doi:10.1002/asl2.561, 2015.
- Church, J.A., Cresswell, G.R., and Godfrey J.S.: The Leeuwin Current, in: Poleward Flows Along Eastern Ocean Boundaries, Coastal and Estuarine Studies (formerly Lecture Notes on Coastal and Estuarine Studies), vol 34, edited by: Neshyba, S.J., Mooers, C.N.K., Smith, R.L., and Barber, R.T., Springer, New York, 230–254, [https://doi.org/10.1007/978-1-4613-8963-7\\_16](https://doi.org/10.1007/978-1-4613-8963-7_16), 1989.
- Cirano, M. and Middleton, J.F.: Aspects of the mean wintertime circulation along Australia's southern shelves: Numerical studies. *J. Phys. Oceanogr.*, 34, 668–684, <https://doi.org/10.1175/2509.1>, 2004.
- Coles, V. J., Wilson, C. and Hood, R. R.: Remote sensing of new production fuelled by nitrogen fixation, *Geophys. Res. Lett.*, doi:10.1029/2003gl019018, 2004.
- Cullen, K. E. and Shroyer, E. L.: Seasonality and interannual variability of the Sri Lanka dome, *Deep. Res. Part II Top. Stud. Oceanogr.*, doi:10.1016/j.dsr2.2019.104642, 2019.
- Currie, J. C., Lengaigne, M., Vialard, J., Kaplan, D. M., Aumont, O., Naqvi, S. W. A., and Maury, O.: Indian Ocean Dipole and El Niño/Southern Oscillation impacts on regional chlorophyll anomalies in the Indian Ocean. *Biogeosciences*, 10, 6677–6698, 2013.
- Cuyppers, Y., X. Le Vaillant, P. Bouruet-Aubertot, J. Vialard and M. J. McPhaden, 2013: Tropical storm-induced near-inertial internal waves during the Cirene experiment: energy fluxes and impact on vertical mixing. *J. Geophys. Res.*, 118, 358–380, doi: 10.1029/2012JC007881.
- Cyriac, A., M. McPhaden, H. Phillips, N. Bindoff, M. Feng: Surface layer heat balance in the subtropical Indian Ocean. *J. Geophys. Res. Oceans*, 124, 6459–6477. <https://doi.org/10.1029/2018JC014559>, 2019.
- Cyriac, A., Phillips, H. E., Bindoff, N. L., Mao, H. & Feng, M.: Observational estimates of turbulent mixing in the southeast Indian Ocean. *J Phys Oceanogr*, doi:10.1175/jpo-d-20-0036.1, 2021.

D'Adamo, N., Fandry, C., Buchan, S., Domingues, C.: Northern sources of the Leeuwin Current and the "Holloway Current" on the North West Shelf, *J. Roy. Soc. Western Australia*, 92(2), 53–66, <http://nora.nerc.ac.uk/id/eprint/526029>, 2009.

Daher, H., Beal, L. M., and Schwarzkopf, F. U.: A new improved estimation of Agulhas Leakage using observations and simulations of Lagrangian floats and drifters, *Journal of Geophysical Research: Oceans*, 125, <https://doi.org/10.1029/2019JC015753>, 2020.

David, D. T., Kumar, S. P., Byju, P., Sarma, M. S. S., Suryanarayana, A., and Murty, V. S. N.: Observational evidence of lower-frequency Yanai waves in the central equatorial Indian Ocean, *Journal of Geophysical Research*, 116 (C06009), doi:10.1029/2010JC006603, 2011..

De Boer, A. M., Graham, R. M., Thomas, M. D., and Kohfeld, K. E.: The control of the Southern Hemisphere Westerlies on the position of the Subtropical Front, *J. Geophys. Res. Oceans*, 118, 5669–5675, doi:10.1002/jgrc.20407, 2013.

de Vos, A., Pattiaratchi, C. B. and Wijeratne, E. M. S.: Surface circulation and upwelling patterns around Sri Lanka, *Biogeosciences*, doi:10.5194/bg-11-5909-2014, 2014.

Demarcq, H., Barlow, R. G. and Shillington, F. A.: Climatology and variability of sea surface temperature and surface chlorophyll in the benguela and agulhas ecosystems as observed by satellite imagery, *African J. Mar. Sci.*, doi:10.2989/18142320309504022, 2003.

DeMott, C. A., Klingaman, N. P., and Woolnough, S. J.: Atmosphere-ocean coupled processes in the Madden-Julian oscillation, *Rev. Geophys.*, 53, 1099–1154, <http://doi.org/10.1002/2014RG000478>, 2015.

Desbruyères, D. G., McDonagh, E. L., King, B. A., and Thierry, V.: Global and Full-Depth Ocean Temperature Trends during the Early Twenty-First Century from Argo and Repeat Hydrography, *J. Climate*, <https://doi.org/10.1175/JCLI-D-16-0396.1>, 2017.

Deshpande, A., Gnanaseelan, C., Chowdary, J., and Rahul, S.: Interannual spring Wyrkti jet variability and its regional impacts, *Dyn. Atmos. Oceans*, 78, 26–37, 2017.

Dhage, L., and Strub, P. T.: Intra-seasonal sea level variability along the west coast of India, *J. Geophys. Res. Oceans*, 121, 8172–8188, doi:10.1002/2016JC011904, 2016.

Dileepkumar, M.: Biogeochemistry of the North Indian Ocean; IGBP-WCRP-SCOPE Rep. Ser. 1, Indian Nat. Sci. Acad., New Delhi, India, 2006.

Dilmahamod, Ahmad Fehmi: Links between the Seychelles-Chagos thermocline ridge and large scale climate modes and primary productivity and the annual cycle of chlorophyll-a, PhD thesis, University of Cape Town, 2014.

Dilmahamod, A. F., Aguiar-González, B., Penven, P., Reason, C. J. C., De Ruijter, W. P. M., Malan, N., & Hermes, J. C.: SIDDIES corridor: A major east-west pathway of long-lived surface and subsurface eddies crossing the subtropical south indian ocean. *Journal of Geophysical Research: Oceans*, 123, 5406–5425. <https://doi.org/10.1029/2018JC013828>, 2018.

Dilmahamod, A. F., Penven, P., Aguiar-González, B., Reason, C. J. C., & Hermes, J. C.: A new definition of the South-East Madagascar Bloom and analysis of its variability. *Journal of Geophysical Research: Oceans*, 124, 1717–1735. <https://doi.org/10.1029/2018JC014582>, 2019.

Divakaran, P., and Brassington, G.B.: Arterial ocean circulation of the southeast Indian Ocean, *Geophys. Res. Lett.*, 38, L01802, <https://doi.org/10.1029/2010GL045574>, 2011.

Doi, T., Behera, S. K., and Yamagata, T.: Wintertime impacts of the 2019 super IOD on East Asia, *Geophys. Res. Lett.*, doi:10.1029/2020GL089456, 2020.

Domingues, C. M., Wijffels, S. E., Maltrud, M. E., Church, J. A. and Tomczak, M.: Role of eddies in cooling the Leeuwin Current, *Geophys. Res. Lett.*, doi:10.1029/2005GL025216, 2006.

Domingues, C. M., Maltrud, M. E., Wijffels, S. E., Church, J. A., Tomczak, M.: Simulated Lagrangian pathways between the Leeuwin Current System and the upper-ocean circulation of the southeast Indian Ocean, *Deep Sea Res. II*, 54, 797–817, <http://doi.org/10.1016/j.dsr2.2006.10.003>, 2007.

Deleted: .

Formatted: No underline

2569 Dong, L. and M.J. McPhaden: Interhemispheric SST gradient trends in the Indian Ocean prior to and during the recent  
2570 global warming hiatus. *J. Climate*, 29, 9077-9095, 2016.

2571 Dong, L., Zhou, T., Dai, A., Song, F., Wu, B., and Chen, X.: The footprint of the inter-decadal Pacific oscillation in  
2572 Indian Ocean sea surface temperatures, *Sci. Rep.*, 6, 21251, <https://doi.org/10.1038/srep21251>, 2016.

2573 Donohue, K. A. and Toole, J. M.: A near-synoptic survey of the Southwest Indian Ocean, *Deep. Res. Part II Top. Stud.*  
2574 *Oceanogr.*, doi:10.1016/S0967-0645(03)00039-0, 2003.

2575 Drushka, K., Sprintall, J., Gille, S. T. and Brodjonegoro, I.: Vertical structure of Kelvin waves in the Indonesian  
2576 throughflow exit passages, *J. Phys. Oceanogr.*, doi:10.1175/2010JPO4380.1, 2010.

2577 Drushka, K., Sprintall, J., Gille, S. T. and Wijffels, S.: In situ observations of Madden-Julian oscillation mixed layer  
2578 dynamics in the Indian and western Pacific Oceans, *J. Clim.*, 25(7), 2306–2328, doi:10.1175/JCLI-D-11-00203.1,  
2579 2012.

2580 Du, Y., Xie, S.-P., Huang, G., and Hu, K.: Role of air–sea interaction in the long persistence of El Niño–induced north  
2581 Indian Ocean warming, *J. Clim.*, 22, 2023-2038, <https://doi.org/10.1175/2008JCLI2590.1>, 2009.

2582 Du, Y., Cai, W., and Wu, Y.: A new type of the Indian Ocean dipole since the mid-1970s, *J. Climate*, 26, 959-972,  
2583 <https://doi.org/10.1175/JCLI-D-12-00047.1>, 2013.

2584 Du, Y., Y. Zhang, M. Feng, T. Wang, N. Zhang, and S. Wijffels, S.: Decadal trends of the upper ocean salinity in the  
2585 tropical Indo-Pacific since mid-1990s, *Scientific Reports*, 5, 16050, 2015.

2586 Du, Y., Zhang, Y., Zhang, L.-Y., Tozuka, T., Ng, B., & Cai, W.: Thermocline warming induced extreme Indian  
2587 Ocean dipole in 2019, *Geophysical Research Letters*, 47, e2020GL090079, <https://doi.org/10.1029/2020GL090079>,  
2588 2020.

2589 Dufois, F., Hardman-Mountford, N. J., Greenwood, J., Richardson, A. J., Feng, M., Herbet, S. and Matear, R.: Impact  
2590 of eddies on surface chlorophyll in the South Indian Ocean, *J. Geophys. Res. Ocean.*, 119, 8061-77,  
2591 doi:10.1002/2014JC010164, 2014.

2592 Duncan, B. and Han, W.: Influence of atmospheric intraseasonal oscillations on seasonal and interannual variability in  
2593 the upper Indian Ocean, *J. Geophys. Res. Ocean.*, 117, 1-24 doi:10.1029/2012JC008190, 2012.

2594 Duran, E. R.: An investigation of the Leeuwin Undercurrent source waters and pathways. Honours thesis, University of  
2595 Tasmania, 2015.

2596 Duran, E.R., Phillips, H.E., Furue, R., Spence, P., and Bindoff, N.L.: Southern Australia Current System based on a  
2597 gridded hydrography and a high-resolution model, *Prog. Oceanogr.*, 181, 102254,  
2598 <https://doi.org/10.1016/j.pcean.2019.102254>, 2020.

2599 Durgadoo, J. V., Loveday, B. R., Reason, C. J. C., Penven, P. and Biastoch, A.: Agulhas leakage predominantly  
2600 responds to the southern hemisphere westerlies, *J. Phys. Oceanogr.*, 43, 2113-2131, doi:10.1175/JPO-D-13-047.1,  
2601 2013.

2602 Durgadoo, J. V., Rñhs, S., Biastoch, A. and Böning, C. W. B.: Indian Ocean sources of Agulhas leakage, *J. Geophys.*  
2603 *Res. Ocean.*, doi:10.1002/2016JC012676, 2017.

2604 Elipot, S., & Beal, L. M.: Characteristics, energetics, and origins of Agulhas current meanders and their limited  
2605 influence on ring shedding. *Journal of Physical Oceanography*, 45(9), 2294-2314. [https://doi.org/10.1175/JPO-D-14-](https://doi.org/10.1175/JPO-D-14-0254.1)  
2606 [0254.1](https://doi.org/10.1175/JPO-D-14-0254.1), 2015.

2607 Elipot, S. and Beal, L. M.: Observed Agulhas Current Sensitivity to Interannual and Long-Term Trend Atmospheric  
2608 Forcings. *Journal of Climate*. 31 (8) p3077–3098. <https://doi.org/10.1175/JCLI-D-17-0597.1>, 2018

2609 Endo, S., and Tozuka, T.: Two flavors of the Indian Ocean dipole, *Climate Dyn.*, 46, 3371-3385, [https://doi.org/10.1007/s00382-](https://doi.org/10.1007/s00382-015-2773-0)  
2610 [015-2773-0](https://doi.org/10.1007/s00382-015-2773-0), 2016.

2611 England, M. H., and Huang, F.: On the interannual variability on the Indonesian Throughflow and its linkage with  
2612 ENSO, *J. Climate*, 18(9), 1435-1444, <https://doi.org/10.1175/JCLI3322.1>, 2005.

2613 England, M. H., Ummenhofer, C. C. and Santoso, A.: Interannual rainfall extremes over southwest Western Australia  
2614 linked to Indian Ocean climate variability, *J. Clim.*, doi:10.1175/JCLI3700.1, 2006.

Formatted: Font colour: Auto

Formatted: Font: Not Italic, Font colour: Auto

Formatted: Font colour: Auto

Formatted: Font colour: Auto

Formatted: Font colour: Auto

England, M., McGregor, S., Spence, P., Meehl, G., Timmerman, A., Cai, W., Sen Gupta, A., McPhaden, M., Purich, A. and Santoso, A.: Recent intensification of wind-driven circulation in the Pacific and the ongoing warming hiatus. *Nature Clim Change* 4, 222–227, <https://doi.org/10.1038/nclimate2106>, 2014.

Fan, L., Liu, Q., Wang, C., and Guo, F.: Indian Ocean dipole modes associated with different types of ENSO development, *J. Climate*, 30, 2233–2249, <https://doi.org/10.1175/JCLI-D-16-0426.1>, 2017.

Fang, F., and Morrow, R.: Evolution, movement and decay of warm-core Leeuwin Current eddies, *Deep Sea Res. II*, 50(12–13), 2245–2261, [https://doi.org/10.1016/S0967-0645\(03\)00055-9](https://doi.org/10.1016/S0967-0645(03)00055-9), 2003.

Fang, G., Susanto, R. D., Wirasantosa, S., Qiao, F., Supangat, A., Fan, B., Wei, Z., Sulistiyo, B. and Li, S.: Volume, heat, and freshwater transports from the South China Sea to Indonesian seas in the boreal winter of 2007–2008, *J. Geophys. Res. Ocean.*, doi:10.1029/2010JC006225, 2010.

Feng, M., and Wijffels, S.: Intraseasonal variability in the South Equatorial Current of the East Indian Ocean. *Journal of Physical Oceanography*, 32, 265–277, 2002.

Feng, M., Meyers, G., Pearce, A., and Wijffels, S.: Annual and interannual variations of the Leeuwin Current at 32°S, *J. Geophys. Res.*, 108(C11), 3355, <https://doi.org/10.1029/2002JC001763>, 2003.

Feng, M., Wijffels, S., Godfrey, S., and Meyers, G.: Do eddies play a role in the momentum balance of the Leeuwin Current? *J. Phys. Oceanogr.*, 35, 964–975, <https://doi.org/10.1175/JPO2730.1>, 2005.

Feng, M., Majewski, L.J., Fandry, C.B., Waite, A.M., Characteristics of two counter-rotating eddies in the Leeuwin Current system off the Western Australian coast, *Deep Sea Research II*, 54(8–10), 961–980, <https://doi.org/10.1016/j.dsr2.2006.11.022>, 2007.

Feng, M., Biastoch, A., Böning, C., Caputi, N., and Meyers, G.: Seasonal and interannual variations of upper ocean heat balance off the west coast of Australia, *J. Geophys. Res.*, 113, C12025, <http://doi.org/10.1029/2008JC004908>, 2008.

Feng, M., Böning, C.W., Biastoch, A., Behrens, E., Weller, E., Masumoto, Y.: The reversal of the multi-decadal trends of the equatorial Pacific easterly winds, and the Indonesian Throughflow and Leeuwin Current transports. *Geophys. Res. Lett.* 38, L11604, 2011.

Feng, M., McPhaden, M.J., Xie, S.P., and Hafner, J.: La Niña forces unprecedented Leeuwin Current warming in 2011, *Sci. Rep.*, 3, 1277, <https://doi.org/10.1038/srep01277>, 2013.

Feng, M., Benthuisen, J., Zhang, N., and Slawinski, D.: Freshening anomalies in the Indonesian throughflow and impacts on the Leeuwin Current during 2010–2011, *Geophys. Res. Lett.*, 42, 8555–8562, <https://doi.org/10.1002/2015GL065848>, 2015a.

Feng, M., Hendon, H. H., Xie, S.-P., Marshall, A. G., Schiller, A., Kosaka, Y., Caputi, N., and Pearce, A.: Decadal increase in Ningaloo Niño since the late 1990s, *Geophys. Res. Lett.*, 42, 1, 104–112, <https://doi.org/10.1002/2014GL062509>, 2015b.

Feng, M., Zhang, X., Oke, P., Monselesan, D., Chamberlain, M., Matear, R., and Schiller, A.: Invigorating ocean boundary current systems around Australia during 1979–2014: As simulated in a near-global eddy-resolving ocean model. *J. Geophys. Res. Oceans*, 121(5), 3395–3408, <https://doi.org/10.1002/2016JC011842>, 2016.

Feng, M., Zhang, N., Liu, Q. and Wijffels, S.: The Indonesian throughflow, its variability and centennial change, *Geosci. Lett.*, doi:10.1186/s40562-018-0102-2, 2018.

Feng, X., and Shinoda, T.: Air-sea heat flux variability in the southeast Indian Ocean and its relation with Ningaloo Niño. *Front. Mar. Sci.*, 6, 266, <https://doi.org/10.3389/fmars.2019.00266>, 2019.

Fieux, M., Schott, F. and Swallow, J. C.: Deep boundary currents in the western Indian Ocean revisited, *Deep Sea Res. Part A, Oceanogr. Res. Pap.*, doi:10.1016/0198-0149(86)90124-X, 1986.

Fine, R. A., Smethie W. M., Bullister, J. L., Rhein M., Min, D. H., Warner, M. J., Poisson, A., Weiss, R. F.: Decadal ventilation and mixing of Indian Ocean waters. *Deep-Sea Res I*, 55, 20–37, <https://doi.org/10.1016/j.dsr.2007.10.002>, 2008.

Foltz, G. R., Vialard, J., Kumar, B. P. and Mcphaden, M. J.: Seasonal mixed layer heat balance of the southwestern tropical Indian Ocean, *J. Clim.*, doi:10.1175/2009JCLI3268.1, 2010.

Deleted:

Fox-Kemper, B., Hewitt, H. T., Xiao, C., Aðalgeirsdóttir, G., Drijfhout, S. S., Edwards, T. L., Golledge, N. R., Hemer, M., Kopp, R. E., Krinner, G., A. Mix, A., Notz, D., Nowicki, S., Nurhati, I. S., Ruiz, L., Sallée, J.-B., Slangen, A. B. A., Yu, Y.: Ocean, Cryosphere and Sea Level Change. In: Climate Change 2021: The Physical Science Basis. Contribution of Working Group I to the Sixth Assessment Report of the Intergovernmental Panel on Climate Change [Masson-Delmotte, V., P. Zhai, A. Pirani, S. L. Connors, C. Péan, S. Berger, N. Caud, Y. Chen, L. Goldfarb, M. I. Gomis, M. Huang, K. Leitzell, E. Lonnoy, J.B.R. Matthews, T. K. Maycock, T. Waterfield, O. Yelekçi, R. Yu and B. Zhou (eds.)]. Cambridge University Press. In press.

Francis, P.A., Jithin, A. K., Effy, J. B., Chatterjee, A., Chakraborty, K. et al.: High-resolution operational ocean forecast and reanalysis system for the Indian Ocean. Bulletin of the American Met. Soc., 101(8), E1340-E1356, <https://journals.ametsoc.org/view/journals/bams/101/8/bamsD190083.xml>, 2020.

Furnas, M.: Intra-seasonal and inter-annual variations in phytoplankton biomass, primary production and bacterial production at North West Cape, Western Australia: Links to the 1997-1998 El Niño event, Cont. Shelf Res., doi:10.1016/j.csr.2007.01.002, 2007.

Furue, R., McCreary, J. P., Benthuisen, J., Phillips, H. E., and Bindoff, N. L.: Dynamics of the Leeuwin Current: Part 1. Coastal flows in an inviscid, variable-density, layer model, Dyn. Atmos. Oceans, 63, 24–59, <https://doi.org/10.1016/j.dynatmoce.2013.03.003>, 2013.

Furue, R., Guerreiro, K., Phillips, H. E., McCreary, J. P., and Bindoff, N. L.: On the Leeuwin Current System and its linkage to zonal flows in the South Indian Ocean as inferred from a gridded hydrography, J. Phys. Oceanogr., 47, 583–602, <https://doi.org/10.1175/JPO-D-16-0170.1>, 2017.

Furue, R.: The three-dimensional structure of the Leeuwin Current System in density coordinates in an eddy-resolving OGCM, Ocean Modelling, 138, 36–50, <https://doi.org/10.1016/j.ocemod.2019.03.001>, 2019.

Ganachaud, A., Wunsch, C., Marotzke, J. and Toole, J.: Meridional overturning and large-scale circulation of the Indian Ocean, J. Geophys. Res. Ocean., doi:10.1029/2000jc900122, 2000.

Gandhi, N., Singh, A., Prakash, S., Ramesh, R., Raman, M., Sheshshayee, M. and Shetye, S.: First direct measurements of N<sub>2</sub> fixation during a *Trichodesmium* bloom in the eastern Arabian Sea, Global Biogeochemical Cycles, 25(4), 2011.

Garrison, D. L., Gowing, M. M., Hughes, M. P., Campbell, L., Caron, D. A., Dennett, M. R., Shalapyonok, A., Olson, R. J., Landry, M. R., Brown, S. L., Liu, H. Bin, Azam, F., Steward, G. F., Ducklow, H. W. and Smith, D. C.: Microbial food web structure in the Arabian Sea: A US JGOFS study, Deep. Res. Part II Top. Stud. Oceanogr., doi:10.1016/S0967-0645(99)00148-4, 2000.

Gaube, P., Chelton, D. B., Strutton, P. G. and Behrenfeld, M. J.: Satellite observations of chlorophyll, phytoplankton biomass, and Ekman pumping in nonlinear mesoscale eddies, J. Geophys. Res. Ocean., doi:10.1002/2013JC009027, 2013.

George, J. V., Nuncio, M., Chacko, R., Anilkumar, N., Noronha, S. B., Patil, S. M., Pavithran, S., Alappattu, D. P., Krishnan, K. P. and Achuthankutty, C. T.: Role of physical processes in chlorophyll distribution in the western tropical Indian Ocean, J. Mar. Syst., doi:10.1016/j.jmarsys.2012.12.001, 2013.

George, J. V., Vinayachandran, P. N., Vijith, V., Thusaraa, V., Nayaka, A. A., Pargaonkara, S. K., Amol, P., Vijaykumar, K., and Matthews, A. J.: Mechanisms of barrier layer formation and erosion from in situ observations in the Bay of Bengal, J. Phys. Oceanogr., 49, 1183–1200, <https://doi.org/10.1175/JPO-D-18-0204.1>, 2019.

Giddings, Jack, Karen J. Heywood, Adrian J. Matthews, Manoj M. Joshi, Benjamin GM Webber, Alejandra Sanchez-Franks, Brian A. King, and Puthenveetil N. Vinayachandran. "Spatial and temporal variability of solar penetration depths in the Bay of Bengal and its impact on SST during the summer monsoon." *Ocean Science Discussions* (2021): 1-33.

Gilmour, J. P., Cook, K. L., Ryan, N. M., Puotinen, M. L., Green, R. H., Shedrawi, G., Hobbs, J.-P. A., Thmson, D.P., Babcock, R.C., Buckee, J., Foster, T., Richards, Z. T., Wilson, S. K., Barnes, P. B., Coutts, T. B., Radford, B. T., Piggott, C. H., Depczynski, M., Evans, S. N., Schoepf, V., Evans, R. D., Halford, A. H., Nutt, C. D., Bancroft, K. P., Heyward, A. J., Oades, D.: The state of Western Australia's coral reefs, Coral Reefs, 38, 4, 651-667, <https://doi.org/10.1007/s00338-019-01795-8>, 2019.

2709 Girishkumar, M. S., M. Ravichandran and M. J. McPhaden: Temperature inversions and their influence on the mixed  
 2710 layer heat budget during the winters of 2006-07 and 2007-08 in the Bay of Bengal. *J. Geophys. Res.*, 118,  
 2711 doi:10.1002/jgrc.20192, 2013.  
 2712 Girishkumar, M. S., Joseph, J., Thangaprakash, V. P., Pottapinjara, V. and McPhaden, M. J.: Mixed Layer Temperature  
 2713 Budget for the Northward Propagating Summer Monsoon Intraseasonal Oscillation (MISO) in the Central Bay of  
 2714 Bengal, *J. Geophys. Res. Ocean.*, 122(11), 8841–8854, doi:10.1002/2017JC013073, 2017.  
 2715 Girishkumar, M.S., K. Ashin, M.J. McPhaden, B. Balaji, and B. Praveenkumar: Estimation of vertical heat diffusivity at  
 2716 the base of the mixed layer in the Bay of Bengal. *J. Geophys. Res.*, 125, e2019JC015402. doi:10.1029/2019JC015402,  
 2717 2020.  
 2718 Gnanaseelan, C., Deshpande, A. and McPhaden, M. J.: Impact of Indian Ocean Dipole and El Nio/Southern Oscillation  
 2719 wind-forcing on the Wyrki jets, *J. Geophys. Res. Ocean.*, doi:10.1029/2012JC007918, 2012.  
 2720 Godfrey, J. S., and Ridgway, K. R.: The large-scale environment of the poleward-flowing Leeuwin Current, Western  
 2721 Australia: longshore steric height gradients, wind stresses and geostrophic flow, *J. Phys. Oceanogr.*, 15(5), 481–495,  
 2722 https://doi.org/10.1175/1520-0485(1985)015<0481:TLSEOT>2.0.CO;2, 1985.  
 2723 Godfrey, J. S., and Weaver, A.: Why are there such strong steric height gradients off Western Australia? In: Proceedings  
 2724 of the Western Pacific International Meeting and Workshop on TOGA COARE, May 24–30, 1989, Noumea, New  
 2725 Caledonia, 215–222, http://hdl.handle.net/102.100.100/262338, 1989.  
 2726 Godfrey, J.S., and Weaver, A.J.: Is the Leeuwin Current driven by Pacific heating and winds? *Prog. Oceanogr.*, 27(3–4),  
 2727 225–272, https://doi.org/10.1016/0079-6611(91)90026-I, 1991.  
 2728 Godfrey, J. S.: The effect of the Indonesian throughflow on ocean circulation and heat exchange with the atmosphere: A  
 2729 review, *J. Geophys. Res.*, 101(C5), 12,217–12,237, 1996.  
 2730 Goericke, R., Olson, R. J. and Shalapyonok, A.: A novel niche for *Prochlorococcus* sp. in low-light suboxic  
 2731 environments in the Arabian Sea and the Eastern Tropical North Pacific, *Deep. Res. Part I Oceanogr. Res. Pap.*,  
 2732 doi:10.1016/S0967-0637(99)00108-9, 2000.  
 2733 Goes, J. I., Tian, H., Gomes, H. do R., Anderson, O. R., Al-Hashmi, K., deRada, S., Luo, H., Al-Kharusi, L., Al-Azri, A.  
 2734 and Martinson, D. G.: Ecosystem state change in the Arabian Sea fuelled by the recent loss of snow over the  
 2735 Himalayan-Tibetan Plateau region, *Sci. Rep.*, doi:10.1038/s41598-020-64360-2, 2020.  
 2736 Gomes, H. D., Goes, J. I., Matondkar, S. G. P., Buskey, E. J., Basu, S., Parab, S. and Thoppil, P.: Massive outbreaks of  
 2737 *Noctiluca scintillans* blooms in the Arabian Sea due to spread of hypoxia, *Nat. Commun.*, doi:10.1038/ncomms5862,  
 2738 2014.  
 2739 Gordon, A. L., Susanto, R. D. and Vranes, K.: Cool Indonesian throughflow as a consequence of restricted surface layer  
 2740 flow, *Nature*, doi:10.1038/nature02038, 2003.  
 2741 Gordon, A. L., Susanto, R. D., Ffield, A., Huber, B. A., Pranowo, W. and Wirasantosa, S.: Makassar Strait throughflow,  
 2742 2004 to 2006, *Geophys. Res. Lett.*, doi:10.1029/2008GL036372, 2008.  
 2743 Gordon, A. L., Sprintall, J., Van Aken, H. M., Susanto, R. D., Wijffels, S., Molcard, R., Ffield, A., Pranowo, W. and  
 2744 Wirasantosa, S.: The Indonesian throughflow during 2004-2006 as observed by the INSTANT program, *Dyn. Atmos.*  
 2745 *Ocean.*, doi:10.1016/j.dynatmoce.2009.12.002, 2010.  
 2746 Gordon, A. L., Huber, B. A., Metzger, E. J., Susanto, R. D., Hurlburt, H. E. and Adi, T. R.: South China Sea  
 2747 throughflow impact on the Indonesian throughflow, *Geophys. Res. Lett.*, doi:10.1029/2012GL052021, 2012.  
 2748 Gordon, A. L., Shroyer, E. L., Mahadevan, A., Sengupta, D. and Freilich, M.: Bay of Bengal: 2013 Northeast monsoon  
 2749 upper-ocean circulation, *Oceanography*, doi:10.5670/oceanog.2016.41, 2016.  
 2750 Gordon, A., Shroyer, E. & Murty, V.: An Intrathermocline Eddy and a tropical cyclone in the Bay of Bengal. *Sci Rep* 7,  
 2751 46218, https://doi.org/10.1038/srep46218, 2017.  
 2752 Goschen, W. S., Schumann, E. H., Bernard, K. S., Bailey, S. E. and Deyzel, S. H. P.: Upwelling and ocean structures off  
 2753 Algoa Bay and the south-east coast of South Africa, *African J. Mar. Sci.*, doi:10.2989/1814232X.2012.749810, 2012.

Deleted: . (1996),



2755 Goswami, B. B., Mukhopadhyay, P., Khairoutdinov, M. and Goswami, B. N.: Simulation of Indian summer monsoon  
 2756 intraseasonal oscillations in a superparameterized coupled climate model: Need to improve the embedded cloud  
 2757 resolving model, *Clim. Dyn.*, 41(5–6), 1497–1507, <https://doi.org/10.1007/s00382-012-1563-1>, 2013.  
 2758 [Goswami, B.N., S.A. Rao, D. Sengupta, and S. Chakravorty: Monsoons to mixing in the Bay of Bengal: Multiscale air-](#)  
 2759 [sea interactions and monsoon predictability. \*Oceanography\* 29\(2\):18–27, <http://dx.doi.org/10.5670/oceanog.2016.35>,](#)  
 2760 [2016.](#)  
 2761 Gudka, M., Obura, D., Mwaura, J., Porter, S. Yahya, S., and Mabwa, R.: Impact of the 3rd Global Coral Bleaching  
 2762 Event on the Western Indian Ocean in 2016, Global Coral Reef Monitoring Network (GCRMN)/Indian Ocean  
 2763 Commission, pp. 67, <http://hdl.handle.net/20.500.11822/25700>, 2018.  
 2764 Guemas, V., Corti, S., Garcia-Serrano, J., Doblas-Reyes, F. J., Balmaseda, M., and Magnusson, L.: The Indian Ocean:  
 2765 The region of highest skill worldwide in decadal climate prediction. *J. Climate*, 26, 726–739, 2013.  
 2766 Gundersen, J. S., Gardner, W. D., Richardson, M. J. and Walsh, I. D.: Effects of monsoons on the seasonal and spatial  
 2767 distributions of POC and chlorophyll in the Arabian Sea, Deep. Res. Part II Top. Stud. Oceanogr., doi:10.1016/S0967-  
 2768 0645(98)00065-4, 1998.  
 2769 Guo, F., Liu, Q., Sun, S., and Yang, J.: Three types of Indian Ocean dipoles. *J. Climate*, 28, 3073-3092, 2015.  
 2770 Haarsma, R. J., Campos, E. J. D., Drijfhout, S., Hazeleger, W. and Severijns, C.: Impacts of interruption of the Agulhas  
 2771 leakage on the tropical Atlantic in coupled ocean-atmosphere simulations, *Clim. Dyn.*, doi:10.1007/s00382-009-0692-  
 2772 7, 2011.  
 2773 Haine, T. W. N., Watson, A. J., Liddicoat, M. I. and Dickson, R. R.: The flow of Antarctic bottom water to the  
 2774 southwest Indian Ocean estimated using CFCs, *J. Geophys. Res. Ocean.*, doi:10.1029/98JC02476, 1998.  
 2775 Halkides, D. J., Waliser, D. E., Lee, T., Menemenlis, D. and Guan, B.: Quantifying the processes controlling  
 2776 intraseasonal mixed-layer temperature variability in the tropical Indian Ocean, *J. Geophys. Res. Ocean.*, 120(2), 692–  
 2777 715, doi:10.1002/2014JC010139, 2015.  
 2778 Han, W., McCreary, J. P., Anderson, D. L. T. and Mariano, A. J.: Dynamics of the eastern surface jets in the equatorial  
 2779 Indian Ocean, *J. Phys. Oceanogr.*, doi:10.1175/1520-0485(1999)029<2191:DOTESJ>2.0.CO;2, 1999.  
 2780 Han, W., Webster, P., Lukas, R., Hacker, P. and Hu, A.: Impact of atmospheric intraseasonal variability in the Indian  
 2781 Ocean: Low-frequency rectification in equatorial surface current and transport, *J. Phys. Oceanogr.*, doi:10.1175/1520-  
 2782 0485(2004)034<1350:IOAIVI>2.0.CO;2, 2004.  
 2783 Han, W., Yuan, D., Liu, W. T. and Halkides, D. J.: Intraseasonal variability of Indian Ocean sea surface temperature  
 2784 during boreal winter: Madden-Julian Oscillation versus submonthly forcing and processes, *J. Geophys. Res. Ocean.*,  
 2785 112(4), 1–20, doi:10.1029/2006JC003791, 2007.  
 2786 Han, W., Vialard, J., McPhaden, M. J., Lee, T., Masumoto, Y., Feng, M. and De Ruijter, W. P. M.: Indian ocean decadal  
 2787 variability: A review, *Bull. Am. Meteorol. Soc.*, doi:10.1175/BAMS-D-13-00028.1, 2014.  
 2788 Hanson, C. E., Waite, A. M., Thompson, P. A. and Pattiaratchi, C. B.: Phytoplankton community structure and nitrogen  
 2789 nutrition in Leeuwin Current and coastal waters off the Gascoyne region of Western Australia, Deep. Res. Part II Top.  
 2790 Stud. Oceanogr., doi:10.1016/j.dsr2.2006.10.002, 2007.  
 2791 Hazra, A., Chaudhari, H. S., Saha, S. K., Pokhrel, S. and Goswami, B. N.: Progress Towards Achieving the Challenge of  
 2792 Indian Summer Monsoon Climate Simulation in a Coupled Ocean-Atmosphere Model, *J. Adv. Model. Earth Syst.*,  
 2793 doi:10.1002/2017MS000966, 2017.  
 2794 Hermes, J. C. and Reason, C. J. C.: Ocean model diagnosis of interannual coevolving SST variability in the South Indian  
 2795 and South Atlantic Oceans, *J. Clim.*, doi:10.1175/JCLI3422.1, 2005.  
 2796 Hermes, J. C., and Reason, C. J. C.: Annual cycle of the South Indian Ocean (Seychelles-Chagos) thermocline ridge in a  
 2797 regional ocean model, *Journal of Geophysical Research*, 113: C04035, doi:10.1029/2007JC004363, 2008.  
 2798 Hermes J. C., Masumoto Y., Beal L. M., Roxy M. K., Vialard J., Andres M., Annamalai H., Behera S., D'Adamo N.,  
 2799 Doi T., Feng M., Han W., Hardman-Mountford N., Hendon H., Hood R., Kido S., Lee C., Lee T., Lengaigne M., Li J.,  
 2800 Lumpkin R., Navaneeth K. N., Milligan B., McPhaden M. J., Ravichandran M., Shinoda T., Singh A., Sloyan B.,

Deleted: . Reason:



2802 Strutton P. G., Subramanian A. C., Thurston S., Tozuka T., Ummenhofer C. C., Unnikrishnan A. S., Venkatesan R.,  
2803 Wang D., Wiggert J., Yu L., Yu W.: A Sustained Ocean Observing System in the Indian Ocean for Climate Related  
2804 Scientific Knowledge and Societal Needs. *Frontiers in Marine Science*, 6, 355, 1-21, doi/10.3389/fmars.2019.00355,  
2805 2019.

2806 Hernández-Guerra, A. & Talley, L. D.: Meridional overturning transports at 30°S in the Indian and Pacific Oceans in  
2807 2002–2003 and 2009. *Prog Oceanogr* 146, 89–120, 2016.

2808 Hitchcock, G. L., L. Key, E. and Masters, J.: The fate of upwelled waters in the Great Whirl, August 1995, *Deep. Res.*  
2809 Part II Top. Stud. Oceanogr., doi:10.1016/S0967-0645(99)00156-3, 2000.

2810 Ho, C. R., Zheng, Q. and Kuo, N. J.: SeaWiFs observations of upwelling south of Madagascar: Long-term variability  
2811 and interaction with East Madagascar Current, *Deep. Res. Part II Top. Stud. Oceanogr.*,  
2812 doi:10.1016/j.dsr2.2003.05.001, 2004.

2813 Holbrook, N. J., Scannell, H.A., Sen Gupta, A., Benthuisen, J.A., Feng, M., Oliver, E.C.J., Alexander, L.V., Burrow,  
2814 M.T., Donat, M.G., Hobday, A.J., Moore, P.J., Perkins-Kirkpatrick, S.E., Smale, D.A., Straub, S. C., and Wernberg,  
2815 T.: A global assessment of marine heatwaves and their drivers, *Nature Commun.*, 10, 2624,  
2816 <https://doi.org/10.1038/s41467-019-10206-z>, 2019.

2817 Holloway, P. E.: Leeuwin current observations on the Australian North West Shelf, May-June 1993, *Deep. Res. Part I*,  
2818 doi:10.1016/0967-0637(95)00004-P, 1995.

2819 Holloway, P. E. and Nye, H. C.: Leeuwin current and wind distributions on the southern part of the australian north west  
2820 shelf between january 1982 and july 1983, *Mar. Freshw. Res.*, doi:10.1071/MF9850123, 1985.

2821 Holton, L., J. Deshayes, B. C. Backeberg, B. R. Loveday, J. C. Hermes, and C. J. C. Reason, Spatio-temporal  
2822 characteristics of Agulhas leakage: a model inter-comparison study, *Climate Dynamics*, 48(7), 2107-2121, 2017.

2823 Hood, R. R., Coles, V. J. and Capone, D. G.: Modeling the distribution of Trichodesmium and nitrogen fixation in the  
2824 Atlantic Ocean, *J. Geophys. Res. C Ocean.*, doi:10.1029/2002JC001753, 2004.

2825 Hood, R. R., Beckley, L. E., and Wiggert, J. D.: Biogeochemical and ecological impacts of boundary currents in the  
2826 Indian Ocean, *Prog. Oceanogr.*, 156, pp. 290–325, 2017.

2827 Hood, R.R., H.W. Bange, L. Beal, L.E. Beckley, P. Burkill, G.L. Cowie, N. D'Adamo, G. Ganssen, H. Hendon, J.  
2828 Hermes, M. Honda, M. McPhaden, M. Roberts, S. Singh, E. Urban, and W. Yu. : Science Plan of the Second  
2829 International Indian Ocean Expedition (IIOE-2): A Basin-Wide Research Program. Scientific Committee on Oceanic  
2830 Research, Newark, Delaware, USA, 2015

2831 Hood, R. R., V. J. Coles, J. Huggett, M. Landry, M. Levy, J. W. Moffett, and J. Wiggert. in preparation. 'Indian Ocean  
2832 Biogeochemistry: Nutrients, Phytoplankton and Zooplankton Variability and Limitations.' in C. C. Ummenhofer and  
2833 R. R. Hood (eds.), *The Indian Ocean and its Role in the Global Climate System* (Elsevier).

2834 Horii, T., K. Mizuno, M. Nagura, T. Miyama, and K. Ando: Seasonal and interannual variation in the cross-equatorial  
2835 meridional currents observed in the eastern Indian Ocean, *J. Geophys. Res.*, 118, 6658–6671,  
2836 doi:10.1002/2013JC009291, 2013.

2837 [Hormann, V., Centurioni, L. R., Gordon, A. L.: Freshwater export pathways from the Bay of Bengal, Deep Sea Research](#)  
2838 [Part II: Topical Studies in Oceanography, 168, 104645, 0967-0645, https://doi.org/10.1016/j.dsr2.2019.104645, 2019.](#)

2839 Howden, S. D., and Murtugudde, R.: Effects of river inputs into the Bay of Bengal, *J. Geophys. Res. Ocean.*, 106(C9),  
2840 19825–19843, <https://doi.org/10.1029/2000jc000656>, 2001.

2841 Hu, D., Wu, L., Cai, W., [Sen](#) Gupta, A., Ganachaud, A., Qiu, B., Gordon, A. L., Lin, X., Chen, Z., Hu, S., Wang, G.,  
2842 Wang, Q., Sprintall, J., Qu, T., Kashino, Y., Wang, F. and Kessler, W. S.: Pacific western boundary currents and their  
2843 roles in climate, *Nature*, doi:10.1038/nature14504, 2015.

2844 Hu, S. and Sprintall, J.: Interannual variability of the Indonesian Throughflow: The salinity effect, *J. Geophys. Res.*  
2845 *Ocean.*, doi:10.1002/2015JC011495, 2016.

2846 Hu, S., and Sprintall, J.: Observed [strengthening of interbasin exchange](#) via the Indonesian Seas [due to rainfall](#)  
2847 Intensification, *Geophysical Research Letters*, 44(3), 1448-1456, 2017a.

Deleted:

Formatted: Font colour: Auto

Formatted: Font colour: Auto

Deleted: . Sen,

Deleted: Strengthening

Deleted: Interbasin Exchange

Deleted: Due

Deleted: Rainfall

2854 Hu, S., and Sprintall, J.: A stronger Indonesian Throughflow [related to enhanced regional rainfall](#), CLIVAR Exchanges,  
 2855 71, 21–25, 2017b.  
 2856 Hu, K., Huang, G., Xie, S.-P., Long, S. M.: Effect of the mean flow on the anomalous anticyclone over the Indo-  
 2857 northwest Pacific in post-El Niño summers. *Clim. Dyn.*, 53, 5725–5741, 2019.  
 2858 Huhn, F., von Kameke, A., Pérez-Muñuzuri, V., Olascoaga, M. J., and Beron-Vera, F. J.: The impact of advective  
 2859 transport by the South Indian Ocean countercurrent on the Madagascar bloom, *Geophys. Res. Lett.*, 39, L06602,  
 2860 <https://doi.org/10.1029/2012GL051246>, 2012.  
 2861 Hutchinson, K., Beal, L. M., Penven, P., Ansorge, I., & Hermes, J.: Seasonal phasing of Agulhas Current transport tied  
 2862 to a baroclinic adjustment of near-field winds. *Journal of Geophysical Research: Oceans*, 123.  
 2863 <https://doi.org/10.1029/2018JC014319>, 2018  
 2864 Huussen, T. N., Naveira-Garabato, A. C., Bryden, H. L. and McDonagh, E. L.: Is the deep Indian Ocean MOC sustained  
 2865 by breaking internal waves?, *J. Geophys. Res. Ocean.*, doi:10.1029/2012JC008236, 2012.  
 2866 Ibrahim, N., Mohamed, M., Basheer, A., Ismail, H., Nistharan, F., Schmidt, A., Naeem, R., Abdulla, A., and Grimsditch,  
 2867 G.: Status of Coral Bleaching in the Maldives in 2016, Marine Research Centre, Malé, Maldives, 47 pp.,  
 2868 <https://portals.iucn.org/library/node/46803>, 2017.  
 2869 Iskandar, I., Masumoto, Y. and Mizuno, K.: Subsurface equatorial zonal current in the eastern Indian Ocean, *J. Geophys.*  
 2870 *Res. Ocean.*, doi:10.1029/2008JC005188, 2009.  
 2871 Iskandar, I., Sasaki, H., Sasai, Y., Masumoto, Y., and Mizuno, K.: A numerical investigation of eddy-induced  
 2872 chlorophyll bloom in the southeastern tropical Indian Ocean during Indian Ocean Dipole—2006. *Ocean Dyn.*, 60, 731–  
 2873 742, 2010.  
 2874 Iskandar, I. and McPhaden, M. J.: Dynamics of wind-forced intraseasonal zonal current variations in the equatorial  
 2875 Indian Ocean, *J. Geophys. Res. Ocean.*, 116(6), 1–16, doi:10.1029/2010JC006864, 2011.  
 2876 Izumo, T., C. de Boyer Montegut, J.J. Luo, S.K. Behera, S. Masson, and T. Yamagata: The role of the western Arabian  
 2877 Sea upwelling in Indian monsoon rainfall variability. *J. Clim.*, 21, 5603–5623, doi:10.1175/2008JCLI2158.1, 2008.  
 2878 Izumo, T., Vialard, J., Lengaigne, M., de Boyer Montegut, C., Behera, S. K., Luo, J.-J., Cravatte, S., Masson, S. and  
 2879 Yamagata, T.: Influence of the state of the Indian Ocean Dipole on the following year’s El Niño, *Nat. Geosci.*, 3(3),  
 2880 168–172, doi:10.1038/ngeo760, 2010.  
 2881 Jackson, J. M., Rainville, L., Roberts, M. J., McQuaid, C. D. and Lutjeharms, J. R. E.: Mesoscale bio-physical  
 2882 interactions between the Agulhas Current and the Agulhas Bank, South Africa, *Cont. Shelf Res.*,  
 2883 doi:10.1016/j.csr.2012.09.005, 2012.  
 2884 Jain, V., Shankar, D., Vinayachandran, P. N., Kankonkar, A., Chatterjee, A., Amol, P., Almeida, A. M., Michael, G. S.,  
 2885 Mukherjee, A., Chatterjee, M., Fernandes, R., Luis, R., Kamble, A., Hegde, A. K., Chatterjee, S., Das, U. and Neema,  
 2886 C. P.: Evidence for the existence of Persian Gulf Water and Red Sea Water in the Bay of Bengal, *Clim. Dyn.*,  
 2887 doi:10.1007/s00382-016-3259-4, 2017.  
 2888 Jayakumar, A., Vialard, J., Lengaigne, M., Gnanaseelan, C., McCreary, J. P. and Kumar, B. P.: Processes controlling the  
 2889 surface temperature signature of the Madden-Julian Oscillation in the thermocline ridge of the Indian Ocean, *Clim.*  
 2890 *Dyn.*, 37(11–12), 2217–2234, doi:10.1007/s00382-010-0953-5, 2011.  
 2891 Jayakumar, A., Turner, A. G., Johnson, S. J., Rajagopal, E. N., Mohandas, S. and Mitra, A. K.: Boreal summer sub-  
 2892 seasonal variability of the South Asian monsoon in the Met Office GloSea5 initialized coupled model, *Clim. Dyn.*,  
 2893 49(5–6), 2035–2059, doi:10.1007/s00382-016-3423-x, 2017.  
 2894 Jensen, T. G.: Arabian Sea and Bay of Bengal exchange of salt and tracers in an ocean model, *Geophys. Res. Lett.*,  
 2895 28(20), 3967–3970, doi:10.1029/2001GL013422, 2001.  
 2896 Jensen, T. G., Wijesekera, H. W., Nyadjro, E. S., Thoppil, P. G., Shriver, J., Sandeep, K. K. and Pant, V.: Modeling  
 2897 Salinity Exchanges Between the Equatorial Indian Ocean and the Bay of Bengal, *Oceanography*, 29(2), 92–101,  
 2898 doi:10.5670/oceanog.2016.42, 2016.

**Deleted:** Related to Enhanced Regional Rainfall

2900 Jia, F., Wu, L., and Qiu, B.: Seasonal modulation of eddy kinetic energy and its formation mechanism in the southeast  
 2901 Indian Ocean, *J. Phys. Oceanogr.*, 41( 4), 657– 665, <https://doi.org/10.1175/2010JPO4436.1>, 2011a.  
 2902 Jia, F., Wu, L., and Qiu, B.: Interannual modulation of eddy kinetic energy in the southeast Indian ocean by Southern  
 2903 Annular Mode, *J. Geophys. Res.*, 116, C02029, <https://doi.org/10.1029/2010JC006699>, 2011b.  
 2904 Jin, D., Waliser, D. E., Jones, C. and Murtugudde, R.: Modulation of tropical ocean surface chlorophyll by the Madden-  
 2905 Julian Oscillation, *Clim. Dyn.*, 40(1–2), 39–58, doi:10.1007/s00382-012-1321-4, 2013a.  
 2906 Jin, D., Murtugudde, R. G. and Waliser, D. E.: Intraseasonal atmospheric forcing effects on the mean state of ocean  
 2907 surface chlorophyll, *J. Geophys. Res. Ocean.*, 118(1), 184–196, doi:10.1029/2012JC008256, 2013b.  
 2908 Jin, X., Kwon, Y.-O., Ummenhofer, C. C., Seo, H., Schwarzkopf, F. U., Biastoch, A., Böning, C. W. and Wright, J. S.:  
 2909 Influences of Pacific climate variability on decadal subsurface ocean heat content variations in the Indian Ocean. *J.*  
 2910 *Climate*, 31, 4157–4174, 2018a.  
 2911 Jin, X., Kwon, Y.-O., Ummenhofer, C. C., Seo, H., Kosaka, Y., and Wright, J. S.: Distinct mechanisms of decadal  
 2912 subsurface heat content variations in the eastern and western Indian Ocean modulated by tropical Pacific SST. *J.*  
 2913 *Climate*, 31, 7751–7769, 2018b.  
 2914 Jinadasa, S. U. P., Lozovatsky, I., Planella-Morató, J., Nash, J. D., MacKinnon, J. A., Lucas, A. J., Wijesekera, H. W.  
 2915 and Fernando, H. J. S.: Ocean turbulence and mixing around Sri Lanka and in adjacent waters of the northern Bay of  
 2916 Bengal, *Oceanography*, doi:10.5670/oceanog.2016.49, 2016.  
 2917 Johnson, G. C., Musgrave, D. L., Warren, B. A., Ffield, A. and Olson, D. B.: Flow of bottom and deep water in the  
 2918 Amirante Passage and Mascarene Basin, *J. Geophys. Res.*, 103, 30973–30984. doi:10.1029/1998JC90002, 1998.  
 2919 Johnson, G. C., Purkey, S. G., Bullister, J. L.: Warming and freshening in the abyssal southeastern Indian Ocean. *J. Clim.*  
 2920 21, 5351–5363. doi: 10.1175/2008JCLI2384.1, 2008a.  
 2921 Johnson, G. C., Purkey, S. G., Toole, J. M.: Reduced Antarctic meridional overturning circulation reaches the North  
 2922 Atlantic Ocean, *Geophys. Res. Lett.*, 35, L22601. doi:10.1029/2008GL035619, 2008b.  
 2923 José, Y. S., Aumont, O., Machu, E., Penven, P., Moloney, C. L. and Maury, O.: Influence of mesoscale eddies on  
 2924 biological production in the Mozambique Channel: Several contrasted examples from a coupled ocean-  
 2925 biogeochemistry model, *Deep. Res. Part II Top. Stud. Oceanogr.*, doi:10.1016/j.dsr2.2013.10.018, 2014.  
 2926 Joseph, S., Wallcraft, A. J., Jensen, T. G., Ravichandran, M., Shenoi, S. S. C. and Nayak, S.: Weakening of spring  
 2927 Wyrski jets in the Indian Ocean during 2006–2011, *J. Geophys. Res. Ocean.*, doi:10.1029/2011JC007581, 2012.  
 2928 Jyothibabu, R., Madhu, N. V., Maheswaran, P. A., Jayalakshmy, K. V., Nair, K. K. C. and Achuthankutty, C. T.:  
 2929 Seasonal variation of microzooplankton (20–200  $\mu\text{m}$ ) and its possible implications on the vertical carbon flux in the  
 2930 western Bay of Bengal, *Cont. Shelf Res.*, doi:10.1016/j.csr.2007.12.011, 2008.  
 2931 Jyoti, J., Swapna, P., Krishnan, R. and Naidu, C. V.: Pacific modulation of accelerated south Indian Ocean sea level rise  
 2932 during the early 21st Century, *Clim. Dyn.*, doi:10.1007/s00382-019-04795-0, 2019.  
 2933 Kataoka, T., Tozuka, T., Masumoto, Y., and Yamagata, T.: The Indian Ocean subtropical dipole mode simulated in the  
 2934 CMIP3 models, *Climate Dyn.*, 39, 1385–1399, <https://doi.org/10.1007/s00382-011-1271-2>, 2012.  
 2935 Kataoka, T., Tozuka, T., Behera, S., and Yamagata, T.: On the Ningaloo Niño/Niña, *Climate Dyn.*, 43, 1463–1482,  
 2936 <https://doi.org/10.1007/s00382-013-1961-z>, 2014.  
 2937 Kato, S., Loeb, N. G., Rose, F. G., Doelling, D. R., Rutan, D. A., Caldwell, T. E., Yu, L. and Weller, R. A.: Surface  
 2938 irradiances consistent with CERES-derived top-of-atmosphere shortwave and longwave irradiances, *J. Clim.*, 26(9),  
 2939 2719–2740, doi:10.1175/JCLI-D-12-00436.1, 2013.  
 2940 Keen, T. R., Kindle, J. C. and Young, D. K.: The interaction of southwest monsoon upwelling, advection and primary  
 2941 production in the northwest Arabian Sea, *J. Mar. Syst.*, doi:10.1016/S0924-7963(97)00003-1, 1997.  
 2942 Keerthi, M. G., Lengaigne, M., Drushka, K., Vialard, J., Montegut, C. D. B., Pous, S., Levy, M. and Muralledharan, P.  
 2943 M.: Intraseasonal variability of mixed layer depth in the tropical Indian Ocean, *Clim. Dyn.*, 46(7–8), 2633–2655,  
 2944 doi:10.1007/s00382-015-2721-z, 2016.

Kessler, W.S., M.J. McPhaden, and K.M. Weickmann: Forcing of intraseasonal Kelvin Waves in the equatorial Pacific. *J. Geophys. Res.*, 100, 10.613–10.631, 1995.

Kido, S., and Tozuka, T.: Salinity Variability Associated with the Positive Indian Ocean Dipole and Its Impact on the Upper Ocean Temperature. *Journal of Climate*, 30(19), 7885–7907, 2017.

Kim, H. S., Flagg, C. N. and Howden, S. D.: Northern Arabian Sea variability from TOPEX/Poseidon altimetry data: An extension of the US JGOFS/ONR shipboard ADCP study, *Deep. Res. Part II Top. Stud. Oceanogr.*, doi:10.1016/S0967-0645(00)00131-4, 2001.

Kobashi, F., and Kubokawa, A.: Review on North Pacific Subtropical Countercurrents and Subtropical Fronts: role of mode waters in ocean circulation and climate, *J. Oceanogr.*, 68, 21–43, <https://doi.org/10.1007/s10872-011-0083-7>, 2012.

Kosaka, Y. and Xie, SP: Recent global-warming hiatus tied to equatorial Pacific surface cooling. *Nature* 501, 403–407, <https://doi.org/10.1038/nature12534>, 2013.

Kosaka, Y., Takaya, Y., Kamae, Y.: The Indo-western Pacific Ocean capacitor effect. In: *Tropical and Extratropical Air-Sea Interactions*, 141–169, 2021.

Koslow, J. A., Pesant, S., Feng, M., Pearce, A., Fearn, P., Moore, T., Matear, R. and Waite, A.: The effect of the Leeuwin Current on phytoplankton biomass and production off Southwestern Australia, *J. Geophys. Res. Ocean.*, doi:10.1029/2007JC004102, 2008.

Krishnamohan, K. S., Vialard, J., Lengaigne, M., Masson, S., Samson, G., Pous, S., Neetu, S., Durand, F., Shenoi, S. S. C. and Madec, G.: Is there an effect of Bay of Bengal salinity on the northern Indian Ocean climatological rainfall?, *Deep Sea Res. Part II Top. Stud. Oceanogr.*, doi:10.1016/j.dsr2.2019.04.003, 2019.

Krishnamurthy, L., and Krishnamurthy, V.: Decadal and interannual variability of the Indian Ocean SST. *Climate Dyn.*, 46, 57–70, 2016.

Krug, M., & Tourmadre, J.: Satellite observations of an annual cycle in the Agulhas Current. *Geophysical Research Letters*, 39, L15607. <https://doi.org/10.1029/2012GL052335>, 2012

Kubokawa, A.: Ventilated thermocline strongly affected by a deep mixed layer: A theory for subtropical countercurrent. *J. Phys. Oceanogr.*, 29, 1314–1333, [https://doi.org/10.1175/1520-0485\(1999\)029<1314:VTSABA>2.0.CO;2](https://doi.org/10.1175/1520-0485(1999)029<1314:VTSABA>2.0.CO;2), 1999.

Kubokawa, A. and Inui, T.: Subtropical countercurrent in an idealized ocean GCM. *J. Phys. Oceanogr.*, 29, 1303–1313, [https://doi.org/10.1175/1520-0485\(1999\)029<1303:SCIAIO>2.0.CO;2](https://doi.org/10.1175/1520-0485(1999)029<1303:SCIAIO>2.0.CO;2), 1999.

Kumar, S.P., Madhupratap, M., Dileep Kumar, M., Gauns, M., Muraleedharan, P. M., Sarma, V. V. S. S. and De Souza, S. N.: Physical control of primary productivity on a seasonal scale in central and eastern Arabian Sea, *Proc. Indian Acad. Sci. Earth Planet. Sci.*, doi:10.1007/bf02708331, 2000.

Kumar, S.P., Muraleedharan, P. M., Prasad, T. G., Gauns, M., Ramaiah, N., De Souza, S. N., Sardesai, S. and Madhupratap, M.: Why is the Bay of Bengal less productive during summer monsoon compared to the Arabian Sea?, *Geophys. Res. Lett.*, doi:10.1029/2002GL016013, 2002.

Kumar, S. P., Nuncio, M., Narvekar, J., Kumar, A., Sardesai, S., De Souza, S. N., Gauns, M., Ramaiah, N. and Madhupratap, M.: Are eddies nature's trigger to enhance biological productivity in the Bay of Bengal?, *Geophys. Res. Lett.*, doi:10.1029/2003GL019274, 2004.

Kumar, S.P., Nuncio, M., Ramaiah, N., Sardesai, S., Narvekar, J., Fernandes, V. and Paul, J. T.: Eddy-mediated biological productivity in the Bay of Bengal during fall and spring intermonsoons, *Deep. Res. Part I Oceanogr. Res. Pap.*, doi:10.1016/j.dsr.2007.06.002, 2007.

Kumar, P., Singh, A., Ramesh, R. and Nallathambi, T.: N<sub>2</sub> Fixation in the Eastern Arabian Sea: Probable Role of Heterotrophic Diazotrophs, *Frontiers: Marine Science*, 4, 80, 2017.

Kundu, P. K. and McCreary, J. P.: On the dynamics of the throughflow from the Pacific into the Indian Ocean, *J. Phys. Oceanogr.*, 16, 2191–2198, [https://doi.org/10.1175/1520-0485\(1986\)016<2191:OTDOTT>2.0.CO;2](https://doi.org/10.1175/1520-0485(1986)016<2191:OTDOTT>2.0.CO;2), 1986.

Lakshmi, R. S., Chatterjee, A., Prakash, S., and Mathew, T.: Biophysical interactions in driving the summer monsoon chlorophyll bloom off the Somalia coast. *Journal of Geophysical Research: Oceans*, 125, <https://doi.org/10.1029/2019JC015549>, 2020.

2992 Lambert, E., Le Bars, W., and de Ruijter, W. P. M.: The connection of the Indonesian Throughflow, South Indian Ocean  
2993 Countercurrent and the Leeuwin Current, *Ocean Science*, 12(3), 771–780, <https://doi.org/10.5194/os-12-771-2016>,  
2994 2016.

2995 Lamont, T., Barlow, R. G., Morris, T. and van den Berg, M. A.: Characterisation of mesoscale features and  
2996 phytoplankton variability in the Mozambique Channel, *Deep. Res. Part II Top. Stud. Oceanogr.*,  
2997 doi:10.1016/j.dsr2.2013.10.019, 2014.

2998 Lamont, T. and Barlow, R. G.: Environmental influence on phytoplankton production during summer on the KwaZulu-  
2999 Natal shelf of the Agulhas ecosystem, *African J. Mar. Sci.*, doi:10.2989/1814232X.2015.1108228, 2015.

3000 Latasa, M. and Bidigare, R. R.: A comparison of phytoplankton populations of the Arabian Sea during the Spring  
3001 Intermonsoon and Southwest Monsoon of 1995 as described by HPLC-analyzed pigments, *Deep. Res. Part II Top.*  
3002 *Stud. Oceanogr.*, doi:10.1016/S0967-0645(98)00066-6, 1998.

3003 Laurindo, L. C., Mariano, A. J. and Lumpkin, R.: An improved near-surface velocity climatology for the global ocean  
3004 from drifter observations, *Deep. Res. Part I Oceanogr. Res. Pap.*, doi:10.1016/j.dsr.2017.04.009, 2017.

3005 Le Bars, D., Dijkstra, H. A. and De Ruijter, W. P. M.: Impact of the Indonesian Throughflow on Agulhas leakage,  
3006 *Ocean Sci.*, doi:10.5194/os-9-773-2013, 2013.

3007 Le Bars, D., Durgadoo, J. V., Dijkstra, H. A., Biastoch, A. and De Ruijter, W. P. M.: An observed 20-year time series of  
3008 Agulhas leakage, *Ocean Sci.*, doi:10.5194/os-10-601-2014, 2014.

3009 Lee, C. M., Jones, B. H., Brink, K. H. and Fischer, A. S.: The upper-ocean response to monsoonal forcing in the Arabian  
3010 Sea: Seasonal and spatial variability, *Deep. Res. Part II Top. Stud. Oceanogr.*, doi:10.1016/S0967-0645(99)00141-1,  
3011 2000.

3012 Lee, C. M., Jinadasa, S. U. P., Anutliya, A., Centurioni, L. R., Fernando, H. J. S., Hormann, V., Lankhorst, M.,  
3013 Rainville, L., Send, U. and Wijesekera, H. W.: Collaborative observations of boundary currents, water mass  
3014 variability, and monsoon response in the southern Bay of Bengal, *Oceanography*, doi:10.5670/oceanog.2016.43, 2016.

3015 Lee, J. Y., Wang, B., Wheeler, M. C., Fu, X., Waliser, D. E. and Kang, I. S.: Real-time multivariate indices for the  
3016 boreal summer intraseasonal oscillation over the Asian summer monsoon region, *Clim. Dyn.*, 40(1–2), 493–509,  
3017 doi:10.1007/s00382-012-1544-4, 2013.

3018 Lee, S. K., Park, W., Baringer, M. O., Gordon, A. L., Huber, B. and Liu, Y.: Pacific origin of the abrupt increase in  
3019 Indian Ocean heat content during the warming hiatus, *Nat. Geosci.*, doi:10.1038/NGEO2438, 2015.

3020 Lee, T.: Decadal weakening of the shallow overturning circulation in the South Indian Ocean, *Geophys. Res. Lett.*,  
3021 doi:10.1029/2004GL020884, 2004.

3022 Lee, T., Fournier, S., Gordon, A. L. and Sprintall, J.: Maritime Continent water cycle regulates low-latitude chokepoint  
3023 of global ocean circulation, *Nat. Commun.*, doi:10.1038/s41467-019-10109-z, 2019.

3024 Legeckis, R., and Cresswell, G.: Satellite observations of sea-surface temperature fronts off the coast of western and  
3025 southern Australia, *Deep Sea Res. I*, 28, 297–306, [https://doi.org/10.1016/0198-0149\(81\)90069-8](https://doi.org/10.1016/0198-0149(81)90069-8), 1981.

3026 Lewandowsky, S., Cowtan, K., Risbey, S., Mann, M., Steinman, B., Oreskes, N. and Rahmstorf, S.: The ‘pause’ in  
3027 global warming in historical context: (II). Comparing models to observations. *Environmental Research Letters*, 13  
3028 (12): 123007 DOI: 10.1088/1748-9326/aaf372, 2018.

3029 L’Heureux, M. L., Lee, S. Lyon, B.: Recent multidecadal strengthening of the Walker circulation across the tropical  
3030 Pacific. *Nat. Clim. Cha.*, 3, 571–576, 2013.

3031 Li, G., Xie, S., Du, Y. A robust but spurious pattern of climate change in model projections over the tropical Indian  
3032 Ocean, *J. Clim.*, 29, 5589–5608, 2016.

3033 Li, Y., Han, W., Ravichandran, M., Wang, W., Shinoda, T. and Lee, T.: Bay of Bengal salinity stratification and Indian  
3034 summer monsoon intraseasonal oscillation: 1. Intraseasonal variability and causes, *J. Geophys. Res. Ocean.*,  
3035 doi:10.1002/2017JC012691, 2017a.

3036 Li, Y., Han, W., Wang, W., Ravichandran, M., Lee, T. and Shinoda, T.: Bay of Bengal salinity stratification and Indian  
3037 summer monsoon intraseasonal oscillation: 2. Impact on SST and convection, *J. Geophys. Res. Ocean.*, 122(5), 4312–  
3038 4328, doi:10.1002/2017JC012692, 2017b.

3039 Li, Y., Han, W., Wang, W., Zhang, L. and Ravichandran, M.: The Indian summer monsoon intraseasonal oscillations in  
3040 CFSv2 forecasts: Biases and importance of improving air-sea interaction processes, *J. Clim.*, 31(14), 5351–5370,  
3041 doi:10.1175/JCLI-D-17-0623.1, 2018a.

3042 Li, Y., Han, W., Hu, A., Meehl, G. A. and Wang, F.: Multidecadal changes of the upper Indian ocean heat content  
3043 during 1965-2016, *J. Clim.*, doi:10.1175/JCLI-D-18-0116.1, 2018b.

3044 Liu, Q.-Y., Feng, M., Wang, D., and Wijffels, S.: Interannual variability of the Indonesian Throughflow transport: A  
3045 revisit based on 30 year expendable bathythermograph data, *J. Geophys. Res.: Oceans*, 120(12), 8270-8282,  
3046 <https://doi.org/10.1002/2015JC011351>, 2015.

3047 Lovel, W. and Lee, T.: Importance and origin of halosteric contribution to sea level change in the southeast Indian  
3048 Ocean during 2005-2013, *Geophys. Res. Lett.*, doi:10.1002/2014GL062611, 2015.

3049 Longhurst, A.: A major seasonal phytoplankton bloom in the Madagascar Basin, *Deep. Res. Part I Oceanogr. Res. Pap.*,  
3050 doi:10.1016/S0967-0637(01)00024-3, 2001.

3051 Lotliker, A. A., Omand, M. M., Lucas, A. J., Laney, S. R., Mahadevan, A. and Ravichandran, M.: Penetrative radiative  
3052 flux in the Bay of Bengal, *Oceanography*, doi:10.5670/oceanog.2016.53, 2016.

3053 Lourey, M. J., Dunn, J. R. and Waring, J.: A mixed-layer nutrient climatology of Leeuwin Current and Western  
3054 Australian shelf waters: Seasonal nutrient dynamics and biomass, *J. Mar. Syst.*, doi:10.1016/j.jmarsys.2005.10.001,  
3055 2006.

3056 Lourey, M. J., Thompson, P. A., McLaughlin, M. J., Bonham, P. and Feng, M.: Primary production and phytoplankton  
3057 community structure during a winter shelf-scale phytoplankton bloom off Western Australia, *Mar. Biol.*,  
3058 doi:10.1007/s00227-012-2093-4, 2013.

3059 Loveday, B. R., Durgadoo, J. V., Reason, C. J. C., Biastoch, A. and Penven, P.: Decoupling of the Agulhas leakage from  
3060 the Agulhas Current, *J. Phys. Oceanogr.*, doi:10.1175/JPO-D-13-093.1, 2014.

3061 Lu, B., and Ren, H. L.: What caused the extreme Indian Ocean Dipole event in 2019? *Geophys. Res. Lett.*,  
3062 [doi:10.1029/2020GL087768](https://doi.org/10.1029/2020GL087768), 2020.

3063 Lübbecke, J. F., Durgadoo, J. V. and Biastoch, A.: Contribution of increased agulhas leakage to tropical Atlantic  
3064 warming, *J. Clim.*, doi:10.1175/JCLI-D-15-0258.1, 2015.

3065 Lucas, A., Nash, J., Pinkel, R., MacKinnon, J., Tandon, A., Mahadevan, A., Omand, M., Freilich, M., Sengupta, D.,  
3066 Ravichandran, M. and Le Boyer, A.: Adrift Upon a Salinity-Stratified Sea: A view of upper-ocean processes in the  
3067 Bay of Bengal during the Southwest Monsoon, *Oceanography*, doi:10.5670/oceanog.2016.46, 2016.

3068 Luis, A. J. and Kawamura, H.: Air-sea interaction, coastal circulation and primary production in the eastern Arabian Sea:  
3069 A review, *J. Oceanogr.*, 60, 205-18, doi:10.1023/B:JOCE.0000038327.33559.34, 2004.

3070 Lumpkin, R., and Speer, K.: Global ocean meridional overturning, *J. Phys. Oceanogr.*, 37, 2550–2562,  
3071 doi:10.1175/JPO3130.1, 2007.

3072 Lutjeharms, J. R. E.: *The Agulhas Current*, Springer: Berlin, Heidelberg, New York, 2006.

3073 Lutjeharms, J. R. E., Meyer, A. A., Ansorge, I. J., Eagle, G. A. and Orren, M. J.: The nutrient characteristics of the  
3074 Agulhas bank, *South African J. Mar. Sci.*, doi:10.2989/025776196784158464, 1996.

3075 Lutjeharms, J. R. E. and Machu, E.: An upwelling cell inshore of the East Madagascar Current, *Deep. Res. Part I*  
3076 *Oceanogr. Res. Pap.*, doi:10.1016/S0967-0637(00)00026-1, 2000.

3077 Ma, J., Feng, M., Sloyan, B. M. and Lan, J.: Pacific influences on the meridional temperature transport of the Indian  
3078 Ocean, *J. Clim.*, doi:10.1175/JCLI-D-18-0349.1, 2019.

3079 Macdonald, A. M., Mecking, S., Robbins, P. E., Toole, J. M., Johnson, G. C., Talley, L. D., Cook, M., Wijffels, S., E.:  
3080 The WOCE-era 3-D Pacific Ocean Circulation and Heat Budget, *Progress in Oceanography*, 48, 281–325, 2009.

**Deleted:** View

**Deleted:** Upper-Ocean Processes

**Deleted:** During

**Deleted:** ,

**Formatted:** Font: Not Italic

**Formatted:** Font: Bold

**Formatted:** Font: Not Italic

3085 Machu, E. and Garçon, V.: Phytoplankton seasonal distribution from sea WiFS data in the Agulhas current system, J.  
3086 Mar. Res., doi:10.1357/002224001762674944, 2001.

3087 MacKinnon, J. A., Johnston, T. M. S. and Pinkel, R.: Strong transport and mixing of deep water through the Southwest  
3088 Indian Ridge, Nat. Geosci., doi:10.1038/ngeo340, 2008.

3089 Madden, R. A. and Julian, P. R.: Description of Global-Scale Circulation Cells in the Tropics with a 40–50 Day Period,  
3090 J. Atmos. Sci., doi:10.1175/1520-0469(1972)029<1109:dogsc>2.0.co;2, 1972.

3091 Madden, R. A. and Julian, P. R.: Detection of a 40–50 Day Oscillation in the Zonal Wind in the Tropical Pacific, J.  
3092 Atmos. Sci., 28(5), 702–708, doi:10.1175/1520-0469(1971)028<0702:DOADOI>2.0.CO;2, 1971.

3093 Madhupratap, M., Gauns, M., Ramaiah, N., Prasanna Kumar, S., Muraleedharan, P. M., De Sousa, S. N., Sardessai, S.  
3094 and Muraleedharan, U.: Biogeochemistry of the Bay of Bengal: Physical, chemical and primary productivity  
3095 characteristics of the central and western Bay of Bengal during summer monsoon 2001, Deep. Res. Part II Top. Stud.  
3096 Oceanogr., doi:10.1016/S0967-0645(02)00611-2, 2003.

3097 Maes, C., Grima, N., Blanke, B., Martinez, E., Paviet-Salomon, T. and Huck, T.: A Surface “Superconvergence”  
3098 Pathway Connecting the South Indian Ocean to the Subtropical South Pacific Gyre, Geophys. Res. Lett.,  
3099 doi:10.1002/2017GL076366, 2018.

3100 Mahadevan, A.: Eddy effects on biogeochemistry, Nature, doi:10.1038/nature13048, 2014.

3101 Mahadevan, A., D’Asaro, E., Lee, C. and Perry, M. J.: Eddy-driven stratification initiates North Atlantic spring  
3102 phytoplankton blooms, Science (80- ), doi:10.1126/science.1218740, 2012.

3103 Mahadevan, A., Paluszkievicz, T., Ravichandran, M., Sengupta, D. and Tandon, A.: Introduction to the Special Issue on  
3104 the Bay of Bengal: From Monsoons to Mixing, Oceanography, doi:10.5670/oceanog.2016.34, 2016a.

3105 Mahadevan, A., Spiro Jaeger, G., Freilich, M., Omand, M., Shroyer, E. and Sengupta, D.: Freshwater in the Bay of  
3106 Bengal: Its Fate and Role in Air-Sea Heat Exchange, Oceanography, 29(2), 72–81, doi:10.5670/oceanog.2016.40,  
3107 2016b.

3108 Maher, N., England, M.H., Gupta, A.S. et al.: Role of Pacific trade winds in driving ocean temperatures during the  
3109 recent slowdown and projections under a wind trend reversal. Clim Dyn 51, 321–336, [https://doi.org/10.1007/s00382-](https://doi.org/10.1007/s00382-017-3923-3)  
3110 [017-3923-3](https://doi.org/10.1007/s00382-017-3923-3), 2018.

3111 Manatsa, D. and Behera, S. K.: On the epochal strengthening in the relationship between rainfall of East Africa and IOD,  
3112 J. Clim., 26, 5655–5673, doi:10.1175/JCLI-D-12-00568.1, 2013.

3113 Manghnani, V., Morrison, J. M., Hopkins, T. S. and Böhm, E.: Advection of upwelled waters in the form of plumes off  
3114 Oman during the Southwest Monsoon, Deep. Res. Part II Top. Stud. Oceanogr., doi:10.1016/S0967-0645(98)00062-9,  
3115 1998.

3116 Mantyla, A. W. and Reid, J. L.: On the origins of deep and bottom waters of the Indian Ocean, J. Geophys. Res.,  
3117 doi:10.1029/94JC02564, 1995.

3118 Marra, J., Dickey, T. D., Ho, C., Kinkade, C. S., Sigurdson, D. E., Weller, R. A. and Barber, R. T.: Variability in  
3119 primary production as observed from moored sensors in the central Arabian Sea in 1995, Deep. Res. Part II Top. Stud.  
3120 Oceanogr., doi:10.1016/S0967-0645(98)00070-8, 1998.

3121 Marsac, F. and Blanc, J.: Oceanographic changes during the 1997–1998 El Niño in the Indian Ocean and their impact on  
3122 the purse seine fishery, IOTC Proc. no. 2, 1999.

3123 Marin, M., and Feng, M.: Intra-annual variability of the North West Shelf of Australia and its impact on the Holloway  
3124 Current: Excitement and propagation of coastally trapped waves, Cont. Shelf Res.,  
3125 <https://doi.org/10.1016/j.csr.2019.08.001>, 2019.

3126 Marin, M., Feng, M., Phillips, H. F., and Bindoff, N. L.: A global, multiproduct analysis of coastal marine heatwaves:  
3127 distribution, characteristics, and long-term trends. J. Geophys. Res. Oceans, 126,  
3128 <http://dx.doi.org/10.1029/2020JC016708>, 2021.

3129 Marshall, A.G. and Hendon, H. H.: Impacts of the MJO in the Indian Ocean and on the Western Australian coast.  
3130 Climate Dyn., 42(3–4), 579–595, <https://doi.org/10.1007/s00382-012-1643-2>, 2014.

Deleted: . &

Deleted: , 2021:

Deleted: <http://dx.doi.org/10.1029/2020JC016708>.

3134 Marshall, A. G., Hendon, H. H., Feng, M., and Schiller, A.: Initiation and amplification of the Ningaloo Niño, *Climate*  
3135 *Dyn.*, 45, 2367–2385, <https://doi.org/10.1007/s00382-015-2477-5>, 2015.

3136 Martin, A. P. and Richards, K. J.: Mechanisms for vertical nutrient transport within a North Atlantic mesoscale eddy,  
3137 *Deep. Res. Part II Top. Stud. Oceanogr.*, doi:10.1016/S0967-0645(00)00096-5, 2001.

3138 Masumoto, Y. and Meyers, G.: Forced Rossby waves in the southern tropical Indian Ocean, *J. Geophys. Res. Ocean.*,  
3139 doi:10.1029/98JC02546, 1998.

3140 Masumoto, Y., Hase, H., Kuroda, Y., Matsuura, H. and Takeuchi, K.: Intraseasonal variability in the upper layer  
3141 currents observed in the eastern equatorial Indian Ocean, *Geophys. Res. Lett.*, doi:10.1029/2004GL021896, 2005.

3142 Matthews, A. J., Singhruck, P. and Heywood, K. J.: Deep ocean impact of a Madden-Julian oscillation observed by Argo  
3143 floats, *Science*, 318(5857), 1765–1769, doi: 10.1126/science.1147312, 2007.

3144 Maximenko, N., Niiler, P., Centurioni, L., Rio, M.-H., Melnichenko, O., Chambers, D., Zlotnicki, V., Galperin, B.:  
3145 Mean dynamic topography of the ocean derived from satellite and drifting buoy data using three different techniques,  
3146 *J. Atmos. Oceanic Technol.* 26 (9), 1910–1919, <https://doi.org/10.1175/2009JTECHO672.1>, 2009.

3147 Mayer, M., Alonso Balmaseda, M. and Haimberger, L.: Unprecedented 2015/2016 Indo-Pacific Heat Transfer Speeds  
3148 Up Tropical Pacific Heat Recharge, *Geophys. Res. Lett.*, doi:10.1002/2018GL077106, 2018.

3149 McCreary, I. N., Kiefer, T., Thornalley, D. J. R. and Elderfield, H.: Deep flow in the Madagascar-Mascarene Basin over  
3150 the last 150 000 years, *Philos. Trans. R. Soc. A: Math. Phys. Eng. Sci.*, doi:10.1098/rsta.2004.1480, 2005.

3151 McCreary, J.P.: Equatorial beams. *J. Mar. Res.*, 42(2), 395–430, <https://doi.org/10.1357/002224084788502792>, 1984.

3152 McCreary, J. P., Fukamachi, Y., and Lu, P.: A nonlinear mechanism for maintaining coastally trapped eastern boundary  
3153 currents, *J. Geophys. Res.*, 97 (C4), 5677–5692, <https://doi.org/10.1029/92JC00035>, 1992.

3154 McCreary, J.P., Kundu, P. K. and Molinari, R. L.: A numerical investigation of dynamics, thermodynamics, and mixed  
3155 layer processes in the Indian Ocean, *Prog. Oceanogr.*, 31, 181-224, 1993.

3156 McCreary, J. P., Han, W., Shankar, D. and Shetye, S. R.: Dynamics of the East India Coastal Current 2. Numerical  
3157 solutions; *J. Geophys. Res.*, 101, 13993–14010, 1996.

3158 McCreary, J. P., Shetye, S. R., and Kundu, P. K.: Thermohaline forcing of eastern boundary currents: With application  
3159 to the circulation off the west coast of Australia, *J. Mar. Res.*, 44, 71–92,  
3160 <https://doi.org/10.1357/002224086788460184>, 1986.

3161 McCreary, J. P., Kohler, K. E., Hood, R. R., Smith, S., Kindle, J., Fischer, A. S. and Weller, R. A.: Influences of diurnal  
3162 and intraseasonal forcing on mixed-layer and biological variability in the central Arabian Sea, *J. Geophys. Res.*  
3163 *Ocean.*, doi:10.1029/2000jc900156, 2001.

3164 McCreary, J.P., Murtugudde, R., Vialard, J., Vinayachandran, P.N., Wiggert, J.D., Hood, R.R., Shankar, D. and Shetye,  
3165 S.: Biophysical Processes in the Indian Ocean. In *Indian Ocean Biogeochemical Processes and Ecological Variability*  
3166 (eds J.D. Wiggert, R.R. Hood, S.A. Naqvi, K.H. Brink and S.L. Smith). <https://doi.org/10.1029/2008GM000768>,  
3167 2009.

3168 McCreary, J. P., Yu, Z., Hood, R. R., Vinayachandran P. N., Furue, R., Ishida, A., Richards, K. J.: Dynamics of the  
3169 Indian-Ocean oxygen minimum zones, *Prog. Oceanogr.*, 112, 15–37, 2013.

3170 McDonagh, E. L., Bryden, H. L., King, B. A. & Sanders, R. J. The circulation of the Indian Ocean at 32°S. *Prog*  
3171 *Oceanogr* 79, 20–36, 2008.

3172 McGillicuddy, D. J., Anderson, L. A., Bates, N. R., Bibby, T., Buesseler, K. O., Carlson, C. A., Davis, C. S., Ewart, C.,  
3173 Falkowski, P. G., Goldthwait, S. A., Hansell, D. A., Jenkins, W. J., Johnson, R., Kosnyrev, V. K., Ledwell, J. R., Li,  
3174 Q. P., Siegel, D. A. and Steinberg, D. K.: Eddy/Wind interactions stimulate extraordinary mid-ocean plankton blooms,  
3175 *Science* (80-. ), doi:10.1126/science.1136256, 2007.

3176 McPhaden, M.J.: Genesis and evolution of the 1997-98 El Niño, *Science*, 283, 950-954, 1999.

3177 McPhaden, M. J., Meyers, G., Ando, K., Masumoto, Y., Murty, V. S. N., Ravichandran, M., Syamsudin, F., Vialard, J.,  
3178 Yu, L., & Yu, W. : RAMA: The Research Moored Array for African–Asian–Australian Monsoon Analysis and

Moved (insertion) [1]

Deleted: .

Formatted: Font: Not Italic

Formatted: Font: Not Italic

Formatted: Font: Not Bold



Prediction, *Bulletin of the American Meteorological Society*, 90(4), 459–480.  
[https://journals.ametsoc.org/view/journals/bams/90/4/2008bams2608\\_1.xml](https://journals.ametsoc.org/view/journals/bams/90/4/2008bams2608_1.xml), 2009.

McPhaden, M. J. and Foltz, G. R.: Intraseasonal variations in the surface layer heat balance of the central equatorial Indian Ocean: The importance of zonal advection and vertical mixing, *Geophys. Res. Lett.*, 40(11), 2737–2741, <https://doi.org/10.1002/grl.50536>, 2013.

McPhaden, M. J. and M. Nagura: Indian Ocean Dipole interpreted in terms of Recharge Oscillator theory. *Clim. Dyn.*, 42, 1569–1586. doi 10.1007/s00382-013-1765-1, 2014.

McPhaden, M. J., Wang, Y. and Ravichandran, M.: Volume transports of the Wyrtki jets and their relationship to the Indian Ocean dipole, *J. Geophys. Res. Oceans*, 120(8), 5302–5317, 2015.

Menezes, V. V., Phillips, H.E., Schiller, A., Domingues, C.M., and Bindoff, N.L.: Salinity dominance on the Indian Ocean Eastern Gyral current, *Geophys. Res. Lett.*, 40, 5716–5721, <https://doi.org/10.1002/2013GL057887>, 2013.

Menezes, V. V., Phillips, H. E., Schiller, A., Bindoff, N. L., Domingues, C. M., and Vianna, M. L.: South Indian Countercurrent and associated fronts, *J. Geophys. Res. Oceans*, 119, 6763–6791, <https://doi.org/10.1002/2014JC010076>, 2014.

Menezes, V. V.: The structure and dynamics of the eastward flows of the South Indian Ocean, PhD Thesis, University of Tasmania, 244pp, <http://eprints.utas.edu.au/23392/>, 2015.

Menezes, V. V., Phillips, H. E., Vianna, M. L., and Bindoff, N. L.: Interannual variability of the South Indian Countercurrent, *J. Geophys. Res. Oceans*, 121, 3465–3487, <https://doi.org/10.1002/2015JC011417>, 2016.

Merle, J., Rotschi, H., and Voituriez, B.: Zonal circulation in the tropical western South Pacific at 170°E. *Bull. Japan Soc. Fish. Oceanogr., Special Issue (Prof. Uda's Commemorative Papers)*, 91–98, 1969.

Meuleners, M.J., Pattiaratchi, C.B., and Ivey, G.N.: Numerical modelling of the mean flow characteristics of the Leeuwin Current System, *Deep Sea Res. II*, 54(8–10), 837–858, <https://doi.org/10.1016/j.dsr2.2007.02.003>, 2007.

Meuleners, M.J., Ivey, G.N., and Pattiaratchi, C.B.: A numerical study of the eddying characteristics of the Leeuwin Current System, *Deep Sea Res. I*, 55(3), 261–276, <https://doi.org/10.1016/j.dsr.2007.12.004>, 2008.

Meyers, G., R. J. Bailey, and A. P. Worby, 1995: Geostrophic transport of Indonesian Throughflow. *Deep-Sea Res. I*, 42, 1163–1174.

Meyers, G.: Variation of Indonesian throughflow and the El Niño Southern Oscillation, *J. Geophys. Res.*, 101, C5, 12255–12263, <https://doi.org/10.1029/95JC03729>, 1996.

Miyama, T., McCreary, J.P., Jensen, T.G., Loschnigg, J.L., Godfrey, S., and Ishida, A.: Structure and dynamics of the Indian-Ocean cross-equatorial cell, *Deep Sea Res. II*, 50, 2023–2047, [https://doi.org/10.1016/S0967-0645\(03\)00044-4](https://doi.org/10.1016/S0967-0645(03)00044-4), 2003.

Miyama, T., McCreary, J.P. Sengupta, D., and Senan, R.: Dynamics of biweekly oscillations in the equatorial Indian Ocean, *J. Phys. Oceanogr.*, 36, 827–846, <https://doi.org/10.1175/JPO2897.1>, 2006.

Moore, T. S., Matear, R. J., Marra, J. and Clementson, L.: Phytoplankton variability off the Western Australian Coast: Mesoscale eddies and their role in cross-shelf exchange, *Deep. Res. Part II Top. Stud. Oceanogr.*, doi:10.1016/j.dsr2.2007.02.006, 2007.

Morel, A. and Antoine, D.: Heating Rate within the Upper Ocean in Relation to its Bio-optical State, *J. Phys. Oceanogr.*, 24(7), 1652–1665, doi:10.1175/1520-0485(1994)024<1652:HRWTUO>2.0.CO;2, 1994.

Morioka, Y., Tozuka, T. and Yamagata, T.: Climate variability in the southern Indian Ocean as revealed by self-organizing maps, *Clim. Dyn.*, doi:10.1007/s00382-010-0843-x, 2010.

Morioka, Y., Tozuka, T., Masson, S., Terray, P., Luo, J. J. and Yamagata, T.: Subtropical dipole modes simulated in a coupled general circulation model, *J. Clim.*, doi:10.1175/JCLI-D-11-00396.1, 2012.

Moum, J. N. and Nash, J. D.: Mixing Measurements on an Equatorial Ocean Mooring, *J. Atmos. Ocean. Technol.*, doi:10.1175/2008jtecho617.1, 2009.

Deleted: \*

3225 Moum, J. N., de Szeke, S. P., Smyth, W. D., Edson, J. B., DeWitt, H. L., Moulin, A. J., Thompson, E. J., Zappa, C. J.,  
3226 Rutledge, S. A., Johnson, R. H. and Fairall, C. W.: Air–Sea Interactions from Westerly Wind Bursts During the  
3227 November 2011 MJO in the Indian Ocean, *Bull. Am. Meteorol. Soc.*, 95(8), 1185–1199, doi:10.1175/BAMS-D-12-  
3228 00225.1, 2014.

3229 Moum, J. N., Pujiana, K., Lien, R. C. and Smyth, W. D.: Ocean feedback to pulses of the Madden-Julian Oscillation in  
3230 the equatorial Indian Ocean, *Nat. Commun.*, 7(May), 1–7, doi:10.1038/ncomms13203, 2016.

3231 Mukherjee, A., Shankar, D., Fernando, V. *et al.* Observed seasonal and intraseasonal variability of the East India Coastal  
3232 Current on the continental slope. *J Earth Syst Sci* 123, 1197–1232 , <https://doi.org/10.1007/s12040-014-0471-7>, 2014.

3233 [Mukherjee, A., Shankar, D., Chatterjee, A. and Vinayachandran, P. N.: Numerical simulation of the observed near](https://doi.org/10.1007/s00382-017-3856-x)  
3234 [surface East India Coastal Current on the continental slope, \*Clim. Dyn.\*, 50, 3949–3980,](https://doi.org/10.1007/s00382-017-3856-x)  
3235 <https://doi.org/10.1007/s00382-017-3856-x>, 2018.

3236 Mukhopadhyay, S., Shankar, D., Aparna, S.G., Mukherjee, A., Fernando, V., Kankonkar, A., Khalap, S. T., Satelkar,  
3237 N.P., Gaonkar, M.G., Tari, A.P., Khedekar, R.R., Ghatkar, S.: Observed variability of the East India Coastal Current  
3238 on the continental slope during 2009–2018. *J. Earth Syst. Sci.*, 129, p. 77, 10.1007/s12040-020-1346-8, 2020.

3239 Mulholland, M. R., Bernhardt, P. W., Ozmon, I., Procise, L. A., Garrett, M., O’Neil, J. M., Heil, C. A. and Bronk, D. A.:  
3240 Contribution of diazotrophy to nitrogen inputs supporting *Karenia brevis* blooms in the Gulf of Mexico, *Harmful*  
3241 *Algae*, doi:10.1016/j.hal.2014.04.004, 2014.

3242 Muraleedharan, K. R., Jasmine, P., Achuthankutty, C. T., Revichandran, C., Dinesh Kumar, P. K., Anand, P. and  
3243 Rejomon, G.: Influence of basin-scale and mesoscale physical processes on biological productivity in the Bay of  
3244 Bengal during the summer monsoon, *Prog. Oceanogr.*, doi:10.1016/j.pocean.2006.09.012, 2007.

3245 Murtugudde, R. and Busalacchi, A. J.: Interannual variability of the dynamics and thermodynamics of the tropical Indian  
3246 Ocean, *J. Clim.*, doi:10.1175/1520-0442(1999)012<2300:ivotda>2.0.co;2, 1999.

3247 Murtugudde, R., McCreary, J. P. and Busalacchi, A. J.: Oceanic processes associated with anomalous events in the  
3248 Indian Ocean with relevance to 1997–1998, *J. Geophys. Res. Ocean.*, 105(C2), 3295–3306,  
3249 doi:10.1029/1999JC900294, 2000.

3250 Murtugudde, R., Beauchamp, J., McClain, C. R., Lewis, M. and Busalacchi, A. J.: Effects of penetrative radiation of the  
3251 upper tropical ocean circulation, *J. Clim.*, 15(5), 470–486, doi:10.1175/1520-  
3252 0442(2002)015<0470:EOPROT>2.0.CO;2, 2002.

3253 Murty, V. S. N., Gupta, G. V. M., Sarma, V. V., Rao, B. P., Jyothi, D., Shastri, P. N. M. and Supraveena, Y.: Effect of  
3254 vertical stability and circulation on the depth of the chlorophyll maximum in the Bay of Bengal during May–June,  
3255 1996, *Deep. Res. Part I Oceanogr. Res. Pap.*, doi:10.1016/S0967-0637(99)00071-0, 2000.

3256 Nagura, M. and McPhaden, M. J.: Wyrtki jet dynamics: Seasonal variability, *J. Geophys. Res. Oceans*, 115(C7), 1–17,  
3257 2010a.

3258 Nagura, M. and McPhaden, M. J.: Dynamics of zonal current variations associated with the Indian Ocean dipole, *J.*  
3259 *Geophys. Res. Oceans*, 115 (C11), 1–12, 2010b.

3260 Nagura, M. and McPhaden, M. J.: The dynamics of wind-driven intraseasonal variability in the equatorial Indian Ocean,  
3261 *J. Geophys. Res. Oceans*, 117(2), 1–16, doi: 10.1029/2011JC007405, 2012.

3262 Nagura, M. and M. J. McPhaden: Zonal momentum budget along the equator in the Indian Ocean from a high resolution  
3263 ocean general circulation model. *J. Geophys. Res.*, 119, 4444–4461, doi:10.1002/2014JC009895, 2014.

3264 Nagura, M. and McPhaden, M. J.: Zonal Propagation of Near-Surface Zonal Currents in Relation to Surface Wind  
3265 Forcing in the Equatorial Indian Ocean, *J. Phys. Ocean.*, 46, 3623–3638, doi: 10.1175/JPO-D-16-0157.1, 2016.

3266 Nagura, M. & McPhaden, M. J. The Shallow Overturning Circulation in the Indian Ocean. *J. Phys. Oceanogr.* 48, 413–  
3267 434, 2018.

3268 Nagura, M., & McPhaden, M. J.: Interannual variability in sea surface height at Southern midlatitudes of the Indian  
3269 Ocean, *J. Phys. Oceanog.*, 51, 1595-1609, 2021.

3270 Naqvi, S. W. A., Jayakumar, D. A., Narvekar, P. V., Naik, H., Sarma, V. V. S. S., D'Souza, W., Joseph, S. and George,  
3271 M. D.: Increased marine production of N<sub>2</sub>O due to intensifying anoxia on the Indian continental shelf, *Nature*,  
3272 doi:10.1038/35042551, 2000.

3273 [Naqvi, S. W., Narvekar, P. V. and Desa, E.: Coastal biogeochemical processes in the North Indian Ocean \(14, S-W\), \*The\*](#)  
3274 [Sea, 14, 723–780, 2006.](#)

3275 Narayanasetti, S., Swapna, P., Ashok, K., Jadhav, J., and Krishnan, R.: Changes in biological productivity associated  
3276 with Ningaloo Niño/Niña events in the southern subtropical Indian Ocean in recent decades, *Scientific Reports*, 6,  
3277 27467, <https://doi.org/10.1038/srep27467>, 2016.

3278 Nethery, D., and Shankar, D.: Vertical propagation of baroclinic Kelvin waves along the west coast of India, *J. Earth*.  
3279 *Syst. Sci.*, 116, 331–339, <https://doi.org/10.1007/s12040-007-0030-6>, 2007.

3280 Nicholson, S. E.: Long-term variability of the East African “short rains” and its links to large-scale factors. *Internat. J.*  
3281 *Climatol.*, doi:10.1002/joc.4259, 2015.

3282 Nieves, V., Willis, J. K. and Patzert, W. C.: Recent hiatus caused by decadal shift in Indo-Pacific heating, *Science*,  
3283 <https://doi.org/10.1126/science.aaa4521>, 2015.

3284 Niiler, P. P., Maximenko, N. A., and McWilliams, J. C.: Dynamically balanced absolute sea level of the global ocean  
3285 derived from near-surface velocity observations, *Geophys. Res. Lett.*, 30, 2164,  
3286 <https://doi.org/10.1029/2003GL018628>, 2003.

3287 Nof, D. and Olson, D. B.: How do western abyssal currents cross the equator?, *Deep. Res. Part I*, doi:10.1016/0967-  
3288 0637(93)90002-K, 1993.

3289 Nyadjro, E. and M. J. McPhaden: Variability of zonal currents in the eastern equatorial Indian Ocean on seasonal to  
3290 interannual time scales. *J. Geophys. Res.*, 119, 7969–7986, doi:10.1002/2014JC010380, 2014.

3291 O'Donoghue, S. H., Drapeau, L., Dudley, S. F. J. and Peddemors, V. M.: The KwaZulu-Natal sardine run: Shoal  
3292 distribution in relation to nearshore environmental conditions, 1997–2007, *African J. Mar. Sci.*,  
3293 doi:10.2989/1814232x.2010.501587, 2010.

3294 Ogata, T., and Masumoto, Y.: Interannual modulation and its dynamics of the mesoscale eddy variability in the  
3295 southeastern tropical Indian Ocean, *J. Geophys. Res.*, 116, C05005, doi:10.1029/2010JC006490, 2011.

3296 Ogata, T., and Xie, S.-P.: Semiannual cycle in zonal wind over the equatorial Indian Ocean. *J. Climate*, 24, 6471–6485,  
3297 doi:10.1175/2011JCLI4243.1, 2011.

3298 Oke, P. R., Griffin, D. A., Rykova, T., and de Oliveira, H. B.: Ocean circulation in the Great Australian Bight in an  
3299 eddy-resolving ocean reanalysis: The eddy field, seasonal and interannual variability, *Deep Sea Res. II*, 157–158, 11–  
3300 26, <https://doi.org/10.1016/j.dsr2.2018.09.012>, 2018.

3301 Oliver, E. C. J., and Thompson, K. R.: Madden-Julian oscillation and sea level: Local and remote forcing, *J. Geophys.*  
3302 *Res. Ocean.*, 115(1), 1–15, <https://doi.org/10.1029/2009JC005337>, 2010.

3303 Oliver, E.C.J., Herzfeld, M., and Holbrook, N.J.: Modelling the shelf circulation offeastern Tasmania. *Continent. Shelf*  
3304 *Res.*, 130, 14–33, 2016.

3305 Oliver, E. C., Donat, M. G., Burrows, M. T., Moore, P. J., Smale, D. A., Alexander, L. V., Benthuyssen, J. A., Feng, M.,  
3306 Sen Gupta, A., Hobday, A. J., Holbrook, N. J., Perkins-Kirkpatrick, S. E., Scannell, H. A., Straub, S. C., and  
3307 Wernberg, T.: Longer and more frequent marine heatwaves over the past century, *Nature Commun.*, 9, 1324,  
3308 <https://doi.org/10.1038/s41467-018-03732-9>, 2018.

3309 Palastanga, V., van Leeuwen, P. J., Schouten, M. W., and de Ruijter, W. P. M.: Flow structure and variability in the  
3310 subtropical Indian Ocean: instability of the South Indian Ocean Countercurrent, *J. Geophys. Res.*, 112, C01001,  
3311 <https://doi.org/10.1029/2005JC003395>, 2007.

3312 Parab, S. G., Prabhu Matondkar, S. G., Gomes, H. do R. and Goes, J. I.: Monsoon driven changes in phytoplankton  
3313 populations in the eastern Arabian Sea as revealed by microscopy and HPLC pigment analysis, *Cont. Shelf Res.*, 26  
3314 (20), doi:10.1016/j.csr.2006.08.004, 2006.

3315 Paris, M. L., Subrahmanyam, B., Trott, C. B. and Murty, V. S. N.: Influence of ENSO Events on the Agulhas Leakage  
3316 Region, *Remote Sens. Earth Syst. Sci.*, doi:10.1007/s41976-018-0007-z, 2018.

3317 Paterson, H. L., Feng, M., Waite, A. M., Gomis, D., Beckley, L. E., Holliday, D. and Thompson, P. A.: Physical and  
3318 chemical signatures of a developing anticyclonic eddy in the Leeuwin Current, eastern Indian Ocean, *J. Geophys. Res.*  
3319 *Ocean.*, doi:10.1029/2007JC004707, 2008.

3320 Paterson, J. S., Nayar, S., Mitchell, J. G. and Seuront, L.: Population-specific shifts in viral and microbial abundance  
3321 within a cryptic upwelling, *J. Mar. Syst.*, doi:10.1016/j.jmarsys.2012.12.009, 2013.

3322 Pearce, A. F., and Griffiths, R.W.: The mesoscale structure of the Leeuwin Current: A comparison of laboratory model  
3323 and satellite images, *J. Geophys. Res.*, 96, 16730–16757, <https://doi.org/10.1029/91JC01712>, 1991.

3324 Pearce, A. and Feng, M.: Observations of warming on the Western Australian continental shelf. *Marine Freshw. Res.*,  
3325 58, 914–920, 2007.

3326 Pearce, A., Lenanton, R., Jackson, G., Moore, J., Feng, M., and Gaughan, D.: The “marine heat wave” off Western  
3327 Australia during the summer of 2010/11, Fisheries Research Report No. 222, Department of Fisheries, Western  
3328 Australia, 40pp, [http://fish.wa.gov.au/Documents/research\\_reports/fr222.pdf](http://fish.wa.gov.au/Documents/research_reports/fr222.pdf), 2011.

3329 Peatman, S. C. and Klingaman, N. P.: The Indian summer monsoon in MetUM-GOML2.0: Effects of air-sea coupling  
3330 and resolution, *Geosci. Model Dev.*, 11(11), 4693–4709, doi:10.5194/gmd-11-4693-2018, 2018.

3331 Philander, S. G. H., and Yoon, J.-H.: Eastern boundary currents and coastal upwelling, *J. Phys. Oceanogr.*, 12(8), 862–  
3332 879, [https://doi.org/10.1175/1520-0485\(1982\)012<0862:EBCACU>2.0.CO;2](https://doi.org/10.1175/1520-0485(1982)012<0862:EBCACU>2.0.CO;2), 1982.

3333 Phillips, H.E., Wijffels, S.E. and Feng, M.: Interannual variability in the freshwater content of the Indonesian-Australian  
3334 Basin. *Geophysical Research Letters*. Vol. 32, L03603, doi:10.1029/2004GL021755, 2005.

3335 Pirro, A., Fernando, H. J. S., Wijesekera, H. W., Jensen, T. G., Centurioni, L. R. and Jinadasa, S. U. P.: Eddies and  
3336 currents in the Bay of Bengal during summer monsoons, *Deep. Res. Part II Top. Stud. Oceanogr.*,  
3337 doi:10.1016/j.dsr2.2019.104728, 2020a.

3338 Pirro, A., Wijesekera, H. W., Jarosz, E. and Fernando, H. J. S.: Dynamics of intraseasonal oscillations in the Bay of  
3339 Bengal during summer monsoons captured by mooring observations, *Deep. Res. Part II Top. Stud. Oceanogr.*,  
3340 doi:10.1016/j.dsr2.2019.104718, 2020b.

3341 Poulton, A. J., Stinchcombe, M. C. and Quartly, G. D.: High numbers of *Trichodesmium* and diazotrophic diatoms in the  
3342 southwest Indian Ocean, *Geophys. Res. Lett.*, doi:10.1029/2009GL039719, 2009.

3343 Prerna, S., Chatterjee, A., Mukherjee, A., Ravichandran, M. and Shenoi, S. S. C.: Wyrki Jets: Role of intraseasonal  
3344 forcing, *J. Earth Syst. Sci.*, doi:10.1007/s12040-018-1042-0, 2019.

3345 Probyn, T., Mitchellinnes, B., Brown, P., Hutchings, L. and Carter, R.: A review of primary production and related  
3346 processes on the Agulhas Bank, *S. Afr. J. Sci.*, 1994.

3347 Pujiana, K., Gordon, A. L. and Sprintall, J.: Intraseasonal Kelvin wave in Makassar strait, *J. Geophys. Res. Ocean.*,  
3348 doi:10.1002/jgrc.20069, 2013.

3349 Pujiana, K. and M.J. McPhaden: Ocean's response to the convectively coupled Kelvin waves in the eastern equatorial  
3350 Indian Ocean. *J. Geophys. Res.*, 123, 5727– 5741. <https://doi.org/10.1029/2018JC013858>, 2018.

3351 Pujiana, K. and McPhaden, M. J.: Intraseasonal Kelvin Waves in the Equatorial Indian Ocean and Their Propagation  
3352 into the Indonesian Seas, *J. Geophys. Res. Oceans*, 125(5), 1–18, doi: 10.1029/2019JC015839, 2020.

3353 Pujiana, K. and M. J. McPhaden: Biweekly mixed Rossby-Gravity waves in the equatorial Indian Ocean. *J. Geophys.*  
3354 *Res.*, <https://doi.org/10.1029/2020JC016840>, 2021.

3355 Pujiana, K., M.J. McPhaden, A.L. Gordon, and A.M. Napitu, 2019: Unprecedented response of Indonesian throughflow  
3356 to anomalous Indo-Pacific climatic forcing in 2016. *J. Geophys. Res.*, 124, 3737-3754.  
3357 <https://doi.org/10.1029/2018JC014574>.

Purkey, S. G., Johnson, G. C.: Warming of global abyssal and deep Southern Ocean waters between the 1990s and 2000s: Contributions to global heat and sea level rise budgets. *J. Clim.* 23, 6336–6351. doi: 10.1175/2010JCLI3682.1, 2010.

Purkey, S. G. and Johnson, G. C.: Global contraction of Antarctic Bottom Water between the 1980s and 2000s, *J. Clim.*, doi:10.1175/JCLI-D-11-00612.1, 2012.

Qiu, B., and Chen, S.: Seasonal modulations in the eddy field of the South Pacific Ocean, *J. Phys. Oceanogr.*, 34(7), 1515–1527, [https://doi.org/10.1175/1520-0485\(2004\)034<1515:SMITEF>2.0.CO;2](https://doi.org/10.1175/1520-0485(2004)034<1515:SMITEF>2.0.CO;2), 2004.

Qiu, Y., Li, L., and Yu, W.: Behavior of the Wyrki jet observed with surface drifting buoys and satellite altimeter. *Geophys. Res. Lett.*, 36, L18607, <https://doi.org/10.1029/2009GL039120>, 2009.

Qiu, Y., Han, W., Lin, X., West, J., Li, Y., Xing, W., Zhang, X., Arulananthan, K. and Guo, X.: Upper-ocean response to the super tropical cyclone Phailin (2013) over the freshwater region of the Bay of Bengal, *J. Phys. Oceanogr.*, doi:10.1175/JPO-D-18-0228.1, 2019.

Qu, T., Fukumori, I. and Fine, R. A.: Spin-Up of the Southern Hemisphere Super Gyre, *J. Geophys. Res. Ocean.*, doi:10.1029/2018JC014391, 2019.

Quadfasel, D. and Cresswell, G. R.: A note on the seasonal variability of the South Java Current. *Journal of Geophysical Research*, 97(C3), 3685– 3688. <https://doi.org/10.1029/91JC03056>, 1992.

Quartly, G. D. and Srokosz, M. A.: Eddies in the southern Mozambique Channel, *Deep. Res. Part II Top. Stud. Oceanogr.*, doi:10.1016/j.dsr2.2003.03.001, 2004.

Rahaman, H., Bharath Raj, G.N. & Ravichandran, M. Coupled Ocean–Atmosphere Summer Intraseasonal Oscillation over the Bay of Bengal. *Pure Appl. Geophys.* 176, 5415–5429, <https://doi.org/10.1007/s00024-019-02275-4>, 2019.

Raj, R. P., Peter, B. N. and Pushpadas, D.: Oceanic and atmospheric influences on the variability of phytoplankton bloom in the Southwestern Indian Ocean, *J. Mar. Syst.*, doi:10.1016/j.jmarsys.2010.05.009, 2010.

Ramanantsoa, J. D., Penven, P., Krug, M., Gula, J., and Rouault, M.: Uncovering a new current: The Southwest Madagascar Coastal Current. *Geophysical Research Letters*, 45, 1930–1938. <https://doi.org/10.1002/2017GL075900>, 2018.

Rao, R. R., Molinari, R. L. and Festa, J. F.: Evolution of the climatological near-surface thermal structure of the tropical Indian Ocean. 1. Description of mean monthly mixed layer depth, and sea surface temperature, surface current, and surface meteorological fields, *J. Geophys. Res.*, doi:10.1029/jc094ic08p10801, 1989.

Rao, R. R., and Sivakumar, R.: Seasonal variability of sea surface salinity and salt budget of the mixed layer of the north Indian Ocean, *J. Geophys. Res.*, 108(C1), 3009, doi:10.1029/2001JC000907, 2003.

Rathore, S., Bindoff, N. L., Phillips, H. E. and Feng, M.: Recent hemispheric asymmetry in global ocean warming induced by climate change and internal variability, *Nat. Commun.*, doi:10.1038/s41467-020-15754-3, 2020.

Ratna, S. B., Cherchi, A., Osborn, T. J., Joshi, M. and Uppara, U.: The extreme positive Indian Ocean Dipole of 2019 and associated Indian summer monsoon rainfall response. *Geophysical Research Letters*, 48, e2020GL091497, doi:10.1029/2020GL091497, 2021.

Ravichandran, M., Girishkumar, M. S. and Riser, S.: Observed variability of chlorophyll-a using Argo profiling floats in the southeastern Arabian Sea, *Deep. Res. Part I Oceanogr. Res. Pap.*, doi:10.1016/j.dsr.2012.03.003, 2012.

Reason, C. J. C.: Subtropical Indian Ocean SST dipole events and southern African rainfall, *Geophys. Res. Lett.*, doi:10.1029/2000GL012735, 2001.

Reason, C.J.C.: Sensitivity of the southern African circulation to dipole sea-surface-temperature patterns in the south Indian Ocean. *Int. J. Climatol.* 22, 377–393. <https://doi.org/10.1002/joc.744>, 2002.

Reppin, J., Schott, F. A., Fischer, J. and Quadfasel, D.: Equatorial currents and transports in the upper central Indian Ocean: Annual cycle and interannual variability, *J. Geophys. Res. Ocean.*, doi:10.1029/1999jc900093, 1999.

Resplandy, L., Vialard, J., Lévy, M., Aumont, O. and Dandonneau, Y.: Seasonal and intraseasonal biogeochemical variability in the thermocline ridge of the southern tropical Indian Ocean, *J. Geophys. Res. Ocean.*, doi:10.1029/2008JC005246, 2009.

3404 Ridgway, K. R., and Condie, S. A.: The 5500-km-long boundary flow off western and southern Australia, *J. Geophys.*  
3405 *Res.*, 109, C04017, <https://doi.org/10.1029/2003JC001921>, 2004.

3406 Ridgway, K. R., Godfrey, J.: The source of the Leeuwin Current seasonality, *J. Geophys. Res.*, 120(10), 6843–6864,  
3407 <https://doi.org/10.1002/2015JC011049>, 2015.

3408 Rixen, T., Cowie, G., Gaye, B., Goes, J., do Rosário Gomes, H., Hood, R. R., Lachkar, Z., Schmidt, H., Segsneider, J.,  
3409 and Singh, A.: Reviews and syntheses: Present, past, and future of the oxygen minimum zone in the northern Indian  
3410 Ocean, *Biogeosciences*, 17, 6051–6080, <https://doi.org/10.5194/bg-17-6051-2020>, 2020.

3411 Robbins, P. E. and Toole, J. M.: The dissolved silica budget as a constraint on the meridional overturning circulation of  
3412 the Indian Ocean, *Deep. Res. Part I Oceanogr. Res. Pap.*, doi:10.1016/S0967-0637(96)00126-4, 1997.

3413 Roberts, M. J.: Chokka squid (*Loligo vulgaris reynaudii*) abundance linked to changes in South Africa’s Agulhas Bank  
3414 ecosystem during spawning and the early life cycle, *ICES J. Mar. Sci.*, doi:10.1016/j.icesjms.2004.10.002, 2005.

3415 Roberts, M. J., Temon, J. F. and Morris, T.: Interaction of dipole eddies with the western continental slope of the  
3416 Mozambique Channel, *Deep. Res. Part II Top. Stud. Oceanogr.*, doi:10.1016/j.dsr2.2013.10.016, 2014.

3417 Robinson, J., Guillotreau, P., Jiménez-Toribio, R., Lantz, F., Nadzon, L., Dorizo, J., Gerry, C. and Marsac, F.: Impacts  
3418 of climate variability on the tuna economy of Seychelles, *Clim. Res.*, doi:10.3354/cr00890, 2010.

3419 Rochford, D. J.: Seasonal interchange of high and low salinity surface waters off south-west Australia, Technical Paper,  
3420 Division of Fisheries and Oceanography, CSIRO, Australia, <http://hdl.handle.net/102.100.100/321788?index=1>, 1969.

3421 Roemmich, D., W. J. Gould and J. Gilson: 135 years of global ocean warming between the Challenger expedition and the  
3422 Argo Programme. *Nature Climate Change* volume 2, 425–428, 2012.

3423 Roman-Stork, H. L., Subrahmanyam, B., & Trott, C. B.: Monitoring  
3424 intraseasonal oscillations in the Indian Ocean using satellite observations. *Journal of Geophysical Research: Oceans*,  
3425 125, e2019JC015891, <https://doi.org/10.1029/2019JC015891>, 2020.

3426 Rosell-Fieschi, M., Rintoul, S. R., Gourrion, J., and Pelegri, J. L.: Tasman Leakage of intermediate waters as inferred  
3427 from Argo floats, *Geophys. Res. Lett.*, 40, 5456– 5460, <https://doi.org/10.1002/2013GL057797>, 2013.

3428 Roxy, M., Tanimoto, Y., Preethi, B., Terray, P. and Krishnan, R.: Intraseasonal SST-precipitation relationship and its  
3429 spatial variability over the tropical summer monsoon region, *Clim. Dyn.*, 41(1), 45–61, doi:10.1007/s00382-012-1547-  
3430 1, 2013.

3431 Roxy, M. K., Ritika, K., Terray, P. and Masson, S.: The curious case of Indian Ocean warming, *J. Clim.*,  
3432 doi:10.1175/JCLI-D-14-00471.1, 2014.

3433 Roxy, M. K., Modi, A., Murtugudde, R., Valsala, V., Panickal, S., Prasanna Kumar, S., Ravichandran, M., Vichi, M. and  
3434 Lévy, M.: A reduction in marine primary productivity driven by rapid warming over the tropical Indian Ocean,  
3435 *Geophys. Res. Lett.*, doi:10.1002/2015GL066979, 2016.

3436 Roxy, M.K., P. Dasgupta, M.J. McPhaden, T. Suematsu, C. Zhang, and D. Kim: Twofold expansion of the Indo-Pacific  
3437 warm pool warps the MJO life cycle. *Nature*, 575, 647-651. <https://doi.org/10.1038/s41586-019-1764-4>, 2019.

3438 Rouault, M., Penven, P. and Pohl, B.: Warming in the Agulhas Current system since the 1980’s, *Geophys. Res. Lett.*,  
3439 doi:10.1029/2009GL037987, 2009.

3440 Rydbeck, A. V. and Jensen, T. G.: Oceanic impetus for convective onset of the Madden-Julian oscillation in the western  
3441 Indian ocean, *J. Clim.*, 30(11), 4299–4316, doi:10.1175/JCLI-D-16-0595.1, 2017.

3442 Rydbeck, A. V., Jensen, T. G. and Nyadjro, E. S.: Intraseasonal sea surface warming in the western Indian Ocean by  
3443 oceanic equatorial Rossby waves, *Geophys. Res. Lett.*, 44(9), 4224–4232, doi:10.1002/2017GL073331, 2017.

3444 Sabeerali, C. T., Ramu Dandi, A., Dhakate, A., Salunke, K., Mahapatra, S. and Rao, S. A.: Simulation of boreal summer  
3445 intraseasonal oscillations in the latest CMIP5 coupled GCMs, *J. Geophys. Res. Atmos.*, 118(10), 4401–4420,  
3446 doi:10.1002/jgrd.50403, 2013.

3447 Sabu, P., M.P. Subeesh, J.V. George et al.: Enhanced subsurface mixing due to near-inertial waves: observation from  
3448 Seychelles-Chagos Thermocline Ridge. *Ocean Dynamics* 71, 391–409. <https://doi.org/10.1007/s10236-020-01430-z>,  
3449 2021

Formatted: No underline, Font colour: Auto

Deleted: 2021Saji

3451 [Sahoo, D., Saxena, H., Tripathi, N., Khan, A., Rahaman, A., Kumar, S., Sudheer, A., and Singh, A.: Non-Redfieldian](#)  
3452 [C:N:P ratio in the inorganic and organic pools of the Bay of Bengal during the summer monsoon, Mar. Ecol. Prog.](#)  
3453 [Ser., 653, 41–55, <https://doi.org/10.3354/meps13498>, 2020.](#)  
3454 [Sahoo, D., Saxena, H., Nazirahmed, S., Kumar, S., Sudheer, A., Bhushan, R., Sahay, A., and Singh, A.: Role of eddies](#)  
3455 [and N<sub>2</sub> fixation in regulating C: N: P proportions in the Bay of Bengal, Biogeochemistry, 1–17, 2021.](#)  
3456 [Saji, N. H., Goswami, B. N., Vinayachandran, P. N. and Yamagata, T.: A dipole mode in the tropical Indian Ocean,](#)  
3457 [Nature, 401\(6751\), 360–363, doi:10.1038/43854, 1999.](#)  
3458 [Saji, N. H., Xie, s.-P., and Tam, C.-Y.: Satellite observations of intense intraseasonal cooling events in the tropical south](#)  
3459 [Indian Ocean, Geophys. Res. Lett., 33, L14704, doi:10.1029/2006GL026525, 2006.](#)  
3460 [Sanchez-Franks, A., Webber, B. G. M., King, B. A., Vinayachandran, P. N., Matthews, A. J., Sheehan, P. M. F., Behara,](#)  
3461 [A. and Neema, C. P.: The railroad switch effect of seasonally reversing currents on the Bay of Bengal high salinity](#)  
3462 [core, Geophys. Res. Lett., doi:10.1029/2019gl082208, 2019.](#)  
3463 [Sanchez-Franks, A., Kent, E. C., Matthews, A. J., Webber, B. G. M., Peatman, S. C. and Vinayachandran, P. N.:](#)  
3464 [Intraseasonal variability of air-sea fluxes over the Bay of Bengal during the Southwest Monsoon, J. Clim.,](#)  
3465 [doi:10.1175/JCLI-D-17-0652.1, 2018.](#)  
3466 [Sarkar, S., H.T. Pham, S. Ramachandran, J.D. Nash, A. Tandon, J. Buckley, A.A. Lotliker, and M.M. Omand: The](#)  
3467 [interplay between submesoscale instabilities and turbulence in the surface layer of the Bay of Bengal. Oceanography](#)  
3468 [29\(2\):146–157, <https://doi.org/10.5670/oceanog.2016.47>, 2016.](#)  
3469 [Sarma, V. V. and Aswanikumar, V.: Subsurface chlorophyll maxima in the north-western Bay of Bengal, J. Plankton](#)  
3470 [Res., <https://doi.org/10.1093/plankt/13.2.339>, 1991.](#)  
3471 [Sasamal, S. K., Panigrahy, R. C. and Misra, S.: Asterionella blooms in the northwestern Bay of Bengal during 2004, Int.](#)  
3472 [J. Remote Sens., <https://doi.org/10.1080/01431160500185391>, 2005.](#)  
3473 [Sawant, S. and Madhupratap, M.: Seasonally and composition of phytoplankton in the Arabian Sea, Curr. Sci., 1996.](#)  
3474 [Schloesser, F.: A dynamical model for the Leeuwin Undercurrent, J. Phys. Oceanogr., 44, 1798–1810,](#)  
3475  [<https://doi.org/10.1175/JPO-D-13-0226.1>, 2014.](#)  
3476 [Schmitz, Jr, W.J.: On the interbasin-scale thermohaline circulation, Reviews of Geophysics, 33, 151–173,](#)  
3477  [<https://doi.org/10.1029/95RG00879>, 1995.](#)  
3478 [Schott, F. A. and McCreary, J. P.: The monsoon circulation of the Indian Ocean, Progr. Oceanogr., 51, 1–123, 2001.](#)  
3479 [Schott, F., Dengler, M., and Schoenefeldt, R.: The shallow overturning circulation of the Indian Ocean. Progress in](#)  
3480 [Oceanography, 53, 57–103, 2002.](#)  
3481 [Schott, F.A., McCreary, J.P., and Johnson, G.C.: “Shallow Overturning Circulations of the Tropical-Subtropical](#)  
3482 [Oceans.” In Earth Climate: The Ocean-Atmosphere Interaction, edited by C. Wang, S.-P. Xie, and J. A. Carton, 261–](#)  
3483 [304. Geophysical Monograph, American Geophysical Union, Washington, D.C., <https://doi.org/10.1029/147GM15>,](#)  
3484 [2004.](#)  
3485 [Schott, F. A., Xie, S.-P. and McCreary, J. P.: Indian Ocean circulation and climate variability, Rev. Geophys., 47,](#)  
3486 [RG1002, <https://doi.org/10.1029/2007RG000245>, 2009.](#)  
3487 [Schmitz, W.J.: On the interbasin-scale thermohaline circulation. Reviews of Geophysics 33:151–173, <http://dx.doi.org/>](#)  
3488 [10.1029/95RG00879, 1995.](#)  
3489 [Schumann, E. H., Churchill, J. R. S. and Zaayman, H. J.: Oceanic variability in the western sector of Algoa Bay, South](#)  
3490 [Africa, African J. Mar. Sci., doi:10.2989/18142320509504069, 2005.](#)  
3491 [Sengupta, D., Senan, R. and Goswami, B. N.: Origin of intraseasonal variability of circulation in the tropical central](#)  
3492 [Indian Ocean, Geophys. Res. Lett., doi:10.1029/2000GL012251, 2001.](#)  
3493 [Sengupta, D., Bharath Raj, G. N. and Shenoi, S. S. C.: Surface freshwater from Bay of Bengal runoff and Indonesian](#)  
3494 [Throughflow in the tropical Indian Ocean, Geophys. Res. Lett., doi:10.1029/2006GL027573, 2006.](#)  
3495 [Sengupta, D., Goddalahundi, B. R. and Anitha, D. S.: Cyclone-induced mixing does not cool SST in the post-monsoon](#)  
3496 [north Bay of Bengal, Atmos. Sci. Lett., doi:10.1002/asl.162, 2008.](#)

Deleted: <https://doi.org/10.1093/plankt/13.2.339>,

Deleted: <https://doi.org/10.1080/01431160500185391>,

Deleted: <https://doi.org/10.1175/JPO-D-13-0226.1>,

Deleted: <https://doi.org/10.1029/95RG00879>,

Deleted: <https://doi.org/10.1029/147GM15>,

Deleted: <https://doi.org/10.1029/2007RG000245>,



3503 Sengupta, D., Senan, R., Goswami, B. N. and Vialard, J.: Intraseasonal variability of equatorial Indian Ocean zonal  
3504 currents, in Journal of Climate., 2007.

3505 Shalapyonok, A., Olson, R. J. and Shalapyonok, L. S.: Arabian Sea phytoplankton during Southwest and Northeast  
3506 Monsoons 1995: Composition, size structure and biomass from individual cell properties measured by flow cytometry,  
3507 Deep. Res. Part II Top. Stud. Oceanogr., doi:10.1016/S0967-0645(00)00137-5, 2001.

3508 Shankar, D., McCreary, J. P., Han, W. and Shetye, S. R.: Dynamics of the East India Coastal Current 1. Analytic  
3509 solutions forced by interior Ekman pumping and local alongshore winds, J. Geophys. Res., 101 13975–13991, 1996.  
3510 Shankar, D. and Shetye, S. R.: On the dynamics of the Lakshadweep high and low in southeastern Arabian Sea; J.  
3511 Geophys. Res. 102 12,551–12,562, 1997.

3512 Shankar, D., Vinayachandran, P. N. and Unnikrishnan, A. S.: The monsoon currents in the north Indian Ocean, Prog.  
3513 Oceanogr., 52(1), 63–120, doi:10.1016/S0079-6611(02)00024-1, 2002.

3514 Shankar, D., Remya, R., Vinayachandran, P., Chatterjee, A. and Behera, A.: Inhibition of mixed-layer deepening during  
3515 winter in the northeastern Arabian Sea by the West India Coastal Current, Climate Dynamics, 47(3-4), 1049–1072,  
3516 2016.

3517 Sharma, G. S.: Water characteristics and current structure at 65°E during the southwest monsoon, J. Oceanogr. Soc. Jpn.,  
3518 32, 284–296, <https://doi.org/10.1007/BF02107985>, 1976.

3519 Sharma, G.S., Gouveia, A.D., and Satyendranath, S.: Incursion of the Pacific Ocean Water into the Indian Ocean. Proc.  
3520 Indian Acad. Sci., A (E & P Sciences) 87, 29–45, <https://doi.org/10.1007/BF02839383>, 1978.

3521 Sharmila, S., Pillai, P. A., Joseph, S., Roxy, M., Krishna, R. P. M., Chattopadhyay, R., Abhilash, S., Sahai, A. K. and  
3522 Goswami, B. N.: Role of ocean-atmosphere interaction on northward propagation of Indian summer monsoon  
3523 intraseasonal oscillations (MISO), Clim. Dyn., 41(5–6), 1651–1669, doi:10.1007/s00382-013-1854-1, 2013.

3524 Sheehan, P. M. F., Webber, B. G. M., Sanchez-Franks, A., Matthews, A. J., Heywood, K. J. and Vinayachandran, P. N.:  
3525 Injection of Oxygenated Persian Gulf Water Into the Southern Bay of Bengal, Geophys. Res. Lett.,  
3526 doi:10.1029/2020GL087773, 2020.

3527 Shenoi, S., Shankar, D. and Shetye, S. R.: Differences in heat budgets of the near-surface Arabian Sea and Bay of  
3528 Bengal: Implications for the summer monsoon; J. Geophys. Res. 107, <https://doi.org/10.1029/2000JC000679>, 2002.

3529 Shetye, S. R. and Shenoi, S. S. C.: Seasonal cycle of surface circulation in the coastal North Indian Ocean; Proc.  
3530 Indian Acad. Sci. (Earth Planet Sci.) 97 53–62, 1988.

3531 Shetye, S. R., Gouveia, A. D., Shankar, D., Shenoi, S. S. C., Vinayachandran, P. N., Sundar, D., Michael, G. S. and  
3532 Nampoothiri, G.: Hydrography and circulation in the western Bay of Bengal during the northeast monsoon, J.  
3533 Geophys. Res. C Ocean., doi:10.1029/95JC03307, 1996.

3534 Shetye, S. R., Gouveia, A.D., Shenoi, S. S. C., Sundar, D., Michael, G. S. and Nampoothiri, G.: The western boundary  
3535 current of the seasonal subtropical gyre in the Bay of Bengal, J. Geophys. Res., 98, 945-954, 1993.

3536 Shinoda, T., Hendon, H. H. and Glick, J.: Intraseasonal Variability of Surface Fluxes and Sea Surface Temperature in  
3537 the Tropical Western Pacific and Indian Oceans, J. Clim., 11, 1685–1702, 1998.

3538 Shinoda, T., Kiladis, G. N. and Roundy, P. E.: Statistical representation of equatorial waves and tropical instability  
3539 waves in the Pacific Ocean, Atmos. Res., 94, 37– 44, doi:10.1016/j.atmosres.2008.06.002, 2009.

3540 Shinoda, T., Han, W., Joseph Metzger, E. and Hurlburt, H. E.: Seasonal variation of the Indonesian throughflow in  
3541 Makassar Strait, J. Phys. Oceanogr., doi:10.1175/JPO-D-11-0120.1, 2012.

3542 Shroyer, E., Rudnick, D., Farrar, J. T., Lim, B., Venayagamoorthy, S. K., St. Laurent, L., Garanaik, A. and Moum, J.:  
3543 Modification of Upper-Ocean Temperature Structure by Subsurface Mixing in the Presence of Strong Salinity  
3544 Stratification, Oceanography, 29(2), 62–71, doi:10.5670/oceanog.2016.39, 2016.

3545 Siedler, G., Rouault, M., and Lutjeharms, J.: Structure and origin of the subtropical South Indian Ocean Countercurrent,  
3546 Geophys. Res. Lett., 33, L24609, <https://doi.org/10.1029/2006GL027399>, 2006.

Deleted: <https://doi.org/10.1007/BF02107985>,

Deleted: <https://doi.org/10.1007/BF02839383>,

Deleted: intra-seasonal

Formatted: Indent: First line: 0 cm

Formatted: Highlight

Deleted: <https://doi.org/10.1029/2006GL027399>,



3551 Siedler, G., Rouault, M., Biastoch, A., Backeberg, B. C., Reason, C. J. C., and Lutjeharms, J.: Modes of the southern  
3552 extension of the East Madagascar Current, J. Geophys. Res., 114, C01005, <https://doi.org/10.1029/2008JC004921>,  
3553 2009.

3554 Singh, A., Gandhi, N., Ramesh, R. and Prakash, S.: Role of cyclonic eddy in enhancing primary and new production in  
3555 the Bay of Bengal, J. Sea Res., doi:10.1016/j.seares.2014.12.002, 2015a.

3556 Singh, A. and Ramesh, R.: Environmental controls on new and primary production in the northern Indian Ocean, Prog.  
3557 Oceanogr., doi:10.1016/j.pocean.2014.12.006, 2015b.

3558 Singh, D., Tsiang, M., Rajaratnam, B. and Diffenbaugh, N. S.: Observed changes in extreme wet and dry spells during  
3559 the south Asian summer monsoon season, Nat. Clim. Chang., doi:10.1038/nclimate2208, 2014.

3560 Smith, R. L., Huyer, A., Godfrey, J. S., and Church, J. A.: The Leeuwin Current off Western Australia, 1986–1987, J.  
3561 Phys. Oceanogr., 21, 323–345, [https://doi.org/10.1175/1520-0485\(1991\)021<0323:TLCOWA>2.0.CO;2](https://doi.org/10.1175/1520-0485(1991)021<0323:TLCOWA>2.0.CO;2), 1991.

3562 Smyth, W.D., Durland, T. and Moun, J.N.: Energy and heat fluxes due to vertically-propagating Yanai waves observed  
3563 in the equatorial Indian Ocean, J. Geophys. Res. Oceans, 120, doi:10.1002/2014JC010152, 2014.

3564 Sorokin, Y., Kopylov, A. and Mamaeva, N.: Abundance and dynamics of microplankton in the central tropical Indian  
3565 Ocean, Mar. Ecol. Prog. Ser., doi:10.3354/meps024027, 1985.

3566 Speich, S., Blanke, B. and Cai, W.: Atlantic meridional overturning circulation and the Southern Hemisphere supergyre,  
3567 Geophys. Res. Lett., doi:10.1029/2007GL031583, 2007.

3568 Sperber, K. R. and Annamalai, H.: Coupled model simulations of boreal summer intraseasonal (30–50 day) variability,  
3569 Part I: Systematic errors and caution on use of metrics, Clim. Dyn., 31(2–3), 345–372, doi:10.1007/s00382-008-0367-  
3570 9, 2008.

3571 Sprintall, J., Chong, J., Syamsudin, F., Morawitz, W., Hautala, S., Bray, N. and Wijffels, S.: Dynamics of the South Java  
3572 current in the Indo-Australian Basin, Geophys. Res. Lett., 26, 2493–2496, 1999.

3573 Sprintall, J., Wijffels, S. E., Molcard, R. and Jaya, I.: Direct estimates of the Indonesian Throughflow entering the Indian  
3574 Ocean: 2004–2006, J. Geophys. Res. Ocean., doi:10.1029/2008JC005257, 2009.

3575 Sprintall, J., Gordon, A. L., Koch-Larrouy, A., Lee, T., Potemra, J. T., Pujiana, K. and Wijffels, S. E.: The Indonesian  
3576 seas and their role in the coupled ocean-climate system, Nat. Geosci., doi:10.1038/ngeo2188, 2014a.

3577 Sprintall, J. and Révelard, A.: The Indonesian Throughflow response to Indo-Pacific climate variability, J. Geophys.  
3578 Res. Ocean., doi:10.1002/2013JC009533, 2014b.

3579 Sprintall, J., Gordon, A. L., Wijffels, S. E., Feng, M., Hu, S., Koch-Larrouy, A., Phillips, H., Nugroho, D., Napitu, A.,  
3580 Pujiana, K., Dwi Susanto, R., Sloyan, B., Yuan, D., Riama, N. F., Siswanto, S., Kuswardani, A., Arifin, Z., Wahyudi,  
3581 A. J., Zhou, H., Nagai, T., Ansong, J. K., Bourdalle-Badié, R., Chanut, J., Lyard, F., Arbic, B. K., Ramdhani, A. and  
3582 Setiawan, A.: Detecting change in the Indonesian seas, Front. Mar. Sci., doi:10.3389/fmars.2019.00257, 2019.

3583 Sree Lekha, J., Buckley, J. M., Tandon, A. and Sengupta, D.: Subseasonal Dispersal of Freshwater in the Northern Bay  
3584 of Bengal in the 2013 Summer Monsoon Season, J. Geophys. Res. Ocean., doi:10.1029/2018JC014181, 2018.

3585 Srinivasan, A., Garraffo, Z. and Iskandarani, M.: Abyssal circulation in the Indian Ocean from a 1 / 12° resolution global  
3586 hindcast, Deep. Res. Part I Oceanogr. Res. Pap., doi:10.1016/j.dsr.2009.07.001, 2009.

3587 Srokosz, M. A., Quartly, G. D. and Buck, J. J. H.: A possible plankton wave in the Indian Ocean, Geophys. Res. Lett.,  
3588 doi:10.1029/2004GL019738, 2004.

3589 Srokosz, M. A. and Quartly, G. D.: The madagascar bloom: A serendipitous study, J. Geophys. Res. Ocean.,  
3590 doi:10.1029/2012JC008339, 2013.

3591 Srokosz, M. A., Robinson, J., McGrain, H., Popova, E. E., and Yool, A.: Could the Madagascar bloom be fertilized by  
3592 Madagascan iron?, J. Geophys. Res. Oceans, 120, 5790–5803, <https://doi.org/10.1002/2015JC011075>, 2015.

3593 Stramma, L., Bange, H. W., Czeschel, R., Lorenzo, A. and Frank, M.: On the role of mesoscale eddies for the biological  
3594 productivity and biogeochemistry in the eastern tropical Pacific Ocean off Peru, Biogeosciences, doi:10.5194/bg-10-  
3595 7293-2013, 2013.

Deleted: <https://doi.org/10.1029/2008JC004921>,

Moved up [1]: Oceanogr.,

Deleted: 21, 323–345, [https://doi.org/10.1175/1520-0485\(1991\)021<0323:TLCOWA>2.0.CO;2](https://doi.org/10.1175/1520-0485(1991)021<0323:TLCOWA>2.0.CO;2),

Formatted: Font colour: Custom Colour (RGB(28,29,30)), Highlight

Deleted: indonesian throughflow

Deleted: indian ocean

3602 Strutton, P. G., Coles, V. J., Hood, R. R., Matear, R. J., McPhaden, M. J. and Phillips, H. E.: Biogeochemical variability  
3603 in the central equatorial Indian Ocean during the monsoon transition, *Biogeosciences*, doi:10.5194/bg-12-2367-2015,  
3604 2015.

3605 Stuecker, M. F., Timmermann, A., Jin, F. F., Chikamoto, Y., Zhang, W., Wittenberg, A. T., Widiasih, E., and Zhao, S.:  
3606 Revisiting ENSO/Indian Ocean Dipole phase relationships, *Geophys. Res. Lett.*, 44, 2481–2492, 2017.

3607 Suhas, E., Neena, J. M. and Goswami, B. N.: An Indian monsoon intraseasonal oscillations (MISO) index for real time  
3608 monitoring and forecast verification, *Clim. Dyn.*, 40(11–12), 2605–2616, doi:10.1007/s00382-012-1462-5, 2013.

3609 Sun, S., Lan, J., Fang, Y., Tana, and Gao, X.: A triggering mechanism for the Indian Ocean dipoles independent of  
3610 ENSO. *J. Climate*, 28, 5063–5076, <https://doi.org/10.1175/JCLI-D-14-00580.1>, 2015.

3611 Suresh, I., Vialard, J., Lengaigne, M., Han, W., McCreary, J., Durand, F., Muraleedharan, P. M.: *Origins of wind-driven*  
3612 *intraseasonal sea level variations in the north Indian Ocean coastal waveguide*. *Geophys Res Lett* 40:5740–5744,  
3613 [doi:10.1002/2013GL058312](https://doi.org/10.1002/2013GL058312), 2013.

3614 Suresh, I., Vialard, J., Izumo, T., Lengaigne, M., Han, W., McCreary, J. P. and Muraleedharan, P. M.: *Dominant role*  
3615 *of winds near Sri Lanka in driving seasonal sea level variations along the west coast of India*, *Geophys. Res. Lett.*,  
3616 43,7028–7035, doi:10.1002/2016GL069976, 2016.

3617 Susanto, R.D., Gordon, A.L. and Zheng, Q.N.: *Upwelling along the coasts of Java and Sumatra sand its relation to*  
3618 *ENSO*. *Geophys. Res. Lett.*, 28, 1599–1602, 2001.

3619 Susanto, R. D., Wei, Z., Adi, R. T., Fan, B., Li, S. and Fang, G.: Observations of the Karimata Strait throughflow from  
3620 December 2007 to November 2008, *Acta Oceanol. Sin.*, doi:10.1007/s13131-013-0307-3, 2013.

3621 Suzuki, R., Behera, S. K., Iizuka, S. and Yamagata, T.: Indian Ocean subtropical dipole simulated using a coupled  
3622 general circulation model, *J. Geophys. Res. C Ocean.*, doi:10.1029/2003JC001974, 2004.

3623 Swallow, J. C. and Pollard, R. T.: Flow of bottom water through the Madagascar Basin, *Deep Sea Res. Part A*,  
3624 *Oceanogr. Res. Pap.*, doi:10.1016/0198-0149(88)90095-7, 1988.

3625 Takaya, Y., Ishikawa, I., Kobayashi, C., Endo, H., & Ose, T.: Enhanced Meiyu-Baiu rainfall in early summer 2020:  
3626 Aftermath of the 2019 super IOD event, *Geophysical Research Letters*, 47, e2020GL090671,  
3627 <https://doi.org/10.1029/2020GL090671>, 2020.

3628 Takeuchi, K.: Numerical study of the Subtropical Front and the Subtropical Countercurrent. *J. Oceanogr. Soc. Japan*, 40,  
3629 371–381, <https://doi.org/10.1007/BF02303341>, 1984.

3630 Talley, L. D., and Sprintall, J.: Deep expression of the Indonesian Throughflow: Indonesian Intermediate Water in the  
3631 South Equatorial Current, *Journal of Geophysical Research, Oceans*, 110: doi:10.1029/2004JC002826, 2005.

3632 Talley, L. D.: Freshwater transport estimates and the global overturning circulation: Shallow, deep and throughflow  
3633 components, *Progress in Oceanography*, 78(4), 257-303. doi: 10.1016/j.pocean.2008.05.001, 2008.

3634 Talley, L. D.: Closure of the global overturning circulation through the Indian, Pacific, and Southern Oceans:  
3635 Schematics and transports. *Oceanography* 26 (1), 80-97. doi: 10.5670/oceanog.2013.07, 2013.

3636 Talley, L. D., Pickard, G. L., Emery, W. J. and Swift, J. H.: *Descriptive Physical Oceanography: An Introduction*, 6th  
3637 Edition. Academic Press, Elsevier Ltd. 983pp, 2011.

3638 Talley, L. D., Feely, R. A., Sloyan, B. M., Wanninkhof, R., Baringer, M.O., Bullister, J. L., et al.: Changes in ocean  
3639 heat, carbon content, and ventilation: A review of the first decade of GO-SHIP global repeat hydrography. *Annu. Rev.*  
3640 *Mar. Sci.* 8, 185-215. doi: 10.1146/annurev-marine-052915-100829, 2016.

3641 Talley, L., Johnson, G. C., Purkey, S., Feely, R. A. and Wanninkhof, R.: Global Ocean Ship-based Hydrographic  
3642 Investigations Program (GO-SHIP) provides key climate-relevant deep ocean observations, *US CLIVAR Variations*,  
3643 15, 8-14, 2017.

3644 Tarran, G. A., Burkill, P. H., Edwards, E. S. and Woodward, E. M. S.: Phytoplankton community structure in the  
3645 Arabian Sea during and after the SW monsoon, 1994, *Deep. Res. Part II Top. Stud. Oceanogr.*, doi:10.1016/S0967-  
3646 0645(98)00122-2, 1999.

Formatted: Font colour: Auto

Formatted: Font: Not Italic, Font colour: Auto

Formatted: Font colour: Auto

Formatted: Font colour: Auto

Formatted: Font colour: Auto

Deleted: <https://doi.org/10.1007/BF02303341>,

Deleted: .

Formatted: Font: Not Italic

3649 Taylor, B. M., Benkwitt, C. E., Choat, H., Clements, K. D., Graham, N. A., and Meekan, M. G.: Synchronous biological  
3650 feedbacks in parrotfishes associated with pantropical coral bleaching, *Global Change Biology*, 26, 3, 1285-1294,  
3651 <https://doi.org/10.1111/gcb.14909>, 2019.

3652 Terray, P., Delecluse, P., Labattu, S. and Terray, L.: Sea surface temperature associations with the late Indian summer  
3653 monsoon, *Clim. Dyn.*, doi:10.1007/s00382-003-0354-0, 2003.

3654 Thadathil, P., Muraleedharan, P. M., Rao, R. R., Somayajulu, Y. K., Reddy, G. V. and Revichandran, C.: Observed  
3655 seasonal variability of barrier layer in the Bay of Bengal, *J. Geophys. Res. Ocean.*, 112(2),  
3656 doi:10.1029/2006JC003651, 2007.

3657 Thadathil, P., Suresh, I., Gautham, S., Prasanna Kumar, S., Lengaigne, M., Rao, R. R., Neetu, S. and Hegde, A.: Surface  
3658 layer temperature inversion in the Bay of Bengal: Main characteristics and related mechanisms, *J. Geophys. Res.*  
3659 *Ocean.*, doi:10.1002/2016JC011674, 2016.

3660 Thangaprakash, V. P., Girishkumar, M. S., Suprit, K., Kumar, N. S., Chaudhuri, D., Dinesh, K., Kumar, A.,  
3661 Shivaprasad, S., Ravichandran, M., Farrar, J. T., Sundar, R. and Weller, R.: What Controls Seasonal Evolution of Sea  
3662 Surface Temperature in the Bay of Bengal? Mixed Layer Heat Budget Analysis Using Moored Buoy Observations  
3663 Along 90°E, *Oceanography*, 29(2), 202–213, doi:10.5670/oceanog.2016.52, 2016.

3664 Thompson, P. A., Pesant, S. and Waite, A. M.: Contrasting the vertical differences in the phytoplankton biology of a  
3665 dipole pair of eddies in the south-eastern Indian Ocean, *Deep. Res. Part II Top. Stud. Oceanogr.*,  
3666 doi:10.1016/j.dsr2.2006.12.009, 2007.

3667 Thompson, P. A., Wild-Allen, K., Lourey, M., Rousseaux, C., Waite, A. M., Feng, M., and Beckley, L. E.: Nutrients in  
3668 an oligotrophic boundary current: evidence of a new role for the Leeuwin Current. *Progress in Oceanography* 91, 345–  
3669 359, 2011.

3670 Thompson, R. O. R. Y.: Observations of the Leeuwin Current off Western Australia, *J. Phys. Oceanogr.*, 14, 623–628,  
3671 [https://doi.org/10.1175/1520-0485\(1984\)014<0623:OOTLCO>2.0.CO;2](https://doi.org/10.1175/1520-0485(1984)014<0623:OOTLCO>2.0.CO;2), 1984.

3672 Thompson, R. O. R. Y.: Continental-shelf-scale model of the Leeuwin Current, *J. Mar. Res.*, 45(4), 813–827,  
3673 <https://doi.org/10.1357/002224087788327190>, 1987.

3674 Todd, R. E., Chavez, F. P., Clayton, S., Cravatte, S., Goes, M., Graco, M., Lin, X., Sprintall, J., Zilberman, N. V.,  
3675 Archer, M., Aristegui, J., Balmaseda, M., Bane, J. M., Baringer, M. O., Barth, J. A., Beal, L. M., Brandt, P., Calil, P.  
3676 H. R., Campos, E., Centurioni, L. R., Chidichimo, M. P., Cirano, M., Cronin, M. F., Curchitser, E. N., Davis, R. E.,  
3677 Dengler, M., deYoung, B., Dong, S., Escribano, R., Fassbender, A. J., Fawcett, S. E., Feng, M., Goni, G. J., Gray, A.  
3678 R., Gutiérrez, D., Hebert, D., Hummels, R., Ito, S., Krug, M., Lacan, F., Laurindo, L., Lazar, A., Lee, C. M.,  
3679 Lengaigne, M., Levine, N. M., Middleton, J., Montes, I., Muglia, M., Nagai, T., Palevsky, H. I., Palter, J. B., Phillips,  
3680 H. E., Piola, A., Plueddemann, A. J., Qiu, B., Rodrigues, R. R., Roughan, M., Rudnick, D. L., Rykaczewski, R. R.,  
3681 Saraceno, M., Seim, H., Sen Gupta, A., Shannon, L., Sloyan, B. M., Sutton, A. J., Thompson, L., van der Plas, A. K.,  
3682 Volkov, D., Wilkin, J., Zhang, D., and Zhang, L.: Global perspectives on observing ocean boundary current systems.  
3683 *OceanObs'19 white paper. Frontiers in Marine Science*. 6:423. doi: 10.3389/fmars.2019.00423, 2019.

3684 Toole, J. M., and Warren, B. A.: A hydrographic section across the subtropical South Indian Ocean, *Deep-Sea Res I*, 40,  
3685 1973-2019, [https://doi.org/10.1016/0967-0637\(93\)90042-2](https://doi.org/10.1016/0967-0637(93)90042-2), 1993.

3686 Tozuka, T., Kataoka, T., and Yamagata, T.: Locally and remotely forced atmospheric circulation anomalies of Ningaloo  
3687 Niño/Niña, *Clim. Dyn.*, 43, 2197–2205, <https://doi.org/10.1007/s00382-013-2044-x>, 2014.

3688 Trott, C., Bulusu, S. and Washburn, C. E.: Investigating the response of temperature and salinity in the Agulhas Current  
3689 region to ENSO events, *Remote Sensing*, 13(9), 1829, doi:10.3390/rs13091829, 2021.

3690 Turner, A. G., Joshi, M., Robertson, E. S., and Woolnough, S. J.: The effect of Arabian Sea optical properties on SST  
3691 biases and the South Asian summer monsoon in a coupled GCM, *Clim. Dyn.*, 39(3), 811–826,  
3692 <https://doi.org/10.1007/s00382-011-1254-3>, 2012.

3693 Ummerhoyer, C. C., Biastoch, A., and Böning, C. W.: Multidecadal Indian Ocean variability linked to the Pacific and  
3694 implications for preconditioning Indian Ocean dipole events. *J. Climate*, 30, 1739–1751, 2017.

Deleted: ... E., Chavez, F.,... P., Clayton, S,	... [1]
Deleted: ..., Goes, M.,... Graco, M.,... Lin, X,	... [2]
Deleted: ..., Zilberman, N.,... V., Archer, M,	... [3]
Deleted: ,	
Deleted: ..., Bane, J,	... [4]
Deleted: ... O., Barth, J.,... A., Beal, L.,... M., Brandt, P,	... [5]
Deleted: ... H. R., Campos, E,	... [6]
Deleted: ,	
Deleted: ,	
Deleted: ..., Cronin, M,	... [7]
Deleted: ... N., Davis, R,	... [8]
Deleted: ,	
Deleted: ..., Dong, S,	... [9]
Deleted: ..., Fassbender, A.,... J., Fawcett, ... S. E., Feng	... [10]
Deleted: ... J., Gray, A.,... R., Gutiérrez, D.,... Hebert, D	... [11]
Deleted: ..., Ito, S-i.,... Krug, M.,... Lacan, F.,... Laurindo, L.,... Lazar, A.,... Lee, C,	... [12]
Deleted: ..., Levine, N.,... M., Middleton, J.,... Montes, I.,... Muglia, M.,... Nagai, T.,... Palevsky, H.,... I., Palter, J.,... B., Phillips, H.,...	... [13]
Deleted: ,	
Deleted: ,	
Deleted: ..., Rodrigues, R,	... [14]
Deleted: ..., Rudnick, D,	... [15]
Deleted: ,	
Deleted: ,	
Deleted: ..., Sen Gupta, A.,... Shannon, L,	... [16]
Deleted: ... M., Sutton, A,	... [17]
Deleted: ,	
Deleted: ... K., Volkov, D.,... Wilkin, J.,... Zhang, D., and Zhang, L.:... Global Perspectives...erspectives on Observing Ocean Boundary Current Systems	... [18]
Deleted: Response...esponse of Temperature...emperature and Salinity...alinity in the Agulhas Current Region...egion to ENSO Events...vents, Remote Sensing, 13(9):1829DOI:10.3390/rs13091829...	... [19]
Formatted: No underline, Font colour: Auto	

Uz, B. M.: What causes the sporadic phytoplankton bloom southeast of Madagascar?, *J. Geophys. Res. Ocean.*, doi:10.1029/2006JC003685, 2007.

Van Sebille, E., Biastoch, A., Van Leeuwen, P. J. and De Ruijter, W. P. M.: A weaker Agulhas current leads to more Agulhas leakage, *Geophys. Res. Lett.*, doi:10.1029/2008GL036614, 2009.

Van Sebille, E., Van Leeuwen, P. J., Biastoch, A. and De Ruijter, W. P. M.: On the fast decay of Agulhas rings, *J. Geophys. Res. Ocean.*, doi:10.1029/2009JC005585, 2010a.

Van Sebille, E., van Leeuwen, P. J., Biastoch, A. and de Ruijter, W. P. M.: Flux comparison of Eulerian and Lagrangian estimates of Agulhas leakage: A case study using a numerical model, *Deep. Res. Part I Oceanogr. Res. Pap.*, doi:10.1016/j.dsr.2009.12.006, 2010b.

Van Sebille, E., Beal, L. M. and Johns, W. E.: Advective Time Scales of Agulhas Leakage to the North Atlantic in Surface Drifter Observations and the 3D OFES Model, *J. Phys. Oceanogr.*, doi:10.1175/2011jpo4602.1, 2011.

Van Sebille, E., Sprintall, J., Schwarzkopf, F. U., Sen Gupta, A., Santoso, A., England, M. H., Biastoch, A. and Böning, C. W.: Pacific-to-Indian Ocean connectivity: Tasman leakage, Indonesian Throughflow, and the role of ENSO, *J. Geophys. Res. Ocean.*, doi:10.1002/2013JC009525, 2014.

Varna, M., Singh, A., Sahoo, D., and Sengupta, D.: Strengthening of basin-scale ocean currents in winter drives decadal salinity decline in the eastern Arabian Sea, *Geophys. Res. Lett.*, 48, e2021GL094516, 2021.

Vecchi, G. A. and Soden, B. J.: Global warming and the weakening of the tropical circulation, *J. Climate*, 20, 4316–4340, 2007.

Vecchi, G. A. and Harrison, D. E.: Monsoon Breaks and Subseasonal Sea Surface Temperature Variability in the Bay of Bengal, *J. Clim.*, 15(12), 1485–1493, doi:10.1175/1520-0442(2002)015<1485:MBASS>2.0.CO;2, 2002.

Venkatesan, R., Vedachalam, N., Arul Muthiah, M., Sundar, R., Kesavakumar, B., Ramasundaram, S. and Jossia Joseph, K.: Reliability metrics from two decades of Indian ocean moored buoy observation network, *Mar. Technol. Soc. J.*, doi:10.4031/MTSJ.52.3.14, 2018.

Venrick, E. L.: Mid-ocean ridges and their influence on the large-scale patterns of chlorophyll and production in the North Pacific, *Deep. Res. Part A*, doi:10.1016/s0198-0149(12)80006-9, 1991.

Vialard, J., Foltz, G. R., McPhaden, M. J., Duvel, J. P. and de Boyer Montégut, C.: Strong Indian Ocean sea surface temperature signals associated with the Madden-Julian Oscillation in late 2007 and early 2008, *Geophys. Res. Lett.*, 35(19), 1–5, doi:10.1029/2008GL035238, 2008.

Vialard, J., Duvel, J. P., McPhaden, M. J., Bouruet-Aubertot, P., Ward, B., Key, E., Bourras, D., Weller, R., Minnett, P., Weill, A., Cassou, C., Eymard, L., Fristedt, T., Basdevant, C., Dandonneau, Y., Duteil, O., Izumo, T., de Boyer Montégut, C., Masson, S., Marsac, F., Menkes, C. and Kennan, S.: Cirene: Air-sea interactions in the Seychelles-Chagos thermocline ridge region, *Bull. Am. Meteorol. Soc.*, doi:10.1175/2008BAMS2499.1, 2009a.

Vialard, J., Shenoi, S. S. C., McCreary, J. P., Shankar, D., Durand, F., Fernando, V. and Shetye, S. R.: Intraseasonal response of the northern Indian Ocean coastal waveguide to the Madden-Julian Oscillation, *Geophys. Res. Lett.*, 36(14), 1–5, doi:10.1029/2009GL038450, 2009b.

Vialard, J., Jayakumar, A., Gnanaseelan, C., Lengaigne, M., Sengupta, D. and Goswami, B. N.: Processes of 30-90 days sea surface temperature variability in the northern Indian Ocean during boreal summer, *Clim. Dyn.*, 38(9–10), 1901–1916, doi:10.1007/s00382-011-1015-3, 2012.

Vic, C., Roulet, G., Xavier, C. and Capet, X.: Mesoscale dynamics in the Arabian Sea and a focus on the Great Whirl life cycle: A numerical investigation using ROMS, *Journal of Geophysical Research: Oceans*, 119, 6422–6443, <https://doi.org/10.1002/2014JC009857>, 2014.

Vijith, V., Vinayachandran, P., Thushara, V., Amol, P., Shankar, D., and Anil, A.: Consequences of inhibition of mixed-layer deepening by the West India Coastal Current for winter phytoplankton bloom in the northeastern Arabian Sea, *Journal of Geophysical Research: Oceans*, 121, 6583–6603, <https://doi.org/10.1002/2016JC012004>, 2016.

Vinayachandran, P. N., Saji, N. H. and Yamagata T.: Response of the equatorial Indian Ocean to an anomalous wind event during 1994, *Geophys. Res. Lett.* 26 1613–1615, 1999.

Deleted: van

Deleted: van

Deleted: \*,

Deleted: seychelles-chagos

3842 Vinayachandran, P. N., Shetye, S. R., Sengupta, D. and Gadgil, S.: Forcing mechanisms of the Bay of Bengal circulation,  
3843 Curr. Sci., 71, 753–763, 1996.

3844 Vinayachandran, P. N., T. Kagimoto, T. Masumoto, Y., Chauhan, P., Nayak, S. R. and Yamagata, T.: Bifurcation of  
3845 the East India Coastal Current east of Sri Lanka, Geophys. Res. Lett., 32, L15606, doi:10.1029/2005GL022864, 2005.

3846 Vinayachandran, P. N., Shankar, D., Vernekar, S., Sandeep, K. K., Amol, P., Neema, C. P. and Chatterjee, A.: A  
3847 summer monsoon pump to keep the Bay of Bengal salty, Geophys. Res. Lett., 40, 1777–1782, doi:10.1002/grl.50274,  
3848 2013.

3849 Vinayachandran, P. N., Matthews, A. J., Vijay KuMar, K., Sanchez-Franks, A., Thushara, V., George, J., Vijith, V.,  
3850 Webber, B. G. M., Queste, B. Y., Roy, R., Sarkar, A., Baranowski, D. B., Bhat, G. S., Klingaman, N. P., Peatman, S.  
3851 C., Parida, C., Heywood, K. J., Hall, R., King, B., Kent, E. C., Nayak, A. A., Neema, C. P., Amol, P., Lotliker, A.,  
3852 Kankonkar, A., Gracias, D. G., Vernekar, S., D'Souza, A. C., Valluvan, G., Pargaonkar, S. M., Dinesh, K., Giddings,  
3853 J. and Joshi, M.: BoBBLE: Ocean–Atmosphere interaction and its impact on the South Asian monsoon, Bull. Am.  
3854 Meteorol. Soc., doi:10.1175/BAMS-D-16-0230.1, 2018.

3855 Vivekanandan, E. and Krishnakumar, P.K.: Spatial and temporal differences in the coastal fisheries along the east  
3856 coast of India. Indian Journal of Marine Science, 39, 380, 2010.

3857 Volkov, D. L., Lee, S.-K., Gordon, A. L., Rudko, M.: Unprecedented reduction and quick recovery of the South Indian  
3858 Ocean heat content and sea level in 2014–2018. Sci. Adv., 6, doi:10.1126/sciadv.abc1151, 2020.

3859 Wacongne, S., and Pacanowski, R.C.: Seasonal heat transport in a primitive equation model of the tropical Indian  
3860 Ocean, J. Phys. Oceanogr., 26, 2666–2699, 1996.

3861 Wainwright, C. M., Finney, D. L., Kilavi, M., Black, E., and Marsham, J. H.: Extreme rainfall in East Africa,  
3862 October 2019–January 2020 and context under future climate change, Weather, 76(1), 26-31,  
3863 <https://doi.org/10.1002/wea.3824>, 2021.

3864 Waite, A. M., Pesant, S., Griffin, D. A., Thompson, P. A. and Holl, C. M.: Oceanography, primary production and  
3865 dissolved inorganic nitrogen uptake in two Leeuwin Current eddies, Deep. Res. Part II Top. Stud. Oceanogr.,  
3866 doi:10.1016/j.dsr2.2007.03.001, 2007a.

3867 Waite, A. M., Thompson, P. A., Pesant, S., Feng, M., Beckley, L. E., Domingues, C. M., Gaughan, D., Hanson, C. E.,  
3868 Holl, C. M., Koslow, T., Meuleners, M., Montoya, J. P., Moore, T., Muhling, B. A., Paterson, H., Rennie, S.,  
3869 Strzelecki, J., and Twomey, L.: The Leeuwin Current and its eddies: An introductory overview, Deep Sea Res. II,  
3870 54(8–10), 789–796, <https://doi.org/10.1016/j.dsr2.2006.12.008>, 2007b.

3871 Waite, A. M., Beckley, L. E., Guidi, L., Landrum, J. P., Holliday, D., Montoya, J., Paterson, H., Feng, M., Thompson, P.  
3872 A. and Raes, E. J.: Cross-shelf transport, oxygen depletion, and nitrate release within a forming mesoscale eddy in the  
3873 eastern Indian Ocean, Limnol. Oceanogr., doi:10.1002/lno.10218, 2016.

3874 Waliser, D. E., Murtugudde, R. and Lucas, L. E.: Indo-Pacific Ocean response to atmospheric intraseasonal variability:  
3875 1. Austral summer and the Madden-Julian Oscillation, J. Geophys. Res., 108(C5), 3160, doi:10.1029/2002JC001620,  
3876 2003.

3877 Wang, H., McClean, J. L., Talley, L. D., and Yeager, S.: Seasonal cycle and annual reversal of the Somali Current in an  
3878 eddy-resolving global ocean model. Journal of Geophysical Research: Oceans, 123, 6562–6580,  
3879 <https://doi.org/10.1029/2018JC013975>, 2018.

3880 Wang, H., Kumar, A., Murtugudde, R., Narapusetty, B., and Selp, K. L.: Covariations between the Indian Ocean dipole  
3881 and ENSO: a modeling study. Clim. Dyn., doi:10.1007/s00382-019-04895-x, 2019.

3882 Wang, Y. and McPhaden, M. J.: Seasonal cycle of cross-equatorial flow in the Central Indian Ocean. J. Geophys. Res.,  
3883 122, doi:10.1002/2016JC012537, 2017.

3884 Wang, G., and Cai, W.: Two-year consecutive concurrences of positive Indian Ocean Dipole and Central Pacific El Niño  
3885 preconditioned the 2019/2020 Australian “black summer” bushfires. Geosci. Lett. 7, 19  
3886 <https://doi.org/10.1186/s40562-020-00168-2>, 2020.

Deleted: south asian

Formatted: Font colour: Auto

Deleted: R. C.

Formatted: Font colour: Auto

Deleted: (1996),

Formatted: Font colour: Auto

Deleted: .

Formatted: Font colour: Auto

Deleted: <https://doi.org/10.1016/j.dsr2.2006.12.008>.

Deleted: M.J.

Deleted: 2017:

Deleted: Cycle

Deleted: Cross-Equatorial Flow

Deleted:

Deleted: .

3898 Warner, S. J., Becherer, J., Pujiana, K., Shroyer, E. L., Ravichandran, M., Thangaprakash, V. P. and Moum, J. N.:  
3899 Monsoon mixing cycles in the Bay of Bengal: A year-long subsurface mixing record, *Oceanography*,  
3900 doi:10.5670/oceanogr.2016.48, 2016.

3901 Warren, B. A.: Deep flow in the Madagascar and Mascarene basins, *Deep. Res. Oceanogr. Abstr.*, doi:10.1016/0011-  
3902 7471(74)90015-1, 1974.

3903 Warren, B. A.: Bottom water transport through the Southwest Indian Ridge, *Deep. Res.*, doi:10.1016/0146-  
3904 6291(78)90596-9, 1978.

3905 Warren, B.A.: Transindian hydrographic section at Lat. 18°S: Property distributions and circulation in the South Indian  
3906 Ocean. *Deep-Sea Res A.*, 28, 759-788. doi: 10.1016/S0198-0149(81)80001-5, 1981.

3907 Warren, B.A. : Driving the meridional overturning in the Indian Ocean, *Deep. Res. Part I*, doi:10.1016/0967-  
3908 0637(94)90101-5, 1994.

3909 Warren, B. A., Whitworth, T. and LaCasce, J. H.: Forced resonant undulation in the deep Mascarene Basin, *Deep. Res.*  
3910 *Part II Top. Stud. Oceanogr.*, doi:10.1016/S0967-0645(01)00151-5, 2002.

3911 Weaver, A. J., and Middleton, J. H.: On the dynamics of the Leeuwin Current, *J. Phys. Oceanogr.*, 19, 626–648,  
3912 [https://doi.org/10.1175/1520-0485\(1989\)019<0626:OTDOTL>2.0.CO;2](https://doi.org/10.1175/1520-0485(1989)019<0626:OTDOTL>2.0.CO;2), 1989.

3913 Weaver, A.J., and Middleton, J.H.: An analytic model for the Leeuwin Current off western Australia, *Cont. Shelf Res.*,  
3914 10(2), 105–122, [https://doi.org/10.1016/0278-4343\(90\)90025-H](https://doi.org/10.1016/0278-4343(90)90025-H), 1990.

3915 Webber, B. G. M., Matthews, A. J. and Heywood, K. J.: A dynamical ocean feedback mechanism for the Madden-Julian  
3916 Oscillation, *Q. J. R. Meteorol. Soc.*, 136(648), 740–754, doi:10.1002/qj.604, 2010.

3917 Webber, B. G. M., Stevens, D. P., Matthews, A. J. and Heywood, K. J.: Dynamical ocean forcing of the Madden-Julian  
3918 oscillation at lead times of up to five months, *J. Clim.*, 25(8), 2824–2842, doi:10.1175/JCLI-D-11-00268.1, 2012a.

3919 Webber, B. G. M., Matthews, A. J., Heywood, K. J. and Stevens, D. P.: Ocean Rossby waves as a triggering mechanism  
3920 for primary Madden-Julian events, *Q. J. R. Meteorol. Soc.*, 138(663), 514–527, doi:10.1002/qj.936, 2012b.

3921 Webber, B. G. M., Matthews, A. J., Heywood, K. J., Kaiser, J. and Schmidtke, S.: Seaglider observations of equatorial  
3922 Indian Ocean Rossby waves associated with the Madden-Julian Oscillation, *J. Geophys. Res. Ocean.*, 119(6), 3714–  
3923 3731, doi:10.1002/2013JC009657, 2014.

3924 Webber, B. G. M., Matthews, A. J., Vinayachandran, P. N., Neema, C. P., Sanchez-Franks, A., Vijith, V., Amol, P. and  
3925 Baranowski, D. B.: The Dynamics of the Southwest Monsoon Current in 2016 from High-Resolution In Situ  
3926 Observations and Models, *J. Phys. Oceanogr.*, 48(10), 2259–2282, doi:10.1175/JPO-D-17-0215.1, 2018.

3927 Webster, P. J., Moore, A., Loschnigg, J. P. and R., L. R.: Coupled oceanic-atmospheric dynamics in the Indian Ocean  
3928 during 1997-1998, *Nature*, 401(September), 356–360, 1999.

3929 Weijer, W. and van Sebille, E.: Impact of Agulhas leakage on the Atlantic overturning circulation in the CCSM4, *J.*  
3930 *Clim.*, doi:10.1175/JCLI-D-12-00714.1, 2014.

3931 Weller, R. A., Farrar, J. T., Buckley, J., Mathew, S., Venkatesan, R., Lekha, J. S., Chaudhuri, D., Suresh Kumar, N. and  
3932 Praveen Kumar, B.: Air-sea interaction in the Bay of Bengal, *Oceanography*, doi:10.5670/oceanog.2016.36, 2016.

3933 Wiggert, J. D., Jones, B. H., Dickey, T. D., Brink, K. H., Weller, R. A., Marra, J. and Codispoti, L. A.: The Northeast  
3934 Monsoon's impact on mixing, phytoplankton biomass and nutrient cycling in the Arabian Sea, *Deep. Res. Part II Top.*  
3935 *Stud. Oceanogr.*, doi:10.1016/S0967-0645(99)00147-2, 2000.

3936 Wiggert, J. D., Hood, R. R., Banse, K. and Kindle, J. C.: Monsoon-driven biogeochemical processes in the Arabian Sea,  
3937 *Prog. Oceanogr.*, doi:10.1016/j.pocean.2005.03.008, 2005.

3938 Wiggert, J. D., Murtugudde, R. G. and Christian, J. R.: Annual ecosystem variability in the tropical Indian Ocean:  
3939 Results of a coupled bio-physical ocean general circulation model, *Deep. Res. Part II Top. Stud. Oceanogr.*, 53(5–7),  
3940 644–676, doi:10.1016/j.dsr2.2006.01.027, 2006.

3941 Wiggert, J. D., Vialard, J., and Behrenfeld, M. J.: Basin-wide modification of dynamical and biogeochemical processes  
3942 by the positive phase of the Indian Ocean Dipole during the SeaWiFS era. In: *Indian Ocean biogeochemical Processes*

**Deleted:** *Oceanogr.*, 19, 626–648, [https://doi.org/10.1175/1520-0485\(1989\)019<0626:OTDOTL>2.0.CO;2](https://doi.org/10.1175/1520-0485(1989)019<0626:OTDOTL>2.0.CO;2),

**Deleted:** [https://doi.org/10.1016/0278-4343\(90\)90025-H](https://doi.org/10.1016/0278-4343(90)90025-H).



3946 and Ecological Variability, Geophysical Monograph Series, 185, 385–407, <https://doi.org/10.1029/2008GM000776>,  
3947 2009.

3948 Wijesekera, H. W., Jensen, T. G., Jarosz, E., Teague, W. J., Metzger, E. J., Wang, D. W., Jinadasa, S. U. P.,  
3949 Arulanathan, K., Centurioni, L. R. and Fernando, H. J. S.: Southern Bay of Bengal currents and salinity intrusions  
3950 during the northeast monsoon, *J. Geophys. Res. Ocean.*, doi:10.1002/2015JC010744, 2015.

3951 Wijesekera, H. W., Shroyer, E., Tandon, A., Ravichandran, M., Sengupta, D., Jinadasa, S. U. P., Fernando, H. J. S.,  
3952 Agrawal, N., Arulanathan, K., Bhat, G. S., Baumgartner, M., Buckley, J., Centurioni, L., Conry, P., Thomas Farrar,  
3953 J., Gordon, A. L., Hormann, V., Jarosz, E., Jensen, T. G., Johnston, S., Lankhorst, M., Lee, C. M., Leo, L. S.,  
3954 Lozovatsky, I., Lucas, A. J., MacKinnon, J., Mahadevan, A., Nash, J., Omand, M. M., Pham, H., Pinkel, R., Rainville,  
3955 L., Ramachandran, S., Rudnick, D. L., Sarkar, S., Send, U., Sharma, R., Simmons, H., Stafford, K. M., Laurent, L. S.,  
3956 Venayagamoorthy, K., Venkatesan, R., Teague, W. J., Wang, D. W., Waterhouse, A. F., Weller, R. and Whalen, C. B.:  
3957 ASIRI: An ocean-atmosphere initiative for Bay of Bengal, *Bull. Am. Meteorol. Soc.*, doi:10.1175/BAMS-D-14-  
3958 00197.1, 2016a.

3959 Wijesekera, H., Teague, W., Jarosz, E., Wang, D., Jensen, T., Jinadasa, S. U. P., Fernando, H., Centurioni, L., Hallock,  
3960 Z., Shroyer, E. and Moum, J.: Observations of Currents Over the Deep Southern Bay of Bengal—With a Little Luck,  
3961 *Oceanography*, 29(2), 112–123, doi:10.5670/oceanog.2016.44, 2016b.

3962 Wijesekera, H. W., Teague, W. J., Wang, D. W., Jarosz, E., Jensen, T. G., Jinadasa, S. U. P., Fernando, H. J. S. and  
3963 Hallock, Z. R.: Low-frequency currents from deep moorings in the southern bay of Bengal, *J. Phys. Oceanogr.*,  
3964 doi:10.1175/JPO-D-16-0113.1, 2016c.

3965 Wijffels, S., and G. Meyers: An intersection of oceanic waveguides: Variability in the Indonesian throughflow region, *J.*  
3966 *Phys. Oceanogr.*, 34, 1232–1253, 2004.

3967 Wijffels, S., Meyers, G. and Godfrey, J. S.: A 20-yr average of the Indonesian throughflow: Regional currents and the  
3968 interbasin exchange, *J. Phys. Oceanogr.*, 38, 1965–1978, 2008.

3969 Wijffels, S., Roemmich, D., Monselesan, D., Church, J. and Gilson, J.: Ocean temperatures chronicle the ongoing  
3970 warming of Earth. *Nature Clim Change* 6, 116–118 <https://doi.org/10.1038/nclimate2924>, 2016.

3971 Williams, A. P. and Funk, C.: A westward extension of the warm pool leads to a westward extension of the Walker  
3972 circulation, drying eastern Africa. *Clim. Dyn.*, 37, 2417–2435, 2011.

3973 Wilson, C. and Qiu, X.: Global distribution of summer chlorophyll blooms in the oligotrophic gyres, *Prog. Oceanogr.*,  
3974 doi:10.1016/j.pocean.2008.05.002, 2008.

3975 Woo, M., Pattiaratchi, C. and Schroeder, W.: Summer surface circulation along the Gascoyne continental shelf, Western  
3976 Australia. *Cont Shelf Res* 26, 132–152, 2006.

3977 Woo, L. M., Pattiaratchi, C. B.: Hydrography and water masses off the western Australian coast, *Deep Sea Res. I*, 55(9),  
3978 1090–1104, <https://doi.org/10.1016/j.dsr.2008.05.005>, 2008.

3979 Wyrtki, K.: An equatorial jet in the Indian Ocean, *Science*, 181 (4096), 262–264, doi:10.1126/science.181.4096.262,  
3980 1973.

3981 Xi, J., L. Zhou, R. Murtugudde, and L. Jiang: Impacts of intraseasonal SST anomalies on precipitation during Indian  
3982 summer monsoon. *J. Clim.*, 28, 4561–4575, <http://dx.doi.org/10.1175/JCLI-D-14-00096.1>, 2015.

3983 Xie, S.-P., Annamalai, H., Schott, F. A., and McCreary, J. P.: Structure and mechanisms of South Indian Ocean climate  
3984 variability, *J. Clim.*, 15, 864–878, 2002.

3985 Xie, S.-P., Du, Y., Huang, G., Zheng, X.-T., Tokinaga, H., Hu, K. M., and Liu, Q. Y.: Decadal shift in El Niño  
3986 influences on Indo–Western Pacific and East Asian climate in the 1970s. *J. Climate*, 23, 3352–3368, 2010.

3987 Xie, S., Hu, K., Hafner, J., Tokinaga, H., Du, Y., Huang, G., and Sampe, T.: Indian Ocean Capacitor Effect on Indo–  
3988 Western Pacific Climate during the Summer following El Niño. *Journal of Climate* 22, 3, 730–747,  
3989 <https://doi.org/10.1175/2008JCLI2544.1>, 2009.

Deleted: bay

Deleted: G.

Deleted: J. S.

Deleted: :

Deleted: <https://doi.org/10.1038/nclimate2924>.

Deleted: C.

Deleted: <https://doi.org/10.1016/j.dsr.2008.05.005>.

Formatted: Indent: Hanging: 0.28 cm, Space After: 3 pt

Deleted: : <http://dx.doi.org/10.1175/JCLI-D-14-00096.1>,

Deleted: <https://doi.org/10.1175/2008JCLI2544.1>.

3999 Xie, S.-P., Kosaka, Y., Du, Y., Hu, K., Chowdary, J. S., & Huang, G.: Indo-western Pacific ocean capacitor and  
4000 coherent climate anomalies in post-ENSO summer: A review. *Adv. in Atmos. Sci.*, 33(4, SI), 411–432.  
4001 <https://doi.org/10.1007/s00376-015-5192-6>, 2016.

4002 Yamagami, Y. and Tozuka, T.: Interdecadal changes of the Indian Ocean subtropical dipole mode, *Clim. Dyn.*,  
4003 doi:10.1007/s00382-014-2202-9, 2015.

4004 Yanai, M. and Maruyama, T.: Stratospheric wave disturbances propagating over the equatorial Pacific, *J. Meteorol.*  
4005 *Soc. Jap.*, 44, 291–294, 1966.

4006 Yang, J., Liu, Q., Xie, S.-P., Liu, Z. and Wu, L.: Impact of the Indian Ocean SST basin mode on the Asian summer  
4007 monsoon. *Geophys. Res. Lett.*, 34, L02708. doi:10.1029/2006GL028571, 2007.

4008 Yang, L., Murtugudde, R., Zhou, L., & Liang, P.: A potential link between the Southern Ocean warming and the South  
4009 Indian Ocean heat balance. *Journal of Geophysical Research: Oceans*, 125, e2020JC016132, 2020.  
4010 <https://doi.org/10.1029/2020JC016132>

4011 Yang, Y., Xie, S.-P., Wu, L., Kosaka, Y., Lau, N. C., and Vecchi, G. A.: Seasonality and predictability of the Indian  
4012 Ocean dipole mode: ENSO forcing and internal variability, *J. Clim.*, 28, 8021–8036, 2015.

4013 Yit Sen Bull, C., and van Sebille, E.: Sources, fate, and pathways of Leeuwin Current water in the Indian Ocean and  
4014 Great Australian Bight: A Lagrangian study in an eddy-resolving ocean model, *J. Geophys. Res. Oceans*, 121, 1626–  
4015 1639, <https://doi.org/10.1002/2015JC011486>, 2016.

4016 Yoshida, K., and Kidokoro, T.: A subtropical countercurrent II: A prediction of eastward flows at lower subtropical  
4017 latitudes, *J. Oceanogr. Soc. Japan*, 23(5), 231–246, 1967.

4018 Yu, L., Jin, X. and Weller, R. A.: Annual, seasonal, and interannual variability of air-sea heat fluxes in the Indian Ocean,  
4019 in *Journal of Climate*, 2007.

4020 Yu, L.: Sea Surface Exchanges of Momentum, Heat, and Fresh Water Determined by Satellite Remote Sensing, in  
4021 *Encyclopedia of Ocean Sciences*, 1, pp. 15–23, Elsevier, <https://doi.org/10.1016/B978-0-12-409548-9.11458-7>, 2009.

4022 Yuan, D., Zhou, H. and Zhao, X.: Interannual climate variability over the tropical Pacific ocean induced by the Indian  
4023 ocean dipole through the Indonesian Throughflow, *J. Clim.*, doi:10.1175/JCLI-D-12-00117.1, 2013.

4024 Zang, N., Sprintall, J., Jemmy, R., Wang, F., *Seasonality of the Somali Current/Undercurrent System, Deep-Sea Research*  
4025 *Part II*, <https://doi.org/10.1016/j.dsr2.2021.104953>, 2021.

4026 Zhang, C.: Madden-Julian Oscillation, *Rev. Geophys.*, 43(2), RG2003, <https://doi.org/10.1029/2004RG000158>, 2005.

4027 Zhang, L., Han, W., Li, Y., and Maloney, E. D.: Role of North Indian Ocean air-sea interaction in summer monsoon  
4028 intraseasonal oscillation, *J. Clim.*, 31(19), 7885–7908, <https://doi.org/10.1175/JCLI-D-17-0691.1>, 2018.

4029 Zhang, N., Feng, M., Hendon, H.H., Hobday, A.J., and Zinke, J.: Opposite polarities of ENSO drive distinct patterns of  
4030 coral bleaching potentials in the southeast Indian Ocean. *Scientific Reports*, 7(1), 1–10,  
4031 <https://doi.org/10.1038/s41598-017-02688-y>, 2017.

4032 Zhang, D., McPhaden, M. J., and Lee, T.: Observed Interannual Variability of Zonal Currents in the Equatorial Indian  
4033 Ocean Thermocline and Their Relation to Indian Ocean Dipole. *Geophys. Res. Lett.*, 41, 7933–7941, doi:  
4034 10.1002/2014GL061449, 2014.

4035 Zhang, W., Wang, Y., Jin, F.-F., Stuecker, M. F., and Turner, A. G.: Impact of different El Niño types on the El  
4036 Niño/IOD relationship. *Geophys. Res. Lett.*, 42, 8570–8576, 2015.

4037 Zhang, Y., Feng, M., Du, Y., Phillips, H. E., Bindoff, N. L., McPhaden, M. J.: Strengthened Indonesian Throughflow  
4038 drives decadal warming in the Southern Indian Ocean. *Geophys. Res. Lett.*, 45, 6167–6175, 2018.

4039 Zheng, X.-T., Xie, S.-P., Du, Y., Liu, L., Huang, G., and Liu, Q. Y.: Indian Ocean Dipole response to global warming in  
4040 the CMIP5 multimodel ensemble. *J. Climate*, 26, 6067–6080, 2013.

4041 Zheng, S., Feng, M., Du, Y., Meng, X., and Yu, W.: Interannual variability of eddy kinetic energy in the subtropical  
4042 southeast Indian Ocean associated with the El Niño–Southern Oscillation. *J. Geophys. Res.: Oceans*, 123, 1048–1061,  
4043 <https://doi.org/10.1002/2017JC013562>, 2018.

Deleted: <https://doi.org/10.1007/s00376-015-5192-6>,

Deleted: <https://doi.org/10.1029/2020JC016132>

Deleted: <https://doi.org/10.1002/2015JC011486>,

Deleted: M. J.

Deleted: T.

Deleted: :

Deleted: M.

Deleted: Y.

Deleted: H. E.

Deleted: N. L.

Deleted: M. J.

Deleted: :



4056 Zhou, X., Alves, O. Marsland, S. J., Bi, D., and Hirst, A.C.: Multi-decadal variations of the south Indian Ocean  
4057 subsurface temperature influenced by Pacific Decadal Oscillation. Tellus, 69A, 1308055,  
4058 <https://doi.org/10.1080/16000870.2017.1308055>, 2017.

4059 Zhou, L., Murtugudde, R., Chen, D. and Tang, Y.: A Central Indian Ocean mode and heavy precipitation during Indian  
4060 Summer Monsoon. J. Clim., DOI: 10.1175/JCLI-D-16-0347.1, 2017a.

4061 Zhou, L., Murtugudde, R., Chen, D. and Tang, Y.: Seasonal and interannual variabilities of the Central Indian Ocean. J.  
4062 Clim., doi: 10.1175/JCLI-D-16-0616.1, 2017b.

4063 Zhou, Z.-Q., Zhang, R., Xie, S.-P.: Interannual variability of summer surface air temperature over central India:  
4064 Implications for monsoon onset. J. Clim., 32, 1693–1706, 2019.

4065 Zhou, Z.-Q., Xie, S.-P., and Zhang, R.: Historic Yangtze flooding of 2020 tied to extreme Indian Ocean conditions,  
4066 Proceedings of the National Academy of Sciences, 118(12), e2022255118, doi: 10.1073/pnas.2022255118, 2021.

4067 Zhuang, W., Feng, M., Du, Y., Schiller, A. and Wang, D.: Low-frequency sea level variability in the southern Indian  
4068 Ocean and its impacts on the oceanic meridional transports, J. Geophys. Res. Ocean., doi:10.1002/jgrc.20129, 2013.

4069 Zinke, J., Rountrey, A., Feng, M., Xie, S.-P., Dissard, D., Rankenburg, K., Lough, J. M., and McCulloch, M. T.: Corals  
4070 record long-term Leeuwin current variability including Ningaloo Niño/Niña since 1795, Nature Comm., 5, 3607,  
4071 <https://doi.org/10.1038/ncomms4607>, 2014.

- Deleted: R.
- Deleted: D.
- Deleted: Y.
- Deleted: :
- Deleted: Mode
- Deleted: Heavy Precipitation
- Deleted: R.
- Deleted: , D.
- Deleted: Y.
- Deleted: :
- Deleted: Interannual Variabilities
- Deleted: .
- Deleted: . DOI
- Deleted: Zhen-Qiang, Shang-Ping
- Deleted: Renhe
- Deleted: . "
- Deleted: . "
- Deleted: .
- Formatted: Highlight

Page 117: [1] Deleted	Helen Phillips	10/09/2021 07:52:00
-----------------------	----------------	---------------------

▼

Page 117: [1] Deleted	Helen Phillips	10/09/2021 07:52:00
-----------------------	----------------	---------------------

▼

Page 117: [1] Deleted	Helen Phillips	10/09/2021 07:52:00
-----------------------	----------------	---------------------

▼

Page 117: [2] Deleted	Helen Phillips	10/09/2021 07:52:00
-----------------------	----------------	---------------------

▼

Page 117: [2] Deleted	Helen Phillips	10/09/2021 07:52:00
-----------------------	----------------	---------------------

▼

Page 117: [2] Deleted	Helen Phillips	10/09/2021 07:52:00
-----------------------	----------------	---------------------

▼

Page 117: [2] Deleted	Helen Phillips	10/09/2021 07:52:00
-----------------------	----------------	---------------------

▼

Page 117: [3] Deleted	Helen Phillips	10/09/2021 07:52:00
-----------------------	----------------	---------------------

▼

Page 117: [3] Deleted	Helen Phillips	10/09/2021 07:52:00
-----------------------	----------------	---------------------

▼

Page 117: [3] Deleted	Helen Phillips	10/09/2021 07:52:00
-----------------------	----------------	---------------------

▼

Page 117: [4] Deleted	Helen Phillips	10/09/2021 07:52:00
-----------------------	----------------	---------------------

▼

Page 117: [4] Deleted	Helen Phillips	10/09/2021 07:52:00
-----------------------	----------------	---------------------

▼

Page 117: [5] Deleted	Helen Phillips	10/09/2021 07:52:00
-----------------------	----------------	---------------------

▼

Page 117: [5] Deleted	Helen Phillips	10/09/2021 07:52:00
-----------------------	----------------	---------------------

▼

Page 117: [5] Deleted	Helen Phillips	10/09/2021 07:52:00
-----------------------	----------------	---------------------

▼

Page 117: [5] Deleted	Helen Phillips	10/09/2021 07:52:00
-----------------------	----------------	---------------------

▼

Page 117: [6] Deleted	Helen Phillips	10/09/2021 07:52:00
-----------------------	----------------	---------------------

▼

Page 117: [6] Deleted	Helen Phillips	10/09/2021 07:52:00
-----------------------	----------------	---------------------

▼

Page 117: [7] Deleted	Helen Phillips	10/09/2021 07:52:00
-----------------------	----------------	---------------------

Page 117: [8] Deleted	Helen Phillips	10/09/2021 07:52:00
-----------------------	----------------	---------------------

▼

Page 117: [9] Deleted	Helen Phillips	10/09/2021 07:52:00
-----------------------	----------------	---------------------

▼

Page 117: [9] Deleted	Helen Phillips	10/09/2021 07:52:00
-----------------------	----------------	---------------------

▼

Page 117: [10] Deleted	Helen Phillips	10/09/2021 07:52:00
------------------------	----------------	---------------------

▼

Page 117: [10] Deleted	Helen Phillips	10/09/2021 07:52:00
------------------------	----------------	---------------------

▼

Page 117: [10] Deleted	Helen Phillips	10/09/2021 07:52:00
------------------------	----------------	---------------------

▼

Page 117: [10] Deleted	Helen Phillips	10/09/2021 07:52:00
------------------------	----------------	---------------------

▼

Page 117: [11] Deleted	Helen Phillips	10/09/2021 07:52:00
------------------------	----------------	---------------------

▼

Page 117: [11] Deleted	Helen Phillips	10/09/2021 07:52:00
------------------------	----------------	---------------------

▼

Page 117: [11] Deleted	Helen Phillips	10/09/2021 07:52:00
------------------------	----------------	---------------------

▼

Page 117: [11] Deleted	Helen Phillips	10/09/2021 07:52:00
------------------------	----------------	---------------------

▼

Page 117: [12] Deleted	Helen Phillips	10/09/2021 07:52:00
------------------------	----------------	---------------------

▼

Page 117: [12] Deleted	Helen Phillips	10/09/2021 07:52:00
------------------------	----------------	---------------------

▼

Page 117: [12] Deleted	Helen Phillips	10/09/2021 07:52:00
------------------------	----------------	---------------------

▼

Page 117: [12] Deleted	Helen Phillips	10/09/2021 07:52:00
------------------------	----------------	---------------------

▼

Page 117: [12] Deleted	Helen Phillips	10/09/2021 07:52:00
------------------------	----------------	---------------------

▼

Page 117: [12] Deleted	Helen Phillips	10/09/2021 07:52:00
------------------------	----------------	---------------------

▼

Page 117: [12] Deleted	Helen Phillips	10/09/2021 07:52:00
------------------------	----------------	---------------------

▼

Page 117: [13] Deleted	Helen Phillips	10/09/2021 07:52:00
------------------------	----------------	---------------------

Page 117: [13] Deleted    Helen Phillips    10/09/2021 07:52:00

▼

Page 117: [13] Deleted    Helen Phillips    10/09/2021 07:52:00

▼

Page 117: [13] Deleted    Helen Phillips    10/09/2021 07:52:00

▼

Page 117: [13] Deleted    Helen Phillips    10/09/2021 07:52:00

▼

Page 117: [13] Deleted    Helen Phillips    10/09/2021 07:52:00

▼

Page 117: [13] Deleted    Helen Phillips    10/09/2021 07:52:00

▼

Page 117: [14] Deleted    Helen Phillips    10/09/2021 07:52:00

▼

Page 117: [14] Deleted    Helen Phillips    10/09/2021 07:52:00

▼

Page 117: [15] Deleted    Helen Phillips    10/09/2021 07:52:00

▼

Page 117: [15] Deleted    Helen Phillips    10/09/2021 07:52:00

▼

Page 117: [16] Deleted    Helen Phillips    10/09/2021 07:52:00

▼

Page 117: [16] Deleted    Helen Phillips    10/09/2021 07:52:00

▼

Page 117: [16] Deleted    Helen Phillips    10/09/2021 07:52:00

▼

Page 117: [17] Deleted    Helen Phillips    10/09/2021 07:52:00

▼

Page 117: [17] Deleted    Helen Phillips    10/09/2021 07:52:00

▼

Page 117: [18] Deleted    Helen Phillips    10/09/2021 07:52:00

▼

Page 117: [18] Deleted    Helen Phillips    10/09/2021 07:52:00

▼

Page 117: [18] Deleted    Helen Phillips    10/09/2021 07:52:00

▼

Page 117: [18] Deleted    Helen Phillips    10/09/2021 07:52:00

**Page 117: [19] Deleted    Helen Phillips    10/09/2021 07:52:00**

▼

**Page 117: [19] Deleted    Helen Phillips    10/09/2021 07:52:00**

▼

**Page 117: [19] Deleted    Helen Phillips    10/09/2021 07:52:00**

▼

**Page 117: [19] Deleted    Helen Phillips    10/09/2021 07:52:00**

▼

**Page 117: [19] Deleted    Helen Phillips    10/09/2021 07:52:00**

▼

**Page 117: [19] Deleted    Helen Phillips    10/09/2021 07:52:00**

▼